# Kinky Structures

**Neil George Roy Currie**

**BEng(Hons) FIStructE MICE CEng PGCAP FHEA**

**School of Computing, Science and Engineering**

**University of Salford**

**This thesis is submitted in part fulfilment of the requirements for a doctoral degree in Structural Engineering.**

**April 2020**

# Dedication…

Developing and refreshing a set of academic and modelling skills has been incredibly hard work with everything else that I've taken on over the years and this would not have been possible without the support of my wife and children who have given Daddy time to go and sit in the garage and work on his 'rubbish PhD' and to my wife for making time to proofread entire chapters whilst debating the benefits of the Oxford comma.

I've really enjoyed working with my supervisor, Laurence, on developing the research strands within this thesis and not many PhD candidates get to have their supervisory meeting down the pub with a pint and a burger, brainstorming and plotting with a beer has made the process much more fun.

Through the development of various models and strategies I've managed to push several pieces of software to the limits (and broken quite a few) and I've been incredibly grateful for the patience and guidance of Ronald at Ingeciber for his support with CivilFEM.

It has also been enjoyable integrating my research into the curriculum and projects by sharing the methods developed in this thesis and watching them develop new skills on deployable structures.

Some of the concepts are initially complex to understand and Phil and Antony in the Structural Engineering Lab have tolerated my strange requests, drilling holes in snooker balls and creating huge swords from Unistrut whilst secretly fearing for my sanity.

Many thanks to Jen from the Business School for making time to proofread my thesis and for the constructive comments regarding how some of my graphs resemble ovaries.

Also, thanks to Nick for making time to read through my thesis and for spotting too many thats.

Finally, an apology to my parents who are excited that I may become a doctor, I haven't the heart to tell them I won't be able to write prescriptions.

Thank you also to my examiners who rightly kicked my arse in the first viva and provided some much needed constructive criticism that has helped change the work, I feel, for the better.

# Abstract…

Rotational springs are not widely used in structural engineering other than within undergraduate texts to aid with the understanding of strut buckling or other similar theoretical exercises.

The inclusion of rotational springs can significantly alter the behaviour of a structure, bringing several potential benefits if inserted strategically. For instance, allowing a frame to be delivered to site as a single deployable piece, where the rotational springs introduce an element of temporary stability during erection; by ensuring hinges form in specific locations during extreme loading events, creating reliable load paths whilst retaining structural integrity; or by limiting the axial force in specific elements, forcing an element to buckle at specific loads.

Currently, there is a significant gap in the existing research with regards the analysis and behaviour of structures that have springs distributed through the frame. The inclusion of springs within structural frames will typically encourage gross, yet controlled and predictable displacements that are challenging to analyse. Equally, deployable structures require an element of instability to deploy. With most research focusing on the packed and deployed states of these structures, there is still considerable research to be done on the structural performance of the intermediate stages of deployment.

Several forms of deployable structure, such as cable-chain arches for example, are vulnerable and unstable during their intermediate deployment phase and it is proposed that the integration of rotational springs in these types of structure could help control the deployment and maintain stability from a packed shape into the final in-service form as well as preventing phenomenon such as snap-through buckling under large loads.

Original work within this thesis creates several repeatable and reliable methods for undertaking buckling analysis of sprung chains to determine an initial balanced equilibrium form to which in-service loadings can then be applied as well as determining the post-buckled behaviour for sprung structures.

The application of numerical analysis methods is demonstrated as giving reliable results for single

and multiple degrees of freedom systems, but due to the potential for incompatibilities between the stiffnesses of the rotational springs and beam elements there are issues associated with ill-conditioning and methods have been established to identify and mitigate these effects.

Alternative structural forms, beyond simple arches, have also been developed through seeking inspiration from the higher buckling modes. Shapes resembling these higher modes have been generated through the careful manipulation of spring stiffnesses (mobilising linear and non-linear springs) combined with the introduction of initial geometrical imperfections allowing the structures to adopt alternative stable states in direct response to specific loading conditions.

The analysis methods contained within this thesis are currently more advanced than the manufacturing techniques required to realise these designs in the real world. Although, flexible springs are already being cut into stiff plywood panels using living hinges and multi-material 3D printing is commonplace within the maker community, but these techniques have not yet progressed through to the scale and consistency needed to fabricate a large structural element.

However, as these manufacturing techniques mature, the work presented within this thesis will provide a solid base from which the effective analysis of multi-stiffness structures will be possible.

# Declaration…

"I, Neil Currie, declare that this thesis is my own work. Any section, part or phrasing of more than 20 consecutive words that is copied from any other work or publication has been clearly referenced at the point of use and also fully described in the reference section of this thesis.

Signed

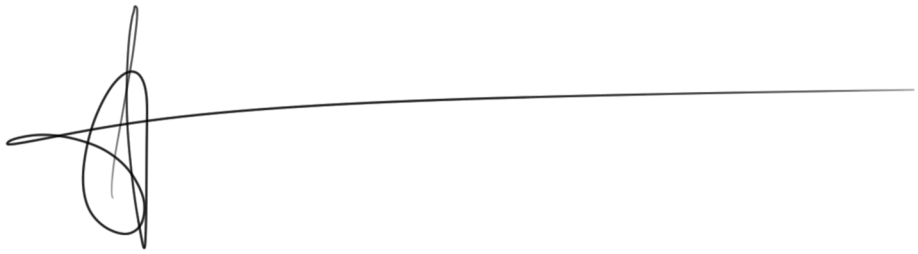

# Contents...

# Table of Figures…

# Chapter 1

## 1 Introduction.

The research within this thesis develops an under-researched area of structural analysis associated with the integration of springs into a structural frame.

The introduction of springs into a structure is hypothesised to bring about benefits that could be advantageous in certain specific scenarios. For example, maintaining the stability of a deployable or metamorphic structure during its deployment phase or in more traditional structures by developing predictable and controlled load relieving mechanisms.

Currently, there is a significant gap in the existing research with regards the behaviour of structures that have springs distributed through the frame. Structures with integral springs appear frequently in undergraduate texts as examples typically associated with axial buckling of struts, but the development of more complex arrangements is an under-researched area.

The lack of implementation of springs within real everyday structures is in part due to the impracticality of creating springs with large rotational stiffnesses compactly and economically and in part due to the complexities of analysing structures formed with rotational springs.

However, modern digital fabrication techniques are becoming more widely available, such as metal and multi-material 3D printing, and the manufacture of bespoke structural elements formed with either integral rotational springs, mixed materials allowing elements to locally flex, or varied geometrical properties to influence the flexural stiffness may become more commonplace. The structure of this thesis is as follows.

Chapter 2 introduces the concept of deployable structures and identifies some of their more common forms. Many deployable structures have similarities to lightweight structures as the lightweight nature makes them easier to deploy plus the associated reduction in weight for the payload in rockets when employed in extra-terrestrial applications.

Deployable structures change between a stable packed state into their deployed shape by introducing an element of controlled instability. Linkage based deployable structures such as pantographs are relatively straightforward to control in this intermediate state, whereas structures with tension elements such as cable-chain arches are unstable until the cables achieve a working tension and this uncontrolled instability can make them more problematic to deploy as a result.

Deployable structures often have inherent structural instabilities associated with their intermediate deployment phase and it is proposed that the integration of rotational springs in certain types of deployable structures, for example a kinematic façade element, could help control the deployment from a flat shape into the final in-service shape. The integration of hinges in arch structures could also overcome the issues associated with snap-through on cable-chain arches and enable large deflections to occur without the associated risk of snap-through.

Establishing controlled equilibrium states is critical when determining the behaviour of deployable structures and this process has similarities to form-finding techniques that are used in tensile fabric structures. Determining a balanced equilibrium form for a structure (or deployable structure) with springs in it can be challenging. This can be made easier through identifying the buckling modes of structures with springs within them. The need for a repeatable methodology that can establish forms that are balanced and retain equilibrium for sprung struts will be required to be researched and developed within this thesis.

The buckling analysis of struts with a single spring is a common example utilised at undergraduate level and can be undertaken using a variety of methods and various methods are discussed in Chapter 2. However, structures with multiple springs present analytical challenges and their solution is non-trivial and these are covered in more depth in Chapter 4.

Chapter 3 presents a detailed investigation into the geometrical construction of cable-chain arches, which are typically a stable and lightweight structure, but have an unbalanced intermediate form when adopted as a deployable structure. The literature for cable-chain arches is scant in the journals and was covered in Chapter 2, but a more detailed investigation into the potential for these structures to snap-through and their geometrical properties is undertaken in this chapter to better understand their behaviour. Specific arrangements of cable-chain structures can be vulnerable to snap-through behaviour, especially where shallow angles between the cable and the struts are present or where overly flexible elements are incorporated into the design. Shallow angles for the cables are usually governed by the arch being split up into too many uniplets, with parabolic curves having an extra level of susceptibility associated with curves

where the significant portions of the curve are relatively flat.

It is proposed that a similar arch formed of struts, but with the cables removed could be formed and where the pins are exchanged for revolute springs, could provide an alternative structure that is stable in both the final and intermediate stages. This requires the development of analytical methods for generating stable arches formed of springs and then applying external loads to these structures to determine their behaviour post-buckling these methods are developed in the subsequent chapter.

Chapter 4 establishes different methods for conducting buckling analysis for struts with infinitely stiff strut elements and a single spring to cross-validate the approaches being used against the classical methods presented in Chapter 2.

New work has been developed within this thesis that establishes a repeatable and reliable method for undertaking buckling analysis of sprung chains using a variety of methods to obtain these equilibrium forms. Starting with traditional geometrically defined buckling analysis and energy methods which are trivial to solve for simple arrangements, but quickly become unwieldy and impractical for structures with several degrees of freedom, through to more robust analysis methods such as a novel finite difference approach and two methodologies that make use of finite element analysis to establish the behaviour during deployment.

The effects of ill-conditioning present challenges when undertaking analysis where the rotational stiffness of the springs vary in comparison to the infinitely rigid links and an investigation is undertaken to flag markers that can be used for identifying when ill-conditioning may be affecting the analysis results. Within this thesis, particularly within the buckling and cable-chain chapters, Mathematica is used and small snippets of code will be presented in black boxes and formatted in such a way as to be clear that they are Mathematica syntax.

Chapter 5 develops the analysis methods developed in the previous chapter and applies these numerical methods to investigate increasingly complex spring structures, specifically arches. The finite element and forced displacement methods are utilised to create solutions for structures formed of numerous linear springs arranged in a linear chain and then also with evenly distributed non-linear springs formed in a chain. Each additional spring introduces an additional degree of freedom and the complexity of analysis becomes greater, with 18 spring arches requiring taking significant amounts of time to solve.

Non-linear springs are introduced into chains that allow the struts to lock into pre-defined angles when displacement reaches a predetermined threshold and this principle can be used to generate

deployable structures that fold into portal frames.

In line with the hypothesis, the analysis methods developed have created a framework to allow sprung structures to be analysed. The introduction of springs brings about theoretical benefits such as: controlling motion under certain loading conditions, creating predictable motion, enabling stability for deployable structures during deployment, or limiting axial forces at key positions. Chapter 5 also includes some initial thoughts as to how springs of suitable magnitudes may be formed if they are to be integrated into a building.

Chapter 6 applies the methodologies established in the earlier chapters to two specific examples to identify if the springs bring about benefits to the structures proposed.

An arched structure is developed using the form-finding techniques established and spring stiffnesses are selected to enable the arch to displace laterally into a more aerodynamic shape under an assumed wind loading. The theoretical arch is then re-modelled with more reasonable glue-laminated timber sizes to identify the scale of spring stiffnesses required for a structure of this scale.

The final example presented is of a kinetic structure that is designed to change shape using the Miura-Ori origami folding technique to introduce a single degree of freedom ensuring a repeatable deployment path. A mixed material approach is used to develop an analytical model based on real material properties to establish a model that is both well behaved and can be deployed as part of a kinetic façade.

Chapter 7 summarises and concludes the work contained within this thesis with chapter8 outlining further work for the research, including the development two particular aspects, including:

- Development of a practical sprung hinge that is of a scale that would be suitable for deployment in a façade element or structure as outlined in Chapter 6.
- Expansion of the modelling process to time-dependent behaviours, particularly accidental and blast loadings where damping in the springs could be used to provide further benefits.

## 1.1 Aim.

The thesis aims to develop an appropriate method for the analysis and modelling of structures (static and deployable) with integral rotational springs with regards to their structural behaviour, performance, and ability to adapt the structure.

## 1.2 Objectives.

1) To undertake a literature review to identify the general forms of deployable, metamorphic and adaptive structures to identify how articulation can influence structures.
2) To investigate the cable-chain structural form and identify shortcomings in this structural form that could be improved upon.
3) To identify the potential benefits of rotational springs on arched structures and to determine their potential in being integrated to deployable, metamorphic or adaptive structures.
4) To identify, implement, and validate methods of determining the buckling capacity of struts formed with lightweight infinitely stiff struts and linear rotational springs.
5) To implement linear rotational springs in an arch structure and identify appropriate methods of analysing and determining balanced forms of arch structures.
6) To investigate different forms of springs that may be integrated within a spring chained strut/arch and identify potential implementations.
7) Develop novel structures that make use of the principles identified within the sprung struts that have clear and distinct advantages that may be applied to a real-world scenario.

# Chapter 2

## 2 Review of Non-Stationary Structures.

### 2.1 Introduction.

As stated in the introduction, the hypothesis presented within this thesis is that the introduction of rotational springs into a structure may bring about benefits that could be advantageous in certain scenarios. For example, maintaining the stability of a deployable or metamorphic structure during its deployment phase or in more traditional structures by developing predictable and controlled load relieving mechanisms.

For this hypothesis to be developed further it is first important to consider the existing literature available and the literature review within this thesis is spread over three distinct regions to enable this to occur.

1. The behaviour and motion of deployable structures and how they are analysed.
2. Cable-chain arches, their vulnerability to snap-through and how they are formed and analysed.
3. Buckling of struts containing rotational springs.

#### 2.1.1 The Behaviour And Motion Of Deployable Structures.

This first section of the literature review explores the literature surrounding the analysis and behaviour of structures that are intentionally designed to not always remain static; either by changing their behaviour under certain loading conditions (specifically, buckling) or structures that can be folded for easy transportation to be then unfolded when they have reached their final destination through the integration of specific connections and additional control methods such as hydraulic actuators that can hold a deployed structure in position.

This thesis overall focuses on the hypothesis that the introduction of rotational springs within a structure can bring about changes in structural behaviour that may be beneficial. This is largely a

theoretical proposal given that the manufacture of springs of suitable stiffnesses is still relatively expensive and unproven, but the first step will be establishing suitable analysis methods that may be used to develop structural forms that may be able to be physically realised in the near future, perhaps using 3D printing or other digital fabrication techniques.

Reviewing the research on deployable structures will establish the concept that not all structures are static and that certain forms of structure can be intentionally designed to embrace an approach to their geometry or structural behaviour that introduces an element of controlled instability.

Most structures designed by structural engineers are, by design, static. However, the primary hypothesis within this thesis is that the introduction of rotational springs within a structure can bring about changes in behaviour that may lead to structures that do not always remain static and that, under certain loading conditions, may more closely resemble balanced mechanisms or deployable structures.

The literature review within this chapter explores the principles of deployable structures initially, identifying the importance of stable states, maintaining equilibrium, and looking at some of the more common forms of deployable structures such as pantographs, identifying how linkage and flexible structures can adjust between their packed and deployed shapes.

### 2.1.2 Cable-Chain Arches.

The second section of the literature review focuses on cable-chain arches, where there is very little existing literature available. Cable-chain arches are formed using pinned links draped into an arched shape that have their stability induced through various stringing patterns of cables to hold them into place and create a stable, sometimes self-stabilising, structural form. Cable-chain arches are a lightweight form of structure that can be deployed through the controlled shortening of the cables but in certain geometrical arrangements, these structures can be susceptible to a phenomenon known as snap-through. Cable-chain arches have not widely been investigated, with only a small number of papers dedicated to the accidental damage and robustness of similar cable and strut structures and therefore the geometrical development of specific cable-chains has undertaken in Chapter 3 to verify that snap-through can be developed. This is to simply establish that snap-through occurs rather than establish the precise limits of when it occurs as this would be a separate line of research.

Cable-chain arches can be divided into smaller sub-units, known as uniplets that are formed from 2 struts connected via a free pin and one further cable tied across the toes, see Figure 2-1.

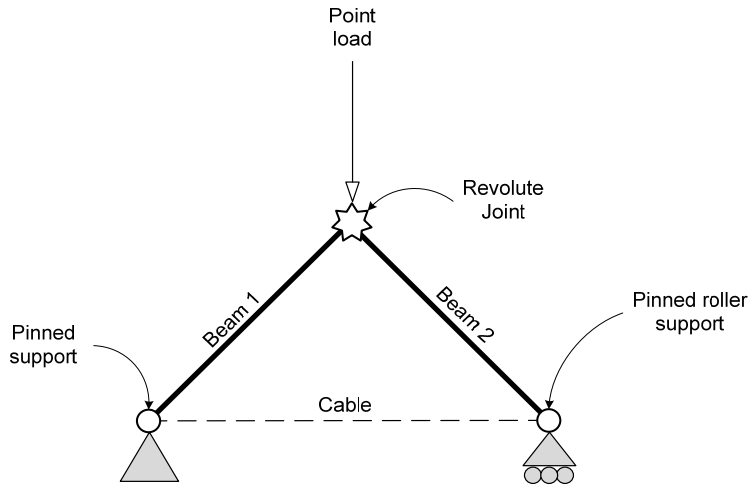


*Figure 2-1 - Cable-Chain Uniplet.*

It is proposed that the free pin and cable could be exchanged for a rotational spring, but that whilst the rotational spring reduces the risk of snap-through, it introduces a new mechanism via axial buckling of the chains struts which will need to be considered if the structure is to remain predictable.

### 2.1.3 Buckling Of Sprung Struts.

The final thread in the literature review presents the concept that the replacement of the free pin and a cable in a cable-chain arch with a rotational spring may help overcome issues associated with snap-through. However, to investigate this concept further it is important to appreciate that the introduction of a rotational spring into a strut creates a structural system that behaves non-linearly and that the method of analysis and the associated prediction of the critical buckling capacity may require a different approach to that of normal uniform struts.

Once again, there is a lack of literature available with determining the critical buckling load and post-buckling capacity of sprung struts and this is the drive behind Chapter 4 for the development of a suitable analysis method for chains of linear springs and Chapter 5 where the method is expanded for the form-finding of arches, the introduction of more complex spring configurations, potential practical spring prototypes, and inclusion of springs in a framed structure.

## 2.2 Non-stationary Structures.

Most structures used within buildings are designed to remain static and even under extreme loadings such as earthquakes are designed to resist excessive movement, either through carefully designed stiffness of the structure or through the use of damping devices.

However, not all structures are designed to be persistently static and are designed to be flexible and move under certain design scenarios. These non-static types of structures can be divided into three distinct types:

| | Description | Application. |
|---|---|---|
| **Demountable Structures** | Structural forms that are typically divided into interconnecting components that can be assembled and dismantled ready for relocation. | Temporary stages, nomad tents, advertising stands. |
| **Deployable Structures** | These are structures that typically have a single degree of freedom to develop a motion that enables deployment from a compact folded state into a fully deployed state. Frequently the intermediate or transitional state has no load-carrying capacity. | Deployable masts, satellites, medical devices, inflatable structures, umbrella. |
| **Adaptive Structures** | Adaptive structures possess a unique ability to change their structural behaviour in response to either applied loads or by being controlled via external stimulus with a stable intermediate state. | Adaptive facades, aerofoils, load relieving structures. |

Each of these types, with examples, will be discussed in more detail in the following sections.

## 2.3 Demountable Structures.

Some of the earliest forms of demountable structures were developed through the nomadic nature of humans tracking and following herds across the plains. The need for the development of a shelter that could be packed and relocated as the herds migrated developed a demountable structure that could be easily transported.

More recent applications include structures such as demountable stages used for concerts and arena tours (see Figure 2-2), although it could also be argued that temporary works used in excavations and formwork also possess many similarities to demountable structures.


*Figure 2-2 - Part Assembled Demountable Structure.*[1]

Typically, demountable structures are implemented as a temporary structure over a relatively short period. Demountable structures are often more expensive than their static equivalent due primarily to the increase in costs with the connections and the use of more expensive materials, such as aluminium, to aid with transportability through weight reduction. Demountable structures and the associated design process has resulted in the need for detailed and specific guidance to be developed by the IStructE (2007) for engineers and those responsible for procuring demountable structures.

Whilst demountable structures may often bring about thoughts associated with ridge tents and smaller-scale structures, it should be noted that many modern demountable structures are of a considerable scale, requiring cranes to lift sections and these have been implemented successfully on several largescale events such as the London Olympics. Anecdotally, Schlaich Bergmann are developing a demountable football stadium as part of the 2022 Qatar FIFA World Cup which can be subdivided to create smaller football facilities for other parts of the country following the completion of the World Cup.

However, the analysis and design of demountable structures are not too dissimilar to a traditional

[1] IStructE. (2007). *Temporary demountable structures: Guidance on procurement, design and use* (Third ed.). London: The Institution of Structural Engineers.

structure in terms of the analysis of the frames and design of the elements, with the key differences being how the connections are designed and fabricated (bolted rather than welded for example) so that they able to be easily taken apart again when it is time to relocate.

Given that demountable structures can be developed and designed using both traditional construction techniques and analysis methods they will not be considered further within this thesis.

## 2.4 Deployable Structures.

A deployable structure, however, has a different set of criteria than most typical building structures (Petroski, 2004) in that the governing criteria is not necessarily about how long the structure will stand for, but instead how will it transform from a compact folded form into a larger enclosure in an autonomous manner (Pellegrino, 2001). The complexity in designing and analysing these types of structures is well documented as being laborious and iterative for engineers (Gantes, 1997).

Deployable structures exist in a broad range of structural forms and arrangements and are in use in everyday application such as train electrification (see Figure 2-3), some of the more common deployable structures and their associated overall properties will be covered in this chapter. Traditional structures are designed to be inherently stable and rigid, with structural instability being seen both as a defect and a potentially catastrophic property for a structure to possess. A structure that is too flexible or able to develop uncontrolled resonant motion, such as the Tacoma Narrows Crossing, for example, can have catastrophic consequences.

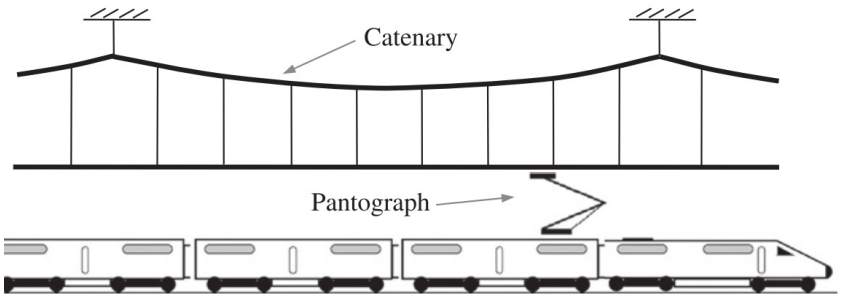


*Figure 2-3 - Pantographic Deployable Structure Use.*[2]

[2] Zhou, N., & Zhang, W. (2011). Investigation on dynamic performance and parameter optimization design of pantograph and catenary system. *Finite Elements in Analysis and Design, 47*(3), 288-295. doi:10.1016/j.finel.2010.10.008

A deployable structure has many performance criteria in common with traditional static structures, such as the need for structural robustness, the creation of a contained environment, structural framing, adequate strength and load-carrying capability, and serviceability requirements. However, it has a distinctly unique difference to traditional static structures: its ability to deploy and/or retract.

Permanent structures are commonly designed to comply with design codes, with well-trodden paths determining structural configurations and element sizes. Whilst this approach works well for most structures, deployable structures differ in that they are, by necessity, driven by ingenious invention and cannot be broken down into a set of simple rules and have no specific design code. To allow a structure to undergo large geometric transformations it is necessary to introduce some form of controlled structural instability (Schleicher, Lienhard, Poppinga, Speck, & Knippers, 2015). The nature of this instability and the ability for it to control and govern the form of movement that allows the structure to fold is crucial (Knippers & Speck, 2012).

Deployable structures must meet their operational requirements (post-deployment stage) and these are likely to be different from their stowed requirements, but in addition to this their transformation from packaged to deployed status should be 'autonomous and reliable' (Pellegrino, 2001, p1).

### 2.4.1 Common Forms Of Deployable Structures.

The breadth and range of deployable structures forms and methods of deployment is an ongoing area of research and could form the basis of a thesis in itself, this section intends to demonstrate some common forms of deployable structure and introduce the concepts of how the motion can be induced with the integration of certain forms of connection and controlling the degrees of freedom available within the structure.

Deployable structures are everywhere within our everyday lives (You, 2007), from simple telescopic radio aerials on cars to ironing boards that expand and then fold away to allow for convenient storage, their influence on the modern world is subtle but pervasive. Equally, the breadth and scale of deployable structures are broad: ranging from miniature stents used to maintain open flow in veins and arteries (Kuribayashi et al., 2006) through to large deployable dome structures (De Temmerman, Alegria Mira, & Vergauwen, 2012). The fundamental drivers behind deployable structures remain the same regardless of scale, changing size from a small and compact form to a larger yet equally stable form through a controlled and predictable path whilst protecting the structure from potential vulnerabilities during this temporary transitional stage.

For this reason, many deployable structures are designed to harness a single degree of freedom to reduce the complexity not only of the analysis but equally for the construction of the structures. There are of course exceptions, with the deployment process for multi-degree of freedom deployable structures having been researched by Fenci and Currie (2017b), showing how the forces can be minimised during deployment which in turn can help reduce the capital cost of the structure as well as the energy required to deploy.

### 2.4.2 Classifications Of Deployable Structure.

There are a wide range of different forms of deployable structures, with attempts at classification of their varying families being proposed by several researchers with a high-level overview being undertaken in the review paper co-authored by the author of this work (Fenci & Currie, 2017a).

This section intends to present an introduction of the general types of deployable structure and to establish a common language regarding the structural forms, not to rehash the work contained within the above review paper which has been integrated within other previously examined University of Salford postgraduate research.

The earliest recorded attempt at classifying deployable structures began with Merchan (1987) who in their master's thesis submitted on Deployable Structures to MIT set out a basic outline for a fundamental distinction between two high-level groups as ***Strut Structures*** and ***Surface Structures***. This initial sub-division of deployable structures into two high level families is helpful and also important in setting the tone for future work on deployable structures, whilst at this point strut structures were quite common and drew upon existing knowledge associated with linkages and mechanisms, the development of surface structures such as tensile fabric was still developing.

Chronologically the next published work with regards classifying deployable structures is Gantes (2001) whose work largely focuses on linkage based structures (You & Pellegrino, 1997), including pantographs (see Figure 2-4), and follows a different path focussing largely on the distinction between terrestrial and extra-terrestrial applications of deployable structures. This focus on application of the structures is telling because the key difference here is that for extra-terrestrial structures, the effects of self-weight and wind loadings can be completely ignored which is convenient for those assessing it purely from a kinematic perspective.

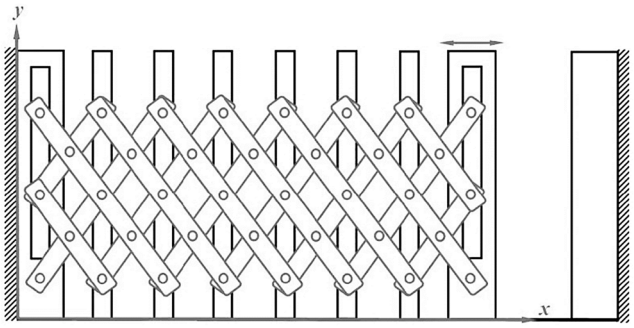


*Figure 2-4 - Pantographic Gate.*[3]

Pellegrino (2001) has a long-standing pedigree in the field of deployable structures, spending a considerable amount of time at Cambridge University after founding their Deployable Structures Laboratory through his research in the field.

Pellegrino's work is wide and varied, but he has spent a significant part of his career investigating pantographs which are defined by their stiff elements being connected with free pins at the ends and near the midpoint and also known as Scissor Like Elements or SLE's (Kwan & Pellegrino, 1991; Tan & Pellegrino, 2008) as well as tensegrity prisms (Tibert & Pellegrino, 2003) with their discontinuous struts linked by a continuous cable system, both concerning their analysis (Pellegrino, 1990, 1993; Pellegrino & Calladine, 1986) and their optimisation (Bel Hadj Ali, Rhode-Barbarigos, & Smith, 2011; Tibert & Pellegrino, 2003). See Figure 2-5 for examples of tensegrity prisms in use.

Whereas most researchers in the field of deployable structures tend to pick a specific family to devote their time and effort towards, Pellegrino is unusual to have such breadth across the many different forms and types of deployable structure. It is perhaps this breadth that gives additional credibility to his classification of deployable structures although it should be noted that it is several decades old now and various new forms have emerged since.

[3] Zhao, J.-S., Chu, F., & Feng, Z.-J. (2009). The mechanism theory and application of deployable structures based on SLE. *Mechanism and Machine Theory, 44*(2), 324-335. doi:10.1016/j.mechmachtheory.2008.03.014

*Figure 2-5 - 3 Strut Tensegrity Prism Supporting Structure.*[4]

Some of Pellegrino's earlier work in flexible tape hinges (Seffen, You, & Pellegrino, 2000) has analogies to rotational springs and these have been developed further in his research to include fabric (Yee & Pellegrino, 2005). His more recent work aligns with the folding of sheets and springs to create compliant mechanisms (Santer & Pellegrino, 2008) for his work undertaken with NASA. Whilst the origami patterns for this research are developed for thin and flexible materials, they may be useful when considering combining them with thicker materials with rigid stiff panels being inter-connected with a flexible filler material to form the valley and creases of the origami fold.

The design of folding sheets with flexible hinges is an area of developing research particularly concerning adaptable structures that make use of flexibility at the hinges for extra-terrestrial applications, see Figure 2-6. Whilst these hinges are not explicitly springs, they demonstrate the

[4] Zhang, J. Y., & Ohsaki, M. (2015). *Tensegrity Structures: Form, Stability, and Symmetry*. London: Springer.

potential for spring-like behaviour by having a rotational stiffness that is recoverable once the load is removed.

The stiffer strut like elements interconnected by the flexible hinges can be differentiated from the SLE's and other linkages considered thus far in that typically SLE's and linkages are formed using free pins whereas the flexible hinges generate a rotational stiffness which could be designed to offer an intermediate stabilising effect that is absent from the traditional free pins used in linkages either during deployment or under extreme loading events.

*Figure 2-6 - CFRP Hinge Boom Hinge for Extra-Terrestrial Applications.*[5]

Given Pellegrino's (2001) extensive research on a wide range of deployable structures, serious consideration should be given to his attempt at classifying deployable structures which can be summarised into the following high-level families:

- Coiled Rods
- Flexible Shells
- Membranes
- Structural Mechanism (Rigid Links)
- Tension Truss Antenna
- Rigid Panel Structure
- Retractable Dome

Not all of the forms on the above list would be necessarily be compatible with the introduction of an additional rotational spring. For example, flexible shells already have an element of flexibility within them that may not be compatible with an additional spring that may be stiffer than the flexible shell element. This initial list, however, has developed and progressed over the years as a combination of new researchers, new methods of analysis, and new materials have

[5] Yee, J. C. H., & Pellegrino, S. (2005). Folding of woven composite structures. *Composites Part A: Applied Science and Manufacturing, 36*(2), 273-278. doi:10.1016/j.compositesa.2004.06.017

been developed.

Building on Pellegrino's list of deployable structures, Hanaor and Levy (2001) expanded the groupings and developed the first tabular representation of different deployable structures, see Figure 2-7. This graphical representation of deployable structures specifically divides deployable structures into distinct groupings and is still widely referenced within deployable structures research, with over 100 citations as of the time of writing this thesis.

Hanaor and Levy's sub-division of deployable structures into two high-level families, rigid links and deformable, is helpful when identifying potential structures that may benefit from the inclusion of a rotational spring. The deployable structures classed as pantographic, bars, and plates all make use of articulated joints formed from free pins or revolute hinged planes that could be modified to be replaced with rotational springs. However, it should be noted that not all of the proposed forms that fit within these high-level families would necessarily be compatible with the integration of rotational springs. For example, reciprocal frames typically deploy in a circular motion, with the deploying motion generally being in an orthogonal axis to the load bearing axis. Thus, including a spring in the deployment axis will be unlikely to impact on the in-service performance of the frame. However, the replacement of the pinned connections in a reciprocal frame with a rotational spring aligned in the direction of load application and that can resist vertical shear may present a clear benefit in the case of accidental damage of an element when considering disproportionate collapse by forming alternative load paths through increased structural redundancy. Ordinarily if an element in a reciprocal frame is damaged it will collapse due to lack of structural redundancy, but if each free pin was able to develop a small additional moment as the result of a spring it could maintain an element of stability until it could be repaired. Whilst a moment connection could generate this behaviour, the spring could differ by maintaining a pinned behaviour in the general condition and having a spring that only activates once a specific angle is rotated through thus developing motion specific behaviour.

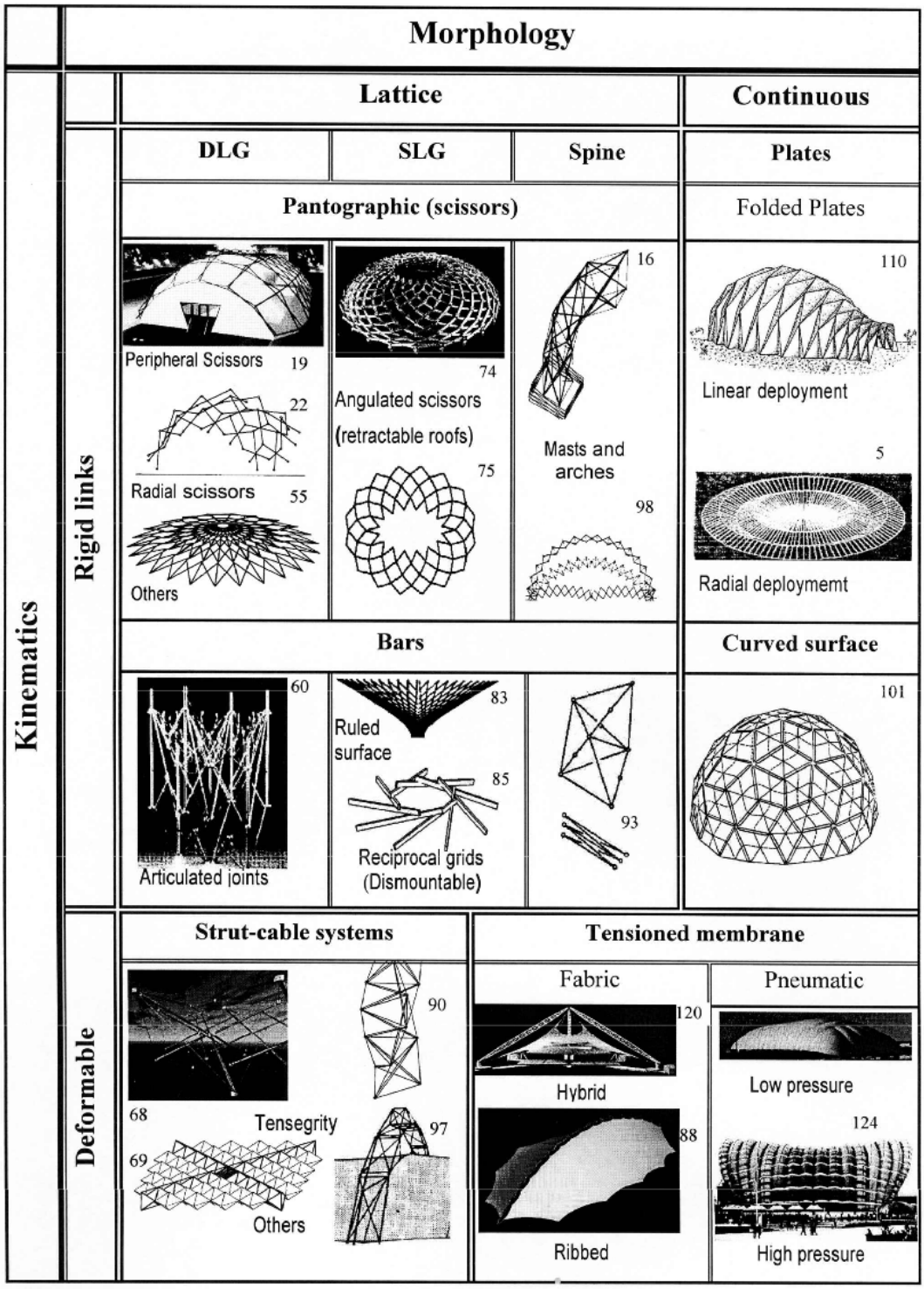


*Figure 2-7 - Hanaor & Levy Proposed Deployable Structures Classification.*[6]

[6] Hanaor, A., & Levy, R. (2001). Evaluation of deployable structures for space enclosures. *International Journal of Space Structures, 16*(4), 211-229.

Hanaor and Levy's early distinction between rigid link structures: such as pantographs, and deformable elements, such as cables and fabric, present a key distinction between the structural behaviour of different types of deployable and metamorphic structural forms used during this period. At this point, tensile fabric structures were used widely for concerts and festivals due to their relatively lightweight nature, the capacity to span large distances, and ability to fold up into compact shapes for storage when stowed away. One example of a retractable roof the author played a small part in was the design of the Rothenbaum arena (see Figure 2-8) where flexible elements in terms of the interwoven cable network support the basket where the fabric covering the roof folds to were developed using dynamic relaxation and form-finding techniques. The design of complex structures such as this, however, would not be compatible with the introduction of rotational springs given the inherent flexibility associated with the fabric roof (Wakefield, 1999) which is designed to be opened and closed to suit the weather conditions to ensure continued play on the tennis courts.

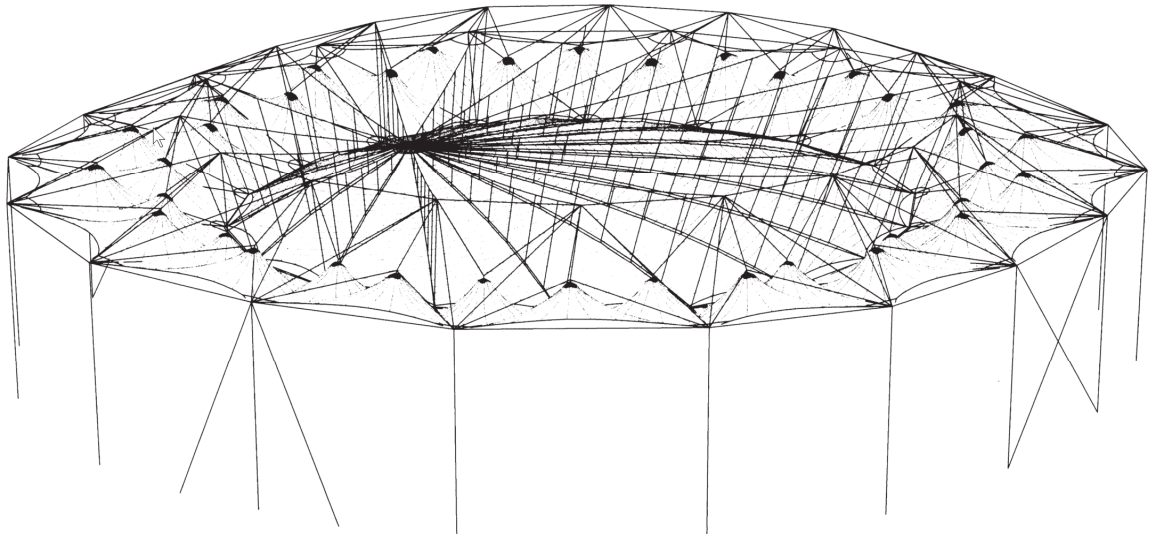

*Figure 2-8 - InTens Analysis and Patterning Model for Deployable Roof at Rothenbaum.*[7]

The next classification of deployable structures was taken by Korkmaz (2004) as part of their PhD thesis. Korkmaz reviewed deployable structures from the perspective of kinetic architecture with types of deployable structure being subdivided more from an architectural perspective. This narrower perspective affected the choice of splitting kinetic architecture into

[7] Wakefield, D. (1999). Engineering analysis of tension structures: theory and practice. *Engineering Structures, 21*(8), 680-690.

two distinct areas that were different from previous assessments: buildings that can change their geometry and buildings that can change their location through mobility. This classification, however, is not helpful with regards deployable structures as typically deployable structures do not self-relocate and Korkmaz's work does not drill down into the structural detail of other classification attempts and so will not be considered any further.

The classification undertaken by Stevenson (2011), has created a detailed classification of deployable structures (see Figure 2-9) which is heavily influenced by her background in architecture and structural morphology yet does not suffer the same short-comings of Korkmaz.

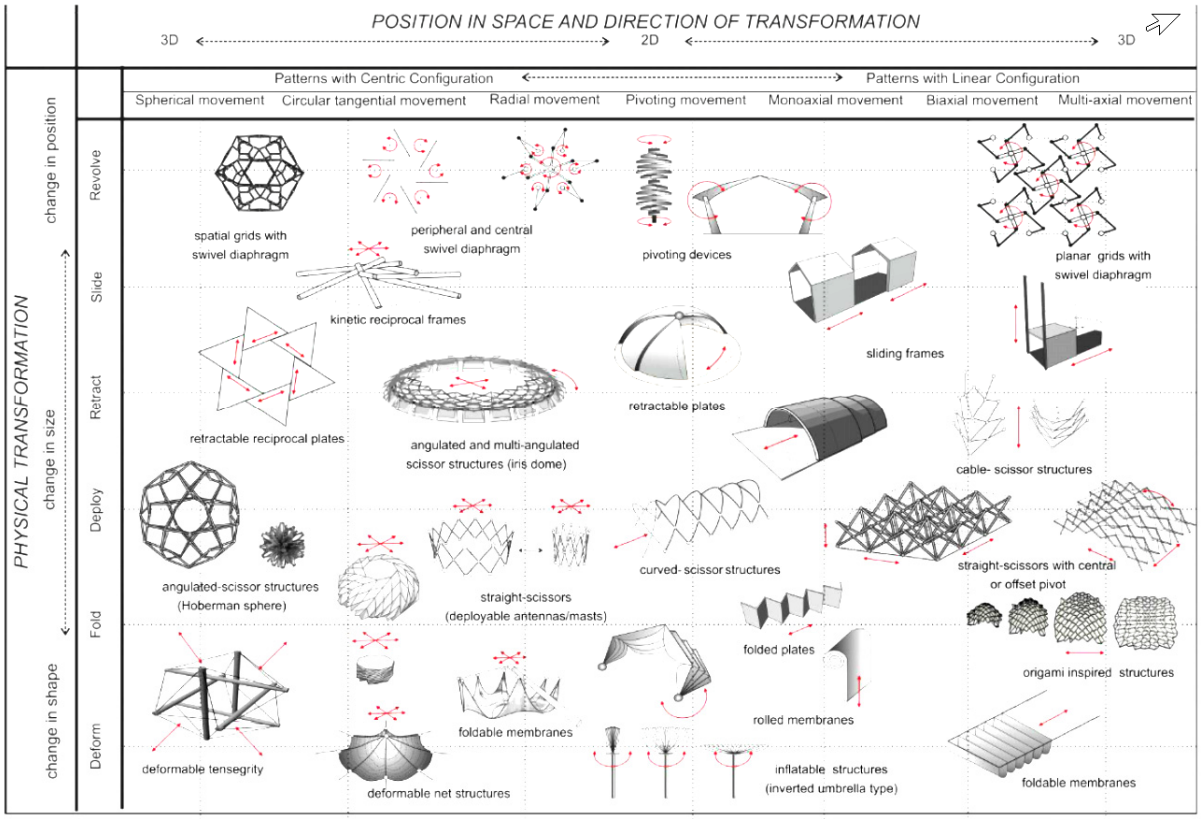


*Figure 2-9 - Stevenson Classification of Deployable Structures.*[8]

Stevenson's classification takes a different approach for the groupings, focussing on the type of motion (folding, deforming, deploying, retracting, sliding, and revolving) rather than the underlying structural behaviour or precise kinematic mechanism type. This categorisation

[8] Stevenson, C. (2011). *Morphological Principles: Current Kinetic Architectural Structures*. Paper presented at the International Adaptive Architecture Conference, Building Centre, London.

contains many of the same forms of deployable structures from previous classification attempts but is the first classification paper that introduces a third type of behaviour other than the well-established rigid and deformable components: smart materials.

Whilst Stevenson's paper does not explicitly include the smart materials in the classification table, it is discussed within the paper as a new development and it is not clear why smart materials were not included within the classification table. The evidence of smart-materials starting to make an appearance within the field of deployable structures is interesting, whilst smart-materials are often activated in response environmental changes, such as temperature, it would initially appear to have little in common with a sprung structure. However, as a concept, springs could potentially be used to increase the flexibility of a structure so that it changes shape in response to an external environmental stimulus such as a wind loading. Whilst the smart materials proposed by Stevenson and also the introduction of springs are both passive controls, recent work by Senatore, Duffour, Hanna, Labbé, and Winslow (2011) has begun to introduce the aspects of smart materials creating actively controlled variable stiffness hinges (Senatore, Duffour, & Winslow, 2018a) these hinges are still being actively developed and if concluded may influence future classifications.

Building on their earlier work with regards adaptive facades Del Grosso and Basso (2010) developed an outline classification (Del Grosso & Basso, 2013) based on the work of Hanaor and Levy (2001) but with the important addition of compliant mechanisms (see Figure 2-10) and morphing truss structures. Compliant mechanisms are becoming particularly pertinent with regards to adaptive structures (Knippers, Nickel, & Speck, 2016) such as those used in active facades. Compliant mechanisms are typically formed from relatively flexible elements such as uniform thickness slender ribbons made from polymers. The direct integration of rotational springs for these forms of structure could prove challenging as they are already inherently flexible. However, compliant mechanisms have an interesting behavioural trait in that they repeatedly switch between dual states when they are manipulated at the end conditions. As an alternative it is proposed that a series of rigid links could be interconnected with rotational springs of varying stiffnesses that could passively mimic the behaviour of a compliant mechanism but with an added benefit that through tailoring spring stiffnesses more complex shapes may be able to developed in comparison to a uniformly thick homogenous ribbon.

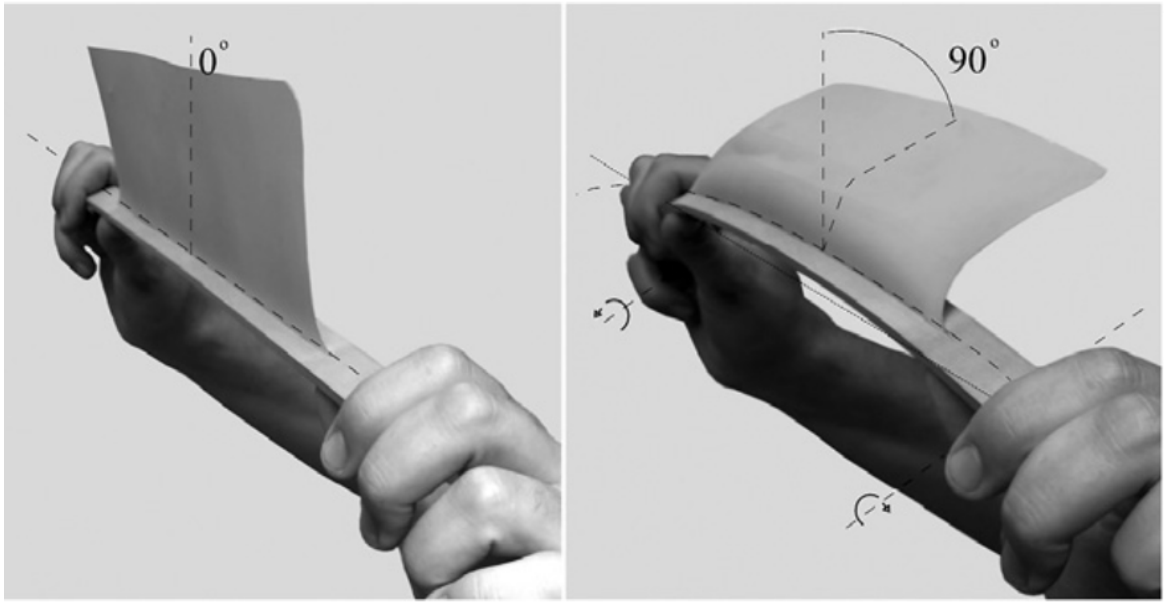


*Figure 2-10 - Compliant Mechanism of Prototype of Flectofin.*[9]

This principle of subdividing a chain of stiff elements with a series of rotational springs is already complex due to the non-linear behaviour of the springs, but the development of a sheet that can flex and snap into new shapes such as those shown in Figure 2-10 would present serious technical challenges in forming the springs. Instead, veins of more flexible material could perhaps be introduced to create predetermined creases through the surface where articulation could occur. If highly elastic materials were used for the formation of these veins, then this may present similar behaviour to that of a rotational spring although likely with a non-linear rotational stiffness.

The most recent published classification attempt is by Adrover (2015) and whilst it has not been peer-reviewed it holds up well to scrutiny when contrasted back to its predecessors. Adrover reverts to the similar high-level headers for classification of ***rigid***, ***deformable***, ***flexible*** and ***combined*** (hybrid) and it shares many similarities with Hanaor and Levy (2001), although there are areas where a more specific classification would be beneficial For example, Adrover has chosen to integrate membranes within the folding roofs section but for the examples presented the membrane provides no structural or kinematic benefit, instead purely acting as a cover to

[9] Schleicher, S., Lienhard, J., Poppinga, S., Speck, T., & Knippers, J. (2015). A methodology for transferring principles of plant movements to elastic systems in architecture. *Computer-Aided Design, 60*, 105-117. doi:10.1016/j.cad.2014.01.005

keep the rain off.

The deployable structures review paper by Fenci and Currie (2017a) has a follow on paper that is currently in review, where a new classification is proposed that brings about the above historical summaries and combines and updates them to integrate new developments in the technologies that can affect deployable structures.

Given the change in terminology across the various classification papers, the rest of this literature review will adopt the terminology set out within Figure 2-11 on page 2-24, with both Strut and Surface Structures being divided into four further sub-categories based around rigid components, deformable components, flexible components and hybrid components.

The critical review of the classification papers presented up to this point has been used to narrow down the wide range of potential forms of deployable structures to forms that may benefit from the inclusion of rotational springs. Exchanging free pins for rotational springs is proposed as a logical intervention to explore given the compatibility between the motion types and the following sections of this literature review will focus on the two areas of deployable structures with most relevance to this thesis and for the research being undertaken: Strut Structures with ***Rigid Components*** and with ***Rigid Components combined with Flexible Components***.

Rigid component-based structures typically make use of free pins to interconnect their elements together and the introduction of rotational springs at these free pin locations make for a convenient and logical strategy to determine any benefits resulting from the inclusion of springs. To investigate this further, several forms of strut or link-based deployable structures will be considered. The class of purely strut based deployable structures will be expanded to include certain hybrid structures (rigid components combined with flexible components) such as tensegrities and cable-chain structures. This expansion to include hybrid structures is included as structures that integrate cables often require the development of an initial stable form under their initial cable tensioning regime and a similar process may be required for a sprung structure to find a balanced equilibrium form before the application of external loads.

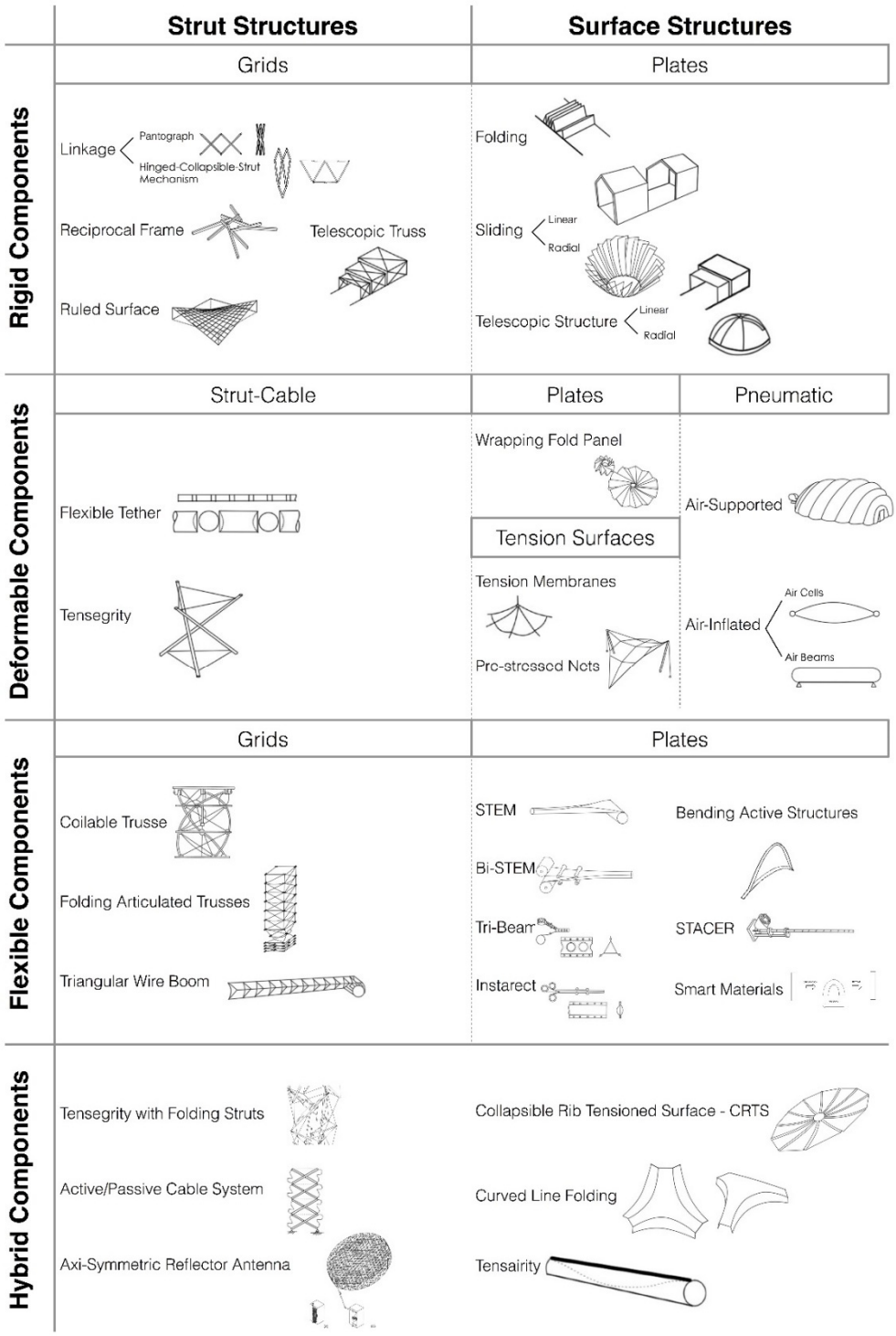


*Figure 2-11 - Proposed Deployable Structures Classification (In Review).*

The classification papers provide an interesting overview of the different families of deployable structures but do not give insight into their general strengths and weaknesses. A transformable structure that can move between the two states of stable (packed or deployed) and unstable (deploying) by its very nature becomes vulnerable to disproportionate collapse due to low

structural redundancy. Planar deployable structures formed from rigid elements (such as pantographs and linkages) are typically formed from either Translational Joints (Planar, Type P) or Rotational Joints (Revolute, Type R) and these forms of joints are covered in greater detail in section 2.7 but it is important to highlight their impact on deployable structures here. Typically to aid with deployment a single restraint is added (to stabilise) to a deployable structure already in motion, or removed (to destabilise) a static deployable structure and this is a common property for many different forms of deployable structure, particularly those based on rigid links.

However, if one of these restraints or a structural element is accidentally damaged and removed from the system, this will create an unintended change in the structural stability and the structure may be become unstable as a result of the low structural redundancy. The free pins which enable the structure to freely articulate need to maintain a minimum configuration to remain stable (see section 2.6 for guidance). It is suggested that these free pins could, in theory, be exchanged wholesale or at key locations for rotational springs within a deployable structure to provide additional redundancy to a deployable structure. This would create alternative load-carrying capacity through the structure which may aid with reducing the vulnerability of disproportionate collapse. Indeed the springs could be placed in the structure to hold the deployable structure in either a permanent position of open or closed which presents a further benefit in that in the instance of loss of pressure for a piston or power for a cable winch the structure can default to a safe position under the action of the springs.

Rotational springs frequently have their springs defined as the moment required to rotate the spring through a specific angle, typically kNm/rad. Therefore, as a structure deploys the angle changes and there will be a subsequent generation of bending moment within the structure that must be resisted. So, whilst the inclusion of rotational springs may initially feel like a positive addition with regards disproportionate collapse it will affect the structural behaviour of the frame and may result in larger (heavier) sections to be designed to resist the additional bending moment. Thus, the greater the number of springs and the stronger the springs, the greater the amount of energy required to transition the structure from between folded and deployed states compared to an equivalent pinned deployable structure.

### 2.4.3 Controlled Instability.

A common criticism of the classification papers above and many of the papers associated with deployable structures is that they often focus purely on the kinematic behaviour of the deployable structure in their folded and deployed stages and neglect the transitional stage.

Deployable structures typically transition between three distinct stages, altering from an initial stable structural form (packed) to the deploying stage which is typically activated through the removal of an external or internal fixity to convert the structure to a mechanism, with the external or external fixity reintroduced at the final deployed state to convert the mechanism back into a stable structure. For a deployable structure to function properly this intermediate transitional stage is just as important as the final deployed position and will influence the design of the structure and it is concerning that this intermediate state is often neglected.

Consider an example of a bridge deploying over a river, the initial packed form may sit on one shore of the river. The deployable bridge may take the form of an idealised beam that could deploy out from the bank and during this initial deployment phase, it would behave as a cantilever with the need for the abutment at the bank to resist the support forces from the cantilever and the bridge itself deflecting like a cantilever with a free tip. Once the bridge has fully deployed then the bridge could gain support from abutments on either side of the river and structurally behave as a simply supported structure. If the bridge had not been designed to consider this intermediate cantilevering stage then the designer may find that the bridge does not perform as intended, with potentially the abutment from where the bridge extends overturning from the reactions of the cantilevered bridge, the different bending moments developed within the bridge during deployment may not be considered in the design resulting in under-sized elements, and the deflections of the bridge whilst it is a cantilever could cause the bridge to deflect so grossly that it is unable to land correctly on the other shore and instead drops down under self-weight deflection and clashes with the abutment.

However, from personal experience with designing metamorphic and articulated facades, it may be that this intermediate stage is often neglected due to environmental controls being in place that prevent the activation of the structure. For example, anemometers limiting when the structure can be deployed and expand in relation to the wind speed, but an assessment should still be undertaken with regards what that maximum wind speed should be and the effects of self-weight during deployment. Indeed, as illustrated with the bridge example above, some structural forms can have completely different structural behaviours between the deploying and the deployed stages. This could be from a change in support conditions, or through effects such as wind reversal on lightweight roofs, but unfortunately for the inexperienced designer, there is little in the available published literature on deployable structures that covers these practical requirements. The concept of maintaining equilibrium will be expanded further in section 2.9 to include cables and other more complex structural elements.

## 2.5 Strut Based Deployable Structures.

The hypothesis within this thesis is that the introduction of springs into structures may bring about positive benefits and from the previous section it is clear that strut based deployable structures rely heavily on free pins to create their deployment mechanism and these same free pins may have potential to be replaced by rotational springs. The free pins are potential locations for the introduction of a rotational spring given that a degree of articulation already exists and thus forms of deployable structures that make use of free pins and rigid struts will be considered in more depth.

Deployable structures based on rigid struts are one of the longest researched areas of deployable structures starting with Piñero's patent in 1961 for his mobile theatre (Del Grosso & Basso, 2013) see Figure 2-12, using infinitely stiff elements in their analysis to develop a load-bearing structure that integrates joints to develop the articulation required to form a deployable structure.

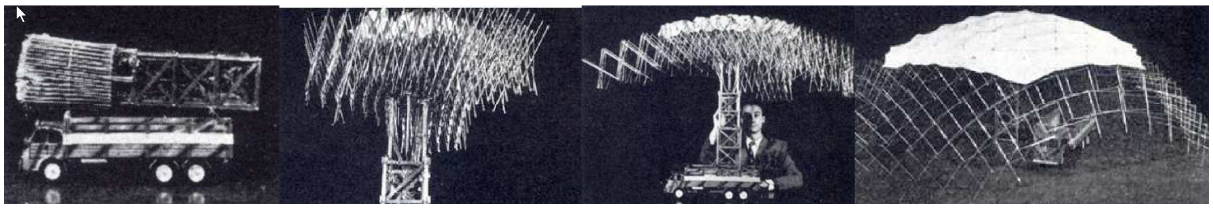

*Figure 2-12 - Piñero's Deployable Theatre Concept.*[10]

The rigid elements may work in compression, tension, or bending: although these types of structures are often configured to remove bending to adhere to the principles of lightweight structures. With the structures being designed using principles adopted from lightweight structures to reduce weight during deployment and to conserve energy it may be that the introduction of rotational springs change this principle because the introduction of a rotational spring will create a bending moment at the point where the spring is located that is in direct proportion to the angle the spring is rotated.

[10] Del Grosso, A. E., & Basso, P. (2013). Deployable structures. *Advances in Science and Technology, 83*, 122-131.

### 2.5.1 Rigid Components.

Linkages have been utilised for centuries with pantographs being employed in a chess-playing automaton (O'Rourke, 2011) known as "The Turk" (Figure 2-13). Invented by Wolfgang von Kemplen in the 18th Century, he travelled the European courts of the day, tricking their attendees that the 'clockwork' automaton could play chess through its own volition, whilst secretly concealing a real person as the chess player within the base.

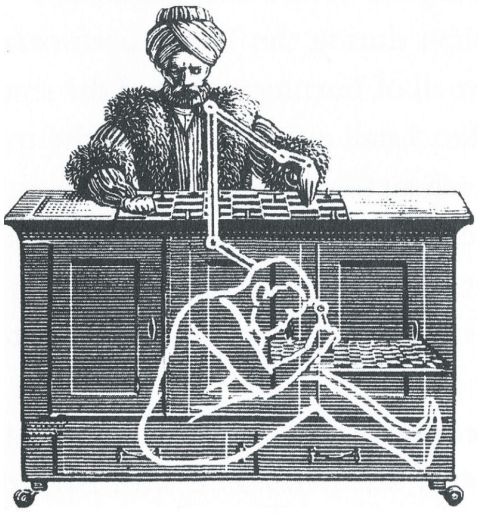

*Figure 2-13 - The Turk Chess Playing Automaton.*[11]

Following the developments of the first industrial revolution, linkages became commonly employed to translate motion from steam engines into useful work in mills and other industrial applications. For example, converting a rotational motion, into linear motion (Demaine & O'Rourke, 2007) as seen in Figure 2-14 where the rotation motion at point y becomes a linear motion at the point $\overline{y}$. Essentially converting the rotation of waterwheels into a linear motion for harnessing within mills and looms. These types of linkages are intended to run in a repeated and continuous cycle, whereas deployable structure often deploy and then play the same motion backwards to retract.

[11] O'Rourke, J. (2011). *How to fold it: The mathematics of linkages, origami and polyhedra* (First ed.). Cambridge: Cambridge University Press.

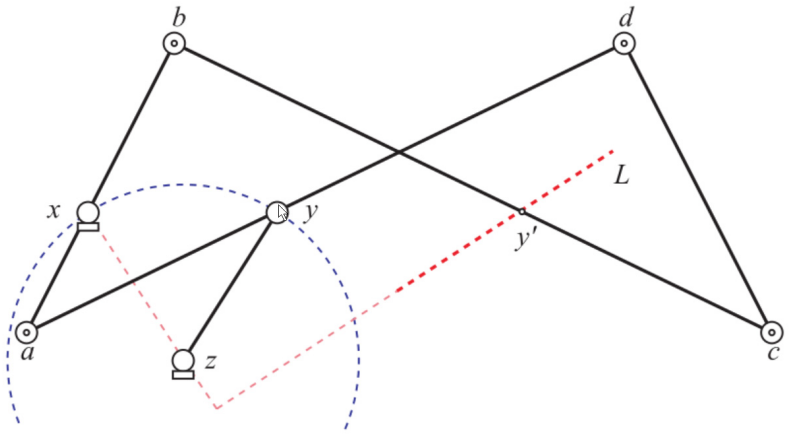


*Figure 2-14 - Hart's Mechanism to Convert Rotational Motion to Linear Motion.*[12]

Linkages have progressed and developed through the centuries, but their principles are inescapably integrated into modern life, for example, the use of deployable structures and robotics. Simple implementations such as those by Hoberman (1990) through his patents that have been used on a wide range of structures ranging from children's toys (Hoberman Sphere) through to the stage at the opening ceremony at Salt Lake City Winter Olympics in 2002 (Brouwer, 2002), see Figure 2-15.


*Figure 2-15 - Hoberman Arch.*[13]

Hoberman spheres are formed using free pins to create scissor like element uniplets that are then inter-linked to create a larger Hoberman structure which can be held in place simply by removing a single degree of freedom, by say connecting to adjacent nodes together once deployed. Once this restraint is removed, however, then the self-weight of the Hoberman sphere will cause the

[12] Demaine, E. D., & O'Rourke, J. (2007). *Geometric Folding Algorithms: Linkages, Origami, Polyhedra*. Cambridge: Cambridge University Press.

[13] Stevenson, C. M. (2011). *Morphological principles: current kinetic architectural structures*. Paper presented at the Adaptive architecture conference. , Building Centre Trust and the University of Nottingham, London.

structure to collapse into the folded position in a violent manner. In practice, this dramatic motion could be overcome through the use of a hydraulic piston controls that control the distance between two or more driving nodes which if they lose pressure would slowly lower the structure into the folded position but this may depend on the speed and nature of the failure of the piston. A more failsafe solution though could be that if a rotational spring was introduced between the scissor elements instead of the free pins then the sphere could be made to close more gently in the event of a complete and instant loss of pressure on the piston or a power cut and this could increase structural safety.

Various combinations of rotational joints are possible to create more complex forms of motion in a single plane to create scaling motion (Kiper, Söylemez, & Kişisel, 2008), such as the use of triangles in a pantographic combination as shown in Figure 2-16.

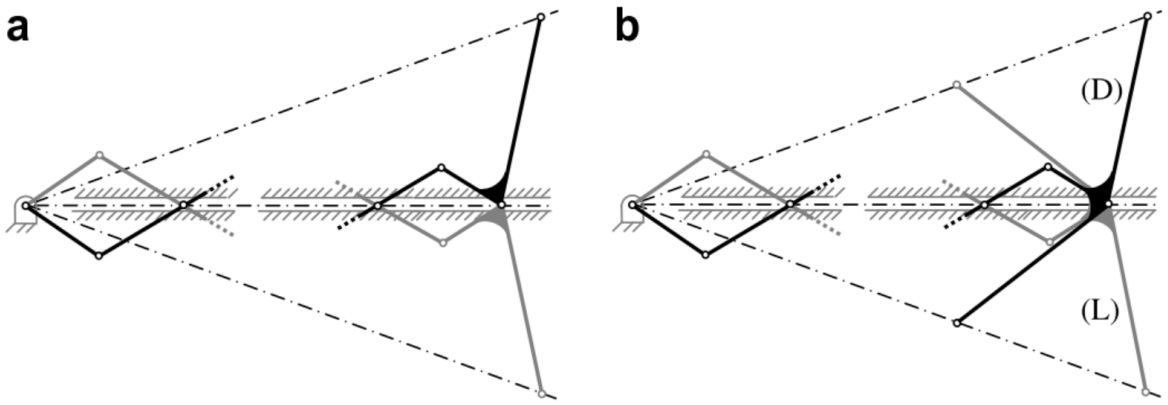


*Figure 2-16 - Scaling of Linear Motion Through Triangles.*[14]

Linkages such as the Bricard Linkages can be configured through the integration of rotation of the hinges and provision of three-fold symmetry (Chen, You, & Tarnai, 2005) to create a single degree freedom linkage. These have been successfully utilised within deployable structures and grillages (Wohlhart, 1993). These forms of linkage present an alternative proposition to pantographs in that they can be configured to act beyond a single flat plane, whilst still only making use of single plane rotational pins. The exchange of the free pins for a rotational spring could alter the behaviour of the Bricard linkage to become self-stabilising as it is formed as a

[14] Kiper, G., Söylemez, E., & Kişisel, A. U. Ö. (2008). A family of deployable polygons and polyhedra. *Mechanism and Machine Theory, 43*(5), 627-640. doi:10.1016/j.mechmachtheory.2007.04.011

closed loop, although clearly the springs must be able to resist the self-weight.

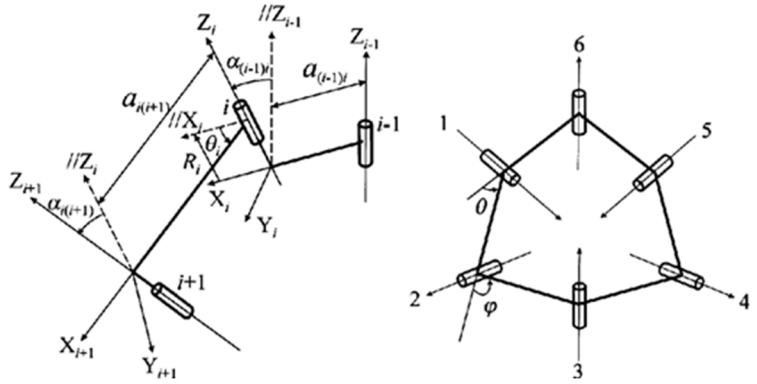


*Figure 2-17 - Threefold Symmetrical Bricard Linkage.*[15]

Bricard linkages (see Figure 2-17) were developed and discovered as planar linkages in 1897 but remain an active area of research through the integration of spherical joints to develop controlled deployments in 3 dimensions (J. Wang & Kong, 2018). Spherical joints are typically formed using ball and socket configurations, like the sockets in the human hip. Whilst 2D planar rotational springs can be purchased readily for small scale structures, true spherical springs with complete freedom comparable to a spherical joint are considerably more specialist and are almost impossible to source. Whilst rotational springs of a larger capacity may be challenging to procure, there are options as covered later in section 5.10, however the same is not true for spherical springs and consequently they will not be considered within this thesis.

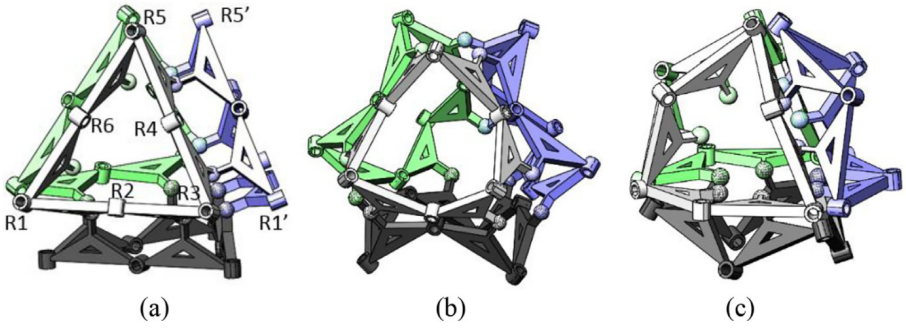


*Figure 2-18 - Tetrahedron LCM based on orthogonal Bricard linkages: (a) initial posture; (b) outward deploying; (c) inward deploying.*[16]

[15] Chen, Y., You, Z., & Tarnai, T. (2005). Threefold-symmetric Bricard linkages for deployable structures. *International Journal of Solids and Structures, 42*(8), 2287-2301. doi:DOI: 10.1016/j.ijsolstr.2004.09.014

[16] Wang, J., & Kong, X. (2018). Deployable mechanisms constructed by connecting orthogonal Bricard linkages, 8R or 10R single-loop linkages using S joints. *Mechanism and Machine Theory, 120*, 178-191.

Much of the research undertaken on the manipulation of mechanisms and the associated degrees of freedom assumes that the joints are perfect and frictionless and concentrate on the kinematic aspects.

Whilst these frictionless models may help determine the initial driving forces and torques required to open the mechanism (Yavin, 1998) and may be of initial interest to practising engineers, the long term degradation through wear, lack of fit, and tolerances cannot be escaped when placing these linkages into practical situations and so these additional effect should be considered. The specific consideration of the forces during deployment has been highlighted as an under-researched area within section 2.4.3, but the energy required to operate a partially seized linkage may alter the structural behaviour where pins are unable to operate freely and start to generate moments that are fed back through to the structural elements. It has been shown that the sequence of deployment for multi-degree of freedom deployable structures can grossly affect the forces required in the hydraulic rams used to deploy certain deployable structure forms (Fenci & Currie, 2017b) and so even the sequence of deployment should be ascertained by the designer. As structures begin to become less static (i.e. material dependent to achieve their stiffness) and increasingly gain their rigidity through the integration of actuators (i.e. energy-dependent to achieve their stiffness) the assessment of embedded and operational energy will become increasingly complicated and yet more important to determine their environmental impact (Senatore et al., 2018a).

Thus far, the majority of linkages considered have been constrained to having their free pin located at the ends of their discrete elements, however, some linkages have self-crossing struts. These linkages are often classified as pantographs (A Kaveh, Jafarvand, & Barkhordari, 1999) and also known as Scissor Like Elements (SLE) (Akgün, Gantes, Kalochairetis, & Kiper, 2010). As illustrated previously with the "The Turk" automaton the pantographic linkage has been widely used for centuries. In everyday life, this is active and most obvious with the connector linkage on electric trains which maintain an even connection with overhead wires, but it is also implemented on mechanisms found within car windscreen wipers.

Early investigations into the potential of pantographs for deployable structures was pioneered by Piñero in 1961 with his proposal for a mobile theatre that leads to Piñero's (1965) patent, with later developments of 3D grillages being developed through the work of Escrig (1984; 1993; Valcárcel & Escrig, 1996).

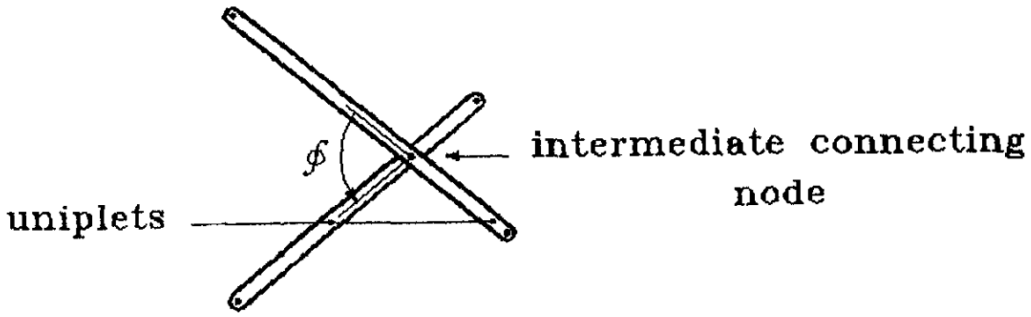


*Figure 2-19 - Typical Pantographic Uniplet.*[17]

Single uniplets, as shown in Figure 2-19 can be combined to create complex planar structures such as masts (Nagaraj, Pandiyan, & Ghosal, 2010), arches (Akgün et al., 2010; Gantes & Konitopoulou, 2004), or 3-dimensional grillages such as domes (Gantes, Connor, Logcher, & Rosenfeld, 1989) to create deployable structures with a single degree of freedom. These uniplets are not stable without receiving additional restraint from external supports to hold them in position, as a simple analogy considering holding a pair of scissors by only one handle as this allows the remaining blade to swing freely. Typically if two ends are connected together on a uniplet then this will form a triangle which is capable of providing the required restraint to lock the uniplet in a specific position, see section 2.9.1 for more detailed examples.

The change from a linearly deploying pantograph to one that follows a curved path is adjusted simply by ensuring that the central pin is moved from being located equidistant (for a linear translational deployment) to a non-symmetrical internal pin location (for a curved deployment) which is also known as a polar arranged SLE (Alegria Mira, Thrall, & De Temmerman, 2014) as shown in Figure 2-20.

[17] Kaveh, A., & Davaran, A. (1996). Analysis of pantograph foldable structures. *Computers & Structures, 59*(1), 131-140. doi:10.1016/0045-7949(95)00231-6

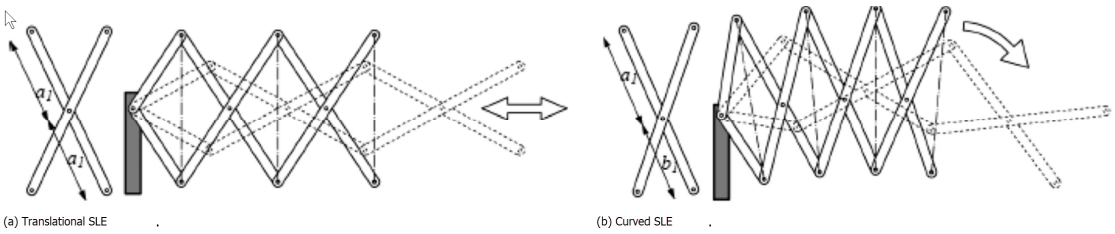


*Figure 2-20 – (a) Linear Translational SLE (b) Curved SLE.*[18]

The deployment of pantographic structures results in highly non-linear behaviour (Gantes et al., 1989) as the structure is sensitive to geometrical imperfections or friction within the hinges (Gantes, Connor, & Logcher, 1993). These non-linear behaviours can have a dramatic effect on the structural behaviour and the ability of the structures to deploy as intended, with seized hinges capable of generating additional bending moments within the elements at the tips.

Through combining linear pantographs in two planes, grillages are easily formed that can be utilised to create a flat surface (A. Kaveh & Davaran, 1996; J.-S. Zhao, Feng, Chu, & Ma, 2014) or a cylindrical surface as shown in Figure 2-21.

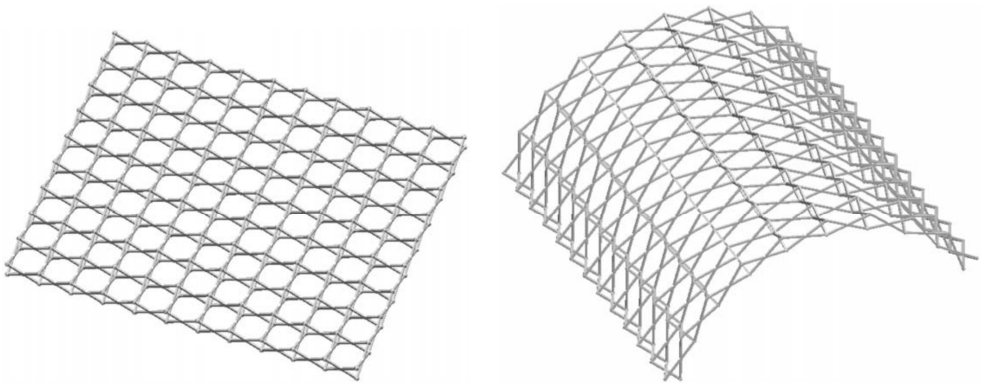

Left: Flat Deployable Structure Right: Cylindrical Deployable Structure

*Figure 2-21 - Flat Deployable Pantographic Roof.*[19]

This principle can be further extended where the use of modified SLE's (Akgün et al., 2010; Cai, Deng, Feng, & Xu, 2014) are integrated to create non-uniform curvatures and paths as seen in

[18] Zhao, J., Feng, Z., Chu, F., & Ma, N. (2014). Chapter 11 - Mechanism Theory and Application of Deployable Structures Based on Scissor-Like Elements. In J. Zhao, Z. Feng, F. Chu, & N. Ma (Eds.), *Advanced Theory of Constraint and Motion Analysis for Robot Mechanisms* (pp. 349-366). Oxford: Academic Press.

[19] Zhao, J.-S., Chu, F., & Feng, Z.-J. (2009). The mechanism theory and application of deployable structures based on SLE. *Mechanism and Machine Theory, 44*(2), 324-335. doi:10.1016/j.mechmachtheory.2008.03.014

the hinged arches of Akgün, Gantes, Sobek, Korkmaz, and Kalochairetis (2011) shown in Figure 2-22. The change in curvature at these points is entirely from the change in shape of the individual uniplet as all of the connections are modelled as a free pin, if the pins were exchanged for rotational springs then geometrically the arch would form the same shape, but with increased and additional bending moments at the positions where the angle of rotation is larger due to the uniplet geometry.

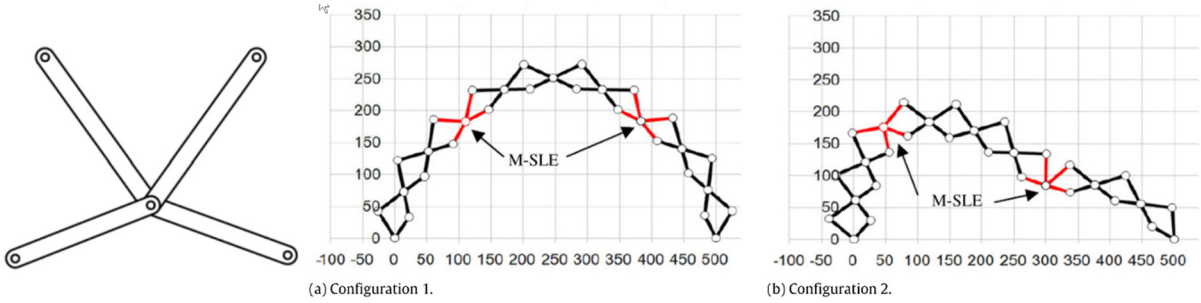


*Figure 2-22 - Modified Scissor Like Elements Adjusting the Shape of a Deployed Arch.*[20]

As evidenced in Figure 2-22 the angle of the units in a uniplet can be set to be different to the angle of adjacent uniplets to create kinks or refine curvatures, however, not all geometries are compatible by default and care should be taken to ensure that there is geometrical compatibility between the uniplets otherwise this may cause the structure to lock and be unable to deploy.

### 2.5.2 Rigid Combined With Flexible Components.

The inclusion of flexible components such as a cable or membrane within a deployable structure is often able to aid with weight reduction and to create specific geometries and control strategies within a deployable structure. However, flexible components are only able to resist tension and have no compressive or bending capacity whatsoever which can bring about challenges. Equally, these deformable and flexible elements have their own practical detailing strategies and issues such as long-term creep and stretching of the flexible elements can also bring about concerns with regards the performance if not designed appropriately.

Deformable components with regards to deployable structures are essentially either cables or membranes that have been employed in such a fashion to generate a stable yet deployable

[20] Akgün, Y., Gantes, C. J., Sobek, W., Korkmaz, K., & Kalochairetis, K. (2011). A novel adaptive spatial scissor-hinge structural mechanism for convertible roofs. *Engineering Structures, 33*(4), 1365-1376. doi:10.1016/j.engstruct.2011.01.014

structure.

For example, a flexible tether structure is proposed by Rauschenbach (2012) as an extra-terrestrial boom that can be folded to allow it to be stowed during launch. The structure is a chain of segments with a central tendon passing through each of the segments, similar to vertebrae with the spinal cord passing through each bone. The end segment has the flexible tether anchored into it and the end connected to the ship is pulled taut to create a rigid element when required, see Figure 2-23.

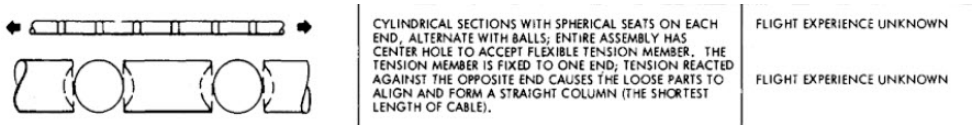


*Figure 2-23 - Flexible Tether Prototype.*[21]

It is the tension only element threaded between the segments which allow the boom to develop rigidity, with the extra-terrestrial deployment allowing the effects of self-weight to be neglected. It is presumed that Rauschenbach intended for the boom to be relatively rigid as part of its deployment which will be influenced by the level of pretension and the tendon material, the selection of tendon material type does raise an interesting question. For example, if a steel wire was selected, the level of pretension that could be developed could be quite high and would create a comparatively rigid strut, but on the other hand, if a highly elastic material was selected the boom would be able to displace under any loading but snap back into a deployed shape once the load is removed with behaviour not too dissimilar to that of a spring.

Whilst the flexible tether outlined by Rauschenbach (2012) would infer only a straight linear boom can be created, some parallels can be drawn through the work of Beatini and Royer-Carfagni (2013) where the use of profiled voussoirs and eccentric tendon profiles are integrated to enable alternative shaped booms to be developed, see Figure 2-24.

[21] Rauschenbach, H. S. (2012). *Solar cell array design handbook: the principles and technology of photovoltaic energy conversion.* London: New York: Von Nostrand Reinhold Company.

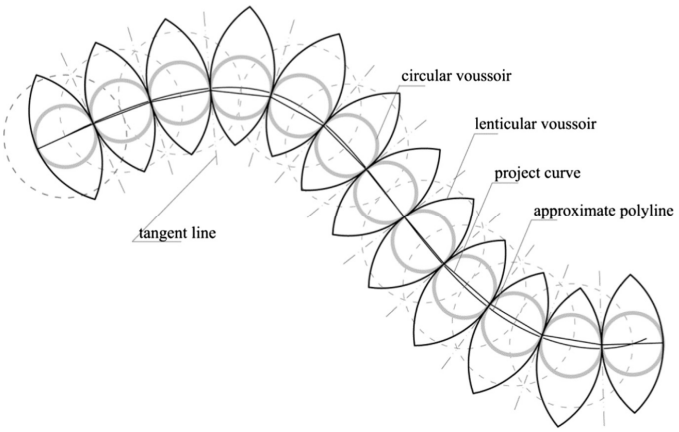


*Figure 2-24 - Curved Cable Stiffened-Elastica with Lenticular Voussoirs.*[22]

Whilst, the cable-stiffened elastica of Beatini are not specifically intended to be deployable, rather it is intended to be a foldable chain of segments, they inevitably present the potential to be deployable and have much in common with the flexible-tether system of Rauschenbach. If carefully designed they would be able to deploy and still vary their rigidity based on the level of pretension developed by the tendon and could have their behaviour further modified with the inclusion of compressible filler between the voussoirs. The arrangement of the tendon and the infill between the voussoirs can create a structure analogous to the human spine with the spinal cord (tendon), vertebra (voussoirs), plus this time additional discs (compressible filler) that may alter the damping and stiffness of the hinges. Even with no infill, the engineering of a highly elastic tendon rather than steel could enable a more flexible curve that would be able to vary its shape under loading. The similarities to the stiffening effects of the tendon in both of the structures considered in this section present similarities to post-tensioned concrete design with the cable imparting an element of interlocking on the elements, the difference though is each segment remains independent and can be unthreaded from the tendon in the structures of Beatini and Rauschenbach. However, there will be similar issues to consider such as duct friction and loss of pre-tension through stretch in the tendons.

A cable lacks any real rigidity without having an anchor point to pull upon or some form of axial rigidity to be combined with, such as a firm anchor point for a cable-net roof or rigid compression struts in tensegrity prisms. But when integrated with a suitably defined system they

[22] Beatini, V., & Royer-Carfagni, G. (2013). Cable-stiffened foldable elastica for movable structures. *Engineering Structures, 56*, 126-136.

can support considerable loads and span large distances with relatively little material. For example, the London Olympics Velodrome roof which has a span of 131m in the longest direction and 119m in the narrowest and is formed by pairs of 36mm spiral strand cables at 3.6m centres pulling against trusses placed around the perimeter, presenting a very shallow structural depth and low self-weight for such a large span. It is the combination of cables and struts however that present opportunities for deployable structures through reduction in structural weight and ease of destabilising for packing/deploying. With either the struts being formed as telescopic elements that can change their overall length to amend the amount of pretension in the structure, or where the cables are pulled taut through the use of motors to aid with deployment or retraction. With each method presenting a different set of challenges. If a strut changes the length to enable folding, this develops the risk of the cables becoming tangled much like a set of Christmas tree lights and then not unfolding neatly on the next deployment, equally though if the structure is controlled through the adjustment of the cable lengths, this can often require large spools for the cables to be wound onto which can increase the complexity and depth of structure needed at the winding positions.

Cable-strut structures with respect to deployable structures may be configured to be self-stabilising through their integration into various forms of tensegrity systems (Motro, 1992), in particular prism-like structures such as icosahedrons or any of the more general platonic polyhedral forms (Chilton, 2000, pp16), see Figure 2-25.

The inventor of tensegrity structures is largely debated but generally agreed to be Snelson (1996) although some of Buckminster Fuller's (Calladine, 1978; B.-B. Wang, 1998) earlier creations adopted tensegrity principles he was not responsible for explicitly naming these systems within his work.

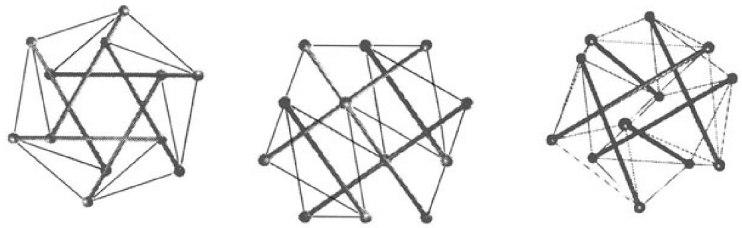

*Figure 2-25 - Six Strut Tensegrity Prisms Based on Icosahedrons.*[23]

[23] Pellegrino, S. (2001). *Deployable Structures* (First ed. Vol. 412). Udine: Springer Wein NewYork. p209

Tensegrity structures take their name from the combination of the words tension and integrity, illustrating that the closed tensioning system is fundamental to these forms of structure developing their stability. Often tensegrity structures are closed systems that are stable regardless of how they are supported by the ground, yet they retain minimal structural redundancy with the loss of a single cable or strut often causing catastrophic failure. The inclusion of cable elements require a geometrical non-linear analysis to be undertaken when assessing their structural performance (Pellegrino, 1990), but for larger tensegrity systems the cables require the introduction of an appreciable level of pretension to stabilise the structure even under self-weight. Whilst cables are the norm for the tension elements within tensegrity structures, alternative elements can be used providing that they are tension only elements with viable tensegrity prisms being formed with the use of fabric panels in lieu of cables (Peña, Llorens, Sastre, Crespo, & Martínez, 2011).

For a structure to be defined as a classical tensegrity structure the compression elements should be fully discontinuous, giving the impression that they are floating, although several forms of tensegrity structure break this rule (Frumar, Zhou, Xie, & Burry, 2009) and have struts in contact with each other. However, all tensegrity structures make use of self-stress states (Maurin, Motro, Raducanu, & Pauli, 2005).

As the rigidity and behaviour of a tensegrity structure are highly dependent on the self-stress state (Bel Hadj Ali, Rhode-Barbarigos, Pascual Albi, & Smith, 2010), this provides exciting opportunities for structures to be tuned to change their dynamic responses and natural frequencies (Bel Hadj Ali & Smith, 2010). As outlined with Beatini's elastica, the exchange of a relatively stiff cable for a highly elastic tension element can create an element of controlled flexibility to the entire structure and indeed this is the basis for several children's toys inspired by icosahedron tensegrity prisms.

There are three common strategies utilised for changing the rigidity of a tensegrity prism, either through directly changing the force within the cables, through indirectly changing the length of the cables by replacing the struts with actuators see Figure 2-26 (Moored & Bart-Smith, 2009), or changing the cables to a material that is highly elastic although this can sometimes result in the prism collapsing under load but, if the material is adequately elastic, it can often recover once the load is removed.

*Figure 2-26 - Tensegrity Facade with Actuators.*[24]

Most tensegrity prisms make use of at least a nominal pretension to hold the structural elements in place and to create a stable structure. Inexperienced engineers are often tempted to increase the pretension excessively to prevent the prism deflecting, but this can result in either oversized compression members to resist the associated increase in compression force from the pretension or huge foundations to act as anchor blocks to resist the pull from the connecting cables.

Determining the initial self-stabilised condition (Williamson, Skelton, & Han, 2003) of a tensegrity structure frequently requires the adoption of form-finding techniques to determine the initial equilibrium state and starting geometry. For example, the author has spent several years designing lightweight and tensegrity systems whilst working at TENSYS with a typical workflow using dynamic relaxation on the inTENS software being:

- Generate the topology, define the connectivity.
- Generate the form, define the boundary conditions and stress system that develops the intended form.
- Analyse, apply the material stiffnesses and external loads.

Establishing a stable form before the application of external loads is fundamental when dealing with structures of this nature as if they are unable to support their self-weight then they are unlikely to be able to support further additional loads. However, creating a balanced form with a

[24] Del Grosso, A., & Basso, P. (2010). Adaptive building skin structures. *Smart Materials and Structures, 19*(12), 124011.

compatible set of forces can be challenging and this problem lends itself well to a form-finding process. Two commonly used methods for form-finding tensegrity prisms include the Force Density Method (Chi Tran & Lee, 2010) and Dynamic Relaxation (Bel Hadj Ali et al., 2011).

Whilst the force density method is arguably the easier to code in software such as Mathematica (with tutorials available in common texts) and is implemented in software such as Rhino's Grasshopper, the author has used InTens whilst working at TENSYS which utilises dynamic relaxation as the primary method of form-finding. However, with experience and with the power of modern non-linear software packages it is becoming increasingly easier to achieve stable pre-stressed states for icosahedrons and related structures without form-finding software. This does, however, require that the user has a good understanding of the expected structural behaviour to create a close approximation of the starting geometry because if the initial guess is too far away from the final form, traditional software will often be incapable of coping with the resulting imbalance of forces and large displacements.

Even in a balanced system, there are risks associated with large displacements. Should a system deflect excessively then the ends of the cable may move closer together and cause the tension only elements to lose their tension and become slack (Deng, Jiang, & Kwan, 2005), effectively reducing the de-tensioned cable to a zero stiffness element and affecting the overall stability of the prism.

Given the complexity of designing tensegrity prisms, they are frequently 'value engineered' out of real-world applications, although the author has designed and constructed numerous tensegrity structures over the years, including the Faith Zone within the Millennium Dome which incorporated flying masts around the perimeter that embraced the principles of tensegrity.

Whilst static tensegrity structures such as the Faith Zone are uncommon, numerous applications have been researched such as pedestrian bridges as shown in Figure 2-27 (Rhode-Barbarigos, Hadj Ali, Motro, & Smith, 2010), active facades (Del Grosso & Basso, 2010), and spine beams on large structures (Adriaenssens & Barnes, 2001).

*Figure 2-27 - Tensegrity Pedestrian Footbridge.*[25]

Another type of strut and cable structure is the cable-chain arch (Li, Vu, & Richard, 2011) where a chain of rigid elements are formed by connecting them using rotational pins, this system on its own would be unstable and would be similar to a bicycle chain. Stability is introduced to the system through the integration of complex ties, forming a series of discontinuous ties linking nodes together to form uniplets, see Figure 2-28.

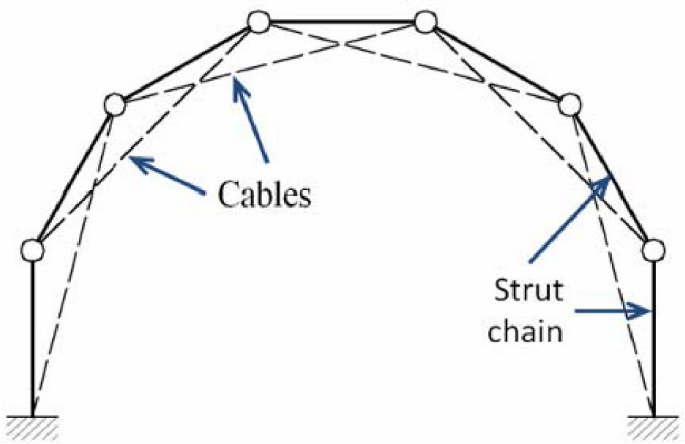


*Figure 2-28 - Cable-Chain Arch.*[26]

These types of structures are becoming increasingly popular given their ability to be deployable or demountable and their given lightweight nature of the resulting structure. Cable-chain arches have even been implemented within glass roofs in Russian shopping centres (Harrhuis, 2012) showing that they are capable of obtaining tight displacement tolerances, but their general behaviour and form will be discussed in greater detail in section 2.11.

[25] Rhode-Barbarigos, L., Hadj Ali, N. B., Motro, R., & Smith, I. F. C. (2010). Designing tensegrity modules for pedestrian bridges. *Engineering Structures, 32*(4), 1158-1167. doi:10.1016/j.engstruct.2009.12.042

[26] Li, Y., Vu, K. K., & Richard, J. Y. (2011). Deployable Cable-Chain Structures: Morphology, Structural Response And Robustness Study. *Journal for the International Association for Shell and Spatial Structures, 52*(168), 83-96.

## 2.6 Kinematic And Static Determinacy.

Structural engineers are used to commonly assessing structures for being statically determinate or indeterminate and are ever conscious of the risks that having a poorly restrained structure can bring. When considering deployable structures, it is essential to introduce a controlled instability (often a single degree) within the structure to allow it to fold in a controlled and monitored fashion (as outlined in section 2.4.3 - Controlled Instability.). The assessment of a structure's ability to be converted into a mechanism easily is directly linked to the degree of static determinacy of the structure. However, it must be noted that this is not cleanly governed through just the application of simple equations and an experienced structural engineer will often use their experience to assess the redundancy of a structure and its comprising elements to develop articulated structures such as the folding bridge shown in Figure 2-29.

*Figure 2-29 - Folding Bridge Kiel by Schlaich Bergermann and Partner.*[27]

Once a structure has sufficient degrees of restraint removed, say by the removal of a brake on a supporting wheel, and it becomes a dynamic structure it can no longer be analysed through the equations of static equilibrium. This is where kinematics comes into play. Kinematics is a study of geometry in motion (Jazar, 2010, p31) and is fundamental when determining the behaviour of perfect structures (no internal deformation) and rarely considered in structural engineering as structures are deemed to be constrained to prevent motion. The kinematic determinacy of a structure is important, particularly when considering rigid body kinematics, as whilst the distance between each 'particle' will remain unchanged the position of those particles is determined by the forces placed upon the structure and the interconnectivity of the particles and their associated degrees of freedom. The kinematic determinacy is crucial (J.-S. Zhao, Chu, & Feng, 2009) when

[27] Knippers, J., & Speck, T. (2012). Design and construction principles in nature and architecture. *Bioinspiration & Biomimetics, 7*(1), 1-10.

exploring and assessing the mobility of a mechanism, typically mechanisms will be constructed from rigid links and a combination of kinematic joints with varying degrees of freedom (see below).

## 2.7 Joints.

Common static structures can be comprised of any number of end constraints, but they are most commonly substituted for the end conditions shown in Figure 2-30 that can easily be constructed within a building.

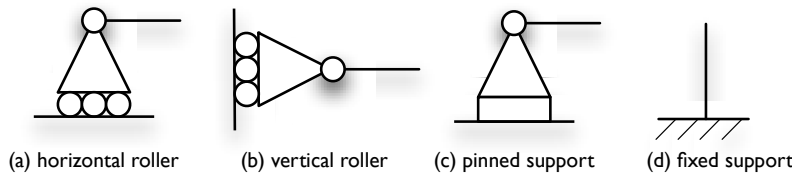


*Figure 2-30 Common Beam Support Conditions.*

In a 2D structure, a node can contain 3 forms of restraint, there are lateral restraints in the x and y-direction and a rotation restraint. The restraints provided by each end condition shown in Figure 2-30 are:

a) 1 – lateral (y-direction).
b) 1 – lateral (x-direction).
c) 2 – lateral (x & y-direction).
d) 3 – lateral (x & y-direction) and rotation restraint.

The combination of these joints and their associated releases can be implemented through Maxwell's rule to determine if a structure is statically determinate or not.

For 2D frames Maxwell's rules are:

(2.1)

*Where:*

$$\begin{array}{l|l} M = 2J - 3 & \text{Statically Determinate} \\ M < 2J - 3 & \text{Unstable} \\ M > 2J - 3 & \text{Statically Indeterminate} \end{array}$$

*M is the number of members*

*J is the number of joints*

This allows a quick appraisal of a potential structure to determine if it will behave as a structure

or as a mechanism, although structural engineering experience must come into play as Maxwell's equations can give results that note that a structure is perfect when it is, in fact, unstable and can behave as a mechanism. As more complex joints are brought into the system, the more complex the behaviour of the system becomes to predict, this leads to the inclusion of lower and higher pair joints. Where a kinematic joint is referred to as a pair.

### 2.7.1 Lower And Higher Pair Joints.

Whilst the joints discussed so far are simply a subset of the lower pair joints, it is worth spending a few minutes briefly discussing the rest of the lower pair joint family, for completeness these joints are replicated below in Figure 2-31 and taken from You and Chan (2012, p5). A lower pair is a joint that maintains contact between two rigid members at every point of one or more surface segments, whereas a higher pair may only maintain contact at isolated points or along line segments.

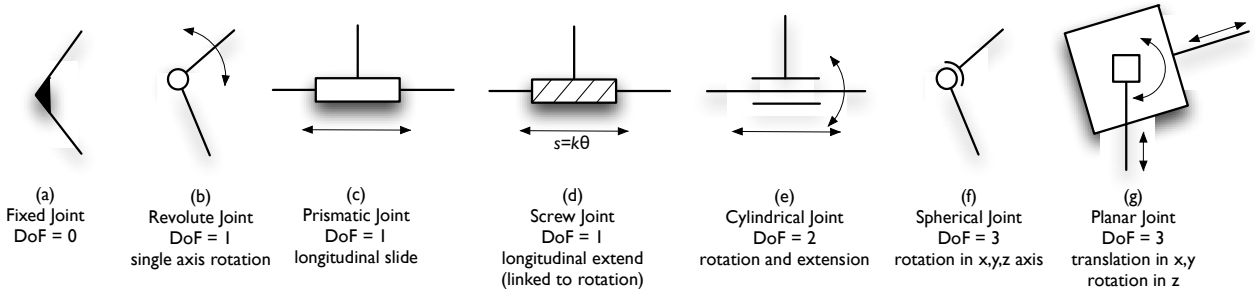


*Figure 2-31 Lower Pair Joints Used In Deployable Structures.*

The number of degrees of freedom is critical when assessing the mobility of a structure (J.-S. Zhao et al., 2009) and the use of revolute joints is a key feature in constraining movement in certain 2-dimensional planes. The distinction between these is important as up until this point we have been using the terms linkage and mechanisms almost interchangeably, but there is a distinct difference between the two that must be appreciated. Essentially and fundamentally a linkage is formed through the inclusion of lower pair joints (and therefore a structure's assessment using the Maxwell rules shows it is unstable it is often a linkage rather than a mechanism) with a mechanism being defined by a chain of links that are formed through kinematic pairs, at least one of which is a higher pair of joints.

The combination of lower pair joints that are brought together in a kinematic chain of linkages will determine the overall range of movement of a chain and how easily this range of movement could be converted into a static structure. The number of degrees of freedom that a mechanism possesses is often referred to as its mobility and just as the Maxwell rule can be used for static

structures, a comparable method is used to determine the degrees of freedom for mechanisms and linkages.

### 2.7.2 Mobility.

The mobility of an assembly is determined by the Grübler-Kutzbach criteria (You, 2007) which is determined by the following equation:

$$m = 6(n - j - 1) + \sum_{i=1}^{f} f_i \tag{2.2}$$

*Where:*

*m is the mobility*

*n is the number of links*

*j is the number of joints*

$f_i$ *is the number of degrees of freedom per joint.*

For an assembly to be considered as a stable structure the mobility should be equal to zero, however, there are limitations on the above equation as identified by (You & Chan, 2012) such as unconstrained local x-axis causing rotational spinning along a link.

### 2.7.3 Planar Mechanisms.

When a mechanism is constrained into a 2-dimensional plane, then it becomes a planar mechanism and each joint can only present 3 degrees of freedom. This reduces the mobility equation to the following:

$$m = 3(n - j - 1) + \sum_{i=1}^{f} f_i \tag{2.3}$$

*Where:*

*m is the mobility*

*n is the number of links*

*j is the number of joints*

$f_i$ *is the number of degrees of freedom per joint.*

As planar structures can only contain ***Revolute*** or ***Prismatic*** joints, the equation can be further simplified to the following expression:

$$m = 3(n-1) - 2j \tag{2.4}$$

*Where:*

*m is the mobility*

*n is the number of links*

*j is the number of joints*

For example, considering a planar linkage formed purely of revolute hinges, more commonly known as a 4R Linkage as shown in *Figure 2-32*:

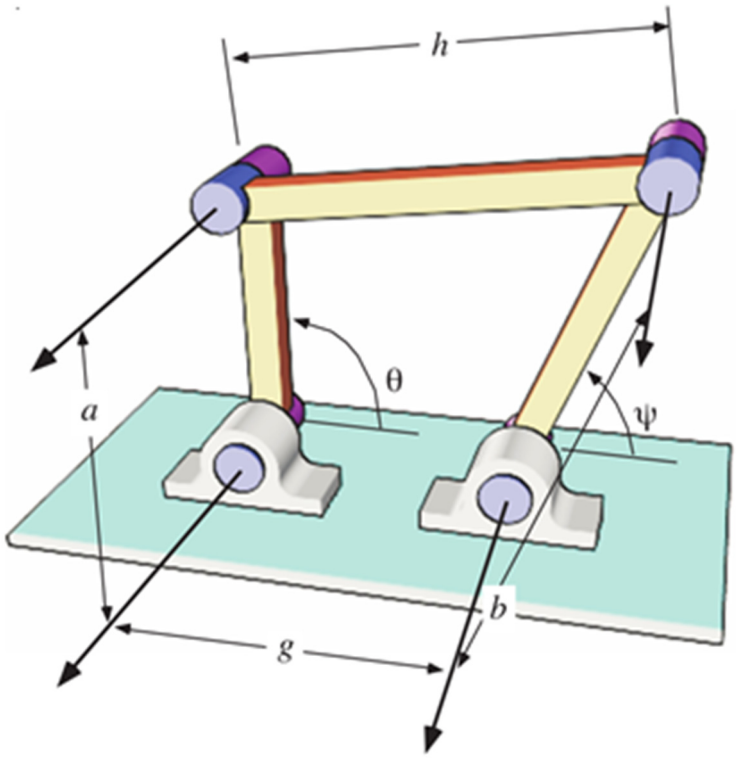


*Figure 2-32 - Typical 4R Planar Linkage.*[28]

As planar linkages can only make use of Revolute or Prismatic joints, each joint may only possess a single degree of freedom. As the links are arranged to form a single-loop closed chain then j=n and the mobility equation can be reduced to the following.

[28] McCarthy, J. M., & Soh, G. S. (2011). *Geometric Design of Linkages* (Second ed.). London: Springer.

$$m = n - 3 \tag{2.5}$$

With a 4R linkage providing 4 single degree of freedom joints, this gives the mobility of the above system as being a single degree (4-3), which is correct.

Following these principles, more complex linkages such as 6 bar linkages would require 7 revolute joints (correctly configured) to provide an overall single degree of freedom (see Figure 2-33).

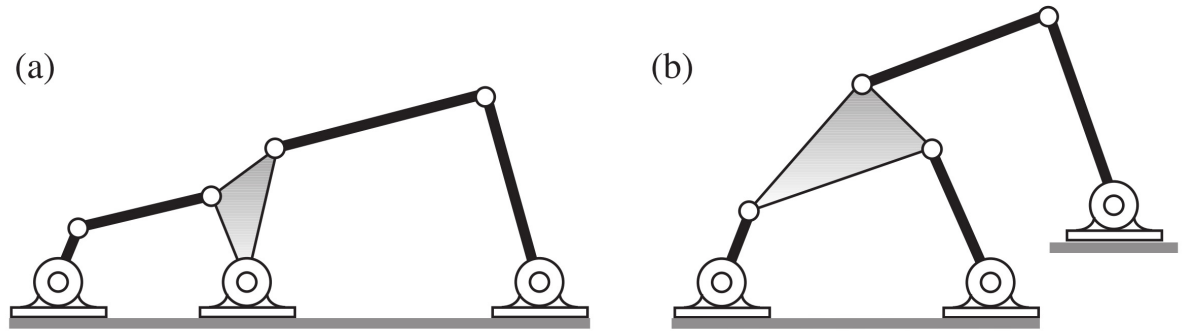


*Figure 2-33 (a) Watt 6 Bar Linkage (b) Stephenson 6 Bar Linkage.*[29]

The above degrees of freedom refers specifically to the common lower pair joints used in mechanisms and deployable structures with the Planar (Type P) and Revolute (Type R) joints being used widely to create linkages. However, if the revolute joint with a single degree of freedom is exchanged for a rotational spring the structure still has a single degree of freedom but the angle of revolution of that hinge is proportional to the forces developed within the structure.

[29] McCarthy, J. M., & Soh, G. S. (2011). *Geometric Design of Linkages* (Second ed.). London: Springer.

## 2.8 Deployable Arches.

Cable-chain arches and arches formed from Scissor Like Elements (SLE's) have been briefly discussed so far in this chapter, however, this section will consider some of the specific considerations associated with precedents for deployable arch structures.

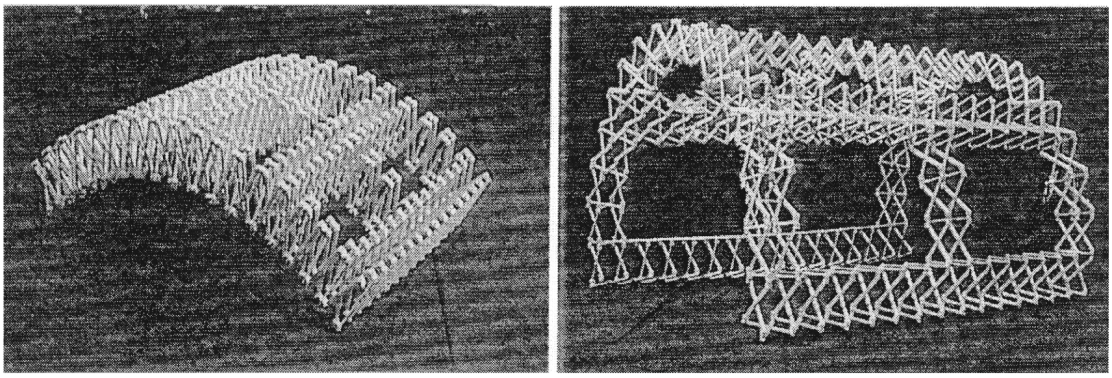

*Figure 2-34 – Folding Barrel Vault Arch Using SLE.*[30]

Folding barrel vault arches based on modular SLE (see Figure 2-34) such as those identified by Langbecker and Albermani (2001) and planar pantographic elements like those by Akgün et al. (2010) give an overall feel for the potential of this structural form to achieve large scale structures. As noted in section 2.4.2, simply by moving the central pin to no longer be in the centre of the strut will convert a linear SLE truss into a curved SLE truss which still folds tightly ready for delivery and deployment. Gantes (Gantes, 2001; Gantes et al., 1989) has been responsible for much of the early work regards SLE behaviour and the assessment of efficient forms of 3D prisms and planar uniplets for deployable structures, but the area is maturing with the inclusion of more advanced forms including those with non-uniform curvatures.

The use of uniform modules is normally key to ensuring a single degree of freedom is retained within the design, simplifying the structural behaviour during deployment. Although the benefits of varying the types of units and combining different types of elements are starting to gain importance (Akgün et al., 2011), as this can lead to the generation of asymmetrical but controlled shapes that still fold and nest just as their symmetrical counterparts, see Figure 2-35.

[30] Langbecker, T., & Albermani, F. (2001). Kinematic and non-linear analysis of foldable barrel vaults. *Engineering Structures, 23*(2), 158-171. doi:10.1016/s0141-0296(00)00033-x

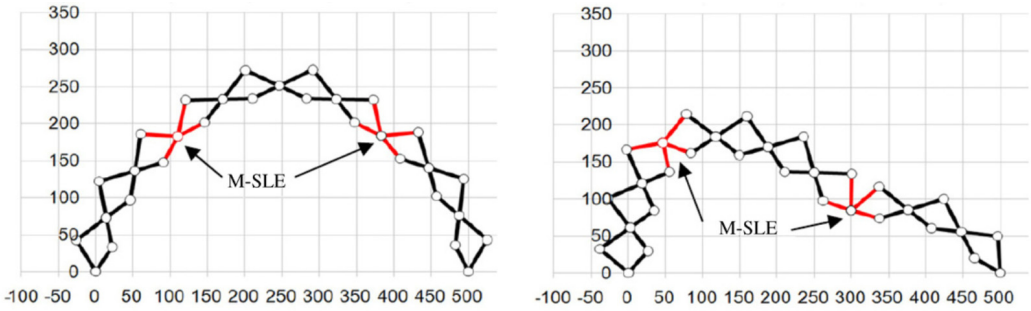


*Figure 2-35 – Varying The Arch Profile Through Varying SLE And Modified SLE (M-SLE) Joints.*[31]

Alternatives to SLE include the curved tape springs such as those proposed by Seffen et al. (2000) on small scale structures, or those not affected by the environment by being extra-terrestrial (Yoshiaki, Yasuhito, Toshihiro, & Makoto, 1992) or through adding beads with pre-tension. Essentially having a low-stress state for packaging, but with increased rigidity post-deployment.

Novel developments of the arched form such as FlexiArch (Long, Kirkpatrick, Gupta, Nanukuttan, & Polin, 2013) for example, have been developed in recent years to speed up construction and simplifying delivery in comparison to traditional methods. FlexiArch makes use of traditional voussoirs but interconnects them with polymeric reinforcement to create a chain of precast units that are inter-linked with pins between each segment. This allows the arch to be stored in a flat shape but once lifted from its storage or delivery position it soon adopts an arched form due to its selfweight.

[31] Akgün, Y., Gantes, C. J., Sobek, W., Korkmaz, K., & Kalochairetis, K. (2011). A novel adaptive spatial scissor-hinge structural mechanism for convertible roofs. *Engineering Structures, 33*(4), 1365-1376. doi:10.1016/j.engstruct.2011.01.014


*Figure 2-36 - FlexiArch Installation Stages, a – delivery via trailer, b-c lifting into place, d- installed between pre-constructed abutments.*[32]

Forming the arch as a series of free-pinned hinged units makes delivery of multiple preformed arches to a site possible using a single trailer (see Figure 2-36a) as they can be laid flat and stacked upon each other, whereas a precast arch would leave dead space on the wagon by nature of the rise of the arch. As the arch is lifted from the trailer (see Figure 2-36b), the self-weight of the structure and the angles of the inter-connected voussoirs cause the structure to 'fold' into an arched form (see Figure 2-36c). The final arch is then lifted into pre-constructed abutments that lock the arch into place and prevent the arch from laterally spreading, (see Figure 2-36d). There are reports that this allows concrete arches to be installed in 15 minutes which can minimise disruption to watercourses. But whilst the FlexiArch make use of hinges and is able to transform its shape from flat to arched during erection they are not truly deployable, instead they are

[32] Long, A., Kirkpatrick, J., Gupta, A., Nanukuttan, S., & Polin, D. M. (2013). *Rapid Construction of arch bridges using the innovative FlexiArch.* Paper presented at the Proceedings of the Institution of Civil Engineers-Bridge Engineering.

intended to adopt a static form once constructed: the arch does not change its shape whilst in service and the pins become redundant as arching action is developed between the voussoirs.

SLE structures are typically deployed by controlling the distance between two principle nodes using the same rationale as closing the handles of a pair of scissors. However, given that the weight of one of these arches is considerable they are not often operated by hand and instead make use of either a hydraulic ram (which has compression and tension load-carrying capabilities) or through the use of a 'driving cable' which pulls two nodes together to force deployment (M. Zhao & Guan, 2005) to deploy, see Figure 2-37. Whilst a cable may initially appear more elegant, the lack of compressive load-carrying capability may prove dangerous during deployment of an arch as often the elements of the pantograph can change from compressive elements whilst the arch is being lifted from the floor to a tension element once the centre of mass has passed over the high point and the pantographic arch is now being lowered into place.

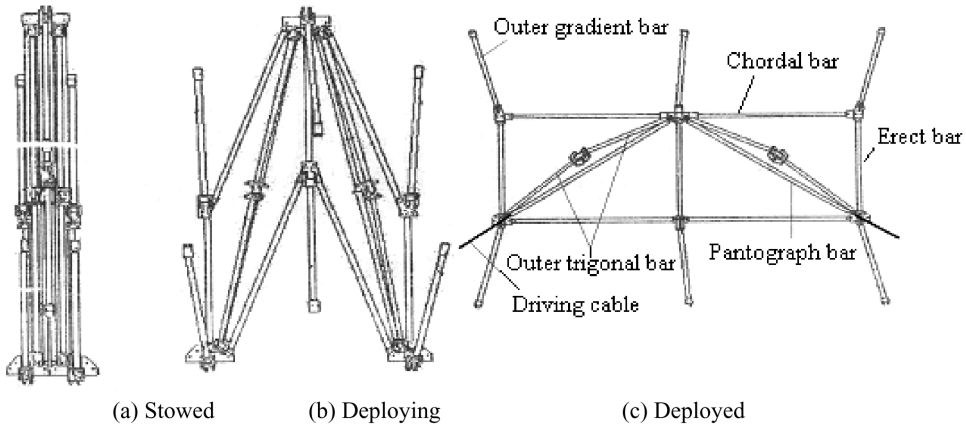


*Figure 2-37 – Deployable Modules Controlled Through Driving Cables.*[33]

The approach of considering deployable structures as 2-dimensional slices is a common approach within the assessment of deployable structures, expanding polygonal movements to polyhedral assemblies through nesting (Kiper et al., 2008) by the simplification of the 2D slices being key to determining the performance. The adaptation from a 1D surface, expanding to a 2D deploying mechanism and then into a 3D curved surface (J.-S. Zhao et al., 2009) helps build

[33] Zhao, M., & Guan, F. (2005). Kinematic analysis of deployable toroidal spatial truss structures for large mesh antenna. *Journal for the International Association for Shell and Spatial Structures, 46*(149), 195-204.

an understanding of behaviour in a deployable structure in much the same way as a more traditional static structure is often subdivided into elements and subframes.

Lightweight structures may give rise to susceptibility to the vibration of the structure under wind, perhaps even giving rise to flutter effects (Barnes & Dickson, 2000). Although the risk to flutter and wind-induced effects could be reduced (Sinan, 2011) with adaptive structures if active control, such as an intelligent structure (Shea, Fest, & Smith, 2002), is selected over passive control as this allows greater control of tuning of the structure in-situ.

### 2.8.1 Types Of Curves.

The type of curve that a structure follows is important as this will determine the in-service behaviour of the arch, but also allows some creative engineering for sculptural pieces that can unfold from a small box into a large open spanning structural sculpture.

As identified by Gantes, Giakoumakis, and Vousvounis (1997) the discovery and development of the geometry is a key component of a deployable structure both for the folded and deployed state. The research into cable-chain structures and their structural behaviour has initially been limited to semi-circular geometries (Harrhuis, 2012; Li et al., 2011) although be it with different methods of stringing the arch to realise differing forms, with (Harrhuis, 2012) creating a transparent and stiff glazed roof structure for a shopping mall in Russia, whilst (Li et al., 2011) investigated the structural performance of a cable-chain shelter including structural robustness. Research into cable strung structures through geometrical optimisation has also been determined through the work of Descamps (2014) although this has been primarily taken from the perspective of the optimization of trusses.

Wu and Sasaki (2007) have chosen to concentrate on the artificial stiffening of arches using an approach analogous to an exoskeleton; using principles similar to an externally stressed stay (Saito & Wadee, 2009), Wu noted that increasing the levels of pretension in the cables can increase the natural frequency of the primary mode and also help with damping. This observation feels logical when comparing it against similar behaviour of tensegrity prisms (Calladine, 1978) which are greatly affected by the self-stress states (Bel Hadj Ali et al., 2010).

### 2.8.2 Nesting Of Arches.

The nesting of arches to create longitudinal tunnels (Thrall & Quaglia, 2014) based on principles found in accordions and origami make for simple structural forms with regards analysis and simplify the connection details between each chain, although great care should be taken with

regards longitudinal stability to avoid the risk of racking through a loss of stability.

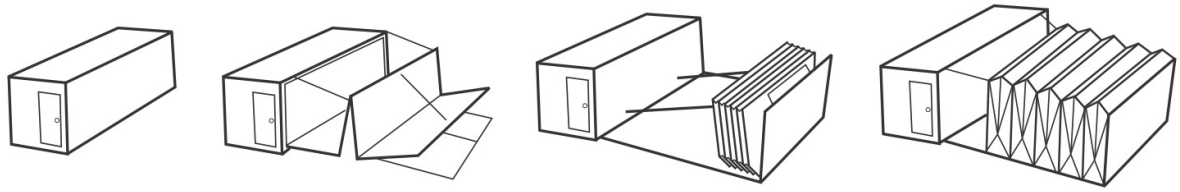

*Figure 2-38 – US Army Disaster Relief Shelter Based On The Accordion Principle.*[34]

The structure in Figure 2-38 deploys laterally from the side of a container, but more common are deployable structures that fold in the primary span direction in terms of a planar structure, or bi-directionally for modular structures, see Figure 2-39. However, for large structures, this can create a structure that requires the use of special lifting equipment to support the structure due to the weight, for example, if a 200 m² structure folds to a small module the overall weight is still the same. This can be overcome through subdivision of the overall structure into smaller interconnected units (Alegria Mira et al., 2014) that can be delivered to site individually and assembled into discrete arches and then tilted into position bay by bay similar to a steel portal frame.

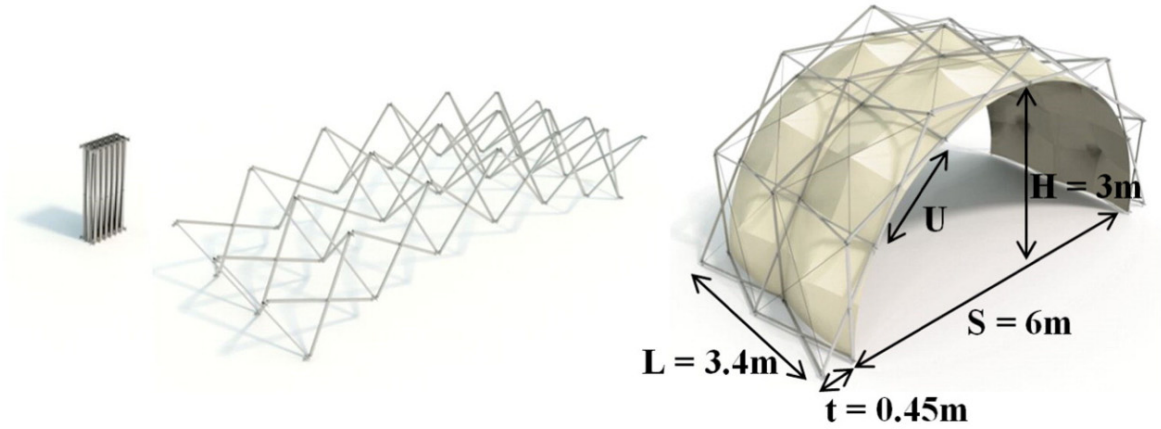


*Figure 2-39 – Deployable Arch That Is Nested As Longitudinal Modules.*[35]

There are a variety of curves that could be investigated for arch structures, but commonly used

[34] Thrall, A. P., & Quaglia, C. P. (2014). Accordion shelters: A historical review of origami-like deployable shelters developed by the US military. *Engineering Structures, 59*, 686-692. doi:10.1016/j.engstruct.2013.11.009

[35] Alegria Mira, L., Thrall, A. P., & De Temmerman, N. (2014). Deployable scissor arch for transitional shelters. *Automation in Construction, 43*, 123-131. doi:10.1016/j.autcon.2014.03.014

curves include:

1. Circular.
2. Cropped circle.
3. Parabolic.

Fundamental differences in the types of curves presented above are apparent from an engineering perspective, particularly at the point where the curves propagate from the supports. Semi-circular arches will have a uniform rate of curvature determined by the angle subtended; this will mean that each segment or uniplet will have the same internal angle and the same angle at the support points. Whereas a parabolic curve, for example, even if subdivided into a series of uniform segments, will have different internal angles for each segment and the angle at the support can be optimised to either minimise the horizontal or vertical reactions.

## 2.9 Equilibrium States.

Controlling and predicting the transformation of a structure from packaged, deploying, to fully deployed; or from deployed, retracting, to folded states is critical and is frequently governed by creating sub-states within the deploying/retracting stages that are inherently stable and in equilibrium that will enable them to be analysed. Methods such as controlling the motion of a mechanical structure as a pseudo-static structure (Fenci & Currie, 2017b) have been used successfully for deployable structures with up to 3 degrees of freedom.

Fundamentally, a deployable or metamorphic structure must develop the ability to change its behaviour from a stable static structure to one that is kinematic and able to move based on a set of well-defined repeatable and controlled mechanisms for it to behave safely.

Enabling these intermediate states (where the structure is kinematic) to be stable requires the introduction of control methods that will introduce constraints and reduce the degrees of freedom that a deployable structure will have available to it. A simple example is seen below where the horizontal roller introduces a single degree of freedom to a pantograph structure resulting in instability for the structure, which allows the structure to move predictably as the Scissor Like Elements expand. Once the degree of freedom from the horizontal roller is removed, say through the introduction of a braking force to the roller mechanism then the mechanism is converted into a static structure, see Figure 2-40.

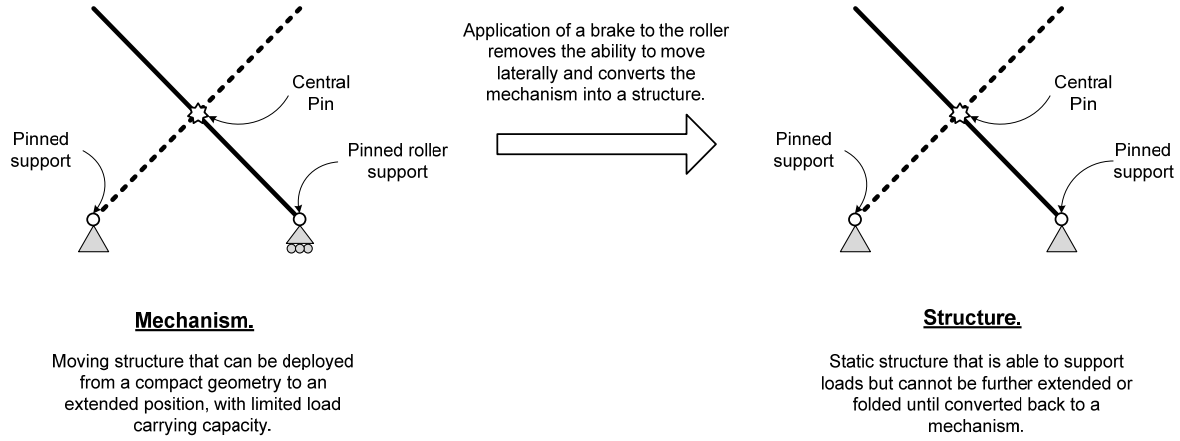


*Figure 2-40 Conversion Of Mechanism To Structure.*

The inclusion of this constraint to the horizontal roller can be seen in the deployable bridge developed by Ario, Nakazawa, Tanaka, Tanikura, and Ono (2013) where the hydraulic ram between points A and C controls the motion during deployment and prevents the bridge from over-extending, see Figure 2-41.

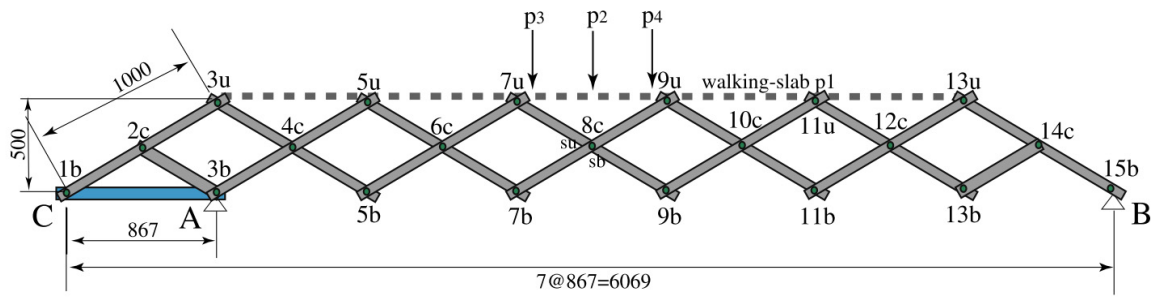


*Figure 2-41 - Deployable Bridge With Control Driven By The Ram Between A And C.*[36]

This is only one way of converting a common deployable mechanism into a static structure. There are a variety of constraints that could be introduced, including the removal of the rotational release at the central revolute joint, through to the introduction of an additional tie cable across the top of the SLE (Figure 2-42) to create a unidirectional stabilised structure. Similar principles have been observed on deployable shelters that also make use of Scissor Like Elements (Alegria Mira et al., 2014).

[36] Ario, I., Nakazawa, M., Tanaka, Y., Tanikura, I., & Ono, S. (2013). Development of a prototype deployable bridge based on origami skill. *Automation in Construction, 32*, 104-111. doi:10.1016/j.autcon.2013.01.012

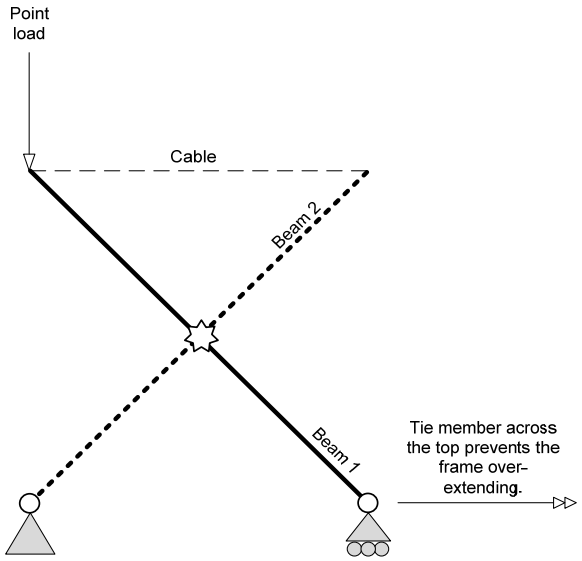


*Figure 2-42 Unidirectionally Stabilised SLE.*

It is this autonomous and reliable transformation between the two states of the packaged form to the deployed form that is fundamental to the success of a deployable structure.

### 2.9.1 Stabilisation Through External Forces.

Maintaining structural equilibrium is essential for deployable structures, with the structure often able to switch between equilibrium states dependent on the stage of deployment or retraction. Although any long-term positions of the structure should be held within a state of stable equilibrium see Figure 2-43.

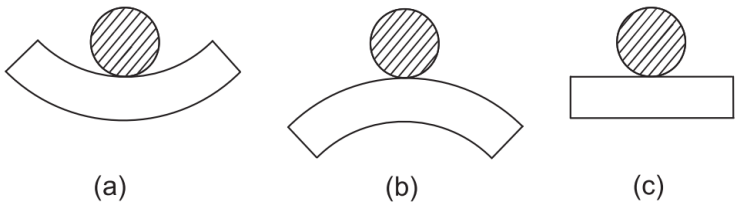


*Figure 2-43 - Equilibrium States - (a) Stable (b) Unstable (c) Neutral.*[37]

Even simple structural assemblies that are stabilised through the application of load, for example, a simple see-saw, need to be considered carefully as specific combinations of loads can create balanced states under certain conditions as seen in Figure 2-44.

[37] Yoo, C. H., & Lee, S. C. (2011). *Stability of Structures: Principles and Applications*. London: Butterworth-Heinemann. p3

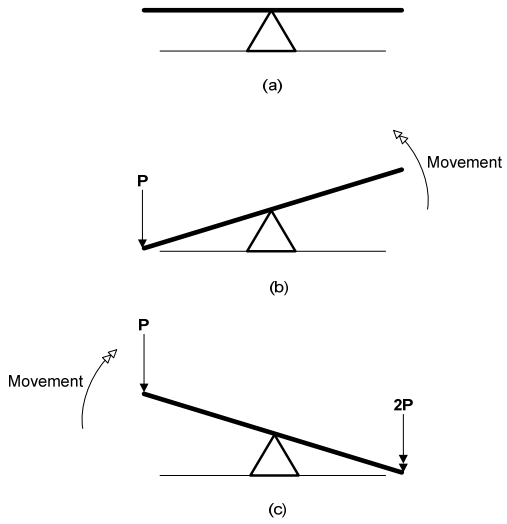


*Figure 2-44 Stabilising Effect Of Loads.*

Where an initial load of P creates a movement within the linkage and converts it into a stable structure, but it is only stable providing that a load not greater than or equal to P is provided on the other end. Once a load is applied to the other end of the see-saw which is more than the initial applied load as can be seen in (Figure 2-44c) then the structure will change form and rebalance showing that the equilibrium was unstable, effectively changing its behaviour to suit the applied loads in a form of structural morphology (Motro & Gerardo Oliva, 2010).

### 2.9.2 Self-Stress.

The relationship between the static and kinematic determinacy is an important parameter when trying to determine the type of linkage being investigated. For example, some structures such as tensegrity prisms, with their discontinuous compressive elements and continuous tensile elements, are only stable when they have achieved an adequate self-stress state (Pellegrino, 1990), and their structural integrity and efficiency of the structure is directly linked to the geometric configuration and the prestress applied within the system (Masic, Skelton, & Gill, 2006). This state of self-stress (Pellegrino, 2001, p120) is defined as a structure which has internal forces that are not zero, whilst maintaining equilibrium without having any external forces applied. Several forms of deployable and lightweight structure require prestress to be manifested within them in order to achieve a stable equilibrium state, preventing nodes displacing grossly in relation to each other.

The relationship of the rigidity ratio between the struts and the cables has been investigated for pedestrian bridges (Rhode-Barbarigos et al., 2010) showing that an increase in this ratio leads to a

reduction in the overall vertical deflections of the bridge. Indeed one of the benefits of a tensegrity structure is its ability to be tuned to vary its stiffness in direct relation to the level of prestressing applied (Juan & Mirats Tur, 2008), although this prestress state should be determined before load analysis can begin in earnest (Adriaenssens & Barnes, 2001).

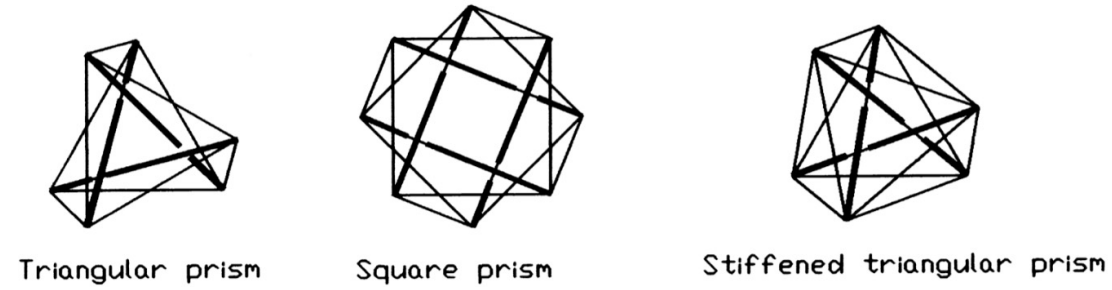


*Figure 2-45 - Common Tensegrity Prisms.*[38]

But tensegrity prisms (see Figure 2-45) and other structural systems that rely on prestress states do not fit well within the structural classification of purely static or kinematic definitions and instead require an approach that sits between both fields. Through a combined approach it is possible to further classify structures that without prestress would behave as unpredictable mechanisms, but through the stabilising effects of a closed system of prestressing could be made practical load-supporting structures (Pellegrino, 2001).

Intentionally allowing cables to de-stress to develop an overall instability can be used to develop deployable behaviour (Friedman & Ibrahimbegovic, 2013) in structures. As the cables have zero compression capacity (Moored & Bart-Smith, 2009) they can be engineered to 'buckle' and no longer contribute to aid with retraction or deployment, but care must be taken that this behaviour is not activated by accident under load cases such as wind reversal for example. To aid with the reduction of risk of a cable losing its tension force under a reversal load condition, it is often beneficial to introduce a suitable prestress to the cable (B.-B. Wang, 1998) which is large enough to ensure that a nominal tension still exists even during inversion. However, there is a balance to be made with the application of pretension as this can affect the forces within the structural system as a whole if an inappropriate value is selected which may again make the structure more vulnerable to snap-through.

[38] Wang, B.-B. (1998). Cable-strut systems: part I - tensegrity. *Journal of Constructional Steel Research, 45*(3), 281-289. doi: 10.1016/s0143-974x(97)00075-8

Research into the effects of cable tensions causing struts to buckle (due to the associated increase in the compressive forces in the struts) and deform by Al-Sadder, Shatnawi, and Dado (2007) gives an interesting insight into the potential for hinges to be locked (Figure 2-68), allowing the arch to flex like a fishing road, see Figure 2-47. This could give a further variation to the cable-chain arches reviewed earlier, which to increase their packability could integrate the slotted pole connections of Laet, Luchsinger, Crettol, Mollaert, and Temmerman (2009) tensairity arches.

Just as correctly prestressed cables in tensegrity structures can increase their overall stability and system rigidity, cables can be used to bring restraint to long-span arch structures (Hosozawa, Shimamura, & Mizutani, 1999). For example, the Miyagi General Gymnasium where they provide restraint to the central arch, see Figure 2-46 for an idealised structural diagram. It should be noted that for the Miyagi General Gymnasium that careful balancing is needed from the restraining force otherwise, the general increase in compression within the structural system can lead to a buckling instability occurring in the trussed arch.

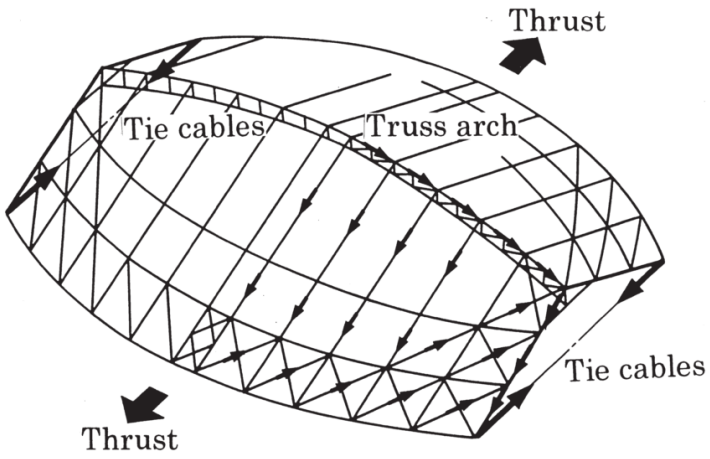


*Figure 2-46 - Miyagi General Gymnasium Load Paths.*[39]

The prestress present within structural systems has been shown to heavily influence the buckling capacity and mode of buckling in flexible struts (Wadee, Gardner, & Osofero, 2013), with the magnitude of the imperfections, present within the structural system also significantly affecting the behaviour of steel stayed columns and struts (Saito & Wadee, 2009).

[39] Hosozawa, O., Shimamura, K., & Mizutani, T. (1999). The role of cables in large span spatial structures: introduction of recent space structures with cables in Japan. *Engineering Structures, 21*(8), 795-804. doi:10.1016/S0141-0296(98)00032-7

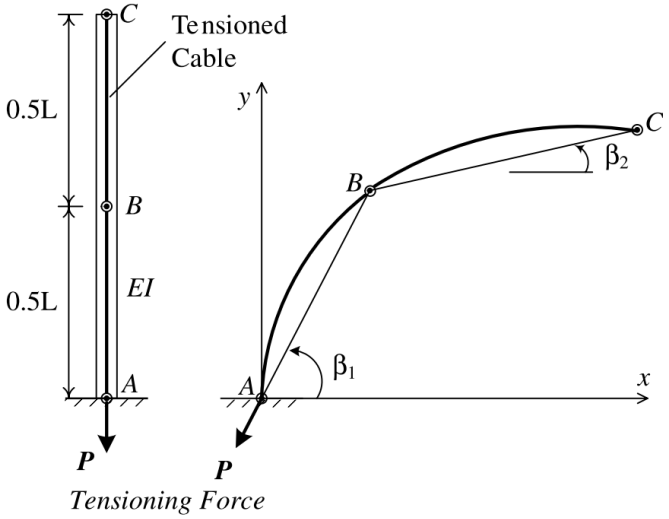


*Figure 2-47 - Strut Buckled Through Application of Cable Tension.*[40]

The stability of structures with cables or tendons integrated into them can be complex and shallow angles for cables where hinges can be problematic for snap-through on structures such as cable-chain arches. Equally, ill-selected values of pretension of cables can cause slender elements to buckle locally which may result in system instabilities.

It may be that if the free pin and the cable to be removed from a cable-chain structure's uniplet and exchanged for a rotational spring then this could reduce the likelihood for the structural elements to snap-through locally. To investigate the buckling and structural behaviour of an element with a rotational spring would require the development of a robust method for analysing and assessing the buckling capacity of the structure though to ensure that stability is maintained.

If all the cables were removed from a complete arch and the free pins exchanged for springs then it is proposed that compressing a series of spring connected struts would naturally form an arched form that is in equilibrium. This buckling of a linear strut into a curved form is not trivial for struts with multiple springs or those formed with non-linear springs. The selection of appropriate spring stiffnesses to maintain the equilibrium of sprung structures under applied external loadings may also prove challenging, later sub-sections will investigate some of the initial theory of buckling of simple sprung struts.

---

[40] Al-Sadder, S., Shatnawi, A. S., & Dado, M. (2007). Exact post-buckling configurations of cantilevered column subjected to forces produced by a tensioned cable. *Mechanics Research Communications, 34*(4), 395-404. doi:10.1016/j.mechrescom.2007.03.001

Potentially it could be argued that for SLE and elements that are formed using free pins that exchanging the free pin for a rotational spring also develops a system of self-stress, with the level of self stress developed being directly linked to the defining geometry and associated spring stiffnesses.

### 2.9.3 Infinitesimal Mechanisms.

The capability of a structure to maintain its equilibrium state is a clear definition of structural stability (Deng & Kwan, 2005). Although, should a system be under-constrained then it may not possess a unique geometric configuration (Kuznetsov, 1999); giving rise to it being kinematically mobile and allowing finite displacements without any corresponding deformations of the structural members. Although under-constrained systems can, in certain configurations, have their kinematic mobility reduced through the introduction of prestress in certain key elements.


*Figure 2-48 - Examples Of Infinitesimal Mechanisms.*[41]

"In kinematical terms, an infinitesimal mechanism is defined as a system that possesses virtual mobility but no kinematic mobility - its geometric configuration is unique." (Kuznetsov, 1999). As can be seen in Figure 2-48a and Figure 2-48b the von Mises truss formed with collinear pins is technically a mechanism as m>0, however it has no kinematic mobility and would require the change in length of the comprising elements to mobilise a change in position of the central pin (Deng & Kwan, 2005). Frequently structures with first-order mechanisms (s=1) can be stiffened through the introduction of a prestress state and this is the basis of the stabilisation of cable-nets and tensegrities (Calladine & Pellegrino, 1991) where the kinematic mobility is subsequently reduced to zero. Indeed if a prestressed state can be applied to a structure possessing m>0 and s>0 that can impart positive first-order stiffness to every mechanism, then the mechanisms are classified as a first-order infinitesimal (Pellegrino & Calladine, 1986).

Pellegrino (2001, p120) defines rigid motion being the motion of an entire space acting as one rigid body. Linkages and mechanisms differ from rigid motions in that they are a structure

[41] Kuznetsov, E. N. (1999). Singular configurations of structural systems. *International Journal of Solids and Structures, 36*(6), 885-897. doi:10.1016/S0020-7683(97)00333-8

which has motion but does not create internal forces. Where prestress mechanisms are the primary mode of controlling the change from stable to unstable states – or from deployed to retractable the internal forces within the structure cannot be zero.

Structures that rely on prestress else would behave as unpredictable mechanisms, as shown in Figure 2-50, are categorised into four subgroups as defined by You and Chan (2012, p35) and also Pellegrino (1990; 2001 ch. 7; 1986). See Figure 2-49 for a summary of the classification of these different structural assemblies.

| | Assembly type | Dimensions of Nullspace and Left-nullspace | Static and kinematic features |
|---|---|---|---|
| I | Statically determinate and kinematically determinate | $s = 0$<br>$m = 0$ | Both (1) and (2) have a unique solution for any r.h.s. |
| II | Statically determinate and kinematically indeterminate | $s = 0$<br>$m > 0$ | (1) has a unique solution for some particular r.h.s., but otherwise no solution. (2) has an infinite number of solutions for any r.h.s. |
| III | Statically indeterminate and kinematically determinate | $s > 0$<br>$m = 0$ | (1) has an infinite number of solutions for any r.h.s. (2) has a unique solution for some particular r.h.s., but otherwise no solution |
| IV | Statically indeterminate and kinematically indeterminate | $s > 0$<br>$m > 0$ | Both (1) and (2) have an infinite number of solutions for some particular r.h.s., but otherwise no solution |

*Figure 2-49 - Classification Of Structural Assemblies.*[42]

[42] Pellegrino, S. (1990). Analysis of prestressed mechanisms. *International Journal of Solids and Structures, 26*(12), 1329-1350.

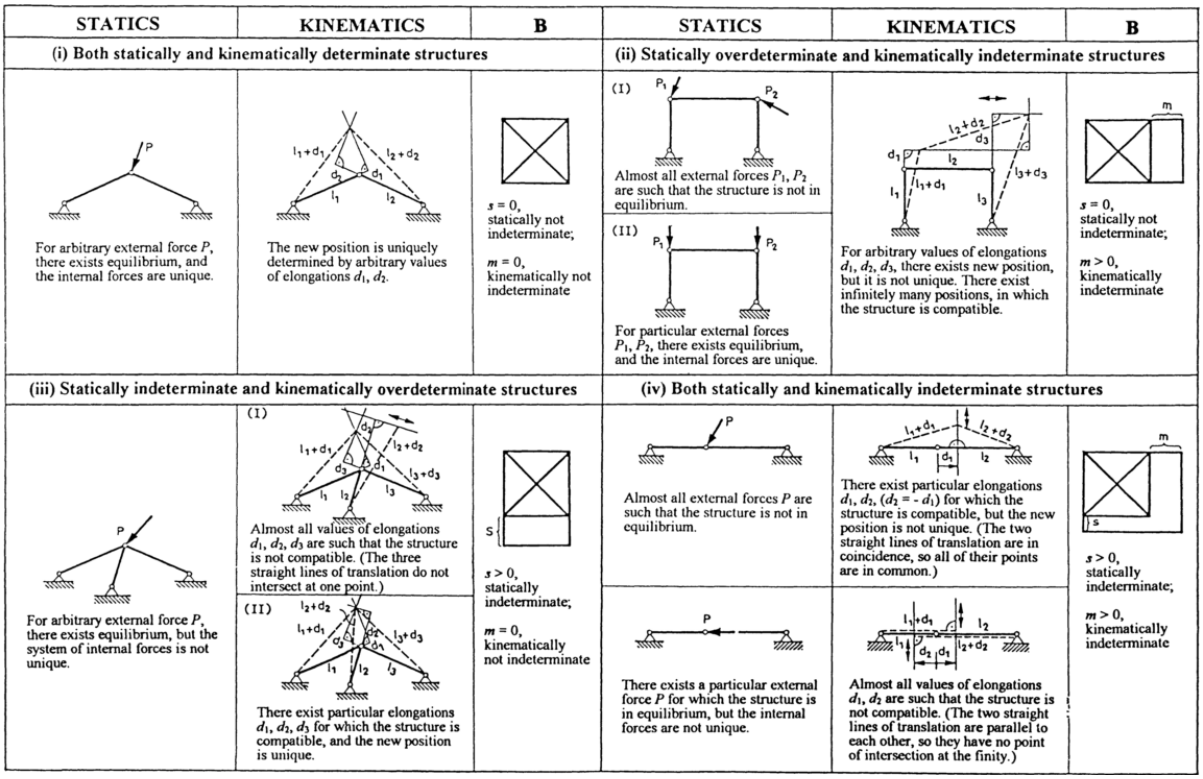


*Figure 2-50 Class (i) to (iv) Mechanisms.*[43]

Each of the above structural assembly types possesses subtly and sometimes quite distinct differences, not just in their overall behaviour but also in the approaches used to analyse them.

### 2.9.4 Class (i) Structural Assemblies.

A class (i) structural assembly is both statically and kinematically determinate and is therefore infinitesimally rigid. It is sometimes referred to as being "simply stiff" (Pellegrino, 2001, p124) and it will possess neither a state of self-stress nor can it be classified as being a mechanism.

### 2.9.5 Class (ii) Structural Assemblies.

A class (ii) structural assembly is statically determinate and kinematically indeterminate. It does not possess a state of self-stress but is a mechanism with a mobility m>0. It, therefore, possesses finite mechanisms.

[43] Pellegrino, S. (2001). *Deployable Structures* (First ed. Vol. 412). Udine: SpringerWeinNewYork. p 125

### 2.9.6 Class (iii) Structural Assemblies.

A class (iii) structural assembly is statically indeterminate and kinematically determinate and has states of self-stress and is classed as infinitesimally rigid. As it is kinematically determinate it cannot be classed as a mechanism. This type of structure can be described as being "over stiff" (Pellegrino, 2001, p124).

### 2.9.7 Class (iv) Structural Assemblies.

A class (iv) structural assembly is both statically and kinematically indeterminate and can maintain states of self-stress whilst also maintaining the capacity to be a mechanism. It is said to possess both infinitesimal or finite mechanisms.

## 2.10 Adaptive Structures.

Adaptive structures have much in common with metamorphic structures in that whilst they may not always be able to completely fold as deployable structures, they can grossly change their form in some capacity (either through a change in stiffness, geometry, or structural massing) to allow the structure to adapt or respond to an external stimulus. Many modern adaptive structures make use of flexible modern materials to form fins such as the flectofin active façade system, but adaptive structures formed from stiff links have recently started to come to the fore using actuators to control the structure in response to the applied loadings.

Adaptive structures are frequently used in kinetic facades (see Figure 2-51) to dynamically control the interior environment (Del Grosso & Basso, 2010). For example, to track the sun path to reduce the effects of solar gain through the course of the day or to ensure that photo-voltaic cells maintain a peak efficiency through the day by maintaining a direct sun path.


*Figure 2-51 - Flectofin Adaptive Facade.*[44]

Adaptive structures are also commonly used for stadium roofs (Ishii, 2000), allowing inclement weather to be locked out during tournaments, for example, the folding roof at Rothenbaum in Germany (Ramzy & Fayed, 2011) where the tennis courts can be either open to the sunshine or closed during inclement weather. This application has also been extended to shopping areas that can become covered using lightweight and transparent cushion structures formed from ethylene tetrafluoroethylene (ETFE) inflatable pillows clipped into rigid frames for sliding roofs when inclement weather appears, with early prototypes being shown in Figure 2-52.

Many of these structures require a forced movement at the ends of the frame where they gain support from the main building to mobilise the façade and it could be argued that the introduction of a preloaded spring at these ends to hold the articulated elements either the closed or the open position may be of benefit, indeed this system is used widely in auto-opening smoke vents for stairwells in tall buildings that open in the event of a fire or power cut.

[44] Knippers, J., & Speck, T. (2012). Design and construction principles in nature and architecture. *Bioinspiration & Biomimetics, 7*(1), 1-10.

*Figure 2-52 - Folding ETFE Cushions For An Animated Roof.*[45]

Just as with deployable structures there are several methods for the roof to articulate, either being gathered as a central basket of fabric as in the Rothenbaum Arena (Figure 2-53) or as a sliding roof as in the Komatsu Dome (Figure 2-54) which both make use of common deployable structural forms.

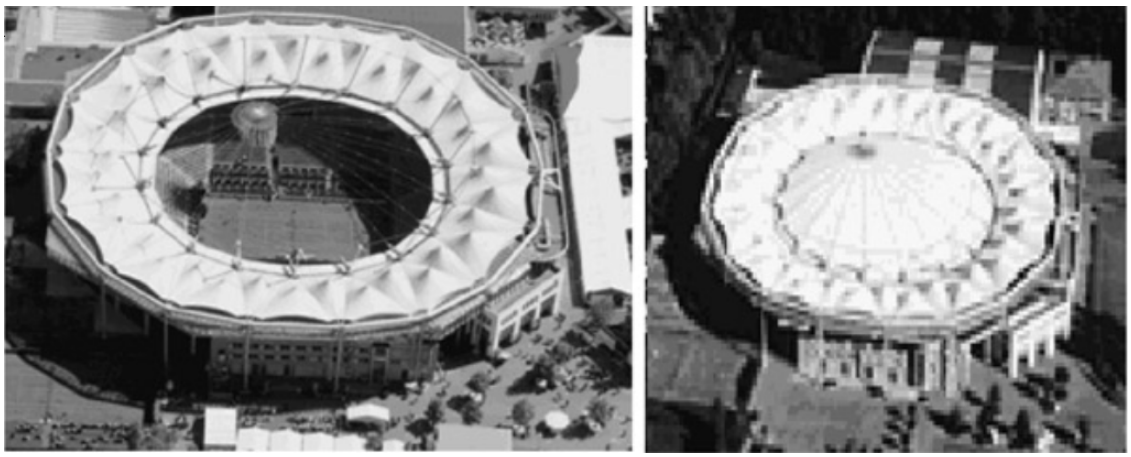

*Figure 2-53 - Rothenbaum Tennis Stadium With Roof Open and Closed.*[46]

[45] Del Grosso, A., & Basso, P. (2010). Adaptive building skin structures. *Smart Materials and Structures, 19*(12), 124011.

[46] Ramzy, N., & Fayed, H. (2011). Kinetic systems in architecture: New approach for environmental control systems and context-sensitive buildings. *Sustainable Cities and Society, 1*(3), 170-177. doi:10.1016/j.scs.2011.07.004

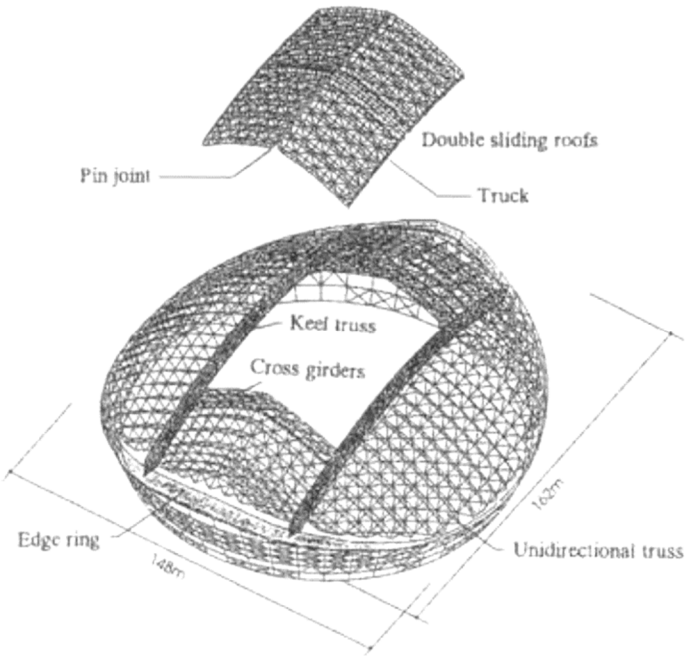


*Figure 2-54 - Framing Arrangement Komatsu Dome.*[47]

Until recently, many adaptive structures made use of well-established, tried and tested deployable structure strategies. These deployable structures were often grafted onto a larger static structure to provide an element of adaptability via controls linked to environmental sensors.

However, with the development of more intelligent control systems, more powerful actuators, and sensors there are structural systems currently under development which are genuinely adaptive. These structures can respond in fractions of a second to changes in loads rather than hours as often associated with stadium roofs. This particular field is currently being dominated by Senatore et al. (2011) through his practical applications and proof of concepts on structures such as the actively controlled cantilever that was installed at the ICE headquarters recently (see Figure 2-55). Discussions with Senatore reveal that one of his biggest challenges is finding actuators that have large enough capacity whilst being able to respond quickly enough to dynamic loads on the scale of a building. It may be that the introduction of a rotational spring at key locations could be used to absorb and dissipate the initial push from the wind whilst the actuators catch up and stiffen the structure globally.

[47] Ishii, K. (Ed.) (2000). *Structural Design of Retractable Roof Structures*. Southampton: WiT Press.

*Figure 2-55 - Adaptive Cantilever.*[48]

In addition to being successfully integrated into adaptive cantilevers (see above) (Senatore, Duffour, Winslow, & Wise, 2017), these same principles have been proposed as systems that could be integrated into skyscraper designs (Senatore, Duffour, & Winslow, 2018b) to generate a variable stiffness lateral stability system to resist the lateral forces such as wind and earthquakes, changing their stiffness to either absorb energy or resist lateral forces, see Figure 2-56.

[48] Senatore, G., Duffour, P., Winslow, P., & Wise, C. (2017). Shape control and whole-life energy assessment of an 'infinitely stiff'prototype adaptive structure. *Smart Materials and Structures, 27*(1), 015022.

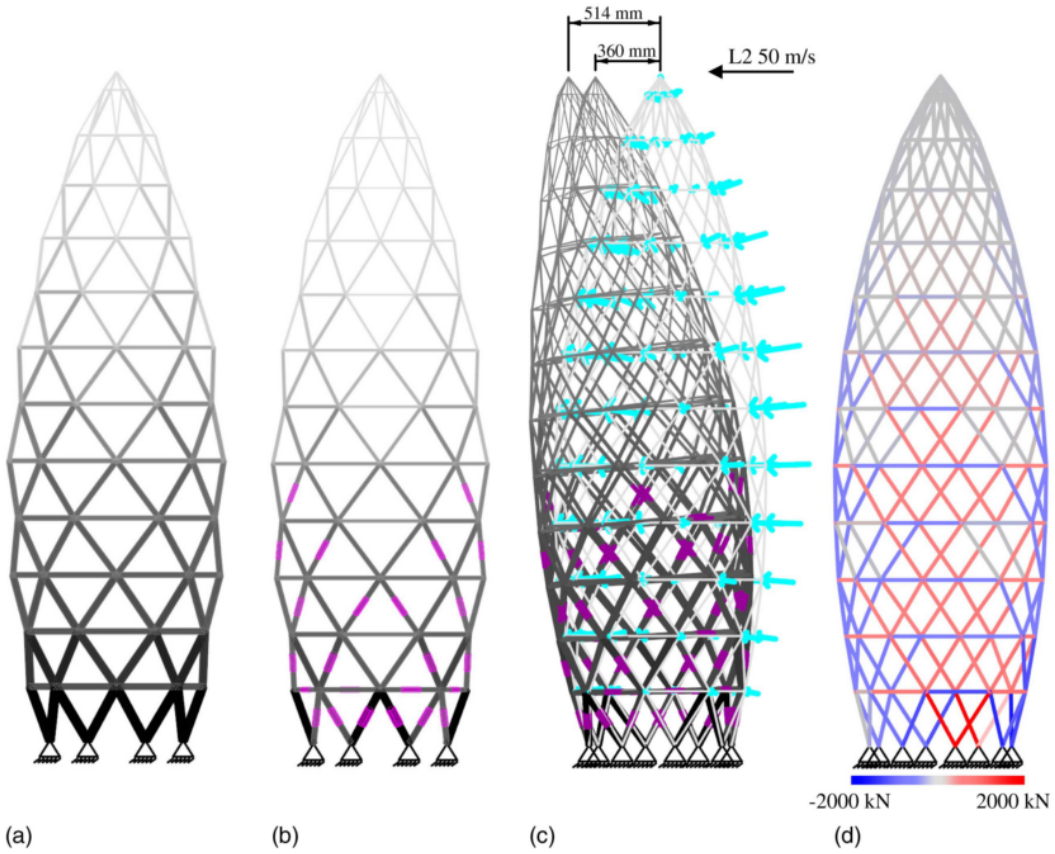


*Figure 2-56 - Lateral Stability Systems (a) Passive (b) Active (c) Controlled & Deformed Shape (d) Redirected Load Path.*[49]

These actively controlled adaptive systems allow buildings to be constructed using less material to create their stiffness thus reducing embedded carbon, instead, consuming energy throughout their life to adapt to dynamic loadings (see Figure 2-57) to minimise forces (Senatore et al., 2018a) within the system yet still potentially saving enough energy to generate a significant carbon saving (Senatore, 2018).

[49] Senatore, G. (2018). Designing and Prototyping Adaptive Structures—An Energy-Based Approach Beyond Lightweight Design *Robotic Building* (pp. 169-189). London: Springer.

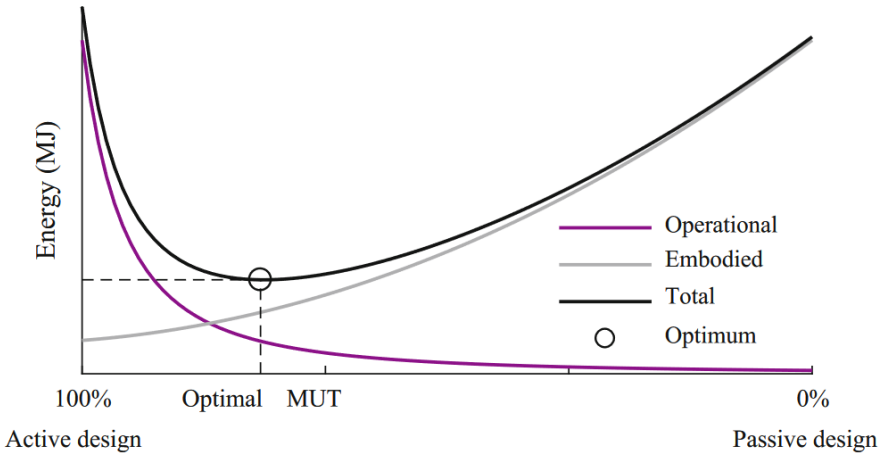


*Figure 2-57 - Active Design Using Adaptable Structures vs Passive Design.*[50]

With the development of 3D printed connections that can create complex hinges and arrangements, future designs may start to move away from heavy cumbersome actuators that are limited by their travel distance and their load-carrying capacity, instead, a lighter more flexible system may be developed.

This is already evident in the work of Knippers and Speck (2012) who actively collaborates with biologists to develop compliant mechanisms that are influenced by nature (Knippers et al., 2016). For example, see the adaptable structure inspired by a flower as shown in Figure 2-58.

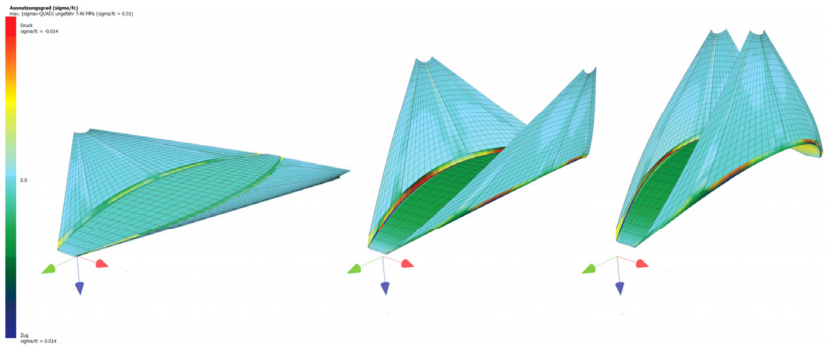

*Figure 2-58 - FEA Model Of Flexible Bioinspired Adaptable Structure.*[51]

These flexible forms of compliant mechanisms are frequently referred to as bending active

[50] Senatore, G. (2018). Designing and Prototyping Adaptive Structures—An Energy-Based Approach Beyond Lightweight Design *Robotic Building* (pp. 169-189). London: Springer.

[51] Schleicher, S., Lienhard, J., Poppinga, S., Speck, T., & Knippers, J. (2015). A methodology for transferring principles of plant movements to elastic systems in architecture. *Computer-Aided Design, 60*, 105-117. doi:10.1016/j.cad.2014.01.005

structures, essentially changing their geometrical form when influenced by external forces that cause these flexible highly elastic structures to bend and flex into a second stable form. These structures are often fabricated using simple 'layup' technologies (Knippers, Cremers, Gabler, & Lienhard, 2011) that have been used for the formation of composites which reduce manufacturing costs and can be undertaken in a general workshop without the need for expensive manufacturing plants.

The principles established on smaller-scale structures such as flectofin (Figure 2-51) have been scaled successfully to larger facades, but care should be taken with bending active structures in that larger fins start to be limited by a combination of their self-weight and the impact of snap-through buckling, which if the displacements are gross will affect the structure's ability to recover/reset (Lienhard & Knippers, 2013).

### 2.10.1 Robustness.

A key behavioural concern of deployable structures is that if they can go between a mechanical and a static state with comparative ease, then they will typically possess reduced structural redundancy compared to other more traditional structures with respect to disproportionate collapse. This can have the calamitous effect that should a critical member be removed then the structure can begin to retract or catastrophically fail, depending on the type of structure deployed and the member removed. A simple example showing the effects of key element removal is shown in Figure 2-59 with a simulation of a key element (coloured red) being removed from a stacked pyramid in a real-time physics simulation undertaken in Physion[52].

[52] http://physion.net

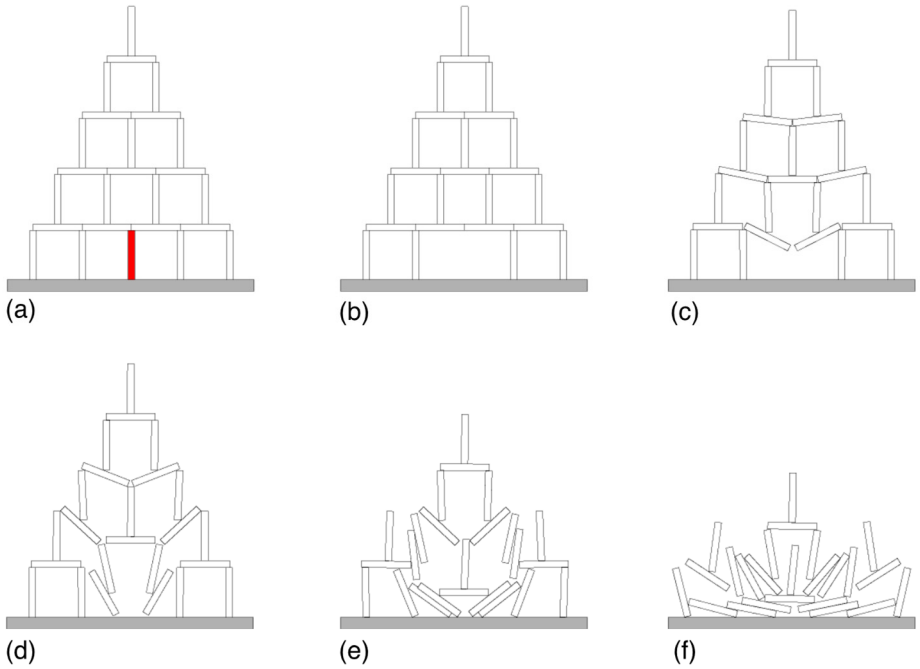


*Figure 2-59 Robustness Through Element Removal.*

This shows that at time step 0 (Figure 2-59b) there is a structural deficiency which as time progresses will spread through the pyramid until ultimately bringing about the full collapse (Figure 2-59f): showing that the effect of element removal brings about a collapse which is disproportionate in scale to the element removed.

Similar research topics have been undertaken by Senatore and Piker (2015) using their bespoke software Catastrophe, that integrates the failure of structures into a simulation environment.

The provision of alternative load paths through the inclusion of additional tie cables and safety cables can create over-constrained mechanisms, but if carefully detailed they can be integrated so that they are only effective when excessive deformations occur, for example when key elements are removed through accidental damage (Li et al., 2011). Figure 2-60 shows a safety tie connected along the ridge of a deployable arch in plan view to create a tie effect should an element be damaged along the grids.

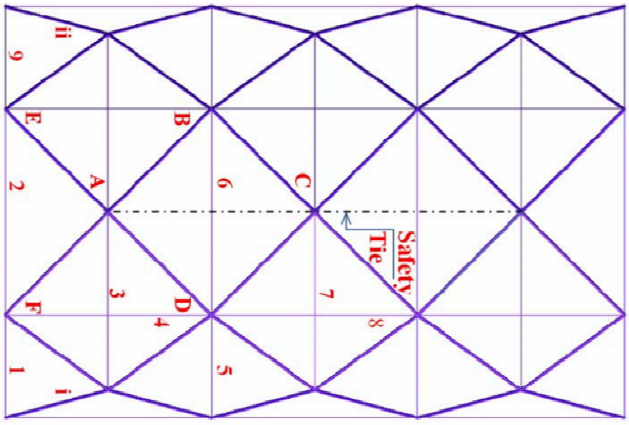


*Figure 2-60 - Plan View Of A Deployable Arch With Safety Tie Cable To Increase Robustness.*[53]

Although a reasonable alternative to the safety tie could be a series of interconnecting springs at the grillage cross over positions, the deployment of the arch would have to overcome the stiffness of the springs which may result in slightly larger element sizes, but would, in the end, result in a more elegant and open structure with no cables crossing the open cells when fully deployed and so may present a more aesthetically pleasing form.

## 2.11 Cable-Chain Arches.

The hypothesis presented within this thesis is that the integration of springs can bring about positive benefits, this sub-section will present a specific type of lightweight deployable structure called a cable-chain structure that makes use of cables and prestress to contain a stable form. This form of structure, however, suffers a vulnerability called snap-through and it is proposed that the introduction of springs could develop a more robust and stable version of this structure. The integration of rotational springs in this cable-chain structure, could also change the behaviour during the erection of the arch and help control the deployment from a flat shape into the final in-service shape.

[53] Li, Y., Vu, K. K., & Richard, J. Y. (2011). Deployable Cable-Chain Structures: Morphology, Structural Response And Robustness Study. *Journal for the International Association for Shell and Spatial Structures, 52*(168), 83-96.

## 2.12 Types Of Arches.

Arched structures are commonplace throughout Europe thanks to the influence of the Romans centuries ago. Masonry arch bridges form the backbone of our highway and rail networks and the UK is dependent on the maintenance and assessment of these arches to ensure safe and efficient transportation of people and goods across the country.

One of the key considerations of arched structures is their ability to resist the applied loads primarily through thrust action when developed as funicular arches. This compressive form of structure has lent itself well historically to the application of masonry forms due to the material behaviour. In later years though, more complex forms of the arch (for example the arch shown in Figure 2-61) have been developed in response to new materials and capabilities in manufacturing techniques, especially the integration of modern and lighter materials such as steel and Fibre Reinforced Plastics (FRP).

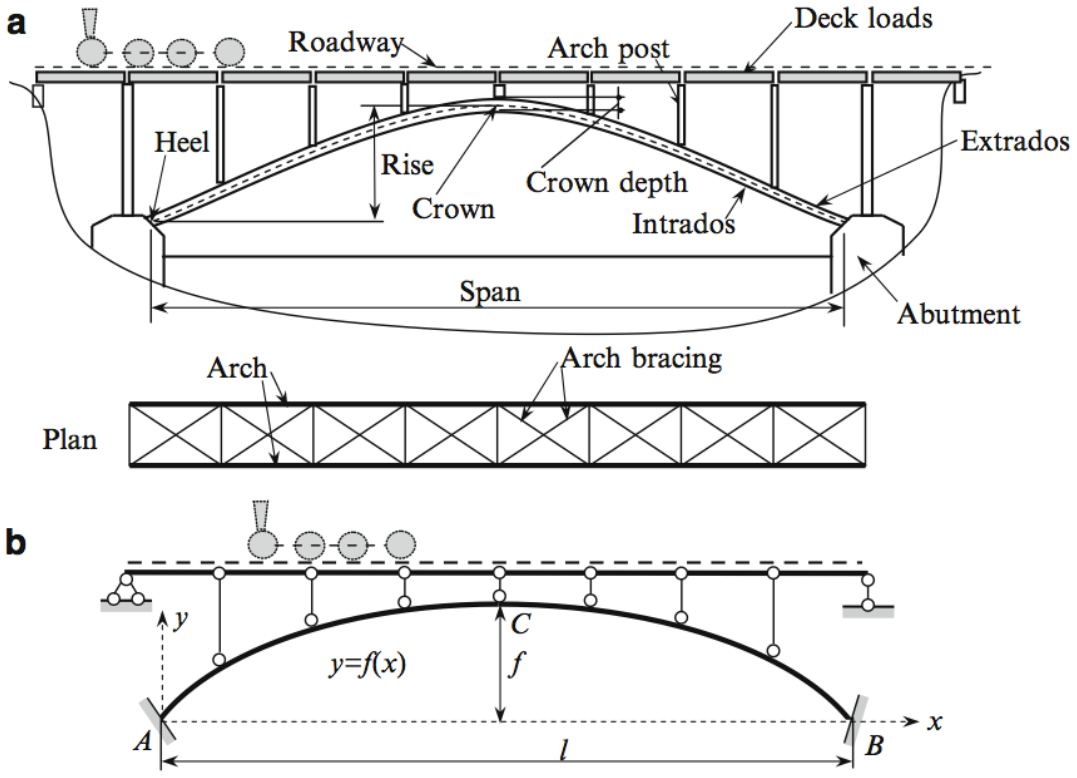


*Figure 2-61 - Anatomy Of A Typical Arch.*[54]

[54] Karnovsky, I. A. (2012). *Theory of Arched Structures: Strength, Stability, Vibration.* London: Springer.

Whilst this simple arch form is used around the world in various iterations and configurations, the focus of this thesis is to investigate how rotational springs may be advantageous when integrated into a deployable or static structure. Given their prevalence to resisting compressive loadings, arches can naturally be dense, heavy structures, not easily relocated or deployed, particularly masonry and concrete arches that require specialist formwork to be constructed. However, one of the key behavioural requirements of a deployable structure is that the structure needs to be lightweight to be deployed. Thus, for the remainder of this chapter, the focus will naturally be on lighter forms of arched structures, with a focus on tied arches to develop suitable forms.

## 2.13 Analysis Of Arches.

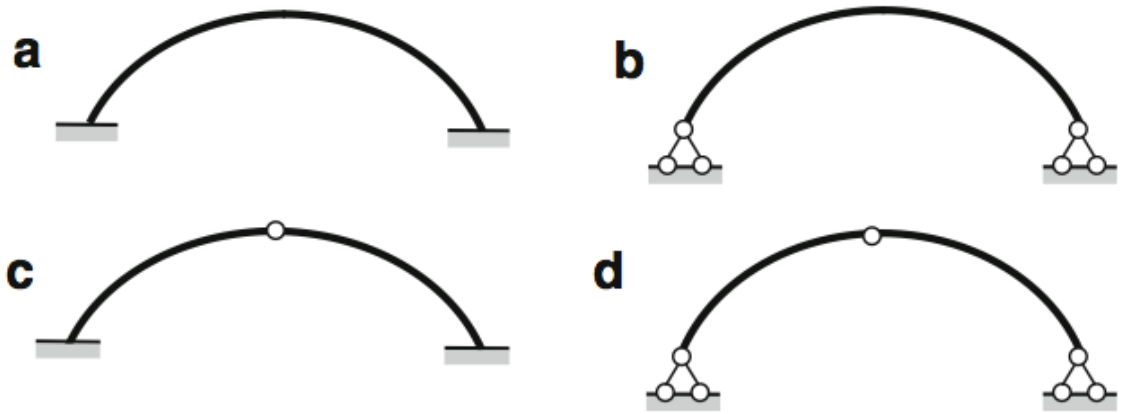


*Figure 2-62 - Arches With Pins.*[54]

A common simplification for arched structures is through the introduction of pins to make it a statically determinate structure to simplify the analysis by creating a 3 pinned arch, see Figure 2-62. Whilst this pin is beneficial in terms of analysis, the introduction of pins presents another positive benefit with regards the ability of the structure to fold and be stored for transportation, with the pins acting as a revolute joint allowing for the structural elements to be folded or rolled up.

## 2.14 Tied Arches.

The introduction of ties to arches (see Figure 2-63) can enable the system to be self-stabilized through the removal of horizontal thrusts at the supports or with the introduction of more complex ties altering the structural behaviour altogether to reduce bending moments and reduce the weight of the materials.

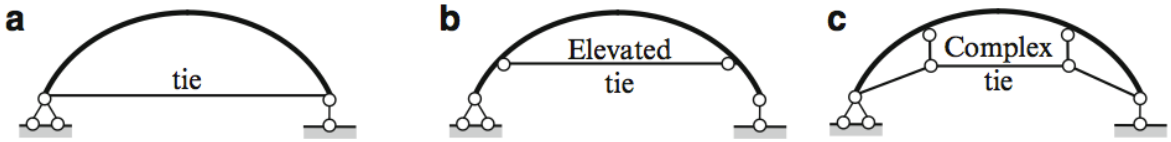


*Figure 2-63 - Common Forms Of Arches With Ties.* [54]

Typically, tension structures are subdivided into two common classifications (Saitoh & Okada, 1999), those being where the tension elements are formed from either membrane or string. Cable-chain arches are commonly classified as Hybrid String Structures (HSS), as opposed to pure tension structures such as cable-nets for example. Figure 2-63 shows some of the common tying patterns for arches, with the ties being introduced for a variety of reasons. In Figure 2-63, for example, the tying cable is introduced across the feet of the arch, helping to prevent the spread of the arch under loadings, an important consideration particularly for sloping structures (Hosozawa et al., 1999). This has the benefit of making the arch self-stabilising by removing the horizontal spread of the arch under vertical loadings, which in softer ground could be advantageous.

The elevated and complex tie (Figure 2-63b & c) is of particular interest with regards deployable structures, and if combined with pins to allow folding, cable-chain arches (Li et al., 2011) can be created that present interesting structural forms that can act as planar structures and also be nested and combined to create more complex structures such as domes and nested arches. Due to the inclusion of the revolute joints, these are more flexible than beam-string structures (Xue & Liu, 2009) which have increased efficiency due to the inclusion of cable elements.

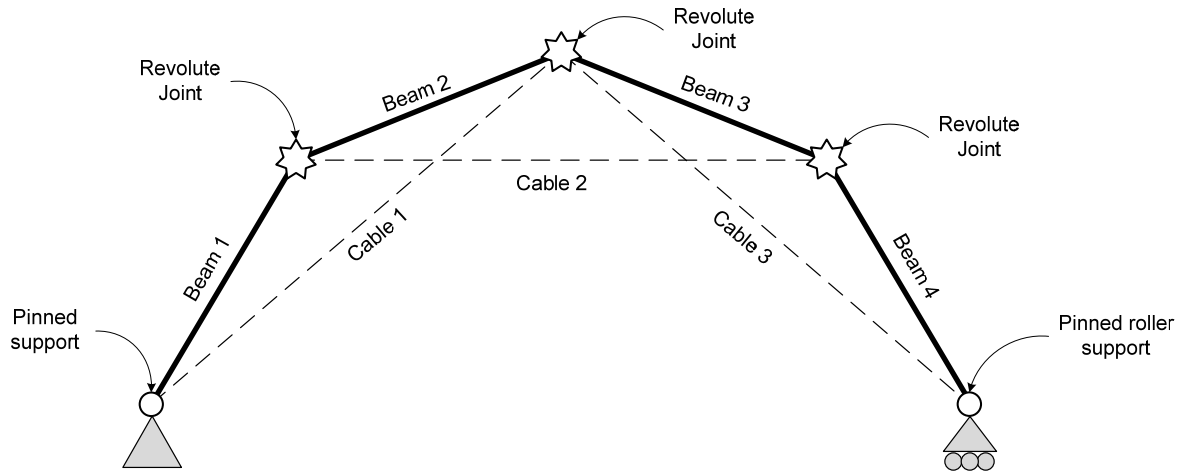


*Figure 2-64 Cable-chain Arch Formed From 3 Uniplets.*

Cable-chain arches are commonly based upon a series of repeatable modules called uniplets, see Figure 2-64. Each of these uniplets are stable in so far that they are triangulated, although the cable spanning between the nodes are tension only elements and should the loading be unfavourable and require the cable to take compression then the uniplets can become unstable.

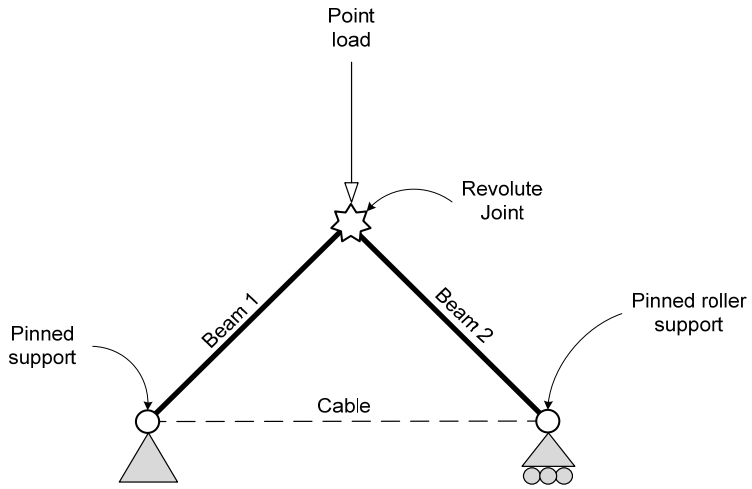


*Figure 2-65 - Stable Uniplet.*

For example, as shown in Figure 2-65, when the point load applied is downwards, this causes the feet to spread and consequently places the cable in tension. However, if the direction of the load was reversed (as in wind uplift say) then the cable has effectively zero capacity in compression and the uniplet ceases to behave as a structure, instead reverting to be a mechanism and becoming a kinematic structure.

Little research has been conducted to date in the behaviour and influences of cable-chain arches, particularly with regards defining the curved geometry and prestress in the cables and it is this

that the next chapter will concentrate on.

Even the classification of these types of structures is still debated, for example following the classification proposed by Saitoh and Okada (1999), see Figure 2-66, depending on the capacity of the revolute joints they may be defined as either being comprised of stiffened beams or as a stiffened arch.

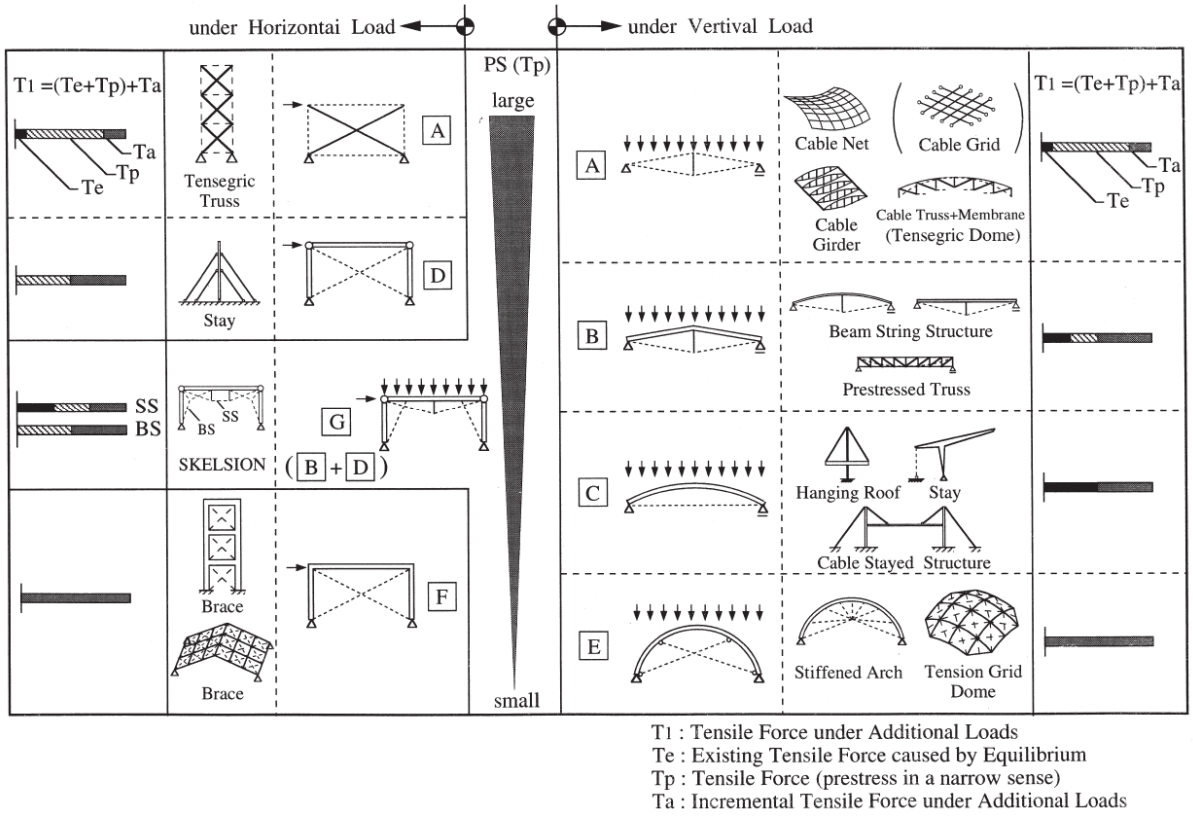


*Figure 2-66 – Hybrid String Structure Classification.*[55]

Alternatives to the free pins have been considered by Al-Sadder et al. (2007), these alternatives may be of interest in investigating adaptations of simple cable-chain arches where springs are considered as an alternative to free pins.

It is noted though that nominal pretensions are required to stabilise arches under gravity loads by Harrhuis (2012) when investigating his glass barrel-vaulted arch, but his investigation focussed mainly on the displacement and performance under accidental damage. The arches investigated

[55]Saitoh, M., & Okada, A. (1999). The role of string in hybrid string structure. *Engineering Structures, 21*(8), 756-769. doi:10.1016/S0141-0296(98)00029-7

are typically semi-circular (Harrhuis, 2012; Li et al., 2011) with a correspondingly low number of segments resulting in wide angles between the cables and the struts.

## 2.15 Snap-through of Arches.

Snap-through of structures are where a structure buckles with an associated gross displacement and shifts into an alternative yet potentially stable geometry. Snap-through structures hold considerable interest for researchers because of their ability to significantly change form and store energy as a result of this change. For small scale electronics and sensors, this presents an opportunity whereby a pressure pod on a mechanical system could 'work' a snap-through arch to generate energy and store this in a small battery (Bruns, Sigmund, & Tortorelli, 2002) to power its sensor. For difficult to access sensors in inhospitable environments, harnessing snap-through behaviour to generate and store power could present interesting opportunities for continued sensing see Figure 2-67. It may even be that the sensors are designed only to awaken once an arch has been forced to snap-through into a position that completes an electrical circuit, meaning that it can be placed in a sleep state when nothing of interest is occurring from the perspective of the sensor.

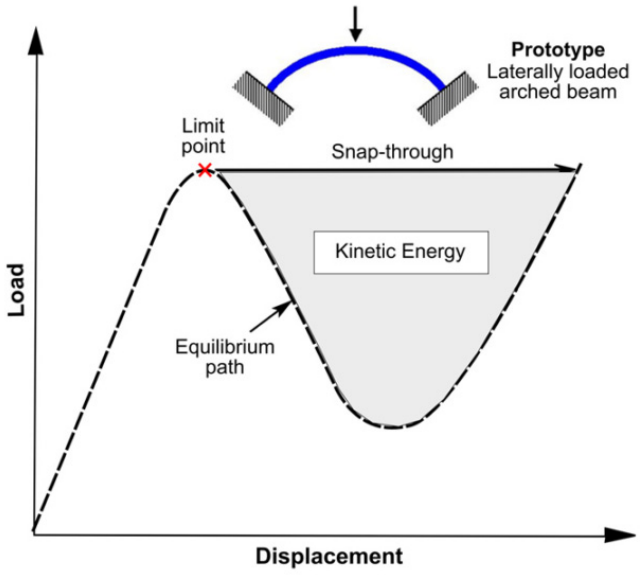


*Figure 2-67 - Snap-Through Arch and Kinetic Energy.*[56]

[56] Hu, N., & Burgueño, R. (2015). Buckling-induced smart applications: recent advances and trends. *Smart Materials and Structures, 24*(6), 063001.

Snap-through behaviour of structures though is not always a positive behaviour. For example, Vu, Richard Liew, and Anandasivam (2006) noted that for their lightweight and deployable structures, a shallow inclination ratio (angle between the strut and the cable) led to undesirable snap-through effects and catastrophic instabilities within certain structures. With the angle between the cable and the strut being directly influenced by the curve type selected and the number of units that the curve is then subdivided into for the structures they were investigating.

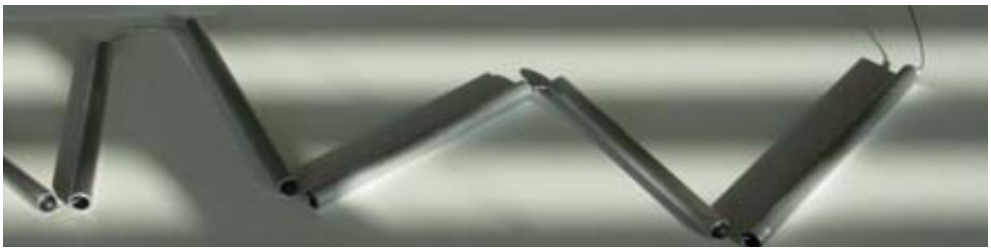

*Figure 2-68 - Segmented Compression Pipe.*[57]

Segmented arch structures can be utilised as deployable structures, for example, the aluminium poles used in tensairity arches (Laet et al., 2009), see Figure 2-68. These types of segmented arches, cable-chain arches, and tensegrity prisms (Motro, 1992; Snelson, 1996) make use of cables to increase their stability but this brings about a risk in that cables within a structure are only effective when placed in tension. Any changes in geometry or gross deflections that move the two connecting points of the cable together will cause the cable to lose tension and if allowed to go slack this element will present no meaningful contribution to the performance of the structure other than perhaps acting as a safety cable in the case of gross failure.

The specific concern with snap-through on cable-chain arches is that whilst snap-through can be controlled and balanced on flexible rods for MEMS and sensor design, for a cable-chain structure if the displacement is gross and inversion of the uniplets occurs then it may be that the tying cable, which is ordinarily beneficial, goes slack and loses all contribution to the stability of the arch. This removal of a structural element will mean that the chain of uniplets which was stable, now transforms into a series of linked pins that is a mechanism and consequently unstable.

To overcome this, it is common to place a pre-tension into cables to counter the potential de-

[57] Laet, L. D., Luchsinger, R. H., Crettol, R., Mollaert, M., & Temmerman, N. D. (2009). Deployable tensairity structures *Journal for the International Association for Shell and Spatial Structures, 50*(161), 121-128.

tensioning of structures under a variety of load cases, the pre-tensioning of cables and how this can be used to alter and control structures as noted in section 2.9.2 of the literature review.

## 2.16 Buckling and Deployable Structures.

Buckling is an active area of research (Hu & Burgueño, 2015) with applications ranging from the consideration of smart sensors and generating power for the cells through buckling motion (Smith & Chase, 2001) and harnessing the energy captive in snap-through buckling (Bruns et al., 2002) to the non-linear stiffness of composite I beams (Lachenal, Daynes, & Weaver, 2014) and the use of smart materials and bio-inspired buckling of rods (Shan & Chen, 2013). The complexity inherent within non-linear geometrical behaviour and materials is gaining momentum and elastic instability is a growing area of research.

Buckling can be used both to aid the deployment of a deployable structure as with elastica and ribbon-based hoops (Yoshiaki et al., 1992) and, just as with permanent structures, buckling needs to be carefully considered when the structure is in service. The introduction of rotational springs (Raskin & Roorda, 1996) to simplify the modelling of a pantographic structure demonstrates that from an analysis perspective the introduction of rotational springs and hinges can aid the simplification of analysis of complex mechanisms, but equally, it is proposed that suitable rotational springs may present similar benefits for physical structures.


*Figure 2-69 - Elastic Instability Papers Published.*[58]

[58] Hu, N., & Burgueño, R. (2015). Buckling-induced smart applications: recent advances and trends. *Smart Materials and Structures, 24*(6), 063001.

Taking the review by Hu and Burgueño (2015) (see Figure 2-69) it is proposed that the application of elastic instability can be defined into two core areas of research, these are energy-related and motion-related applications. Energy-related applications earn their name through either the creation or dissipation of energy (Kalathur & Lakes, 2013). Whereas motion-related elastic instability relates to structures that have gross deformations (Friedman & Ibrahimbegovic, 2013; Knippers & Speck, 2012; Schleicher et al., 2015) such as snap-through behaviour (You, 2007) to lock structures in position or where the geometry is changed radically (Hachem & Hanaor, 2005; Santer & Pellegrino, 2008 ) through buckling to form an adaptive structure (Knippers & Speck, 2012) such as a flectofin façade or the façade of the EXPO Pavilion in Korea (see Figure 2-70 and Figure 2-71).

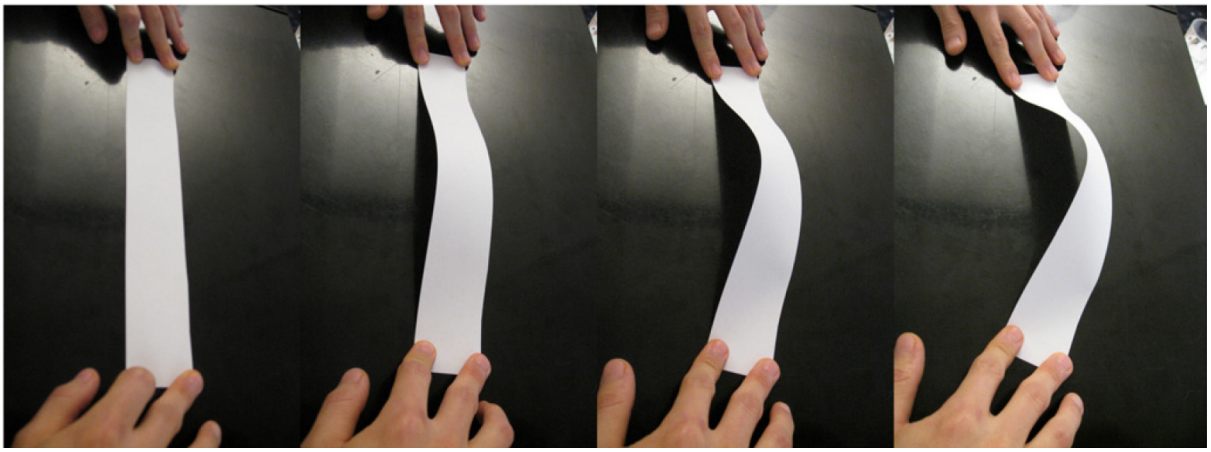

*Figure 2-70 - EXPO 2012 Kinematic Principles Behind Adaptive Façade.*[59]

Adaptive structures are not always of this scale of a large façade as shown in Figure 2-71 and there is considerable research into the use of flexible structures for energy generation in Micro-Electro-Mechanical Systems (MEMS). MEMS are being used to integrate sensors across our industrial sectors as well as our infrastructure, with the ability to provide constant power being a particular challenge. Significant research is underway to develop power sources for sensors connected in remote or difficult to access locations with regards the 'Internet of Things' through micro (and quantum) devices through to looking at similar challenges on larger structures such as predicting and controlling buckled forms (Smith & Chase, 2001).

[59] Knippers, J., & Speck, T. (2012). Design and construction principles in nature and architecture. *Bioinspiration & Biomimetics, 7*(1), 1-10.

*Figure 2-71 - EXPO 2012 Adaptive Façade.*[60]

One point to note is that whilst the examples such as the EXPO 2012 façade are grand in scale, the axial load-carrying capacity of the fins is negligible and the elements are typically manufactured from relatively flexible materials compared to steel or timber structural sections. The fins are generally held in position at their ends with these supports manipulated to push the fins into a specific shape.

It may be that the introduction of a targeted spring (or springs) on a rigid strut could lead to the development of a structure that has greater axial load-carrying potential than the flexible fins considered thus far whilst still maintaining the ability to adjust its geometry in a metamorphic structure kind of behaviour. For a structure of this nature to be appropriately analysed, it is important to first consider the theory of buckling of sprung struts and this is covered in more detail in chapter 4.

During writing this thesis, sample springs of the magnitude required to integrate into a strut of appropriate size were attempted to be procured, but many of the large heavy-duty torsional spring providers were unable to helically wind stock wire of an adequate diameter to achieve the types of rotational stiffnesses required. It is likely that alternative methods of rotational springs

[60] Knippers, J., Nickel, K. G., & Speck, T. (2016). *Biomimetic research for architecture and building construction : biological design and integrative structures*: New York, NY : Springer Berlin Heidelberg.

such as the introduction of a bi-material joint (Gibson, Goenka, Narasimhan, & Bhat, 2010) that could be 3D printed and combining stiff rigid struts with a flexible rubber-like hinge in the middle with a much lower stiffness to achieve flexibility.

Or the introduction of reduced geometrical properties in elements such as a living hinge (González, Kerl, & Engineers, 2008) which can be used to create regions of flexurally compliant structures (Santer & Pellegrino, 2008) that can make rigid plywood (up to 22mm in thickness) able to fold 180 degrees numerous times with no signs of distress. These kinds of manufacturing techniques, however, are still maturing to a scale that is appropriate for a building or large structural element, but they are maturing quickly.

Further thoughts on developing large scale linear springs that are appropriate for integrating into buildings are considered in section 5.10 of this thesis.

## 2.17 Summary.

Non-static structures can be broadly split into three over-arching categories: demountable, deployable and adaptable (sometimes referred to as metamorphic):

- Demountable structures essentially are structures that can be subdivided into smaller components and disassembled to aid with relocation and general transportability.
- Deployable structures can fold into a small form to aid with transportation (for example within a space rocket) that are then able to expand in a controlled fashion, typically with a single degree of freedom, into the final deployed state.
- An Adaptive structure can change its arrangement or geometry to respond either passively or actively to an external force or condition.

Deployable structures and adaptive structures are active areas of research, with step changes in the research typically being driven by leaps in technology: either through materials, analysis methods, or control methods.

Typically, deployable and adaptive structures have much in common with lightweight structures to reduce the self-weight to correspondingly reduce the forces/energy required to deploy.

Strut-based structures are perhaps the longest researched deployable structures, with linkages being developed since the 18$^{th}$ Century to develop motion and movement. The connection of rigid links through a combination of different forms of lower joints can result in a broad range of motion that can be controlled using controlled displacement using elements such as actuators or strategically located cables to develop motion and stabilise structures.

Deformable components, such as cables and membranes, can be brought together to increase structural efficiency for deployable and lightweight structures, for example, to create a tensegrity prism or a cable-chain arch although these types of structure can be vulnerable in certain instances to effects such as snap-though.

Whilst having low structural redundancy can be a positive benefit for a deployable structure, allowing it to transform from a structure to a mechanism and back again, it does increase its vulnerability to collapsing from being misloaded or through accidental damage.

It was suggested that perhaps the introduction of rotational springs to replace free pins may aid with the structural robustness of deployable structures and their ability to resist accidental damage, but that this may affect the size of the structural elements in order for them to resist the additional bending moments generated from rotational springs when the joints rotate.

Snap-through on cable-chain structures is a concern when the angle between the cable and the strut on a uniplet becomes shallow allowing the uniplet to flip as a result of the systems localised stiffness and this angle is often avoided through limiting the number of segments within a cable-chain arch and adopting a semi-circular geometry, both of which help with maintaining a steeper angle of the modules.

An alternative was proposed to limit the effects of snap-through buckling which was to exchange the free pin and the cable in a uniplet arrangement for a rotational spring. Whilst this will locally stop the snap-through as the element will be able to flex around the hinge with resistance from the spring, it brings about an additional problem of ensuring the buckling behaviour of this new uniplet can be determined appropriately.

It was proposed that the introduction of rotational springs to replace free pins could be beneficial for a deployable structure and could be introduced to a structure to have the following potential positive effects:

- Reduction of risk due to disproportionate collapse due to increased structural redundancy,
- Controlling motion during deployment,
- Mimicking the behaviour of a flexible rod such as those used in adaptive facades,
- Remove risk associated with snap-through,
- Forcing a deployable structure to hold a specific position in the event of a mechanical failure or a power cut.

However, the introduction of a rotational spring may impact the behaviour of a lightweight structure as this form of structure is ordinarily designed to act in either tension or compression and the inclusion of a rotational spring will start to develop additional bending moments as the structure displaces and this may result in a more inefficient design due to the larger section sizes needed to resist the additional moment.

However, there is little published literature regarding cable-chain arches and the next chapter will focus more closely on the behaviour of cable-chain arches, their geometrical properties and will demonstrate how instabilities can affect the performance of the arches through modelling of various example arches.

# Chapter 3

## 3 Cable-Chain Arches.

Following the previous section introducing issues associated with snap-through on hybrid deployable structures where cable angles are shallow, this chapter will start to investigate the behaviour of cable-chain arches plus their potential to suffer snap-through behaviour. Given that there is minimal literature available on the specific behaviour of cable-chain arches, this chapter will focus on generating the geometry configured using the common alternate node stringing pattern that is used for the habitable arrangement of a cable-chain arch (such as Rubb structures hangars) as this arrangement has the potential to return shallow angles under certain parameters which may make the structure susceptible to snap-through buckling of the uniplets.

In addition to the structural behaviour under load, other geometrical parameters will need to be considered such as the internal habitable space that will be important when determining the suitability of the structures. Initially, a simple static elastic modelling process will be used with different geometrical curves that will be subdivided into a series of equal length links to maintain an element of regularity to the structure. Initial models will have their geometry generated and assessed through the writing of scripts in Mathematica.

The intention of this chapter is not to determine the precise angle and stiffness relationship for cable-chain arches to develop snap-through, it is instead intended to establish and validate that snap-through can be a governing and critical factor when designing these types of structures and that an alternative connection using rotation springs may aid with removing this susceptibility.

This chapter will also start to introduce basic Mathematica coding principles for generation of geometry and also solving of systems of equations which will be further developed in section 4 where the finite difference method and ill-conditioning will be investigated further. Blocks of Mathematica syntax will be identified clearly within the writing to ensure it is obvious where code has been shared rather than reams of syntax buried in an appendix.

## 3.1 Methodology.

The investigation into the cable-chain arches intends to determine the effects that a change in curve type for the geometrical definition of the arch and its subsequent sub-division into different numbers of equal length segments will have upon the habitable area and structural performance with regards snap-through. See Figure 3-1 for an example of how the number of segments (nSeg) can vary the habitable area (shown in pink) available between the cables.

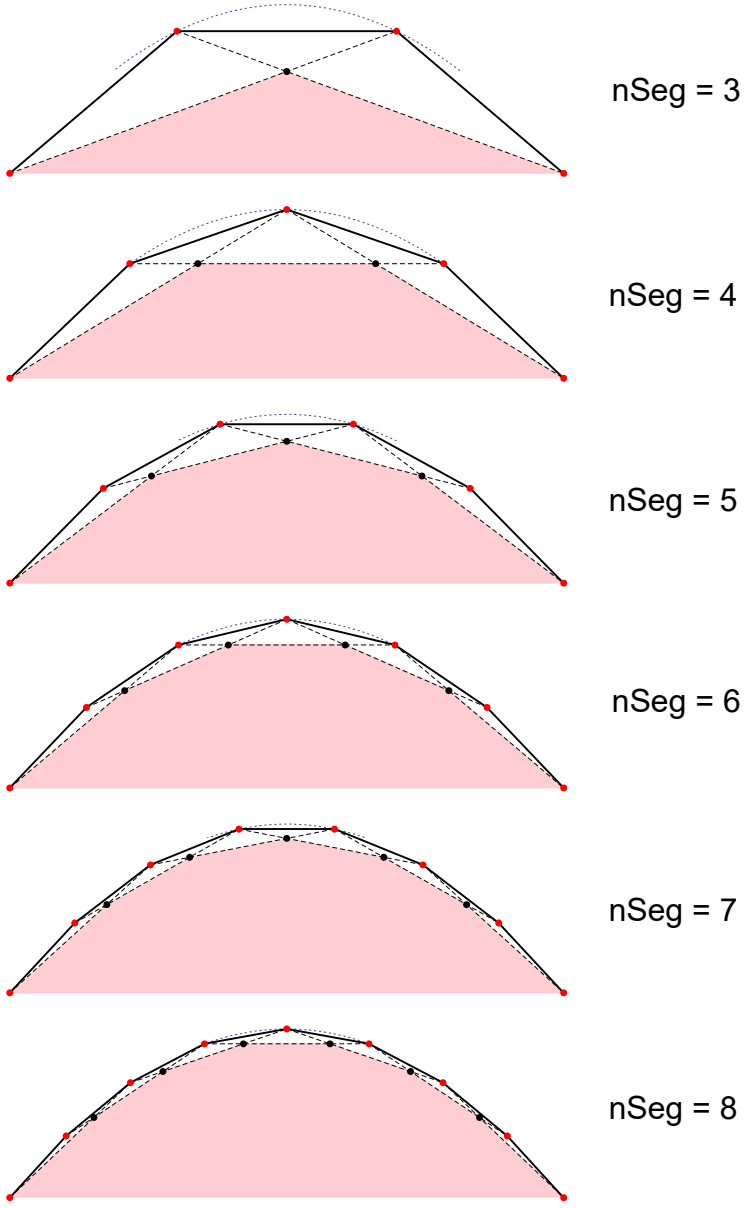


*Figure 3-1 Effective Values Of nSeg For A Cable-Chain.*

Whilst the above demonstrates that a high number of segments provides a greater habitable area, it also reduces the angle between the cables and the struts with this stringing pattern which Vu et al. (2006) have noted as being critical with regards snap-through buckling of tension-strut

structures. Given the large range of different families of curves, the investigation will initially focus on just two types. The first being semi-circular (radial) geometry, which has the benefit of uniform internal angles when divided into equal-length segments. The second type to be considered is parabolic curves, which tend to have flatter sides (and consequently shallower angles between the cables and struts) plus the potential to use different span/depth ratios to control the available internal area.

## 3.2 Radial Geometry.

The radial geometry is defined in part by assuming that the arc being defined is created as a true semi-circle, which lends the associated geometry to be compatible with many of the platonic solids. By allowing the curvature to be limited in this manner means that the span of an arch under consideration will be equal to the diameter of the circle, whilst the rise of the arch will similarly be equal to the radius of the same circle (Figure 3-2).

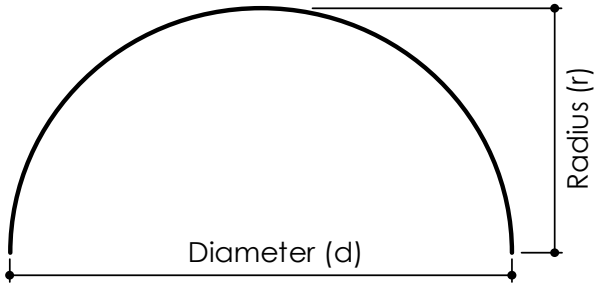


*Figure 3-2 Semi-Circle Geometry Relationship.*

Commonly a cable-chain arch subdivides this curved section into a series of uniplets to allow the mass manufacture of the structural elements within the workshop. The number of subdivisions for the arch varies from design to design with no published guidance available on the optimum number of subdivisions for a cable-chain arch. If the curved section is divided into a series of linear segments, then let the number of linear segments be $n_{seg}$ with the arch shown in Figure 3-3 defined by a value of $n_{seg} = 4$.

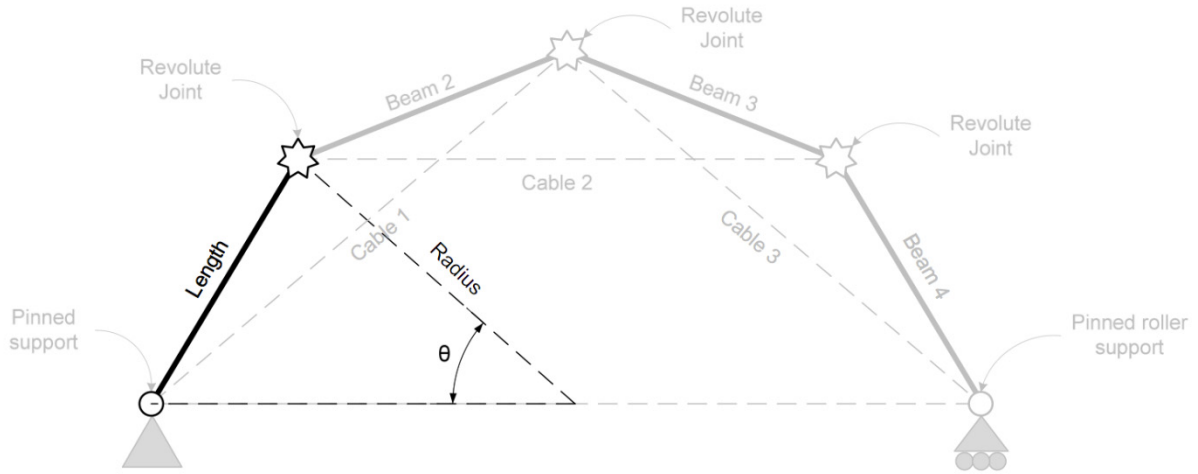


*Figure 3-3 Radial Geometry Defining Single Link.*

As a semi-circle by its definition has a total internal angle of 180°, the internal angle ($\theta$) of each uniplet is defined as follows:

$$\theta = \frac{180}{n_{seg}} \tag{3.1}$$

By assuming that the geometry is based on a semi-circle and thus that the centre of the circle lies at an elevation equal to the supports, it becomes possible to apply the Cosine rule to determine the length of the strut, taking the other two sides of the triangle as being equal in length and both equal to the radius (r) of the enclosing circle.

$$L_{strut} = \sqrt{2r^2 - 2r^2 Cos\left(\frac{180}{n_{seg}}\right)} \tag{3.2}$$

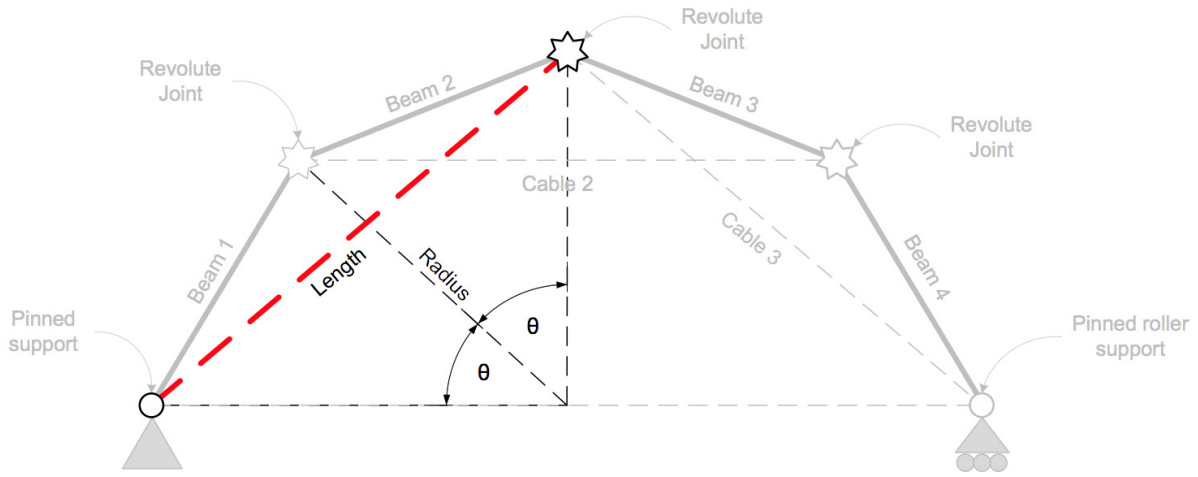


*Figure 3-4 Radial Geometry Defining Single Cable.*

A similar technique can be utilised to determine the lengths of the tie cables within the cable arch shown dashed and in red on Figure 3-4.

$$L_{cable} = \sqrt{2r^2 - 2r^2 Cos\left[2\left(\frac{180}{n_{seg}}\right)\right]} \tag{3.3}$$

These two equations now allow the geometry of a cable-chain arch, based on semi-circular geometry, to be determined. Before moving further into the analysis and development, let us consider the geometry of a cropped circle geometry arch and then a parabolic cable-chain arch.

## 3.3 Cropped Circular Geometry.

Consider a radial segment where the bottom arc of a circle is removed as shown in Figure 3-5 where the bottom portion of the circle is curtailed by a length $\alpha$.

$$\theta = Tan^{-1}\frac{r-\alpha}{\sqrt{(2r-\alpha)\alpha}} \tag{3.4}$$

$$\psi = Cos^{-1}\left(\frac{r^2 - 4r\alpha + 2\alpha^2}{r^2}\right) = 2Tan^{-1}\left(\frac{\sqrt{(2r-\alpha)\alpha}}{r-\alpha}\right) \tag{3.5}$$

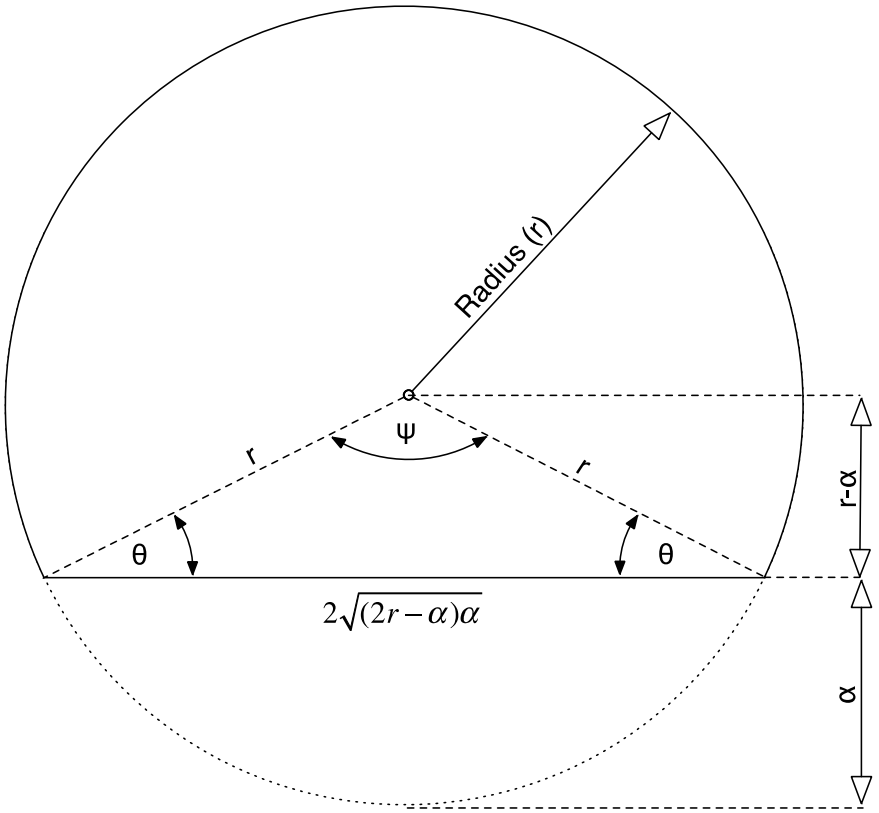


*Figure 3-5 Segmental Geometry.*

Through the removal of part of the circle, this will leave the remaining angle $\psi$ which is defined in the equation (3.5) and can now be used to determine the remaining angle within the circle. Dividing this remaining angle will determine the internal angle ($Angle_{nSeg}$) for each segment of the remaining circle as defined in (3.6).

$$Angle_{nSeg} = \frac{360 - \psi}{n_{Seg}} \tag{3.6}$$

The individual angle for each segment is then defined and strung with tension only elements, shown as dashed lines in Figure 3-6, ready for analysing for its geometrical and structural properties as defined above.

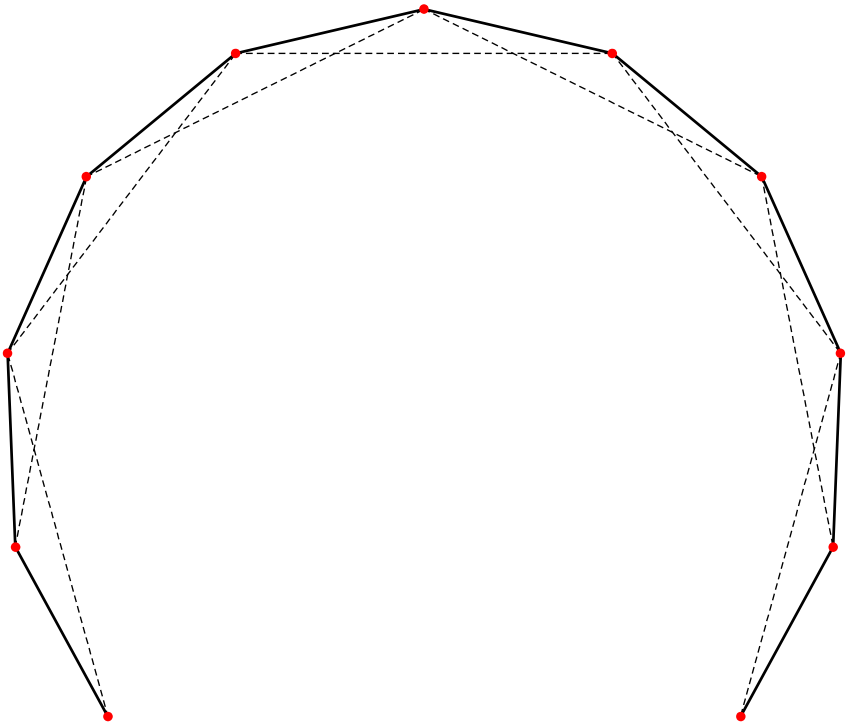

*Figure 3-6 - Cable-Chain Arch With Curtailed Radial Geometry.*

Considering the geometry for a fixed number of segments, the amount that is cropped from the bottom of a series of circular geometry can be seen in Figure 3-7 where the radius (r) is kept constant at 10m, but the amount cropped off the bottom of the circle (α) varies between 1 and 10 creating significant differences in geometry.

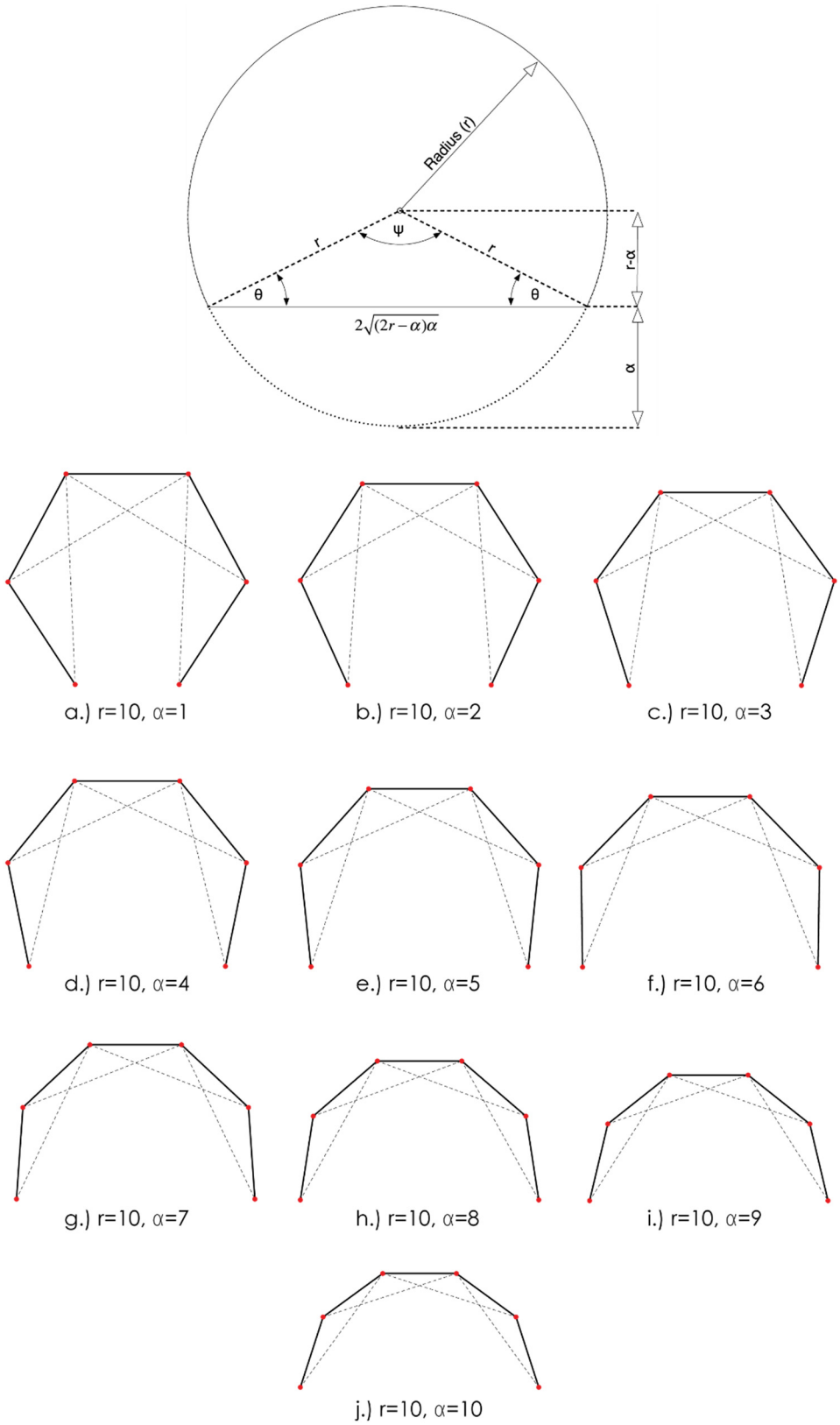


*Figure 3-7 – Varying Semi-Circular Geometries Constant R, Varying Alpha.*

For the same number of segments, it can be seen that cropped circles have a larger internal angle between the cables and the struts compared to semi-circles.

## 3.4 Parabolic Geometry.

Parabolas are widely used in engineering, with parabolic cable profiles being interchanged with catenary cables in structures such as suspension bridges.

A parabolic profile is typically defined using the following expression:-

$$f(x) = ax^2 + bx + c \tag{3.7}$$

This form gives the typical line and layout of a parabolic curve.

Determining the length of a parabolic curve between two defined points, such as point a and point b, can be solved using integration.

$$Length = \int_a^b \sqrt{1 + \left(\frac{dy}{dx}\right)^2}\, dx \tag{3.8}$$

Using Mathematica to profile fit a curve through three defined points, it is possible to solve the resulting simultaneous equations to derive an expression for the resulting parabolic curve.

Considering an example based around a fictitious suspension bridge, spanning 4100m with a dip of 500m (see Figure 3-8), the following points could be used to determine the basic geometry of the resulting parabolic curve:

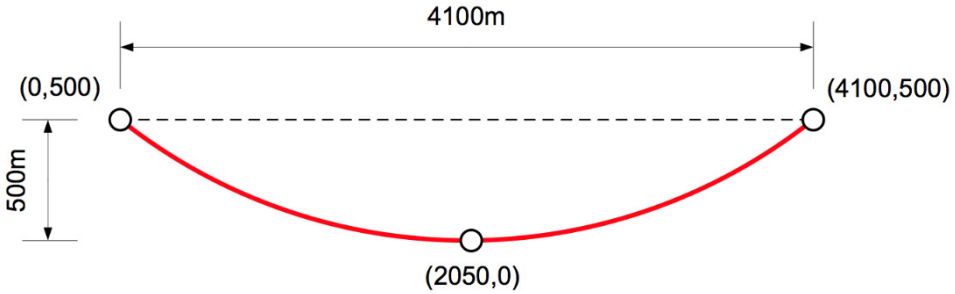


*Figure 3-8 Parabolic cable geometry.*

Taking the points (0,500), (2050,0), (4100,500) the following expression can be derived through solving the associated simultaneous equations.

$$\begin{aligned} ax_1^2 + bx_1 + c &= y_1 \\ ax_2^2 + bx_2 + c &= y_2 \\ ax_3^2 + bx_3 + c &= y_3 \end{aligned} \tag{3.9}$$

This can be solved to determine the variables: a, b, and c using linear algebra.

$$\begin{bmatrix} x_1^2 & x_1 & 1 \\ x_2^2 & x_2 & 1 \\ x_3^2 & x_3 & 1 \end{bmatrix} \begin{bmatrix} a \\ b \\ c \end{bmatrix} = \begin{bmatrix} y_1 \\ y_2 \\ y_3 \end{bmatrix} \tag{3.10}$$

Solving for the above system gives:

$$f(x) = \frac{x^2}{8405} - \frac{20x}{41} + 500 \tag{3.11}$$

Plotting this function against the original points in Mathematica (Figure 3-9) shows that the curve is a good fit and passes through the original points as defined.

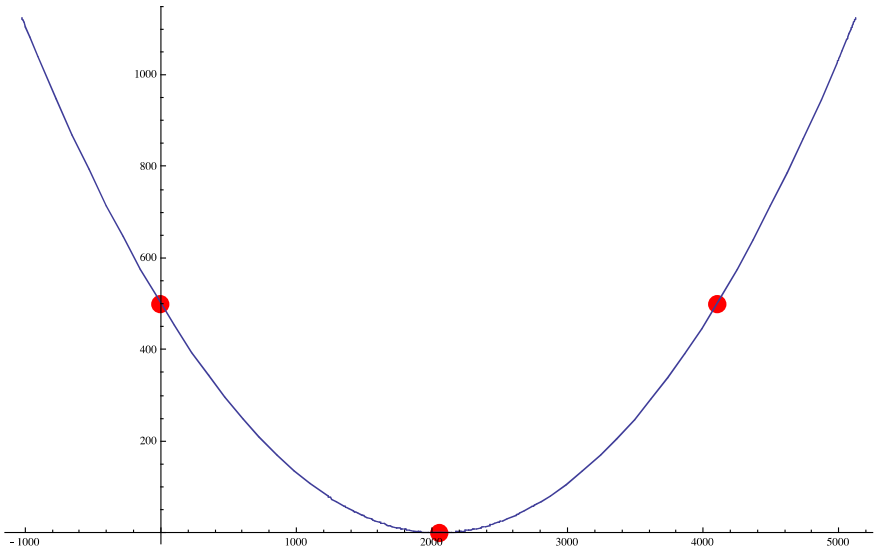


*Figure 3-9 Parabolic Expression And Points Plotted.*

Similarly, as part of the calculation automation process, a Mathematica sheet has been written to not only define and determine the parabolic geometry based on the input of three coordinates but to numerically integrate the expression between the two support points as can be seen in (3.12).

$$Length = \int_0^{4100} \sqrt{1 + \left(\frac{dy}{dx}\right)^2}\, dx \tag{3.12}$$

Where:

$$y = \frac{x^2}{8405} - \frac{20x}{41} + 500 \tag{3.13}$$

Converting this into code that is recognised within Mathematica is straightforward by firstly defining the parabolic equation as a function of x; f(x), then calling upon the NIntegrate function

in the second line. For speed and convenience, the differential of the function is simply referenced as f ′(x) within the code and finally, the limits for the integration are defined as the final variables.

*Mathematica Snippet 1 – Numerically integrate the curve to find the length.*

```
f[x_]:=500 - (20 x)/41 + x^2/8405;

NIntegrate[Sqrt[1 + (f'[x])^2], {x, 0, 4100}]
```

This numerically integrates the expression between the defined limits and provides the overall length of the cable between the supports, which for this example is 4,257.24m.

## 3.5 Number Of Segments.

As previously discussed a semi-circle can be simply divided into even segments ($n_{Seg}$) through determining the internal angle. The greater the number of segments, the smaller the internal angle between the cable and the struts, as can be seen in Figure 3-1. With more and more segments, the combined straight lengths start to approach a good approximation of the total curved length.

Whilst determining the strut lengths ($L_{Strut}$) for semi-circular cable-chain arches is straightforward, see equation (3.2), for a parabolic curve subdividing into segments of equal length, is more complex as the internal angle cannot be easily defined through a common central point. To subdivide a parabolic curve into a series of equal straight lengths between points (rather than even curved lengths) a series of equations need to be established that can be solved simultaneously. Each segment of the curve is equal to $L_{Strut}$ with the length determined using simple trigonometry applied to the Cartesian coordinate.

To ensure that real values can be found for these lengths for parabolic curves, several initial conditions must be met, and whilst these may appear obvious it is important that they are established before trying to solve the series of simultaneous equations using mathematical software, these conditions are listed below:

$$n_{Seg} \in \mathbb{N} \tag{3.14}$$

$$n_{Seg} > 1 \tag{3.15}$$

$$L_{Strut} \in |\mathbb{R}| \tag{3.16}$$

$$x_1 < x_2 < x_3 \ldots < x_{n_{Seg}+1} \tag{3.17}$$

It should be noted however that for a cropped circle where the base span is less than the diameter, or any other curve that as an overall width greater than its base (as shown in Figure 3-10) the conditions of (3.17) will not always be applicable and indeed may prevent the series of equations from solving should they be ill-defined.

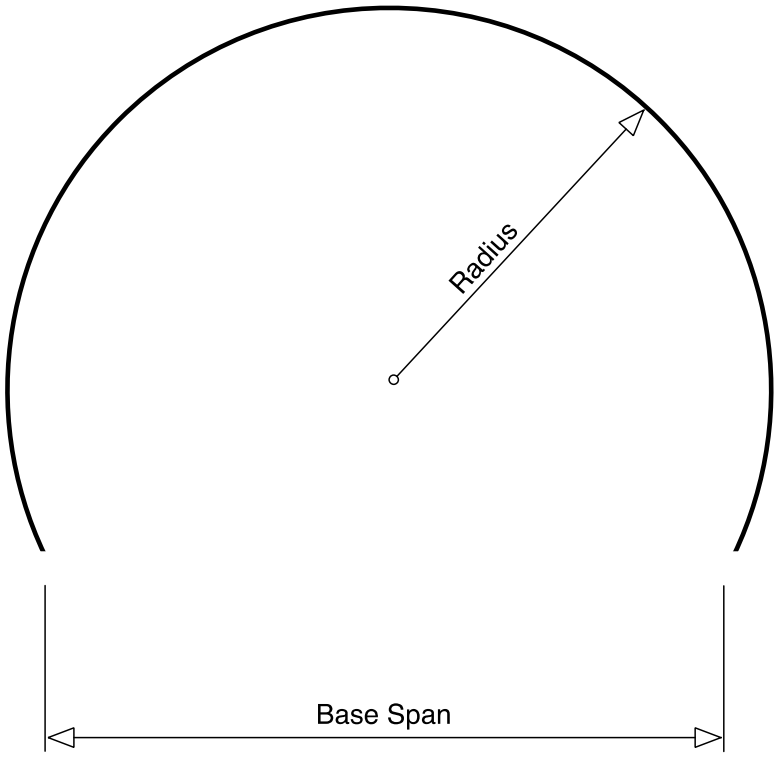


*Figure 3-10 Example Of Curve That Is Wider Than The Base Span.*

Figure 3-11 shows a cable-chain with an $n_{Seg}$ value of 6. As the number of segments is even there is a corresponding uneven number of coordinates along the curve to create the segments. This will help reduce the number of simultaneous equations to be solved due to the symmetry about the centre of the crown for the arch.

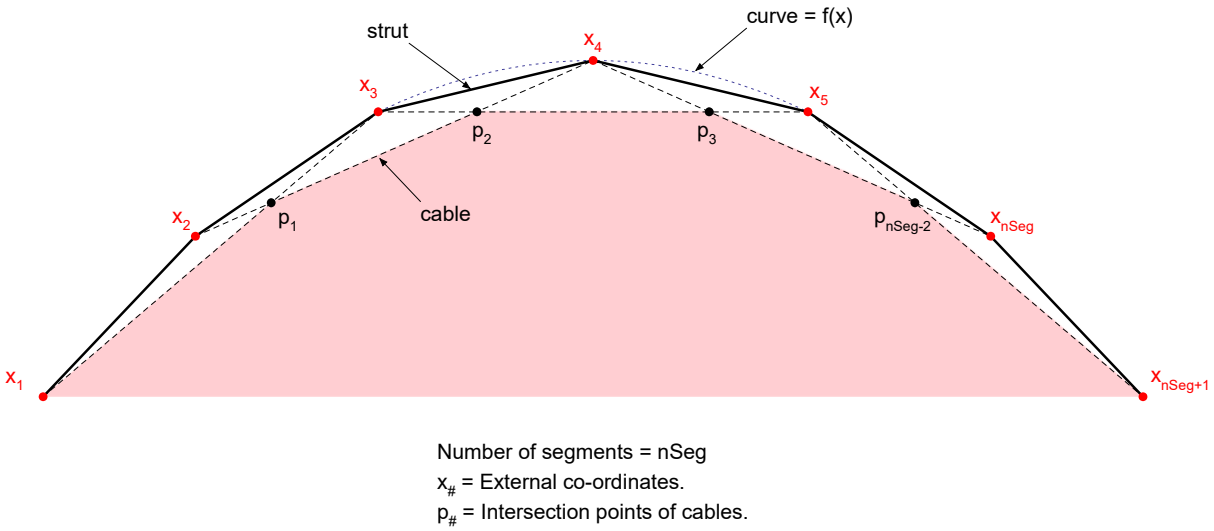


*Figure 3-11 Cable-Chain Structure With nSeg=6.*

Let the length of the element spanning between points $x_1$ and $x_2$ be defined as $L_{Strut}$. As a series of Cartesian coordinates, the point $x_1$ can be defined as $(x_1, f(x_1))$ as the y-ordinate is directly connected to the distance x along the curve's path.

$$L_{Strut} = \sqrt{\left(x_2 - x_1\right)^2 + \left[f(x_2) - f(x_1)\right]^2} \tag{3.18}$$

This expression can be generalised as:

$$L_{Strut} = \sqrt{\left(x_{i+1} - x_i\right)^2 + \left[f(x_{i+1}) - f(x_i)\right]^2} \tag{3.19}$$

*Where:*

*i is the number of the left-hand joint.*

The principle outlined in (3.19) can be nested within a table in Mathematica using the code below. Within this thesis, small snippets of code will be presented in black boxes and formatted in such a way as to be clear that they are Mathematica syntax.

*Mathematica Snippet 2 – Determine the segmental lengths through the chords.*

```
chordL = Table[
    Sqrt[(xi + 1 - xi])^2 + (f[xi + 1] - f[xi])^2],
    {i, 1, nSeg}];
```

In the syntax above, 'i' is an iterator that runs from 1 through to the total number of segments ( $n_{Seg}$) that the arch is formed from.

The above syntax creates a library for all the lengths of the chords along the curved line denoted by f(x) and stores these in a variable defined as chordL *(it is important to note that variables cannot begin with a capital letter as these are reserved within Mathematica for specific commands and functions).* The collection of equations within chordL is stored as a list, but they cannot be solved as a system until they are defined as being equal to a specific value. Essentially the equations are open-ended and by appending a common variable to each equation in the library the equations they can all be made to equal each other, or in other terms, they must all create a line of equal length but not direction. This is precisely what is required for a curve to be divided into equal straight lengths (as opposed to equal curved lengths) and simplifies the creation of the geometry for parabolic arches.

In the above example, the additional text to be appended is "==d" which will define each equation as being precisely equal to d due to the inclusion of the double equal signs, see Mathematica Snippet 3.

*Mathematica Snippet 3 – Make each symbolic chord length equal for solving simultaneous equations.*

```
combEqs = # == d & /@ chordL;
```

Now that a system of equations has been defined they can be solved within Mathematica. Early iterations of this process made use of the Solve[] function which worked well for solving the systems of equations where nSeg was less than 5, but once the level of complexity rose above 10, the solutions could not be arrived at in less than 24 hours of computation time.

Given that the coordinates are typically defined in millimetres, providing the solutions are similar to within 2 or 3 decimal places this would give an acceptable level of error as this would make a minuscule level of difference given typical fabrication tolerances in steelwork if manufactured to the National Structural Steelwork Specification 6th Edition. By exchanging the solving routines within Mathematica from the more complex `Solve[]` engine *(which can symbolically and numerically solve simultaneous equations)* for the `FindRoot[]` solver (*which solves equations numerically, ignoring imaginary roots)* the calculation time was reduced dramatically with no noticeable effect on accuracy. Using the numerical solver, the system of equations up to 20 or 30 segments could be solved in less than 10 seconds on the same computer presenting a significant improvement in solution times. Similar sets of equations have been solved numerically using Microsoft Excel, but limitations of the Solver engine started to show after approximately 12 segments, with different sheets needing to be created for symmetrical and non-symmetrical arches.

*Mathematica Snippet 4 – Numerically solve the equations to give a common root.*

```
ClearAll[vars, x];

vars = Append[{x#], #, Part[a, 1] + 10^-6,

upVal - 10^-6} & /@ Range[2, nSeg], {d, 1}];

sol = {FindRoot[combEqs, vars]}
```

The routine in Mathematica Snippet 4 will save the solutions as a list into the variable `sol`, which helps determine that each solution is identical as it can be inspected and subjected to Boolean validation criterion but cannot be used in further calculations due to its volatile nature. Through assigning the contents of sols for the $x_n$ parameters back into the vals variable, a schedule of coordinates that adequately define the curve can be created, see below.

*Mathematica Snippet 5 – Back-substitute solutions to give coordinates.*

```
vals = Table[xi, {i, 2, nSeg}, {d, 1}] /. sol[[1]]
```

This process can be repeated for any form of curve desired, providing that the y-ordinate can be defined as a function of x and for any reasonable number of segments. Trials with the sensitivity of the solution of the equations have shown that establishing geometry based on dimensions in millimetres increases the success of the solution of the equations, and it is presumed that the increase in magnitude helps reduce errors introduced using MachinePrecision numbering system in Mathematica as a similar process was needed within Excel.

## 3.6 Additional Geometrical Constraints.

The establishment of the external arch geometry for the cable-chain arch has been defined to create uniform strut lengths. This provides benefits in terms of manufacturing and checking for local buckling failure mechanisms, but, where a shelter is to be defined as habitable, either for people or for another purpose such as an aircraft hangar or storage, the available internal area is another important criterion that should be considered during the early stages of geometrical definition.

### 3.6.1 Internal Area.

The total internal area that is available is not always the area contained within the node points of the strut elements as the cables themselves also intrude into the arched structure.

Whilst the internal area of a polygon is relatively straightforward to determine, for a cable-chain structure that is strung in an orthodox manner appropriate for habitation this first requires the

cross over points of the internal cables to be determined. This is critical in that the cables will create a constraint for the internal use of space as they will reduce the available longitudinal cross-sectional area available between ribs if the arches were arranged in a tunnel formation for example.

The least efficient space would be where the nSeg value is at its lowest acceptable value of 3. Conversely, as nSeg approaches ∞, the internal area becomes approximately equal to the area enclosed by the curve itself as the facets become very small. Given that the cables start and end at a defined x coordinate, they can be defined quickly as vectors. For a cable-chain arch with nSeg = 4 the useable internal area is shown below in Figure 3-12 and is enclosed by the points $P_1$, $P_2$, $P_3$, and $P_4$; where the internal cables intersect (note that a new generic local numbering system is in place specifically for this example).

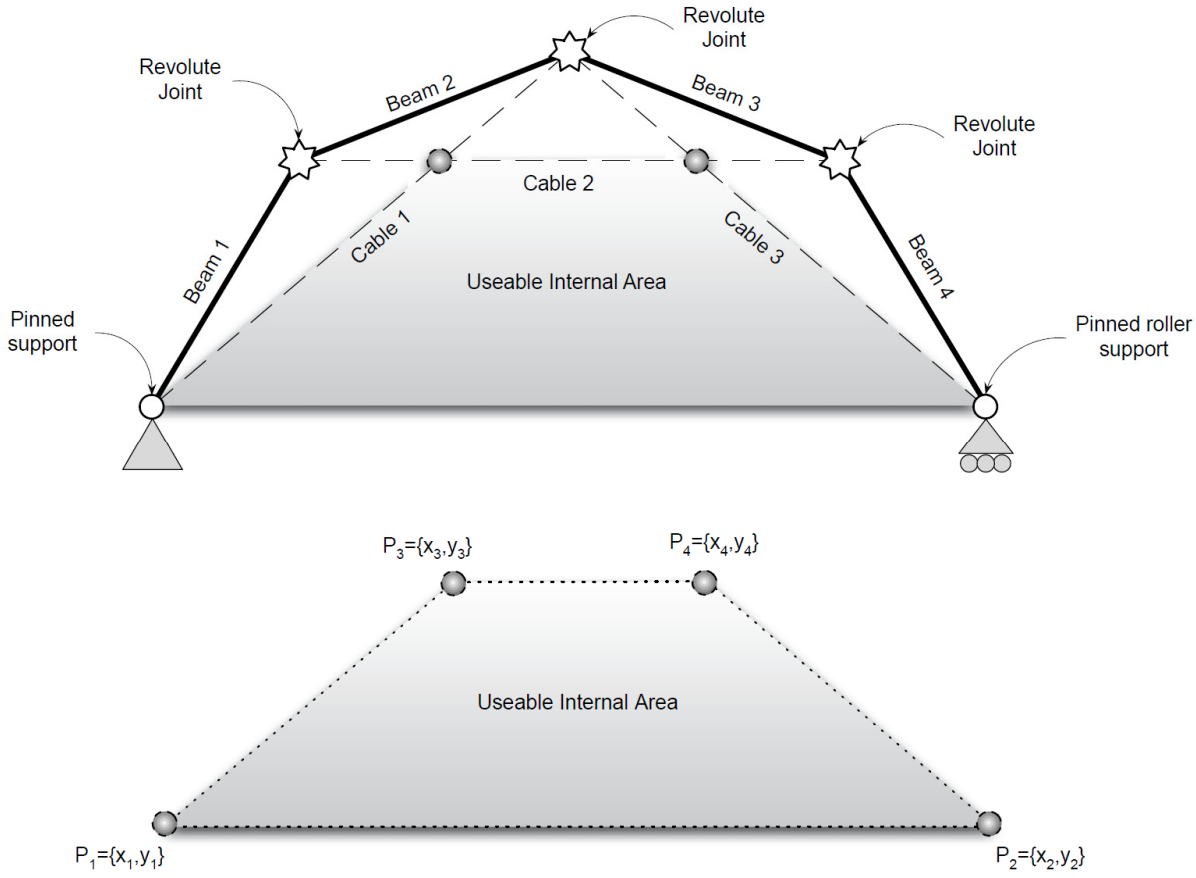


*Figure 3-12 Available Internal Space.*

The internal area of a polygon is defined by:-

$$Area = \left| \frac{(x_1 y_2 - y_1 x_2) + (x_2 y_3 - y_2 x_3) \ldots + (x_n y_1 - y_n x_1)}{2} \right| \tag{3.20}$$

To determine the intermediate coordinates where the lines intersect, vector-based geometry is used to determine the intersection points $P_1$, $P_2$, $P_3$, and $P_4$. To illustrate this principle, two cables are extracted and considered in isolation in Figure 3-13.

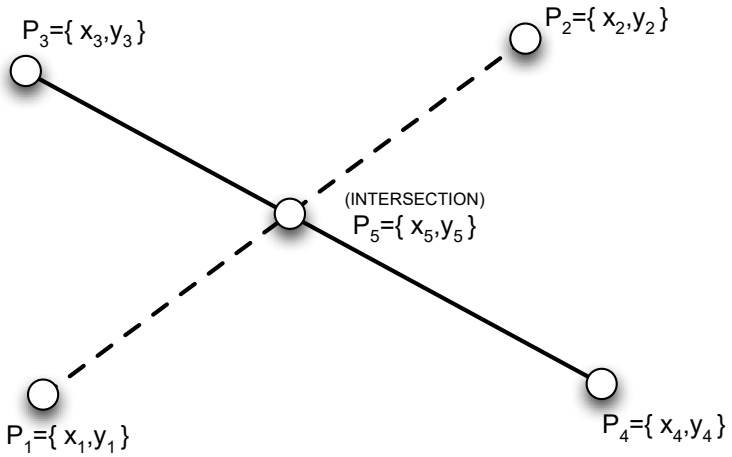


*Figure 3-13 Intersection Of Two Lines.*

To find point $P_5$ in Figure 3-13 the assembly of the Cartesian coordinates into a vector-based equation will be required (Hirst, 1995, p15).

By defining the coordinates as a vector-based equation in the general form below, the intersection can be solved using simultaneous equations.

$$\begin{aligned} Line_1 &= (1-\lambda) P_1 + \lambda P_2 \\ Line_2 &= (1-\mu) P_3 + \mu P_4 \end{aligned} \tag{3.21}$$

Through inputting the coordinates as vectors, the two equations can be solved for $\lambda$ and $\mu$ respectively, then through back substitution, the equation can be solved for $P_5$. Given that the intersection of the two points has a discrete solution for each pair of equations, the Solve[] function can be used within Mathematica with no noticeable time penalty. An example of how this is achieved, complete with Mathematica syntax is illustrated in Figure 3-14 and Mathematica Snippet 6.

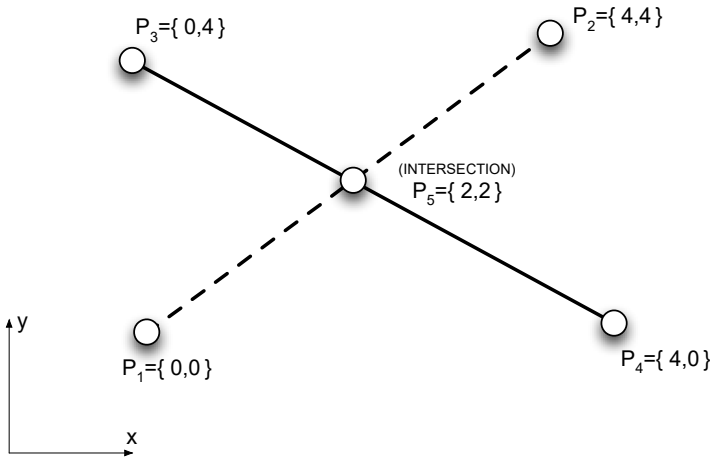


*Figure 3-14 Intersection Example.*

For the four points below, restructure the four points into their vector form and then solve for the remaining variables and back-substitute into Mathematica to determine the point at $P_5$.

*Mathematica Snippet 6 – Solve simultaneous equations for vector cross over points.*

```
{p1, p2, p3, p4} := {{0, 0}, {4, 4}, {0, 4}, {4, 0}};

Solve[{(1 - λ) p1 + λ*p2 == (1 - μ) p3 + μ*p4}, {λ, μ},
                                    Reals];

p5 = Flatten[(1 - λ) p1 + λ*p2 /. %]
```

## 3.7 Habitable Area.

As cable-chained arches can be longitudinally stacked to create tunnel tents, the habitable area is often of interest, but cannot be defined purely as the internal polygonal area as it will also need to be defined concerning the proposed inhabitants of the structure. This could be people, storage, or even machinery that needs to be contained within the structure. To assess the suitability of a proposed geometry to be used for habitation there will be a requirement for a minimum headroom, whilst the structures may be temporary – families could be living in them for several months and so the quality of space will be important. The provision of this taller space does not, however, have to be uniform across the total cross-sectional area as seen in Figure 3-15, this space could be subdivided into prime habitable space and secondary sleeping/storage space.

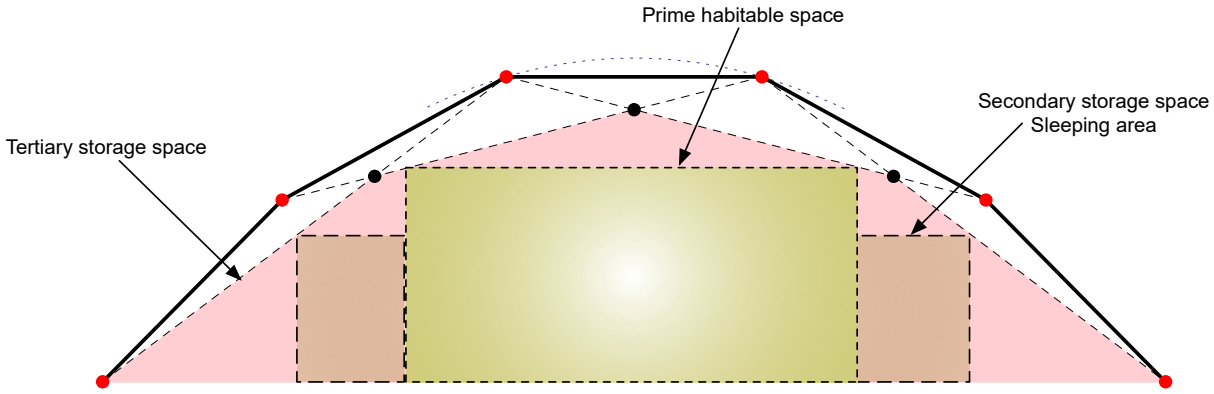


*Figure 3-15 Useable Space.*

The subdivision of internal areas may take into consideration the cable arrangement within the structure as shown by the pink area bounded by the cables, but it should be noted that between the ribs there may be more space, although the intention for the shelters is to not guillotine the occupiers should they run between the ribs.

The use of the internal volume will vary depending on the application, for example, an arch used as an aircraft hangar will only be governed by the volume enclosed by the cables, whereas a disaster relief shelter may make use of the secondary and tertiary areas that are lower than the headroom requirements for storage, as illustrated in Figure 3-15.

Indeed, should the structure be used for human habitation then the habitable area between the cables that achieved a minimum allowable headroom can be defined and an imaginary line can be drawn.

Subdividing this horizontal line into several points, spaced at 1mm intervals, allows each point to have a Winding Number check applied to assess if it sits within the polygon (adequate headroom) or outside the polygon (inadequate headroom).

For a given polygon, a point is said to be located within a polygon if its Winding Number is greater than zero, see Figure 3-16.

$$\text{winding number} = \frac{1}{2\pi}\oint_C \frac{x}{r^2}dy - \frac{y}{r^2}dx \tag{3.22}$$

*Where:*

$$r^2 = x^2 + y^2$$

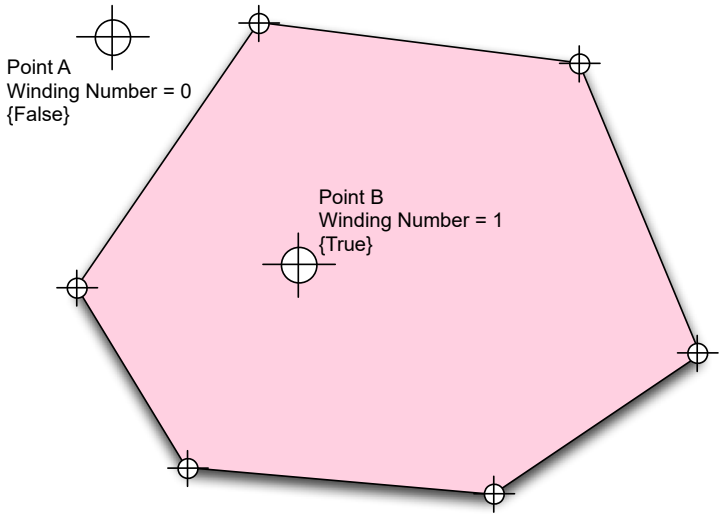


*Figure 3-16 Winding Number Illustration.*

As the winding number is a verification, if a point sits within the polygon, it becomes possible to create a Boolean check for the full width of a flat-bottomed polygon at 1mm increments as shown in Figure 3-17. Through an iterative approach, using simple Boolean logic, it is then possible to sum all the Boolean responses to obtain the total length of the points within the polygon where the winding number is greater than 1 and therefore the headroom requirements are met.

In Mathematica Snippet 7 a new function, inPolyQ, is created which determines the winding number of a point (pt) with reference to a defined polygon (poly). Within the Mathematica sheet created in the Appendix, the internal shaded area is plotted using a polygon that is regenerated each time the script is run and allocated to the variable polyPlot, which is used in the snippet Mathematica Snippet 7.

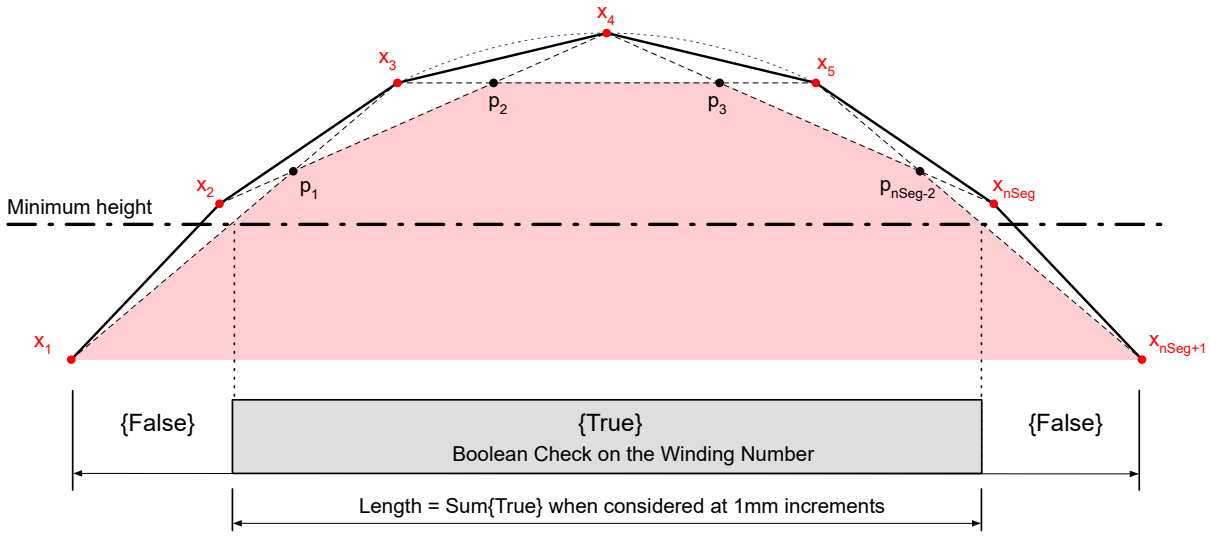


*Figure 3-17 Boolean Check On The Winding Number.*

*Mathematica Snippet 7 - Undocumented Mathematica function for determining the Winding Number*

```
inPolyQ[poly_,pt_]:=Graphics`PolygonUtils`PointWindingNumber
[poly,pt]=!=0

primeArea=Table[inPolyQ[polyPlot,

{x,intHeight}],

{x,0,Subscript[x, nSeg+1]}];

boxNodes=Flatten[Tally[Boole[primeArea]]];

widthBox=boxNodes[[4]]
```

Whilst the assumptions for the calculation of the winding number assumes that the bottom of the polygon is flat, this would be a reasonable assumption in a disaster relief scenario as level ground would ordinarily be selected for a variety of reasons, including providing a level sleeping surface and avoiding risks associated with further landslides and earthquakes. Should the shelters need to be constructed on a hillside it may be preferable to construct some element of terracing initially to provide a suitable founding element.

### 3.7.1 Internal Areas.

Two distinct curves have been considered within this work, with the semi-circular cable-chain arch being adopted in practice by companies such as RUBB it is worth considering if the parabolic form presents any benefits to the designer. Typically, parabolic curves with cable-chain

segments can 'wrap' rectangular habitable areas with less perimeter than their semi-circular counterparts, to illustrate this an example is presented below.

Consider a rectangular block that is to be enclosed to provide 1.8m of headroom (without the cables fouling the space) with a width of 1.809m. This could be for enclosing a specific element of plant machinery or for a habitable area for people.

Taking a 7-segment enclosure, a parabolic and a semi-circular profile are considered purely from a geometrical perspective, each of which is formed with equal length compressive elements. Using the methods outlined in this chapter to solve the geometrical configurations, the following solutions are derived using Mathematica.

*Table 1 - Parabolic vs Semi-Circular Comparison.*

| | Element Length (mm) | Total Linear Perimeter Length (m) | Arch Width (m) | Arch Height (m) | Area Contained Between Cables. ($mm^2$) |
|---|---|---|---|---|---|
| Parabolic | 957.592 | 6.703.1 | 4.100 | 2.050 | $5.889\times10^6$ |
| Semi-Circular | 973.752 | 6.816.3 | 4.376 | 2.188 | $6.306\times10^6$ |

What is clear is that the parabolic profile uses slightly less steelwork to enclose the same habitable area, but that this reduction is relatively nominal in this instance and is likely to only affect a building design if thousands of units were being manufactured. With a parabolic profile, the same habitable area can be contained within a narrower structural footprint, which if used in a humanitarian emergency could result in more tents per square kilometre for example.

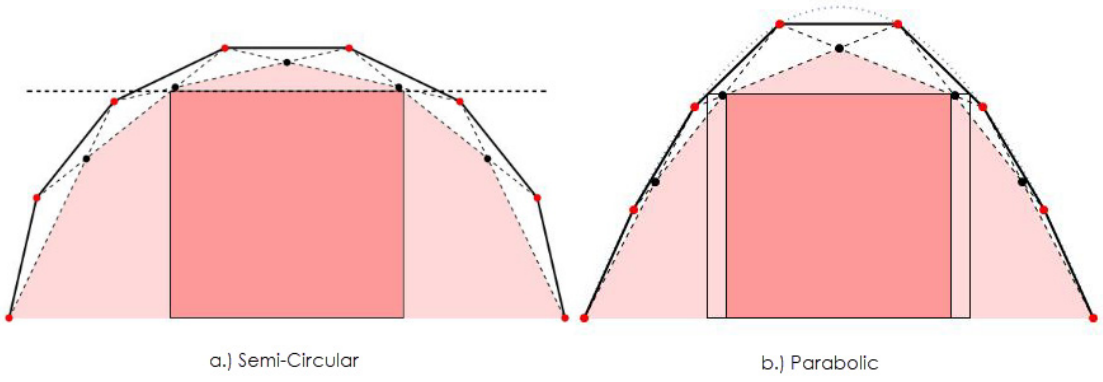


*Figure 3-18 - Comparison Between Semi-Circular and Parabolic Profiles.*

What is also clear from Figure 3-18 is that for a relatively modest saving in perimeter steelwork, there is a clear reduction in the internal angle with the parabolic curve reducing to approximately 3.2° (compared to 12.9° for the semi-circle) along the edges which will make the structure more vulnerable to the effects of snap-through. Increasing the segments generally had a direct impact

on the available internal area due to the refinement of the arc into smaller linear pieces. The natural fall off appears to be about 7 or so segments based on the visual feel of the arch with parabolic profiles suffering shallow angles and snap-through vulnerable geometries at lower numbers of segments when compared to semi-circular.

As an example, consider a parabolic arch with a base span of 4.1m and a height rise of 2.05m, the equation through the curve is:

$$f(x) = \frac{100x}{41} - \frac{x^2}{1681} \tag{3.23}$$

Subdividing this curve into various equal length segments gives the change in internal area as shown in Figure 3-19.

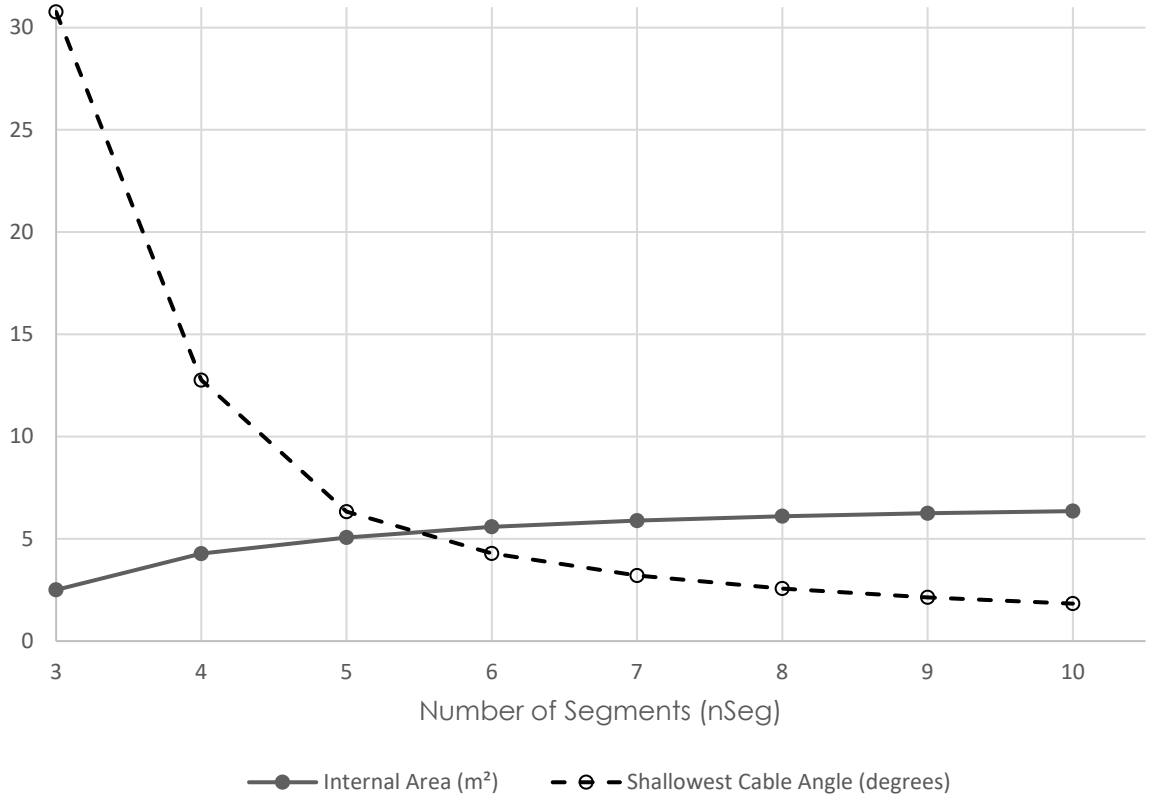


*Figure 3-19 - Graph Showing The Influence Of nSeg On The Internal Area Of A Cable-Chain Arch and Shallowest Cable Angle.*

As can be seen in Figure 3-19 increasing the number of segments from 3 to 5 almost doubles the available internal area, with a substantial amount of internal area being available after 5 or 6 segments which would appear to be a sensible compromise between internal area and shallow internal angles between the cable. This, however, is dependent on the nature of the curve used to define the arch, and the required internal headroom, but could still be used as a reasonable

starting point when modelling future arches. It can also be seen that the shallowest internal angle with the cable drops quite dramatically after 5 segments for this particular curve and consideration should be given with regards the vulnerability of snap-through behaviour on a case by case basis.

## 3.8 Structural Behaviour.

The previous few sections have been concentrated primarily on determining the geometry of the cable-chain arches to enable analysis models to be built. As cables are an integral component of a cable-chain arch, there needs to be consideration of the structural behaviour of the cable and this will require the non-linear geometrical analysis of the structure.

The other parameters that could be considered are almost limitless, such as the consideration of additional rotational stiffnesses at the revolute joints, global buckling behaviour, local buckling, fatigue analysis, and so on, but, before any detailed considerations are evaluated, it is proposed that a fundamental review of the structural behaviour under common loading conditions is considered.

As each arch is subdivided into a series of uniform struts, each strut will have a hinged end that will be incapable of transferring bending moments to the adjacent element. This chain of struts would hang like a cable without the addition of stabilising cables and it is these cables that provide the rigidity to the system.

The only bending moment that will be present within the struts will be through a combination of self-weight and/or additional uniformly distributed or point loads applied to the element itself (as opposed to nodal positions, assuming no applied end moments).

### 3.8.1 Loadings.

Critical loadings that are likely to occur include the lateral load mimicking a crosswind, which depending on the span/rise ratio would create either uplift or a combination of positive pressures and uplift across a dome or arch based on the pressure coefficient from Eurocodes.

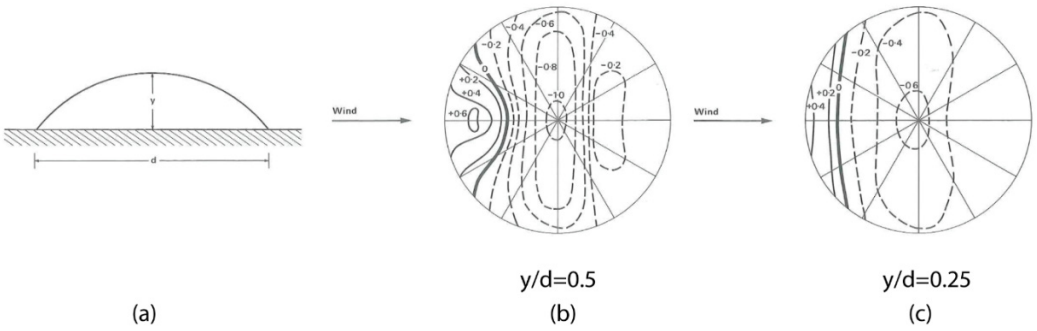


*Figure 3-20 Wind Loading On Domed Structures For Varying Ratios Of y/d.*[61]

As can be seen from the pressure coefficient in Figure 3-20 the flatter the dome the lower the pressure coefficient, whilst this figure is for a dome, the same principles hold for arches. Therefore, if the structure was able to flatten, then by its very nature it would become more aerodynamic and avoid the large positive pressure on the front windward face and have lower suction values on the crown, consequently reducing the net load on the structure.

Generally, though, the wind load creates a lateral pressure which may potentially destabilise an arch or dome structure, see Figure 3-21) which shows a positive pressure ($k(\theta)$) on the windward side ($\theta=0$), with a negative pressure on the leeward side ($\theta=\pi$) which creates a wind loading pattern which can 'rock' an arch, causing it to become unstable if not stiff enough to resist the applied loading.

[61] Newberry, C. W., & Eaton, K. J. (1974). *Wind Loading Handbook*. Watford: Building Research Establishment.

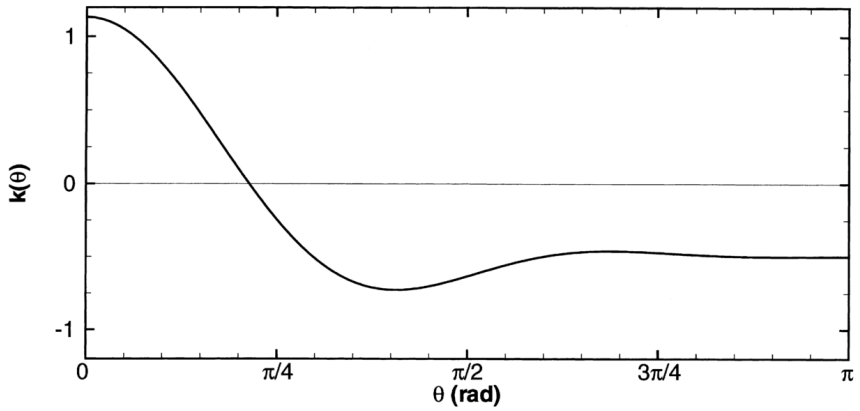


*Figure 3-21 – Pressure Distribution On An Inflatable Arch, Showing Positive Pressure On The Windward Edge.*[62]

The destabilising effect of wind loading has been investigated for inflatable arches (Plaut, Goh, Kigudde, & Hammerand, 2000) and they have determined that just as for normal arches, large positive pressure on the front face is critical, as it creates a positive push against the structure increasing the sway effects on the arch and encouraging lateral buckling of the arch.

Whilst there are geometrical benefits for mobilising a more aerodynamic form for the wind load, there remains the matter of snow and sand drifting which can create a similar lateral load against the arch. These lateral loads cannot be controlled in the same way that the wind loading is and may still be a governing criterion for certain applications.

The second common loading criteria to be applied would be a straightforward gravity load case, considering the self-weight of the structure and an allowance for any additional cladding and secondary support structure spanning the primary ribs.

The final load case to be considered would be the prestress in the cables, which may be required for certain geometries to create a stable structure during the analysis process. A typical analysis method for structures that include cables is to find a stable self-weight condition (which may require prestress to be applied) and then to apply additional loadings to determine the overall behaviour of the structure.

The structural behaviour is largely independent of the material selection at this point, instead of being governed by the geometry and applied loadings, but for the initial structural analysis

[62] Plaut, R. H., Goh, J. K. S., Kigudde, M., & Hammerand, D. C. (2000). Shell analysis of an inflatable arch subjected to snow and wind loading. *International Journal of Solids and Structures, 37*(31), 4275-4288.

circular hollow sections have been selected for the primary struts, with steel cables modelled for the connecting cables to identify that snap-through buckling will be an issue.

Some of the analysis models have had their steelwork designed to respond to the stresses contained within the model, naturally, these sizes have been iterated back through the analysis mode to ensure that the self-weight case has been updated appropriately.

## 3.9 ROBOT Analysis And Local Buckling.

Whilst the overall arch shape has been considered, with regards to the buckling behaviour under static loads, the introduction of non-linear analysis introduces an element of complexity to the models. Local buckling effects (of individual elements) have been considered within the ROBOT modelling to account for local element buckling but only within a planar sense.

As the model complexity is increased there remains a risk that local strut buckling under destabilising loads may become an issue as identified by Wu (2008). This behaviour is dependent on the overall stiffness of the uniplets and will vary depending on the fixities and lateral restraints provided by the overall structural behaviour. However, unstable snap-through buckling is also a risk where the angle between the struts and the connecting cables remains shallow and establishing that this behaviour can occur is the primary purpose of this investigation.

Localised buckling within the ROBOT modelling environment can be identified and works particularly well when using the DSC algorithm, but this algorithm is incompatible with rotational spring stiffnesses. Therefore, the higher modes should always be investigated as there remains a risk that these local element buckling effects are not initially identified within the first or second modes when in fact they may be the defining element with regards overall behaviour and stability.

## 3.10 Results.

Numerous models have been generated by combining the Mathematica scripts to generate geometry and handing these updated geometries through to ROBOT and repeating the analysis.

The intention of this section is not to present detailed output from ROBOT, but to highlight general behaviours that were deemed to be beneficial or detrimental to the development of cable-chain arch structures.

As can be seen in Figure 3-22 under purely self-weight a typical cable-chain structure will act as a series of pin-jointed beams spanning from node to node. With the cables acting under tension

and the struts acting in compression in the same load cases. This is as to be expected as the general overall structural behaviour and shows that the model is well-conditioned when acting under light loads.

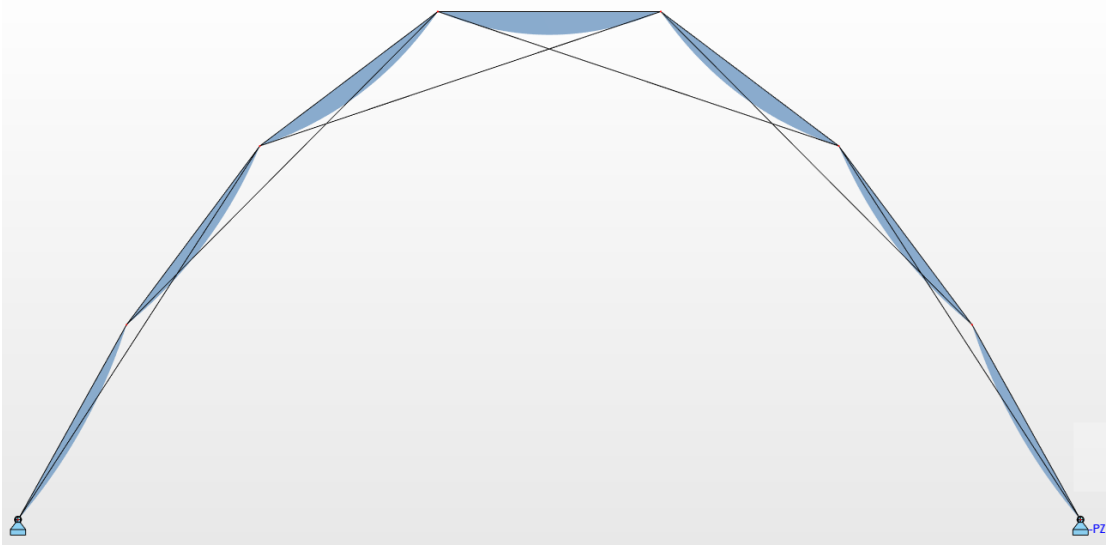


*Figure 3-22 - Bending Moment Diagram Under Self Weight.*

However, under more appreciable or eccentric loadings (see Figure 3-23) the structure will deflect more and the tighter angles near the supports may start to suffer issues associated with snap-through.

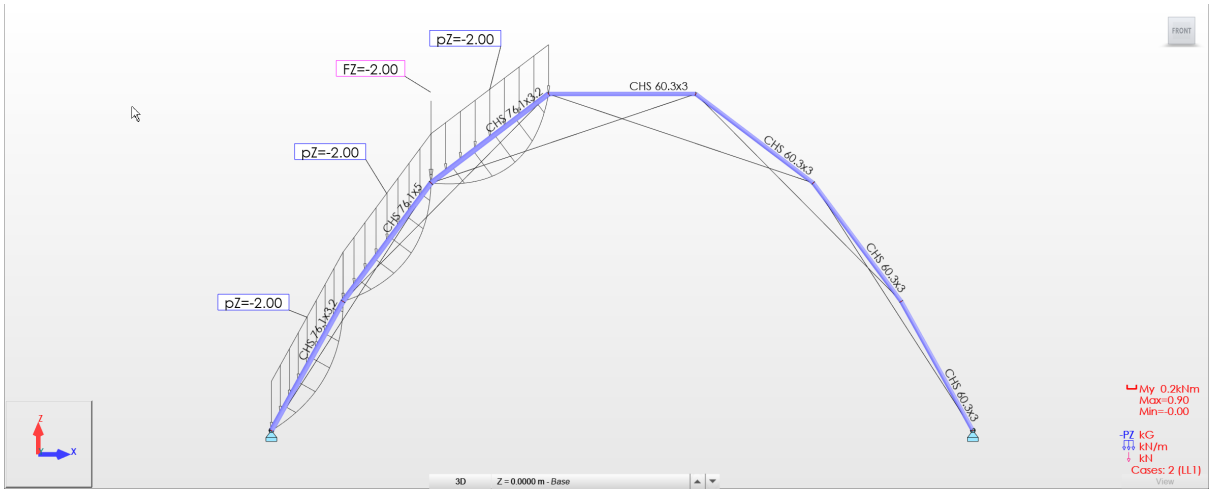


*Figure 3-23 - Typical Asymmetrical Loading And Bending Moment Diagram.*

The applied loadings are focused on creating imbalance within the structure (see Figure 3-23), rather than modelling real-world loads, to determine the general structural behaviour and sensitivities in response to loads that may, in shape, mimic those of say a wind load or drifted snow maybe only so far as being asymmetrical.

As can be seen in Figure 3-24 a point load applied at one of the nodes to create an eccentric net effect on the arch, combined with vertical UDL's along the left-hand side generates a series of bending moments, see Figure 3-23, that indicates that the struts are pinned and working as intended.

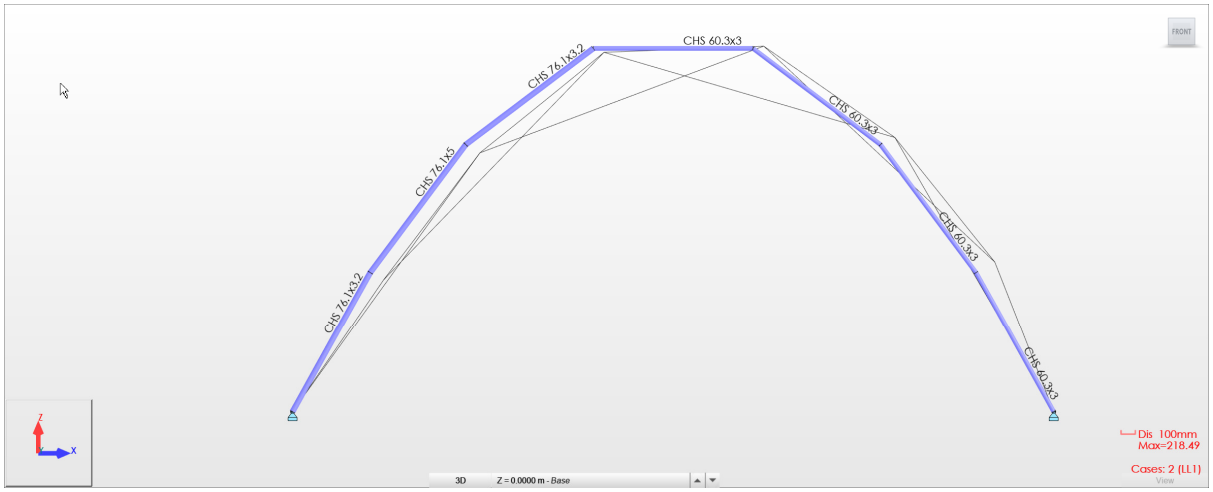


*Figure 3-24 - Lateral Displacement Of Cable-Chain Arch.*

Similarly, the bias and asymmetrical nature of the loadings on the left-hand side of the structure causes the frame to sway to the right as expected, but the structural system is sensitive to the magnitude of the loads applied and care has to be taken when analysing the structures with significant loads, as large loads where the cables angles are shallow, can cause the analysis model to fail to converge and solve, see section 3.10.2 for more discussion regarding the snap-through behaviour.

### 3.10.1 Levels Of Pretension.

For cable-strut structures generally, a small amount of prestressing is a helpful force to integrate for general stability and rigidity of the structure by pulling the frame into position and locking it in a pre-defined state by controlling the distance between connected nodes. As with all things though, there is a fine balance to be maintained and excessive pretension within the cables can force the struts can generate compressive forces that require the struts to be increased in weight (and consequently cost) to resist this force.

Equally, poor detailing of cables can quickly introduce eccentricities at the connections which may generate secondary moments through the structure which may contribute to element failure or developing snap-through behaviour depending on the orientation of the elements.

The pre-tensioning of the cables within the ROBOT model was found to bring mixed effects, a

small amount sometimes aided unstable models to solve, however, sometimes the pre-tension brought about instabilities on particularly shallow angled cables and made the model unstable before the external load was applied.

### 3.10.2 Snap-Through Behaviour.

Snap-through behaviour was noted on certain models, this was particularly evident on certain models being unable to solve without a considerable reduction in applied loads (see Figure 3-25), where either the sides of the arch were steep or where a high number of segments were introduced, as both parameters reduced the internal angle of the cable and increased the likelihood of snap-through behaviour occurring. This observation matches well with the work of Vu et al. (2006) where shallow angles caused issues. This could be overcome in a variety of ways such as making the cables stiffer to prevent extension or including levels of pretension, but ultimately these will only work to a point and shallow angles at the cables will eventually bring about vulnerabilities for hinged tension-strut structures.

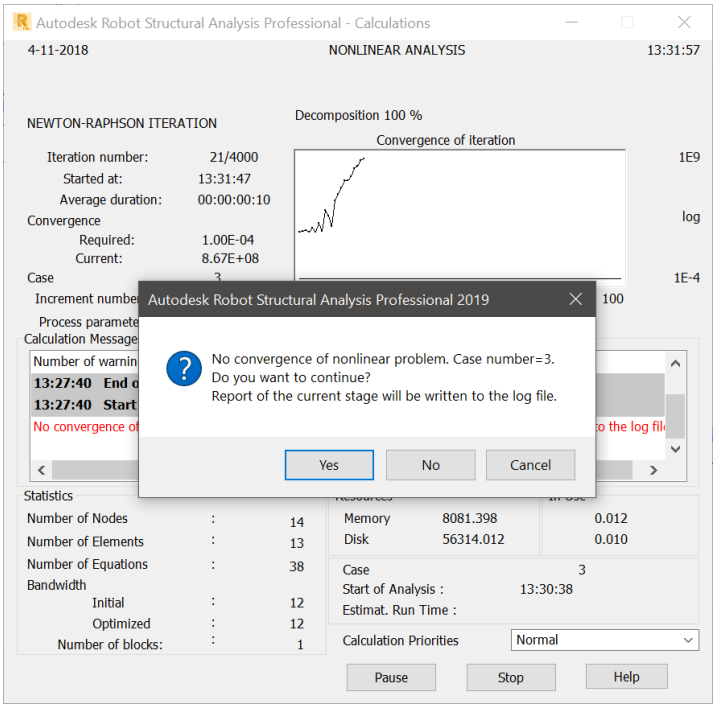


*Figure 3-25 - Error Message on ROBOT Structural Analysis.*

Even with fine adjustments to the analysis engine settings, feeding back the matrix after each iteration and using finer increments with larger target goals, for example, this particular structure was still unable to solve due to the collapsing of the uniplets via snap-through.

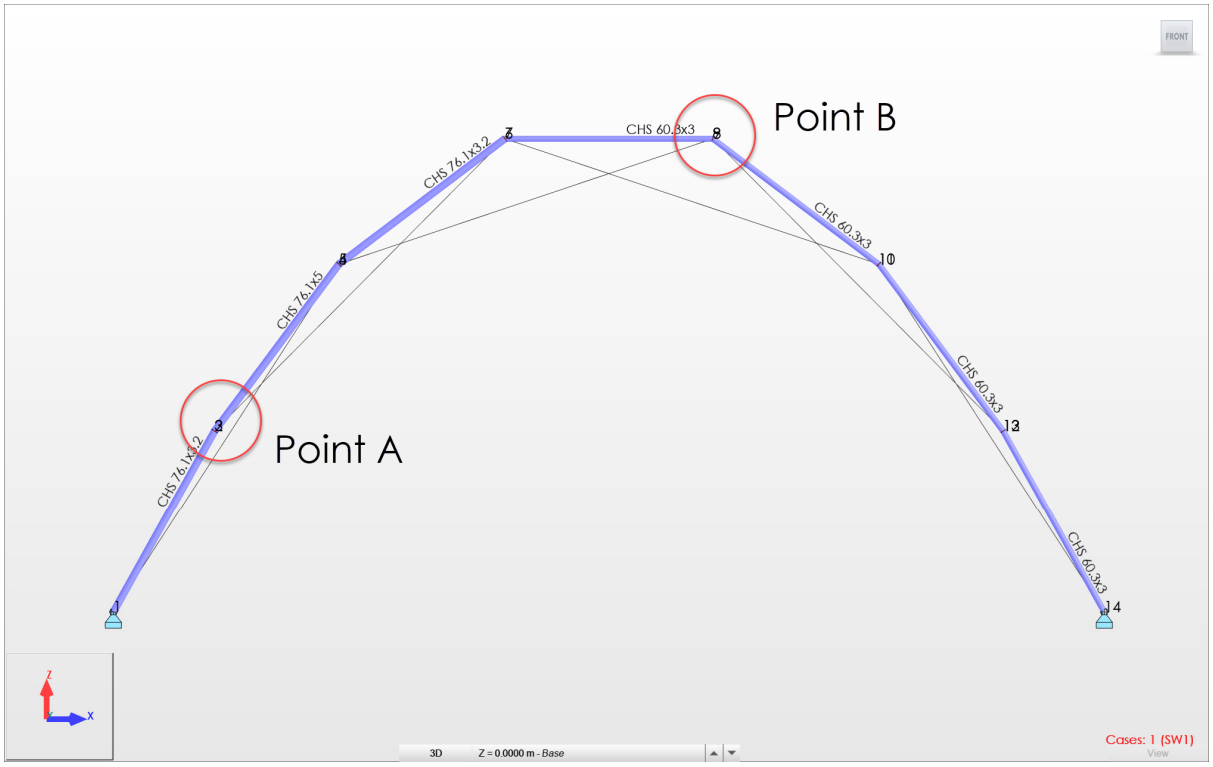


*Figure 3-26 - Tight Internal Angles on Cables at Point A.*

As can be seen in Figure 3-26, at point A the internal angles of the cables are close to 180° and this (depending on the magnitude of the loading and the rigidity of the elements) leaves the uniplet vulnerable to snap-through effects which can lead the structure to become unstable and unable to be solved by ROBOT. However, at Point B, the internal angle is less shallow, allowing the triangle formed by the uniplet to deflect further before pushing point B towards the cable, allowing significant displacements to be developed before becoming vulnerable to snap-through behaviour.

### 3.10.3 Limiting The Effects Of Snap-Through.

Generally, to improve the behaviour of the arches there could be a series of interventions considered to prevent specifically the snap-through behaviour occurring which will be discussed in this section. As identified by Gantes and Konitopoulou (2004) in his assessment of fitting Scissor Like Element (SLE) modules into arches, the shallower elements (see Figure 3-27) tend to have a propensity to buckle first and greatly affect the overall structural performance. Even where buckling does not fully occur, a small displacement of a deployable structure in a snap-through mechanism can result in the structure locking and being unable to free itself to allow folding to happen (Gantes, 1997). This phenomenon was also identified in the practical work of Croll and Walker (1972) who identified that shallow angles also increased the risk of snap-

through behaviour occurring, but that it was also linked to the element stiffness and the flexibility of the struts and the extensibility of the cable and supports.

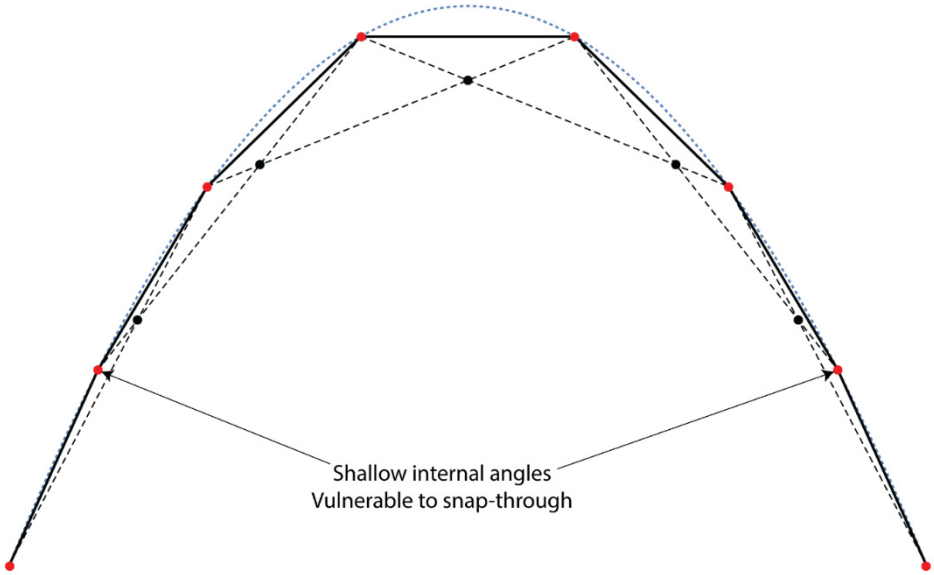


*Figure 3-27 – Steep Sided Parabolic Cable-Chain Arch.*

This is further supported by the work of Bazant and Cedolin (2010, p275) and (Croll & Walker, 1972) which test Von Mises trusses for various central spring stiffnesses to determine the potential energy contained within the system and to identify angles at which snap-through becomes a concern. This snap-through behaviour is a function of the angle between elements and the relative stiffness of these elements and will vary from structural system to structural system.

It should be noted that snap-through behaviour is not always a negative effect though, for certain types of structure such as the Longeron mast (Takatsuka & Ohmori, 2011) the snap-through behaviour benefits the load-carrying capacity, allowing the structure to snap into a more stable form after packing.

To prevent the snap-through behaviour occurring, either the joints where the internal angle is shallow can be locked rigidly in position to increase the resistance or the lower sections of the arch may be replaced by a single piece for continuity (see Figure 3-28), eliminating the shallow internal angle (see Figure 3-29).

However, there is the added complexity that the compressive sections would no longer be of an equal length to those employed at the crown, thus reducing the packability of the steel frame. Similarly, the local buckling lengths of the section would increase for the lower sections, meaning

that the net efficiency of the lower sections and thus the overall weight of the frame would vary. It is worth noting that for this structure to remain structurally stable, the fixity of the internal joints would need varying to prevent failure under lateral loads.

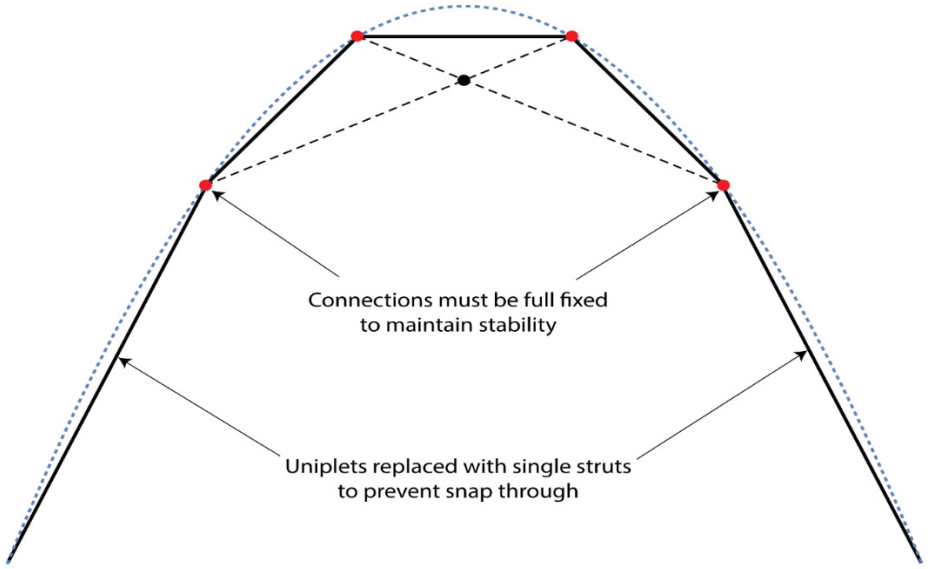


*Figure 3-28 – Parabolic Arch With Lower Section Uniplets Replaced With Solid Strut.*

To increase the packability of the lower sections, they may be formed as a series of hinged structures comprised of struts each the same length as those located at the crown. The hinges could be set to lock into place to create a single strut to create solid strut with regards the overall structural behaviour, similar perhaps in design to modern tent poles.

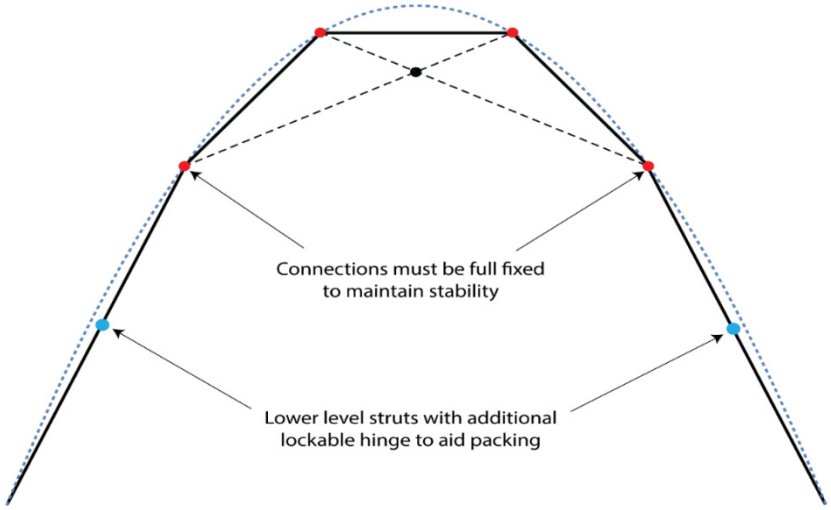


*Figure 3-29 – Solid Lower Level Strut With Locking Hinge For Packing.*

The ability to isolate and remove the snap-through behaviour of the shallow internal angles presents many benefits with regards to the performance of the cable-chain arch. Rather than just inserting a single hinge for the lower section in Figure 3-29 to increase the packability, the strut elements could be completely replaced with a beaded structure, stiffened by a cable. The performance of cable-stiffened elastica has been considered by Beatini and Royer-Carfagni (2013) for adapting arch profiles to meet certain geometrical criteria, but not for changing rotational stiffnesses to facilitate form change.

## 3.11 Beaded chains.

To reduce the susceptibility to snap-through behaviour, whilst still being able to integrate the beneficial properties of a flexible arch with clear load-carrying capabilities, a series of hinged struts connected with rotational springs may prove beneficial in creating a sprung arch that can adjust its geometry and consequently load relieve, or even absorb energy whilst retaining a significant load-carrying capability.

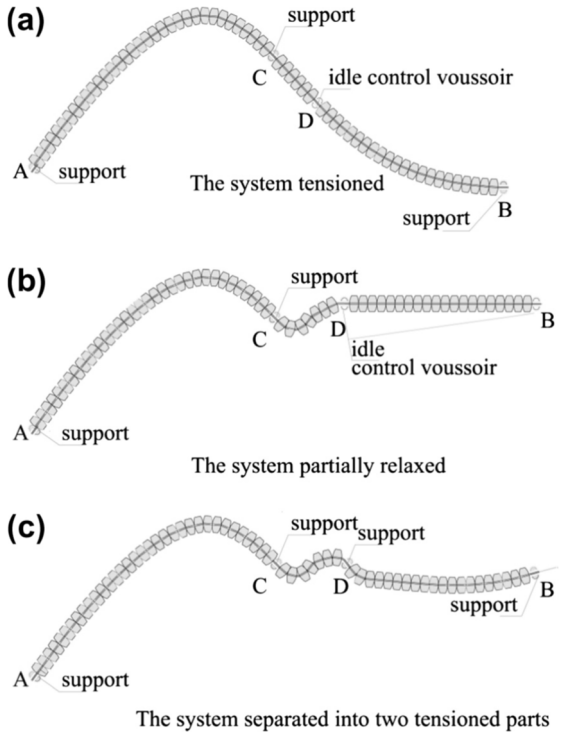


*Figure 3-30 – Tension Controlled Elastica.*[63]

[63] Beatini, V., & Royer-Carfagni, G. (2013). Cable-stiffened foldable elastica for movable structures. *Engineering Structures, 56*, 126-136.

Cable-stiffened elastica (Beatini & Royer-Carfagni, 2013), as shown in Figure 3-30, have not been assessed with regards their use as axial support structures. This is despite being used for many years in children's toys (Figure 3-31) this may be due to the difference in scale of holding up a habitable space compared to a miniature wooden giraffe.

*Figure 3-31 – Children's Toys Supported Through Cable Stiffened Elastica Within The Legs And Neck.*[64]

The types of structures shown in Figure 3-31 are well understood by children around the world; with a spring-loaded plate located in the base that maintains tension in the string threaded through the beads within the animal. When the plate is squeezed this causes the structure to lose its stability and associated load-carrying capabilities as the tension in the stabilising tendon are lost thus causing it to collapse chaotically.

When the tension is restored the structure returns to a recognisable state and becomes the wooden animal it was designed to be initially, although be it in a slightly different configuration as the beads may rotate along their local x-axis during the chaotic collapse stage.

This ability to grossly deform and elastically recover to a rigid form presents many exciting opportunities, both for adaptive and metamorphic structures but also from a ductility

[64] http://goo.gl/uXxBwf

perspective.

This structural system shall be referred to as beaded chains from this point forward in the thesis and their behaviour and functionality will form the basis of the next chapter where rigid, infinitely stiff links with rotational springs will be used to develop an analysis process that potentially mimics the behaviour of beaded chains, initially starting with the buckling analysis of struts with linear and then non-linear springs.

This approach is valid given that the beads are deemed to be infinitely rigid, with controlled rotation motion governed by the tensioned tendon connecting them. This will develop a non-uniform spring tension given the two lenticular surfaces rotating about each other, but the initial models considered in the next chapter will begin with linear rotational springs as part of the validation process given the complexity of the analysis.

Instead of locking hinges, an alternative would be to develop the chain as a series of hinged beaded structures. A system developed by Beatini and Royer-Carfagni (2013) shows a central tendon threaded through voussoirs which would perhaps allow a structure to be developed with varying tendon profiles surface curvatures to create a non-uniform arch. Alternatively, it is argued that the connectivity between voussoirs could be modelled as a series of non-linear rotational springs connected rigid struts, with the spring stiffnesses informed by the geometrical considerations of the cable and arched surface.

These proposed hinged and beaded structures may create a structure that has some parallels with taped structures which encourage snap-through behaviour to occur in predictable paths for space telescopes (Seffen et al., 2000) and indeed this bi-stable behaviour (Kebadze, Guest, & Pellegrino, 2004) is advantageous for load relieving metamorphic arches, and with careful consideration, multiple stable states (Santer & Pellegrino, 2008) can be developed.

## 3.12 Summary

There is very little published literature available on cable-chain arches and snap-through behaviour on these types of structure and so this chapter developed various Mathematica scripts to explore the geometrical configurations of cable-chain arches which were subsequently analysed using Autodesk ROBOT to determine if snap-through failure mechanisms could be invoked.

Defining the geometry of a semi-circular arch is generally straightforward and can be defined either using a polar co-ordinate system or through making use of the consistent internal angle between uniplets.

The creation of the equally sub-divided geometry for a parabolic curve is more complex than a semi-circular arch and this requires the solving of several sets of simultaneous equations to ensure that all compression segments are of equal length which will ease fabrication and rationalise the detailing. Within this chapter, the solving of the equations was undertaken using Mathematica and custom scripts. Efficiencies using the numeric engine over the symbolic engine were identified for solving simultaneous equations within Mathematica, allowing sets of equations that could not be solved in days using the symbolic engine to be able to be solved in seconds with the numeric engine invoked.

Whilst adjusting the arch geometry from semi-circular to parabolic can present some small benefits to the internal habitable area, there is a genuine concern as to the sensitive nature of the snap-through of arched cable-chain structures when adopting parabolic curvatures. Parabolic arches were shown to lead to shallow angles developing within the uniplets at lower levels of subdivision than the semi-circular arches. This was particularly evident near the supports where the curves are straighter. However, shallow angles are an issue even for circular geometries when the curves are sub-divided into too many segments.

Parabolic arches can also present benefits associated with a slightly smaller on-plan footprint compared to semi-circular alternatives when considering the available internal area, which may be helpful when nesting large numbers of units into a small site such as a disaster relief camp. However, these small efficiencies in footprint, come at a penalty of shallow internal angles between the internal cables which may lead to snap-through behaviour in service, this may go some way in demonstrating why temporary aircraft hangars such as the Rubb system generally adopt semi-circular arches.

The investigations within this chapter were not intended to identify the critical angle for snap-

through to develop or the relationship between cable and strut stiffnesses, instead given the general lack of literature available for this structural form, the intention was to establish that snap-through can be invoked on these types of structure at all and this was shown to be the case in particular where the cable angle was shallow.

It is proposed that the removal of the internal cables and the replacement of the free pin structures with rotational springs could lead to an alternative arched structure which could achieve some of the benefits identified for parabolic curvatures such as reduced perimeter and smaller footprints (compared to semi-circular cable-chain arches), and such a structural system could be adaptable enough to make use of various curved profiles or even to displace into favourable forms under loading whilst eliminating the issues associated with snap-through behaviour.

However, to investigate this hypothesis any further it will be necessary to be able to analyse a chain of springs appropriately and the buckling analysis of struts with rotational springs was noted as being notoriously troublesome in chapter 2.

The next chapter seeks to establish and validate an analysis method which enables the ease of determining the critical buckling loads for sprung struts using three distinct computer-based methods, the first method uses the finite difference method with a custom Mathematica notebook which can be adapted for multi sprung linear spring chains.

The second method using Eigen buckling methods within CivilFEM and finally the forced displacement method using CivilFEM, both of these two last methods can be adapted for linear and non-linear multi-spring chains and importantly the forced displacement method of analysis is capable of identifying post-buckling behaviours, particularly with regards the gross deformations that are likely to occur.

However, all three methods are novel with regards their application to sprung struts and potential issues such as ill-conditioning will also be explored in more depth in the following chapter too.

# Chapter 4

## 4 Kinked Struts.

Determining the critical buckling load of a strut with a single linear rotational spring is fairly trivial (section 4.1) but in order to analyse chains of linear springs, chains of non-linear springs, and chains formed of different stiffnesses of springs a robust and practical method needs to be developed to analyse and determine their critical buckling loads and post-buckling behaviour and this will be the focus of this section.

To illustrate some of the initial challenges associated with the analysis of the critical buckling load of a sprung strut, Autodesk ROBOT was initially used (section 4.2.1) as it possesses buckling analysis capabilities and it was deployed successfully for cable-chain arches in chapter 3. Quickly though it became apparent that whilst it could be manipulated to develop critical buckling loads that matched hand analysis verification, it was a trial and error approach and lacked capabilities associated with forced displacement analysis. However, valuable lessons were developed regarding the range of values to be considered for the Young's Modulus of infinitely stiff struts that were integrated into the final methodologies.

Each of the proposed strategies are based on numerical solutions and make use of the computational power of modern PC's. The first proposed method makes use of the finite difference method (section 4.1.3) which has been used for decades but introduces a novel approach for the introduction of the springs into a strut to determine the critical buckling load. This method as presented is limited to linear springs but can efficiently solve numerous springs in a chain.

The next two methods both make use of finite element software, specifically CivilFEM. The first method can determine the critical buckling loads for struts for linear and non-linear springs plus their modal shapes using buckling analysis. With the second forced displacement method used to develop the post-buckled behaviour for linear and non-linear struts and is invaluable for

designing metamorphic structures that are intended to change their shape and structural behaviour under pre-determined loading conditions.

An overview of the methods and their potential applications is presented in the table below.

| | Description | Application |
|---|---|---|
| **Finite Difference** | Mathematica script for infinitely stiff strut elements and user defined springs. | Critical buckling load of chains of sprung struts. |
| **Finite Element** | CivilFEM analysis methodology for undertaking buckling analysis. | Critical buckling load of sprung struts and corresponding modal shapes. |
| **Forced Displacement** | CivilFEM non-linear analysis through forced displacement integrating initial imperfections. | Critical buckling loads of sprung struts, form-finding, and post-buckling behaviour. |

## 4.1 Buckling of Sprung Struts.

Determining the buckling of struts with linear rotational springs (Gere & Goodno, 2012) is more complex than a strut with a uniform cross-section and buckling for deployable structures will be the focus of the rest of the literature review.

Whilst springs possess a single degree of freedom (considering a 2D plane initially), each subsequent spring that is added to a structure increases the analysis complexity accordingly. With a typical arch containing between 6 and 10 uniplets or units (Vu et al., 2006) this may lead to difficulty in analysing structures with regards maintain analytical stability and compatibility of stiffnesses.

Through replacing the cable-chain uniplets with a beaded/sprung chain to increase the packability of the struts to enable the use of parabolic curves to create the arches it is hoped that this type of snap-through behaviour can be removed, however, the complex relationship between the joints on a beaded chain structure introduces additional complexities. Before multi-sprung struts can be analysed though, the behaviour of a single spring strut will be established based on classical methods.

One of the simplest structural forms where nonlinear geometric behaviour is considered is the infinitely stiff strut with a central spring (Allen & Bulson, 1980, p8). Whereas Walker (1975) considers the buckling load from a geometrical aspect, Allen and Bulson (1980) also consider the potential energy contained within the system during buckling.

This structure has a single degree of freedom, with each successive spring that is added to the chain introducing a further additional degree of freedom.

Whilst single uniplets and localised snap-through is of obvious concern, the effects and influence of buckling on deployable structures must be also considered. Indeed, the buckling of certain structural forms is the preferred method of deployment and is an ongoing area of research within itself.

Buckling is taught on virtually all undergraduate Civil Engineering degrees and consequently, it could be construed that it is a well-understood behaviour (Crosby, 2010) that does not warrant further investigation.

### 4.1.1 Geometrical Approach.

Referring to the original hypotheses within this thesis, replacing the free pin and the cable within a uniplet with a rotational spring will require the designers to determine the critical buckling loads to determine the overall behaviour of the arch. Clearly, for each unit of rotation, there will be a corresponding rotational moment required to mobilise movement, but typically arches contain significant axial forces and buckling will also be an important governing behaviour. To start with the initial assessment of the behaviour a single uniplet will be considered.

Consider two of the compressive struts on a cable-chain arch, instead of being linked via a central free pin and a cable, it could be exchanged for a single hinge between the elements with a rotational spring stiffness. This new strut with a central sprung hinge uses the hinge to generate stability within the structural element whilst still retaining the ability to fold ready for shipping.

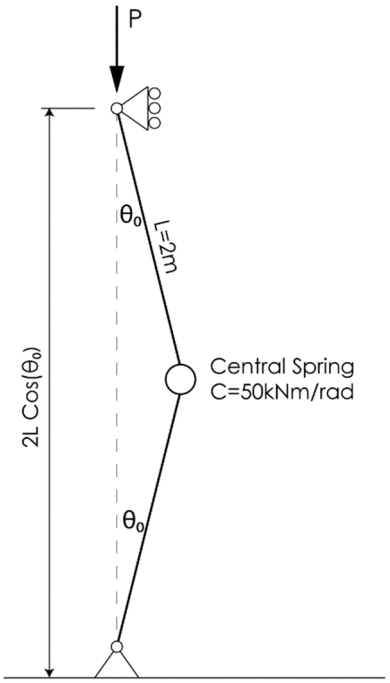


*Figure 4-1 Strut with a central pin and spring.*

Taking the initial arrangement as shown in Figure 4-1 with a central spring of stiffness C=50kNm/radian and an overall length of L=4m the critical buckling load can be determined as the strut displaces. Initially considering the perfect geometry and if the struts are rigid beams, for a vertical load P being applied at the top of the strut at a given load the system will deform.

If the internal angle for the displaced form is $\theta$ then it is evident that no horizontal forces are acting at the top support. Therefore, for equilibrium:

$$M_r = M_L - M_S \tag{4.1}$$

Where $M_r$ is the resultant moment at the central hinge, $M_L$ is the applied moment from the vertical point load and $M_S$ is the moment provided by the spring.

Taking clockwise moments as positive:

$$\begin{aligned} M_L &= PL\,\mathrm{Sin}\,\theta \\ M_S &= 2C\theta \end{aligned} \tag{4.2}$$

Thus:

$$M_r = PL\,\mathrm{Sin}\,\theta - 2C\theta \tag{4.3}$$

For equilibrium, it is worth noting that the resultant moment ($M_r$) should be equal to zero.

$$0 = PL\,\mathrm{Sin}\,\theta - 2C\theta \tag{4.4}$$

Trivial solutions for this system show that the internal angle $\theta = 0$ is a solution for all values of P, which would require a genuinely perfect geometrical arrangement. However, other solutions for this equation also exist where $\theta \neq 0$ and P can be rewritten as.

$$P = \frac{2C}{L} \cdot \frac{\theta}{\mathrm{Sin}\,\theta} \tag{4.5}$$

This shows that where $\theta = 0$

$$P = \frac{2C}{L} \tag{4.6}$$

However, as the load P increases beyond this limit, the structures' overall stability is altered and the system begins to buckle, this is a critical point within the behaviour of the structure and is worth considering further, particularly as the loads begin to increase beyond this limit.

With no load applied the structure is stable, then as the loads are applied it remains in stable equilibrium, however as it starts to displace it can be argued that the structure has become disturbed and if this movement is violent and changes the equilibrium state from one to another for identical loads then the structure can be said to have buckled.

Considering the same system but with an initial displacement on the system of $\theta_o$ before P is applied means that equation (4.5) becomes modified to.

$$P = \frac{2C}{L} \cdot \frac{\theta - \theta_o}{\mathrm{Sin}\,\theta} \tag{4.7}$$

Taking the values for the spring stiffnesses and lengths of the strut from Figure 4-1 and the perfect initial condition (4.5) and (4.7) for a variety of initial defects allows the creation of a plot as shown in Figure 4-2.

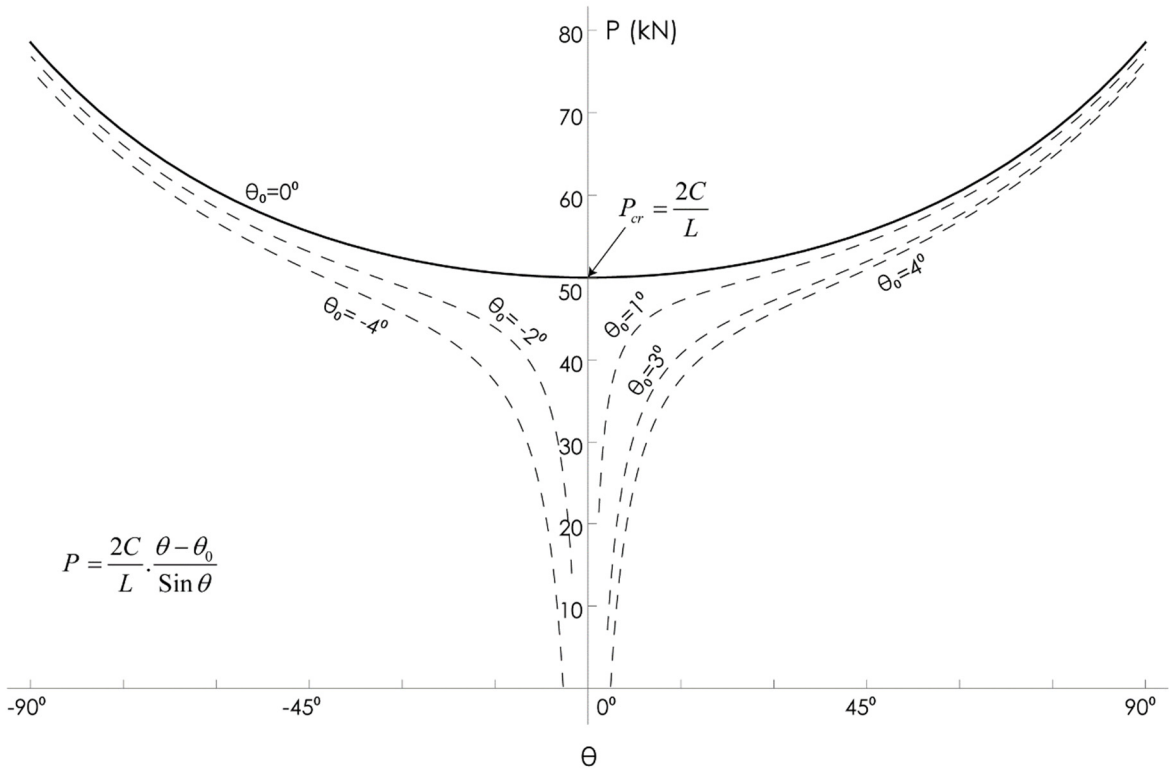


*Figure 4-2 Buckling Curve Ignoring Secondary Effects.*

As can be seen from Figure 4-2 there is an initial mobilisation load of 50kN for the perfect geometry and through the introduction of initial defects, this capacity is greatly reduced. However, after the initial mobilisation load has been added the structure still maintains equilibrium and can carry a load greater than the critical buckling load. This nonlinear behaviour is important when considering the behaviour of spring-loaded struts, for safe design within steel standards the residual capacities are frequently ignored for conservative and safe design as they usually invoke plastic behaviour.

However, in the spring struts, the springs allow the strut to recover elastically providing that the struts themselves are stiff enough and the springs are not over-extended beyond their limits which is an important aspect which can be exploited.

It is important to appreciate though that the even though the vertical load-carrying increases after the structure has buckled, the axial force within the hinged strut does not increase and the additional load-carrying capacity is developed through the bending moment created by the spring and the associated shear forces. Ordinarily, once a uniform strut has buckled it is unable to support any further additional load, whereas in a strut with a sprung hinge (where the spring stiffness is weaker than the flexural capacity of the two connecting struts) the strut is capable of supporting additional load post-buckling providing that the stresses in the connecting struts do

not exceed the safe working limits of the struts (see Figure 4-2).

Whilst the strut will safely support additional load though, the deformations will become gross and the spring will continue to rotate as there is a fundamental change in the method by which the system resists the applied load, moving from a purely axial system into an axial and bending combined system as additional moments are generated in the connecting strut sections.

### 4.1.2 Energy Approach.

Repeating the same exercise, but taking the energy approach for validation shows that energy stored within the spring is the product of the rotation and its associated angle relative from one rod to the other, or $2\theta$ with the mean value of the couple exerted by the spring being:

$$\frac{1}{2}C(2\theta) \tag{4.8}$$

This gives the strain energy to be:

$$U = \frac{1}{2}C(2\theta)(2\theta) = 2C\theta^2 \tag{4.9}$$

As the force P was applied when the strut was originally straight and has been presumed to be maintained, there is an associated loss in potential energy.

If the initial potential energy is taken as a datum and equal to zero, then the change in potential energy is given by.

$$V_P = -P\Delta_1 \tag{4.10}$$

Where $\Delta_1$ is the vertical displacement only at the top roller support.

From simple geometry, the change in vertical length $\Delta_1$:

$$\Delta_1 = 2L(1-\mathrm{Cos}\,\theta) \tag{4.11}$$

And the midpoint lateral displacement $\Delta_2$:

$$\Delta_2 = L\,\mathrm{Sin}\,\theta \tag{4.12}$$

Therefore expressing the total potential energy in terms of $\theta$ using equations (4.9), (4.10) and (4.11) gives.

$$V = U + V_p = 2C\theta^2 - 2PL(1-\mathrm{Cos}\,\theta) \tag{4.13}$$

Hence

$$\frac{dV}{d\theta} = 4C\theta - 2PL\,\mathrm{Sin}\,\theta \tag{4.14}$$

And

$$\frac{d^2V}{d\theta^2} = 4C - 2PL\,\mathrm{Sin}\,\theta \tag{4.15}$$

Given that $V$ is stationary with respect to $\theta$, implies that $\frac{dV}{d\theta} = 0$ in equation (4.14) which has a trivial solution for when $\theta = 0$ but also when:

$$P = \frac{2C}{L}\frac{\theta}{\mathrm{Sin}\,\theta} \tag{4.16}$$

Which is identical to the geometrical approach, shown in (4.5)

Determining the axial buckling capacity of two struts with a single spring is relatively straightforward as can be seen and for that reason, it is often used in undergraduate texts to illustrate the principles of axial buckling. However, for a cable-chain arch to have the cables removed and remain stable would require multiple springs inserting into the arch (one at each pin typically, although it could be reduced to a 3 pin arch if required) and with each spring integrated the number of degrees of freedom increases by 1 for a 2D arch.

The approaches outlined above are convenient for structures with a single spring, but soon start to become unwieldy and complicated for multiple degrees of freedom systems such as would be required to model a chain or arch with between 6 or 10 linked springs.

Given the complex shapes and structural behaviours that a multi-sprung strut would exhibit and the associated complexity an alternative analysis and form finding method will need to be developed.

The development of such an alternative method is likely to require the development of a displaced form that is based on the buckled shape of a multi sprung strut to ensure that the structure will start from an initial position of stable equilibrium. This initial starting position will naturally settle and shift as self-weight load cases are added but will create a sensible starting position for finding the shapes of arches with complex spring arrangements.

### 4.1.3 Finite Difference Approach.

Both of the approaches set out previously have demonstrated that a simple strut with a central hinge can be solved using either a geometrical or an energy-based approach. Buckling of struts with non-uniform cross-sections using finite difference methods is well documented (Coates, Coutie, & Kong, 1988, pp433; Perrone & Kao, 1975) with its accuracy and applicability to buckling problems being well proven (Iremonger, 1980).

However, there is a lack of research or published data on the finite difference approach being applied to a strut with a sprung hinge or hinges. Raskin and Roorda (1996) have reduced pantographic deployable towers to a series of spring linked struts but took a stiffness matrix-based approach rather than a finite difference rationale. This is somewhat like the investigation of the struts being considered here, but a numerical approach offers a flexible and scriptable method of solving the associated differential equations.

An alternative numerical method for determining the critical buckling load of struts through the introduction of rotational springs as an analytical tool was proposed by Hencky (1921) whereby a series of infinitely stiff links could be connected with a series of rotational springs to approximate an equivalent flexural element. As the connecting links were infinitely stiff, the flexural and buckling stiffness of the system is entirely governed both by the number of and the stiffness of the rotational springs.

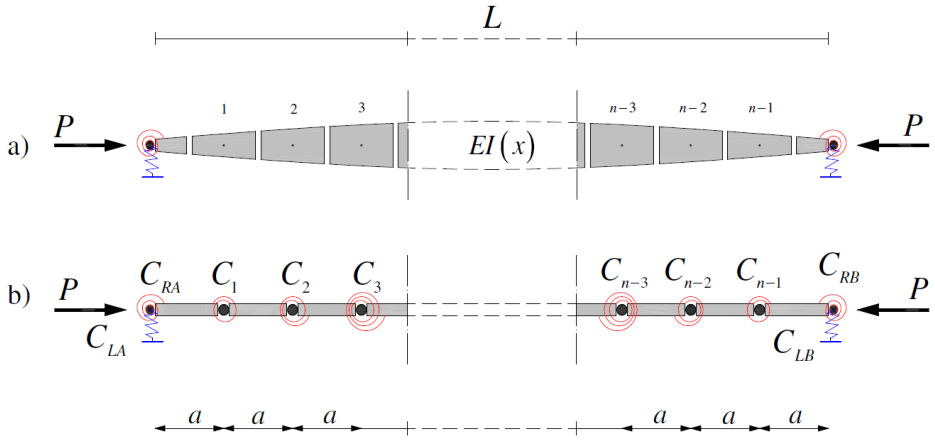


*Figure 4-3 - Non-uniform Strut Idealised as a Hencky Bar-Chain For Buckling Analysis.*[65]

[65] Ruocco, E., Zhang, H., & Wang, C. (2016). Hencky bar-chain model for buckling analysis of non-uniform columns. *Structures, 6*, 73-84.

The primary benefit of modelling an element using Hencky's proposed method was that it allowed for an element to be solved using simpler algebraic techniques rather than having to solve more complex differential equations.

Since the completion of this chapter of the thesis and subsequent examination, it has become clear from the examiners that there has been a recent resurgence of Hencky's proposed methods. Zhang, Wang, and Challamel (2016) have re-established and greatly expanded the application of Hencky's work beyond buckling into vibration assessments and establishing the behaviour of framed structures. Whilst the work of Zhang et al is not specifically focused on the application of determining buckling loads of sprung structures by solving differential equations using finite difference methods, there are similarities with Hencky's work simply by virtue of the method subdividing the structural elements and then reconnected them with rotational springs to model elements.

As noted above, one of the key benefits proposed by Zhang et al for the Hencky bar-chain method is that the beam is simulated through infinitely stiff links connected with springs to represent the equivalent flexural stiffness (C. M. Wang, Zhang, Gao, Duan, & Challamel, 2015) and this allows the solution of simple algebraic rather than differential equations. For example, a column would typically be sub-divided into smaller sub-elements as shown in Figure 4-3 but the number of elements used in the sub-division of the system has been shown to affect the accuracy of the results (Ruocco, Zhang, & Wang, 2016). There is no universal number of sub-elements that provides exact results as the number of sub-elements is influenced by the end conditions and complexity of the internal geometry and associated springs, although for complex non-uniform struts 100 sub-elements was found to give reasonable critical buckling loads that were validated against similar values calculated by Timoshenko.

Investigations specifically into the buckling performance of sprung struts, rather than the behaviour of normal struts approximated with springs as in Hencky's methods, were not identified during the research presented within this thesis. Although Zhang et al. (2016) paper includes an example of a sprung strut with an internal rotational spring which has been established using finite difference methods to enable a comparison with an equivalent Hencky bar-chain model, their paper does not develop the finite difference method beyond establishing the governing equations, does not identify the change in behaviour of the structural systems with springs integrated post-buckling, nor does it identify any challenges that may be present with solving these structural systems. Such as for example, incompatible stiffnesses or ill-conditioning which will be presented later in this chapter (see Section 4.6).

As the output and methods established within this chapter were completed before the papers were published by Zhang et al in 2016 there may be merit in revisiting and comparing the Hencky bar-chain methods in more detail in the future out of intellectual curiosity, however the method established within this chapter using the finite difference method is not rendered redundant by, nor does it duplicate, the research of Zhang and it is still held that the work within this section of the thesis is classed as novel.

As a starting point in applying the finite difference method to sprung struts, a uniform strut will be considered, considering the Euler buckling load but the stiffness matrix will be manipulated to reflect the softening of the struts that will occur through the introduction of the springs. The determination of the Euler buckling load for a uniform cross-sectioned strut will be considered using the well-documented approach for finite difference and this will be coded within Mathematica for ease of calculation with sample elements of code being contained within 'Mathematica Snippets' to allow the reader to follow the process.

Once results from this approach are coded and validated in Mathematica the Mathematica notebook will be modified to integrate a single element hinge of given rotational stiffness at midpoint which can be validated against the other methods presented in section 4.1.1. Once the notebook can accurately determine the buckling load for a single spring model, it will be expanded to include a mapped approach which will let multiple springs integrated at regular intervals and the associated buckling load be determined. Using the following notation:

$$q = -\frac{dV}{dx} \tag{4.17}$$

$$V = \frac{dM}{dx} - Py \tag{4.18}$$

$$EI\frac{d^2y}{dx^2} = -M \tag{4.19}$$

Where: q = Applied (transverse) load on the beam/column

V = Shear force in beam/column

P = Applied axial load on beam/column

M = Bending moment in beam/column

E = Young's Modulus

I = Second Moment of Area of the beam/column

These equations can then be combined to give.

$$EI\frac{d^3y}{dx^3}+P\frac{dy}{dx}=-V \tag{4.20}$$

$$EI\frac{d^4y}{dx^4}+P\frac{d^2y}{dx^2}=q \tag{4.21}$$

Consider modifying each term to convert it into a finite difference equation:

$$EI\frac{y_{i-2}-4y_{i-1}+6y_i-4y_{i+1}+y_{i+2}}{dx^4}+P\frac{y_{i-1}-2y_i+y_{i+1}}{dx^2}=q_i \tag{4.22}$$

If there is no lateral load and given that we're only interested in determining the Euler Buckling loads by extracting the Eigenvalues for an axial load, this gives.

$$EI\frac{y_{i-2}-4y_{i-1}+6y_i-4y_{i+1}+y_{i+2}}{dx^4}+P\frac{y_{i-1}-2y_i+y_{i+1}}{dx^2}=0 \tag{4.23}$$

As we're only considering a pin ended support, the boundary conditions will need modifying to reflect this, taking $y_0=0, y_{-1}=-y_1$ and $y_{-2}=-y_2$, as shown in Figure 4-4.

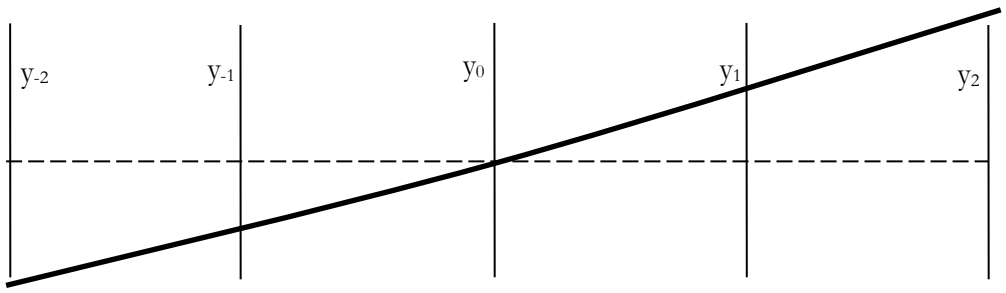


*Figure 4-4 - FD Pinned Boundary Conditions.*

Once the matrices have been modified to accommodate the boundary conditions, then the critical buckling load may be determined.

This is an ***eigenvalue*** problem, of the form:

$$Ay=\lambda y \text{ or } (A-\lambda I)y=0 \tag{4.24}$$

Where A is a square matrix,

I is the identity matrix

One solution to this equation is y=0, i.e. the column does not buckle. Disregarding this trivial solution, the non-trivial solution(s) to this equation is a series of ***eigenvalues*** of λ. For each eigenvalue, there is an associated ***eigenvector*** (found by substituting the eigenvalue into the above equation and solving).

The eigenvalues give the critical load of the column for different failure modes and the eigenvectors give the failure mode shape.

### 4.1.4 Multi-Hinged Example.

Working through the problem set out in the figure below, the finite difference method will be applied to the strut with a pair of hinges, as shown in Figure 4-5.

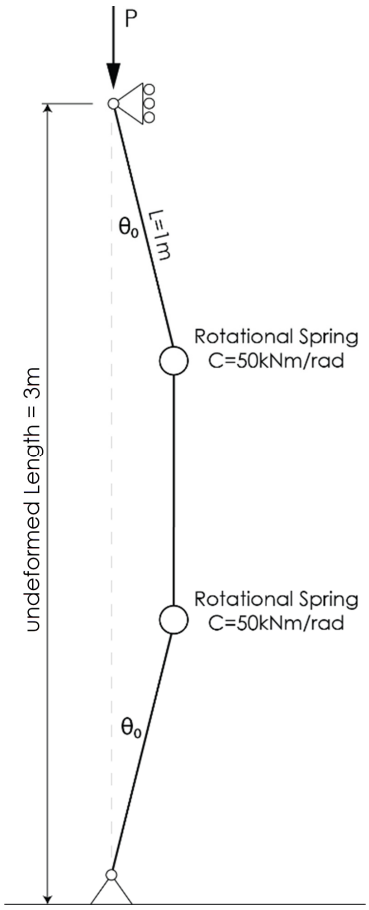


*Figure 4-5 - Twin Hinged Strut.*

The first step is to establish the variables that will require input from the engineer to complete the numerical process, these will be:

Young's Modulus (e) = 200,000,000 N/mm² (lower case e used as E is reserved in Mathematica)

The number of hinges (numhinge) = For this example 2, the range varies between 1 and 8.

Number of nodes each sub-link should be divided into (segments) = 3

Stiffness (i) = 33,500,000 $mm^4$ (lower case i used as I is reserved in Mathematica)

Rotational spring stiffness (moment) = 50kNm/rad

Total length of the strut (l) = 3000mm.

With the variables declared and defined, the next step is to start to calculate the parameters that will be used to construct the matrices, these include determining the total number of nodes required (nn) and the associated segmental length of each piece (lx).

*Mathematica Snippet 8*

```
nn = (numhinge + 1)*segments + 1

lx = 1/(nn - 1)
```

With the outline parameters declared, the next step is to establish the modification required to integrate a rotational hinge within the structural arrangements. Numerous examples and research exist for applying finite difference on uniform struts and indeed for struts of varying sectional stiffness, but the application of the method for the inclusion of a rotational spring in this work is both novel and undocumented.

The equations established above are taught on undergraduate degrees and are both commonplace and well understood by structural engineers the world around. However, they are not generally seen as being compatible with the inclusion of rotational springs, instead typically being applied to solid elements.

The proposed method for integrating a rotational spring within this example is through the modification of the Young's Modulus for the spring segments only, this gives a flexural behaviour that models the rotational spring suitably.

Through manipulating the equation of simple bending, it is possible to mimic the behaviour of a rotation spring.

$$\frac{M}{I} = \frac{\sigma}{y} = \frac{E}{R} \tag{4.25}$$

Taking:

M = Bending Moment.

I = Moment of Inertia about the Bending Axis.

$\sigma$ = Fibre stress at distance y from the centroidal/neutral axis.

E = Young's Modulus

R = Radius of curvature of the bent beam.

This is naturally based on several assumptions which will be held whilst determining the Euler buckling load, those being:

1. Plane sections of the beam remain plane.
2. The material is homogenous and obeys Hooke's Law.
3. The moduli of elasticity are equal for both tension and compression.
4. The beam is initially straight and of a constant cross-section.
5. The plane of loading contains a principal axis of the beam cross-section and the loads must be perpendicular to the longitudinal axis of the beam.
6. The springs are linear.

Rearranging the above equation, it is possible to define the equivalent Young's Modulus for the spring ($E_{spring}$) in terms of the moment (M), the inertia (I) and radius (R).

$$E_{spring} = \frac{MR}{I} \tag{4.26}$$

The spring that is being replicated has been allocated a stiffness of 50kNm/rad, essentially this defines that a forced moment of 50kNm applied to the section will yield a corresponding rotation of 1 radian.

If the flexed arc length of the segment being subjected to the moment remains the same length, then with the angle measured in radians:

$$arc\ length = radius \times angle \tag{4.27}$$

Which, taking the angle to be 1 radian and assuming no change in overall length of the flexed section gives that the radius is equal to the segmental length (lx). The final step is to determine the ratio between the stiffness of the solid elements and the rotational springs (eratio) for use in modifying the matrices later in the calculation.

*Mathematica Snippet 9*

```
radius=lx

ehinge = (moment*1000000*radius)/i

eratio = e/ehinge
```

Taking the strut under consideration, having 2 hinges and 3 segments per section, the matrices for the LHS and the RHS can be assembled.

*Mathematica Snippet 10*

```
lhs = DiagonalMatrix[ConstantArray[6, nn]] +
DiagonalMatrix[ConstantArray[-4, nn - 1], 1] +
DiagonalMatrix[ConstantArray[-4, nn - 1], -1] +
DiagonalMatrix[ConstantArray[1, nn - 2], 2] +
DiagonalMatrix[ConstantArray[1, nn - 2], -2];
```

$$lhs = \begin{pmatrix} 6 & -4 & 1 & 0 & 0 & 0 & 0 & 0 & 0 & 0 \\ -4 & 6 & -4 & 1 & 0 & 0 & 0 & 0 & 0 & 0 \\ 1 & -4 & 6 & -4 & 1 & 0 & 0 & 0 & 0 & 0 \\ 0 & 1 & -4 & 6 & -4 & 1 & 0 & 0 & 0 & 0 \\ 0 & 0 & 1 & -4 & 6 & -4 & 1 & 0 & 0 & 0 \\ 0 & 0 & 0 & 1 & -4 & 6 & -4 & 1 & 0 & 0 \\ 0 & 0 & 0 & 0 & 1 & -4 & 6 & -4 & 1 & 0 \\ 0 & 0 & 0 & 0 & 0 & 1 & -4 & 6 & -4 & 1 \\ 0 & 0 & 0 & 0 & 0 & 0 & 1 & -4 & 6 & -4 \\ 0 & 0 & 0 & 0 & 0 & 0 & 0 & 1 & -4 & 6 \end{pmatrix}$$

*Mathematica Snippet 11*

```
rhs = DiagonalMatrix[ConstantArray[-2, nn]] +
DiagonalMatrix[ConstantArray[1, nn - 1], 1] +
DiagonalMatrix[ConstantArray[1, nn - 1], -1] ;
```

$$rhs = \begin{pmatrix} -2 & 1 & 0 & 0 & 0 & 0 & 0 & 0 & 0 & 0 \\ 1 & -2 & 1 & 0 & 0 & 0 & 0 & 0 & 0 & 0 \\ 0 & 1 & -2 & 1 & 0 & 0 & 0 & 0 & 0 & 0 \\ 0 & 0 & 1 & -2 & 1 & 0 & 0 & 0 & 0 & 0 \\ 0 & 0 & 0 & 1 & -2 & 1 & 0 & 0 & 0 & 0 \\ 0 & 0 & 0 & 0 & 1 & -2 & 1 & 0 & 0 & 0 \\ 0 & 0 & 0 & 0 & 0 & 1 & -2 & 1 & 0 & 0 \\ 0 & 0 & 0 & 0 & 0 & 0 & 1 & -2 & 1 & 0 \\ 0 & 0 & 0 & 0 & 0 & 0 & 0 & 1 & -2 & 1 \\ 0 & 0 & 0 & 0 & 0 & 0 & 0 & 0 & 1 & -2 \end{pmatrix}$$

Once the base matrices have been established, they will require modification to take into consideration the boundary conditions.

*Mathematica Snippet 12*

```
mlhs = lhs[[;; -2, 2 ;;]];

xredlhs = Drop[mlhs, 1, -1];
```

$$xredlhs = \begin{pmatrix} 6 & -4 & 1 & 0 & 0 & 0 & 0 & 0 \\ -4 & 6 & -4 & 1 & 0 & 0 & 0 & 0 \\ 1 & -4 & 6 & -4 & 1 & 0 & 0 & 0 \\ 0 & 1 & -4 & 6 & -4 & 1 & 0 & 0 \\ 0 & 0 & 1 & -4 & 6 & -4 & 1 & 0 \\ 0 & 0 & 0 & 1 & -4 & 6 & -4 & 1 \\ 0 & 0 & 0 & 0 & 1 & -4 & 6 & -4 \\ 0 & 0 & 0 & 0 & 0 & 1 & -4 & 6 \end{pmatrix}$$

*Mathematica Snippet 13*

```
mrhs = rhs[[;; -2, 2 ;;]];

xredrhs = Drop[mrhs, 1, -1];
```

$$xredrhs = \begin{pmatrix} -2 & 1 & 0 & 0 & 0 & 0 & 0 & 0 \\ 1 & -2 & 1 & 0 & 0 & 0 & 0 & 0 \\ 0 & 1 & -2 & 1 & 0 & 0 & 0 & 0 \\ 0 & 0 & 1 & -2 & 1 & 0 & 0 & 0 \\ 0 & 0 & 0 & 1 & -2 & 1 & 0 & 0 \\ 0 & 0 & 0 & 0 & 1 & -2 & 1 & 0 \\ 0 & 0 & 0 & 0 & 0 & 1 & -2 & 1 \\ 0 & 0 & 0 & 0 & 0 & 0 & 1 & -2 \end{pmatrix}$$

*Mathematica Snippet 14*

```
supportend1 = 5;

supportend2 = 5;

xredlhs[[1, 1]] = supportend1;

xredlhs[[nn - 2, nn - 2]] = supportend2;
```

$$xredlhs = \begin{pmatrix} 5 & -4 & 1 & 0 & 0 & 0 & 0 & 0 \\ -4 & 6 & -4 & 1 & 0 & 0 & 0 & 0 \\ 1 & -4 & 6 & -4 & 1 & 0 & 0 & 0 \\ 0 & 1 & -4 & 6 & -4 & 1 & 0 & 0 \\ 0 & 0 & 1 & -4 & 6 & -4 & 1 & 0 \\ 0 & 0 & 0 & 1 & -4 & 6 & -4 & 1 \\ 0 & 0 & 0 & 0 & 1 & -4 & 6 & -4 \\ 0 & 0 & 0 & 0 & 0 & 1 & -4 & 5 \end{pmatrix}$$

With the base matrices defined, the next stage is to start compiling the matrices that generate the base stiffness of the structure and then to map through the amended stiffnesses that will represent the springs.

*Mathematica Snippet 15*

```
stiff = ConstantArray[e, nn - 2];
```

$$stiff = \begin{pmatrix} 200000000 \\ 200000000 \\ 200000000 \\ 200000000 \\ 200000000 \\ 200000000 \\ 200000000 \\ 200000000 \end{pmatrix}$$

Given that two hinges within this matrix need to be modified by eratio, the matrix needs to be adjusted to reflect the integration of these hinges. To automate this a directory is created that will map the modifications needed following the number of hinges specified.

*Mathematica Snippet 16*

```
maptable = Partition[Table[segments i, {i, numhinge}], 1]
```

$$maptable = \begin{pmatrix} 3 \\ 6 \end{pmatrix}$$

The deflection matrix is constructed with the first value from this base matrix extracted and then divided by the spring ratio. With this value stored as the variable 'realspring', it is then mapped back into the matrix at the locations defined by maptable.

*Mathematica Snippet 17*

```
def = (stiff i)/(1000*lx^2);

realspring = def[[1]]/eratio;

def = ReplacePart[def, maptable -> realspring];
```

$$def = \begin{pmatrix} 6.03\times10^{7} \\ 6.03\times10^{7} \\ 150 \\ 6.03\times10^{7} \\ 6.03\times10^{7} \\ 150 \\ 6.03\times10^{7} \\ 6.03\times10^{7} \end{pmatrix}$$

As becomes immediately evident, there are 2 'softened' hinges contained within the matrix that represent the two springs integrated within this example.

*Mathematica Snippet 18*

```
tlhss = def xredlhs;
```

$$tlhss = \begin{pmatrix} 3.015\times10^{8} & -2.412\times10^{8} & 6.03\times10^{7} & 0. & 0. & 0. & 0. & 0. \\ -2.412\times10^{8} & 3.618\times10^{8} & -2.412\times10^{8} & 6.03\times10^{7} & 0. & 0. & 0. & 0. \\ 150. & -600. & 900. & -600. & 150. & 0. & 0. & 0. \\ 0. & 6.03\times10^{7} & -2.412\times10^{8} & 3.618\times10^{8} & -2.412\times10^{8} & 6.03\times10^{7} & 0. & 0. \\ 0. & 0. & 6.03\times10^{7} & -2.412\times10^{8} & 3.618\times10^{8} & -2.412\times10^{8} & 6.03\times10^{7} & 0. \\ 0. & 0. & 0. & 150. & -600. & 900. & -600. & 150. \\ 0. & 0. & 0. & 0. & 6.03\times10^{7} & -2.412\times10^{8} & 3.618\times10^{8} & -2.412\times10^{8} \\ 0. & 0. & 0. & 0. & 0. & 6.03\times10^{7} & -2.412\times10^{8} & 3.015\times10^{8} \end{pmatrix}$$

Conveniently Mathematica has inbuilt routines that can solve an entire Eigen System, the final step is to invoke this routine to extract the Eigen Values and then numerically extract the largest of these to determine the Euler buckling load in kN (negative).

*Mathematica Snippet 19*

```
{gvals, gvecs} = Eigensystem[{tlhss, xredrhs}];

eigenbuckle = Max[gvals] // N
```

$$-49.999806624490006$$

Typically, the output in Mathematica is suppressed to 3 decimal places, but the full value is shown here for completeness to demonstrate the minimal error, even with a coarse mesh the theoretical value for this system should be 50kN.

Generally, when this routine is run within Mathematica it has a computation time of approximately 0.03 seconds on a laptop running Windows 10, Mathematica 11.3 on an i7 Processor with 16Gb of RAM.

The time taken varies minimally depending on the number of hinges used providing they are less than 10, and the number of segments (up to 170), although as can be seen in this example even a relatively coarse mesh has returned values with a very low error.

However, it should be noted that the code has been optimised with a few minor but subtle adjustments to significantly reduce computation time, the largest of which is based on invoking the numerical solving engine within Mathematica rather than the symbolic engine which the

software defaults too.

This is achieved simply through the addition of a decimal point to the variable l which is the overall length of the strut. This declares the value being assigned as a number and consequently all calculations based upon l will equally be a number (rather than a symbol) and Mathematica will invoke the numeric engine as a result. As an example, several of the models that solved in 0.03 seconds in Mathematica under the numeric engine were unable to complete after several hours when processed through the symbolic engine. This builds on the lessons learned within the Mathematica modelling of the arches within chapter 3.

The initial choice for the Young's Modulus that the struts should start with also has a significant effect on the success of the notebook achieving an appropriate solution. If a value for the Young's Modulus is selected that is too low then the flexural stiffness of the struts will reduce the buckling capacity below that of the Euler value sought, as the system is no longer governed purely by the spring stiffness. The counter to this, however, is that if a Young's Modulus is defined that is excessively rigid then numerical instability can be observed (ill-conditioning) which either prevents any solution being found or, more dangerously, an incorrect solution can be found which may be non-conservative.

The influence of the initial choice of Young's Modulus is investigated in more detail later in the thesis where the effect of flexural vs rotational stiffness is investigated within the CivilFEM finite element models.

## 4.2 Computer Analysis.

Whilst simple sprung chains such as those covered within the previous chapter can be idealised through using either energy or geometrical methods, more complex structures will need to make use of Finite Element Methods, the springs introduce an element of non-linear geometrical behaviour and not all software will necessarily be able to reliably predict this behaviour. Whilst CivilFEM was eventually selected to be the final choice of software, numerous packages were evaluated and developed including ROBOT, ANSYS, ABAQUS, Inventor, SolidCAM, Fusion360 and CivilFEM. Some of the investigations are presented before the final methodology to show some of the limitations that were encountered and how these limitations influenced the final working methodology.

To this end, several pieces of software have been investigated with regards determining the buckling loads for a hinged strut with a spring with varying levels of success.

The common problem to be investigated within the various software packages is the structural arrangement shown in Figure 4-1 on page 4-128. With a 4m long, 2m segmented hinged strut. The central hinge should possess a rotational stiffness of 50kNm/rad.

### 4.2.1 Autodesk ROBOT.

Autodesk ROBOT provides free versions of their software for non-commercial use for students and academics alike. Generally, the software is aligned with structural analysis of framed buildings, with wizards and analytical engines being integrated into a common environment that is also extended out to elemental design based on various design codes. Whilst the investigations with regards buckling using Autodesk ROBOT found that the software generally was unable to suitably analyse the buckling of sprung struts an overview is presented here for completeness and to emphasise the non-trivial nature of the analysis being undertaken.

ROBOT is used widely on the curriculum at Salford with the software being logical to use and powerful with regards the integrated analysis. Various forms of structures have been analysed reliably with the software ranging from simple 2D framed structures, through to 3D frames, cable-supported lightweight structures, tensegrity prisms and motion-controlled deployable structures. None of these structures though have had their buckling behaviour investigated, and whilst the analysis is reliable for static behaviour of orthodox structures, the behaviour of non-linear structures has still to be determined.

Given that ROBOT is aimed at structural design, one of the limiting factors is the difficulty with creating custom materials as the software is aimed at creating linear analysis/design paths through the software. One of the strategies employed in creating models that match the theoretical values is through the modification of the Young's Modulus to a value that enables the elements to become infinitely stiff, the limiting value of this within custom materials in ROBOT is $9x10^4$ MPa which will bring limitations in certain models.

Taking a 100mm diameter solid section with a Young's Modulus of $9x10^4$MPa gives a critical buckling load for the first mode of 43.29kN, which would infer that the flexural stiffness of the struts is still governing but that the material stiffness cannot be increased further.

One solution to this would be to use a larger diameter cylinder for the analysis, but this compromises the visual appearance of the strut and may lead to difficulties when constructing the models and selecting nodes for connecting. To develop a buckling load that is broadly comparable with the theoretical buckling value will require the creation of an artificially stiff element to control the influence of the flexural links. ROBOT also allows the creation of a

custom section with values for the second moment of area and cross-section being numerically defined, rather than calculated as a function of the geometry.

Typically, ROBOT colour codes input values to show when limits within the software have been reached, although this is not always the case. For example (see Figure 4-6) when creating custom section properties these limits can be exceeded and only when the properties dialogue is refreshed and reloaded can it be seen that the stiffnesses entered were excessive and have been replaced with infinity which flags up various errors during the solving process, which are believed to be associated with the incorrect buckling loads being calculated.

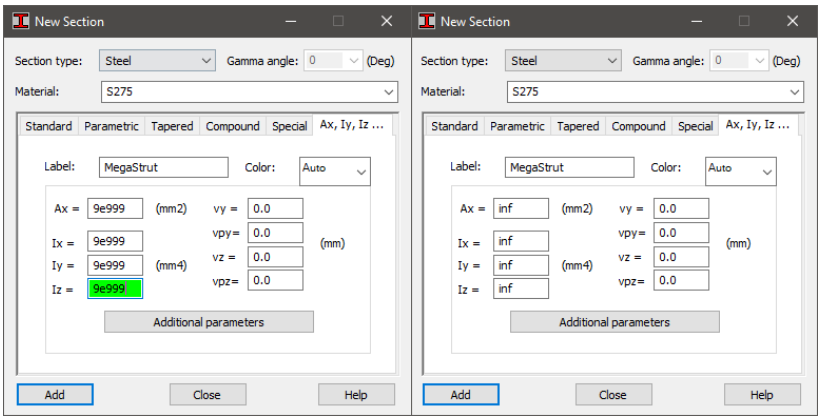


*Figure 4-6 – Section Stiffness In ROBOT Showing Values Defaulting To Infinity After Being Committed.*

Early models showed that there is a fine balance to be had with regards the cross-sectional areas and the stiffness of the elements, whereby elements that were defined as being too stiff lead to errors being generated within ROBOT (see Figure 4-7) that would infer that some form of ill-conditioning is present within the analysis. This is not entirely unexpected given the potentially large differences between the rotational and flexural stiffnesses of the struts.

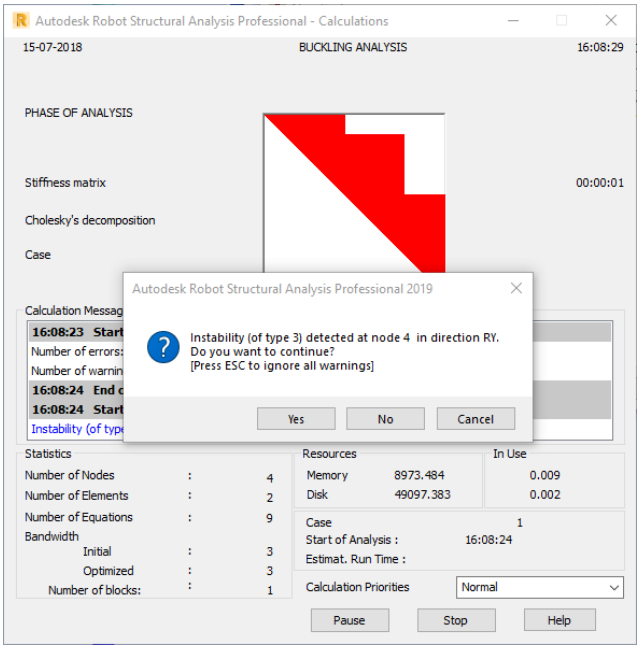


*Figure 4-7 - Analysis Error Messages Within ROBOT When Stiffnesses Increased Significantly.*

A trial and error approach has been undertaken with regards the section properties where the analysis started to converge, and the buckling of the structure was governed entirely by the rotational stiffness of the hinge. Typically for the 2m long strut, this was found to be a section with the Second Moment of Area of 9,000,000,000.0mm$^4$ and a Cross-Sectional Area of 900,000mm$^2$ which results in a critical buckling load of 49.9982kN. This buckling value could be refined to give an exact answer through further adjustment of the section properties but was deemed to be adequate for the initial trials.

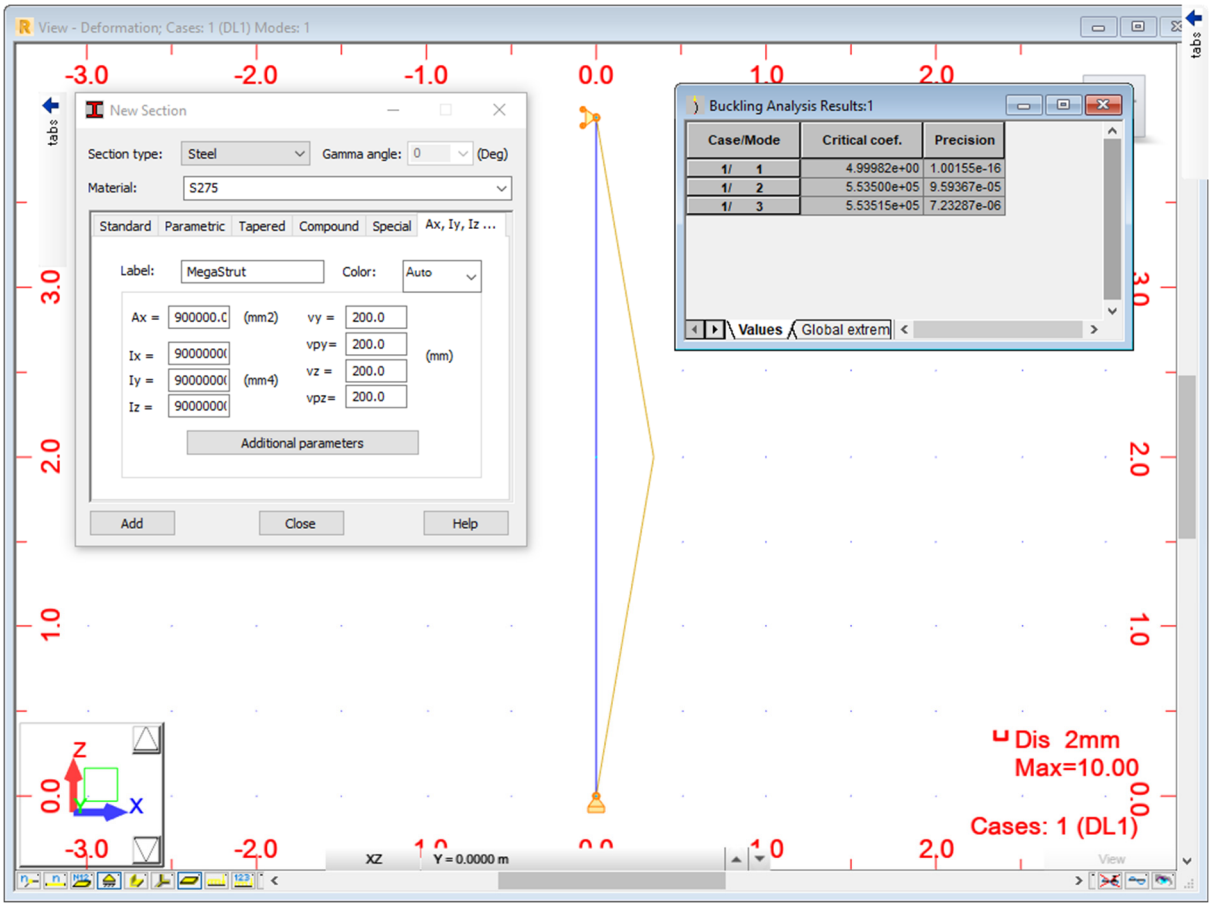


*Figure 4-8 - Critical Buckling For The First Mode Of A Hinged Strut.*

Whilst the buckling loads could be obtained by extracting the Eigenmodes as shown in Figure 4-8, the behaviour of the models through non-linear analysis was met with mixed results when trying to determine the incremental behaviour associated with forced displacement. This is primarily limited to the fact that ROBOT is unable to apply forced displacements within its analysis models at points other than the foundations (presumably to model settlements) and this forced displacement will be an important element to model when investigating adaptive, deployable, or metamorphic structures.

### 4.2.2 Finite Element Analysis.

ANSYS is available at the University, and whilst its prowess and ability to model complex structures have been long-standing within the engineering community for decades, its interface and output has not developed at the same pace as its competitors and visually and from a 'usability' perspective it has been left behind with a cumbersome workflow in parts.

Even ANSYS workbench with its new crisp interface misses the point for structural engineers by not allowing the plotting of commonly used output such as a bending moment diagram for an

entire frame, instead producing bending moments for individual elements, to this end an alternative was sought.

Several pieces of software were trialled and assessed ranging from SCIA and ABAQUS through to mechanical modelling pieces of software such as Inventor, Fusion, and Solid Edge with even small sub-routines being attempted to be custom scripted within Mathematica. The nature of the analysis proposed and the workflows within these pieces of software lead to mixed levels of results with either the motion being dealt with well, but the stresses poorly analysed or vice versa.

Finally, after many years of tinkering and endless model building of the same system a new numerical analysis tool was found that was able to reliably model some of the proposed structures and allowed validation of the simple strut with a central pin. CivilFEM has been used for the modelling of the flexible struts and arches throughout the rest of this thesis.

## 4.3 Modelling Within CivilFEM

CivilFEM originally began life as an add-in for ANSYS to adapt the interface to combat some of the criticisms levied at it by the Civil Engineering community. Since beginning its life as a simple interface hack, it has now grown and developed into a standalone computer package that makes use of the powerful MARC solver.

The following steps give a concise overview of the procedures followed to validate and achieve buckling loads that match the theoretical predictions of a strut with a central rotational spring and infinitely stiff links. Much of the process outlined here draws from the experience of the early ROBOT modelling process.

Whilst CivilFEM can appropriately analyse rotational springs, there is a current limitation within the software with regards the damping of the rotational springs. This will not affect the ability for static analysis to be undertaken with the frames, however, this will prevent the further development of any dynamic analysis associated with the frames, perhaps to demonstrate energy absorption associated with blast loading. This limitation was identified quite late in the research and reported to CivilFEM who too were unaware of this oversight with a patch due to be released sometime in 2020 to include the damping of rotational springs.

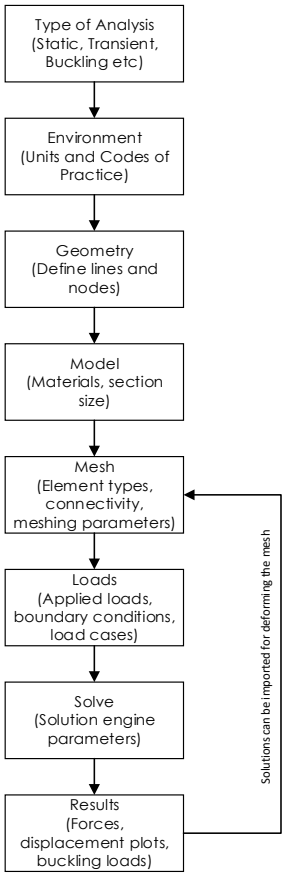


*Figure 4-9 - General Workflow Within CivilFEM for Structural Modelling.*

Essentially there will be two modelling processes investigated within CivilFEM, the first more traditional approach will be to undertake a buckling analysis where the Critical Buckling loads will be determined for a hinged strut. The second method will take the mode shape for the first mode and use this shape to create an initial displaced form via the deform mesh tool (to disrupt the perfect equilibrium) and then a forced displacement will be applied at the head of the strut to determine at what axial force the strut buckles at via a static non-linear geometry analysis. An overview of the general analysis procedure is shown in Figure 4-9.

### 4.3.1 Critical Buckling Load.

To determine the critical buckling load for the structure, the struts will need to be modelled so that for all intents and purposes they are deemed to be infinitely stiff and the buckling loads will be entirely governed by the rotational stiffness of the central spring. This method is primarily used to determine the Euler buckling load at which the struts buckles and the associated buckling shape. This buckling shape can help determine buckling shapes that can be re-introduced to later models as initial imperfections. The critical buckling models, however, do not present any information relating to the post-buckled performance or behaviour of the struts.

As with the earlier ROBOT models, two approaches would seem to be feasible, either through creating a set of geometrical properties that result in the second moment of area that develops a grossly artificial stiffness or through the development of a material with a disproportionately high Young's Modulus (E).

Within CivilFEM the Young's Modulus values are not limited in the same way that they are within ROBOT and so the creation of a custom material with an abnormally high Young's Modulus was selected as the approach to be adopted.

Importantly this allows for the visual appearance of the structure to look 'normal' without introducing custom sections, this was deemed to be important in maintaining a visual appraisal of the structural behaviour, particularly for future models that may have complex behaviour and where the visual appraisal will be important in identifying errors.

Through a trial and error approach, a Young's Modulus of $9x10^9$ MPa (for a 100mm diameter cylinder) appears to produce a model where the spring stiffness of the hinge dictates the buckling behaviour, see Figure 4-10 below, which has a critical buckling load of 50kN that matches the theoretical load.

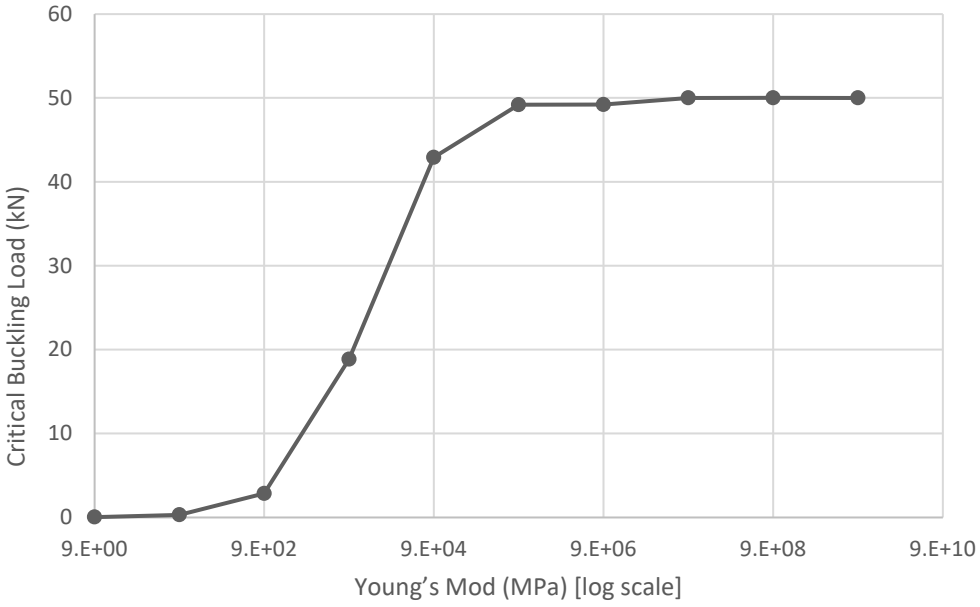


*Figure 4-10 - Material Stiffness (Plotted Logarithmically) Vs Buckling Load For The Strut System.*

The hinges are created within CivilFEM in much of a similar way as they would be within ANSYS and ROBOT where duplicate nodes are created within the software and then coupled with regards their translations and rotationally coupled but with an associated rotational spring

stiffness, in this case, 50kNm/rad.

Boundary conditions are as would be expected and shown in Figure 4-11, with a pinned support at the base (blue arrow in the x and y-direction) and a vertical roller modelled (blue arrow in the x-direction) at the top of the strut with a single 1kN vertical point (red arrow) applied to the head of the strut.

CivilFEM gives flexibility with regards to the number of modes that can be returned, but for this structure, only the first mode is of interest initially to determine the suitability of the analysis and modelling process and the rest will be discounted for now but will be considered in more detail in section 4.7 and section 5.11.3.

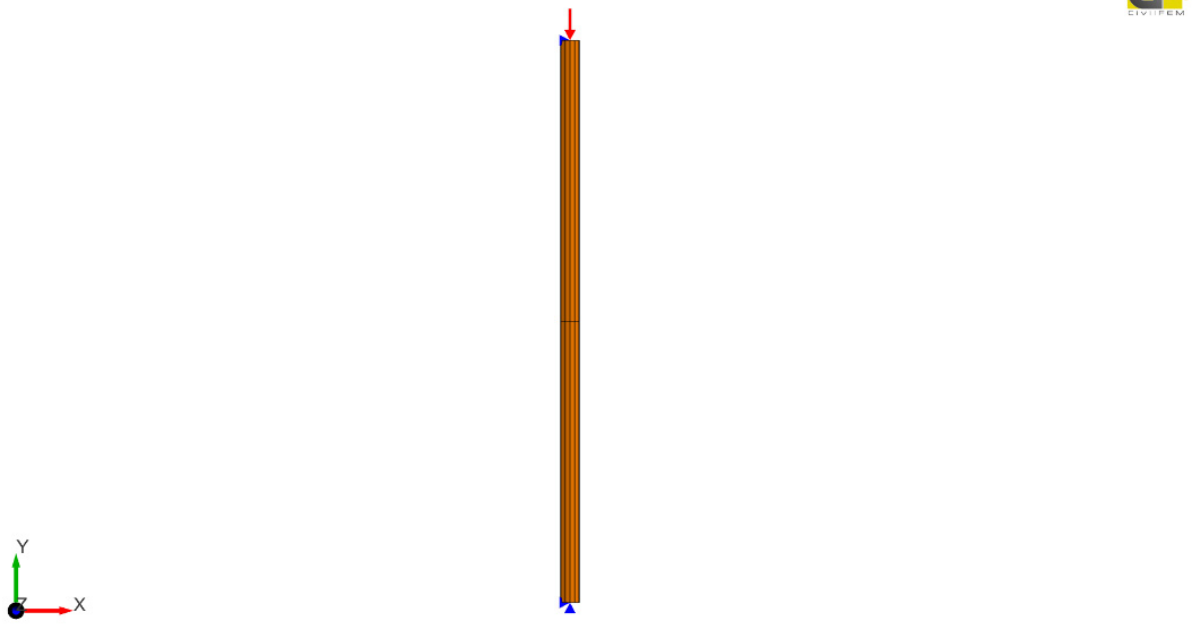


*Figure 4-11 - Boundary Conditions (Blue) And Applied Loads (Red) For Hinged Strut In CivilFEM.*

With the unit load and boundary conditions applied as shown in Figure 4-11, the last step is to combine these into a load case that can be solved. This also allows for refinement to be carried out with regards the fine-tuning of the solution engine, although typically for buckling analysis the default settings suffice. Once analysed the results can be loaded back into the software and the buckling load factor for the various modes can be displayed, see Figure 4-12.

| | Buckling m | Buckling load factor | File |
|---|---|---|---|
| | | Dimensionless | |
| | 1 | 66.667 | Buckling Case_1.rcf |
| | 2 | 13139375104.000 | Buckling Case_2.rcf |
| | 3 | 15981432832.000 | Buckling Case_3.rcf |
| | 4 | 674999959552.000 | Buckling Case_4.rcf |
| | 5 | 727913332736.000 | Buckling Case_5.rcf |
| | 6 | 1937032085504.000 | Buckling Case_6.rcf |
| | 7 | 9999999933815812... | Buckling Case_7.rcf |

*Figure 4-12 - Critical Buckling Loads For Various Modes.*

With the results loaded into CivilFEM, the typical plots such as the deflected form can be plotted to ensure that the mode of failure corresponds with the expectations of the engineer, see Figure 4-13.

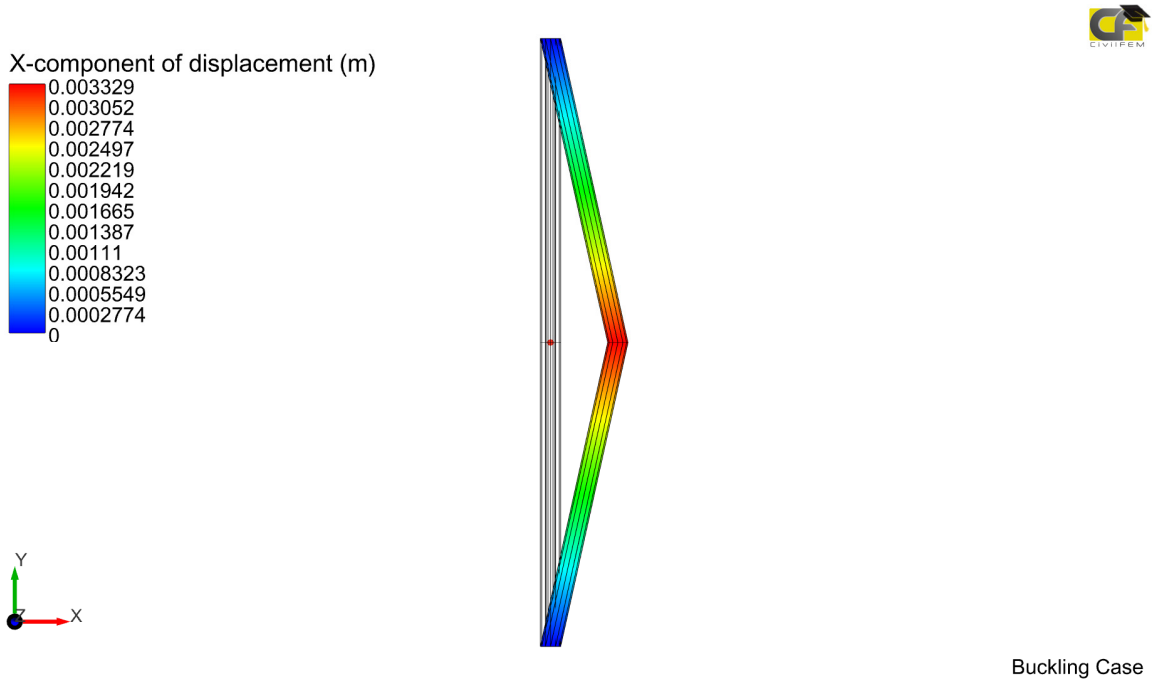


*Figure 4-13 - Deflected Form For The First Buckling Mode.*

From this initial model the critical buckling load for a 3m long strut, with a central spring of 50kNm/rad, is as expected at 66.667kN showing that the model is behaving appropriately and with high accuracy.

### 4.3.2 Forced Displacement Analysis.

Whereas the buckling analysis presented within section 4.3.1 is used to establish simply the Euler buckling load and the associated buckling shape, this analysis method cannot establish subsequent post-buckling behaviour of a structure which is a limitation given that a sprung strut may continue to support additional load post-buckling, see Figure 4-2. If analysis is undertaken through applying forces, then once the structure becomes unstable there may be a catastrophic

failure which will destabilise the loading or provide an accelerated motion which will generate an uneven distribution of data through the range of motion.

A forced displacement analysis, however, is capable of determining the post-buckling behaviour of a structure and maintains beyond the initiation of buckling in even increments, creating a steady controlled set of data points, although controlling the forced displacement is not without certain challenges. For example, if a structure is geometrically 'perfect' then the forced displacement analysis will not replicate the buckling behaviour as it will typically continue to maintain equilibrium and not deform into the correct buckled shape, instead providing misleading results as to the structure's capacity. To overcome this 'perfect' balance an initial defect needs to be introduced to the analysis model. This defect could be applied by a couple of methods such as the introduction of a small additional load positioned to unbalance the structure or via a more controlled measure, such as proposed in this research, that is to reintroduce the preferred buckling shape from an Euler buckling analysis and use this shape as the initial deformation to the strut. Whilst this method of analysis can investigate the post-buckling analysis of a cable sprung strut, it is a two-stage process with the initial stage being the determination of the critical buckling loads and associated buckling mode shape and thus it can be a lengthy process as a workflow.

An interesting difference to the CivilFEM workflow compared to that of ROBOT is the distinction between the buckling analysis and the static analysis requiring two distinct workflows. The static analysis within ROBOT is typically controlled by assigning a different analysis engine to distinct load cases, but ROBOT is limited to the application of loads rather than through forcing displacements (except at support locations to model foundation settlements). CivilFEM, however, requires the user to define the purpose of their analysis from the inception of the modelling process, see Figure 4-14.

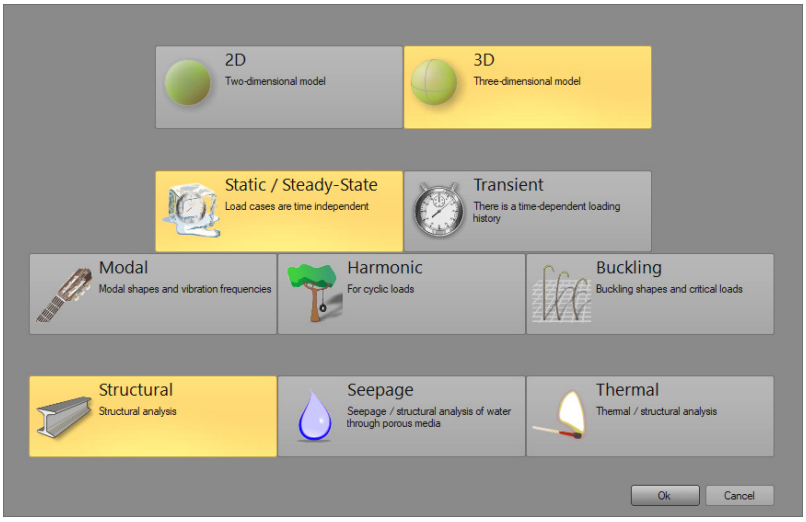


*Figure 4-14 - CivilFEM Model Creation Menu.*

Fortunately, CivilFEM allows the importing of geometry, material properties, and boundary conditions from previous analyses even when created using different analysis engines within CivilFEM. This is helpful in that once the primary buckling mode has been determined its associated displaced form can be re-introduced into the starting geometry as initial imperfection for the same structure through 'deforming' the mesh before solving to encourage the structure to buckle into the primary buckling mode identified.

The application of this displaced form in a manner that replicates the final buckled shape allows the structure to be disturbed from potential neutral equilibrium states and to move into a relevant displaced form and thus allows the solving of the model using a static/steady-state model.

The primary benefit of controlling the behaviour of the strut via a forced displacement rather than an applied load (as was the case for extracting the eigenmodes) is that certain forms of structure will collapse catastrophically under an applied point load and the load itself will become a destabilising load. Typically, analysis models struggle with these catastrophic effects and without additional adjustments to the solution engine will lose refinement in the results and miss data out during the analysis process. Various methods exist such as the arc-length method, but the lack of refined data due to collapse can be overcome more simply by applying a displacement rather than the applied vertical load to control the destabilising effects.

Once a model is imported and the mesh has been deformed from a previous buckling load case using the option shown in Figure 4-15, a displacement can be applied at the head of the column to determine the behaviour of the structure as it becomes destabilised. The deformed mesh can

be applied with scaling factors and clearly the larger the initial 'imperfection' the lower the buckling load.

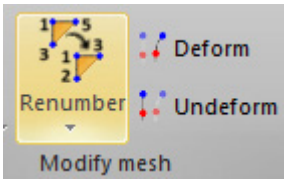


*Figure 4-15 - Modify Mesh Within CivilFEM.*

Following the completion of the analysis, it is possible to make use of the history plots function within CivilFEM to show how the load (measured as a reaction force at the support) relates to the displacement or rotation of the central hinge (see Figure 4-16). The structure still has a residual capacity (based on the support reaction) even though the structure has technically buckled showing that the structure can still support load effectively even when grossly deformed.

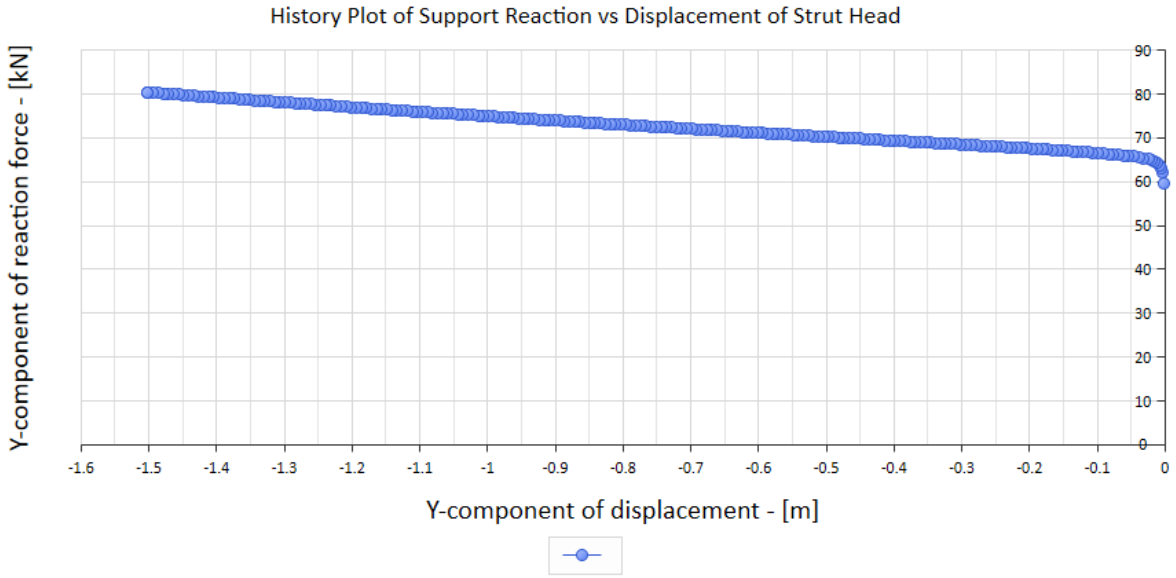


*Figure 4-16 - Sample History Plot From Within CivilFEM.*

As can be seen from the figure above, when the end of the strut is grossly deformed the structure retains an increased load capacity which is retained within the elastic region, the nonlinear behaviour of the rotation spring is evident when taken with respect to the lateral displacement of the strut. It is also clear from the approach above that the magnitude of the scaled deformation has an appreciable effect on the load at which the structure buckles, which corresponds with the underlying philosophy that the magnitude of the initial imperfection has a significant bearing on the buckling capacity.

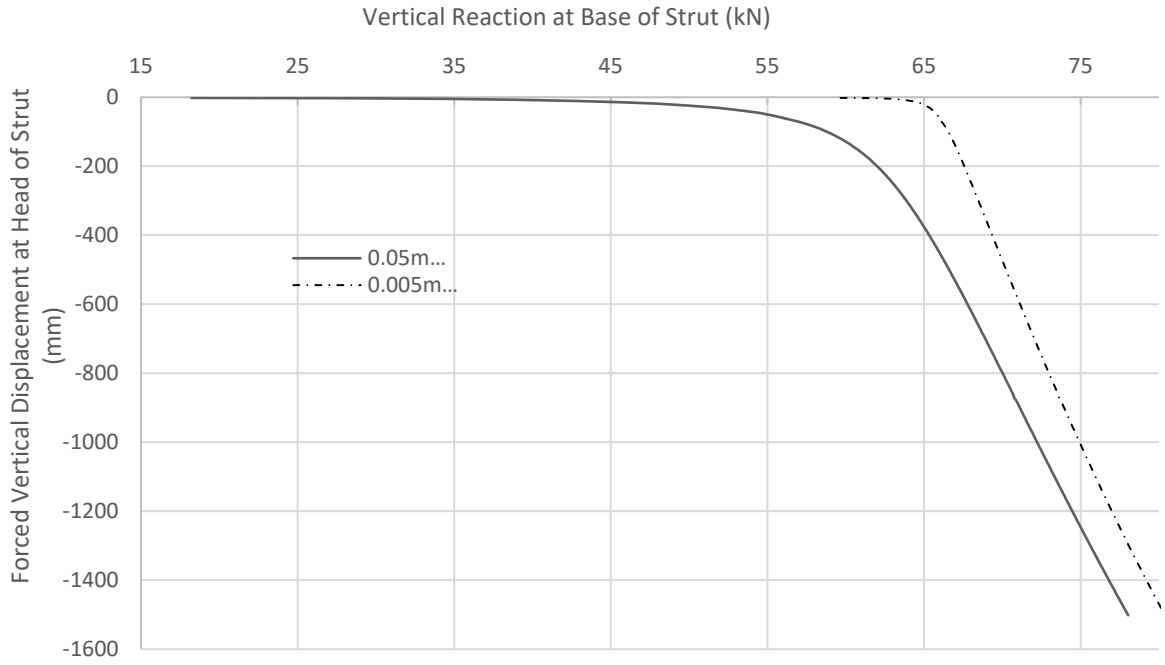


*Figure 4-17 - Effect of Initial Deformation to Strut.*

As can be seen in Figure 4-17 (above) the initial imperfection affects the critical buckling load, should the precise buckling load be required then the scale factor should be reduced to a single 1mm or 0.5mm displacement, although this load will always be slightly lower than the theoretical buckling load due to the initial destabilising imperfection. The ability to determine the change of force associated with a controlled displacement is also helpful when reviewing deployable structures as the intermediate stages during deployment are often omitted in the published research and the methodology proposed here could be used to determine the forces in deployable structures that make use of springs to control their motion.

## 4.4 Increased Number Of Springs.

Following the validation of the single spring model for buckling a Mathematica sheet was constructed to expand the number of segments and springs within a strut to determine the influence the number of springs has on a strut and the associated buckling load. Each spring location through the strut was placed at regular spacings to create a uniformly distributed arrangement of springs.

A series of 3m long struts, with a varying number of rotational springs (always 50kNm/rad), was created both for CivilFEM and using the Mathematica finite difference notebook. The critical buckling load for each of the struts is shown below in Figure 4-18 plotted for just the CivilFEM

models initially.

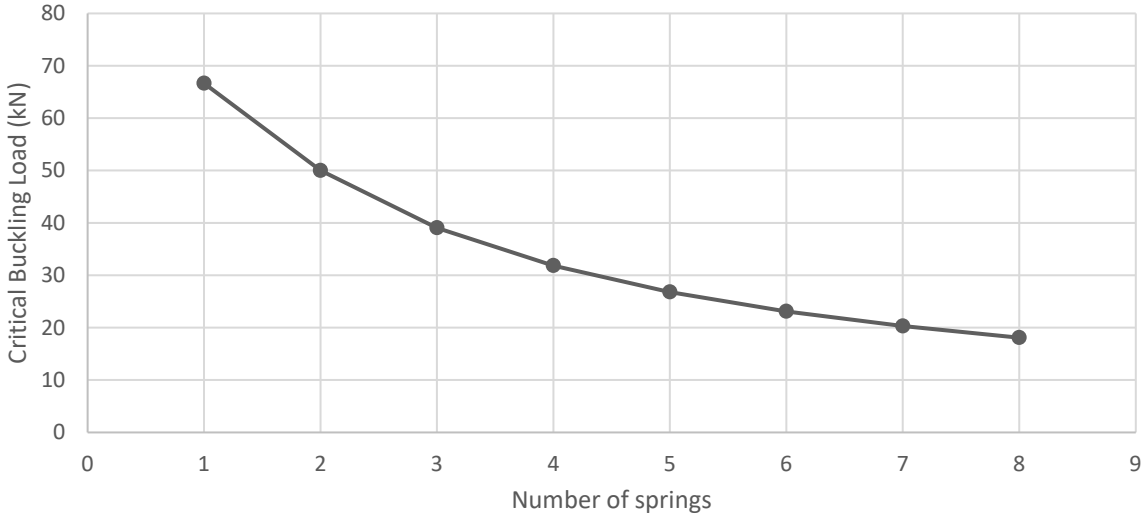


*Figure 4-18 - Buckling Load For Multi-Sprung Struts.*

As can be seen, there is a clear curved path for the graph, which would logically plateau out at the buckling load that is equivalent to when the strut is constructed out of a strut with a uniform stiffness along its length equal to that of being entirely made up of 50kNm/rad springs.

Comparing the output from the finite difference notebook and the output from CivilFEM (Table 2, below) shows that there is a strong agreement between the critical buckling loads (fractions of a per cent error) as the number of springs increase and that the modelling approach outlined is appropriate for the types of structures being investigated using CivilFEM.

*Table 2 - CivilFEM and Finite Difference Critical Buckling Loads Comparison.*

| **Number of hinges** | **Eigen Buckling** | |
|---|---|---|
| | **CivilFEM (kN)** | **Finite Difference (kN)** |
| 1 | 66.667 | 66.666 |
| 2 | 50.000 | 50.000 |
| 3 | 39.052 | 39.052 |
| 4 | 31.830 | 31.830 |
| 5 | 26.793 | 26.795 |
| 6 | 23.097 | 23.107 |
| 7 | 20.298 | 20.299 |
| 8 | 18.085 | 18.092 |

## 4.5 Material Stiffness and Model Conditioning.

The system being investigated requires that the links are infinitely stiff. Whilst this is fine for a theoretical investigation, for the numerical investigation the goal is to model a material that is so stiff that the behaviour is entirely governed by the rotational stiffness of the central spring. Eventually, the material stiffnesses will have to reflect the actual properties of the structure being considered for the real-world structures, but to validate CivilFEM's ability to accurately analyse the validation model the limits for being infinitely stiff had to be determined.

Preliminary investigations identified that depending on the number of decimal points being worked to, that a material stiffness of $9x10^9$ MPa gave acceptable results (clearly if the struts become longer then the material stiffness would require modifying) but CivilFEM does not place numerical limitations in the current version (CivilFEM 2018 64 bit) although there will be a limit at which point the system will cease to solve.

*Table 3 - Young's Modulus vs Critical Buckling Load.*

| **Young's Mod (MPa)** | **Critical Buckling Load (kN)** |
|---|---|
| $9.00\times10^9$ | 50 |
| $9.00\times10^8$ | 49.999 |
| $9.00\times10^7$ | 49.992 |
| $9.00\times10^6$ | 49.197 |
| $9.00\times10^5$ | 49.186 |
| $9.00\times10^4$ | 42.903 |
| $9.00\times10^3$ | 18.839 |
| $9.00\times10^2$ | 2.85 |
| $9.00\times10^1$ | 0.3 |
| $9.00\times10^0$ | 0.03 |

As can be seen from Table 3 above even a single reduction in magnitude for the Young's Modulus starts to affect the critical buckling load, although there is a sharp decline after the Modulus has been approximately halved in magnitude. Reassuringly the very small Young's Modulus gives a result that is almost at zero, a Young's Modulus of zero would not have solved, but when these values are plotted logarithmically they appear sensible, see Figure 4-19.

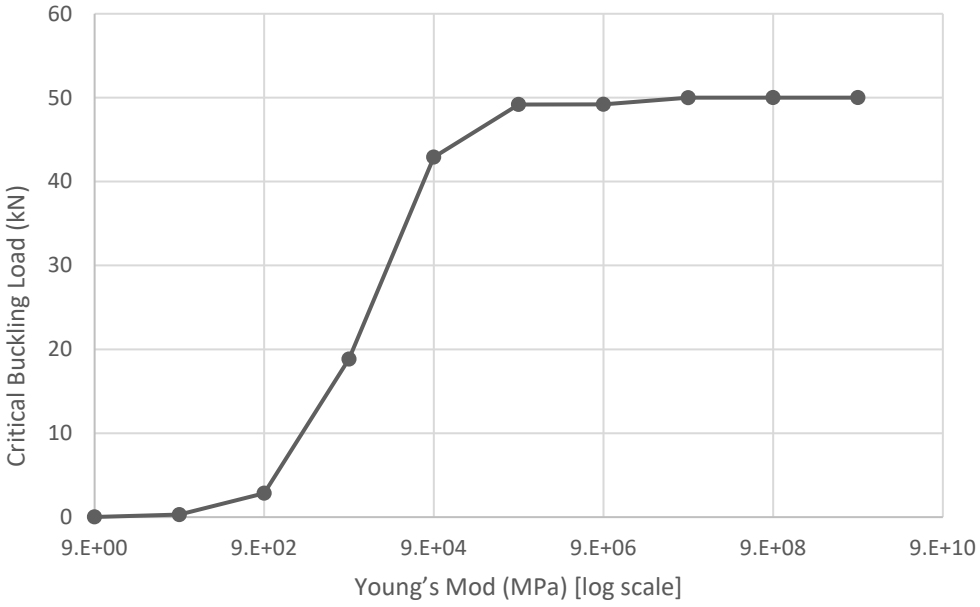


*Figure 4-19 - Material Stiffness (Plotted Logarithmically) Vs Buckling Load For The Strut System.*

Once a numerical value ($9x10^9$ MPa) was integrated into the material properties for the buckling analysis (with geometrical properties being set as a 100mm diameter circular column) the critical buckling values extracted from the analysis matched the theoretical values perfectly.

However, when the Young's Modulus was increased beyond $9x10^9$ MPa issues were noted where the output no longer provided sensible results and the influence of the matrices being ill-conditioned becomes apparent. As the flexural stiffness of the struts and the rotational stiffness of the springs are not directly comparable, their numerical ratio was determined with both stiffnesses being calculated with the input units of N and mm.

$$Flexural\ Stiffness = \frac{EI}{L} \tag{4.28}$$

With:

E = Young's Modulus ($N/mm^2$)

I = Moment of Inertia ($mm^4$)

L = Length (mm)

The rotational spring stiffnesses were multiplied by $1x10^6$ to convert them from kNm/rad to Nmm/rad.

A ratio was then determined between the flexural stiffness (as the length of each strut will reduce

as more springs are added) and the rotational stiffness to determine if there was a correlation or trend that could be identified within the modelling process for future models. As the range of these ratios has a broad spectrum, they were plotted using a logarithmic scale for ease of comparison as can be seen in Figure 4-20.

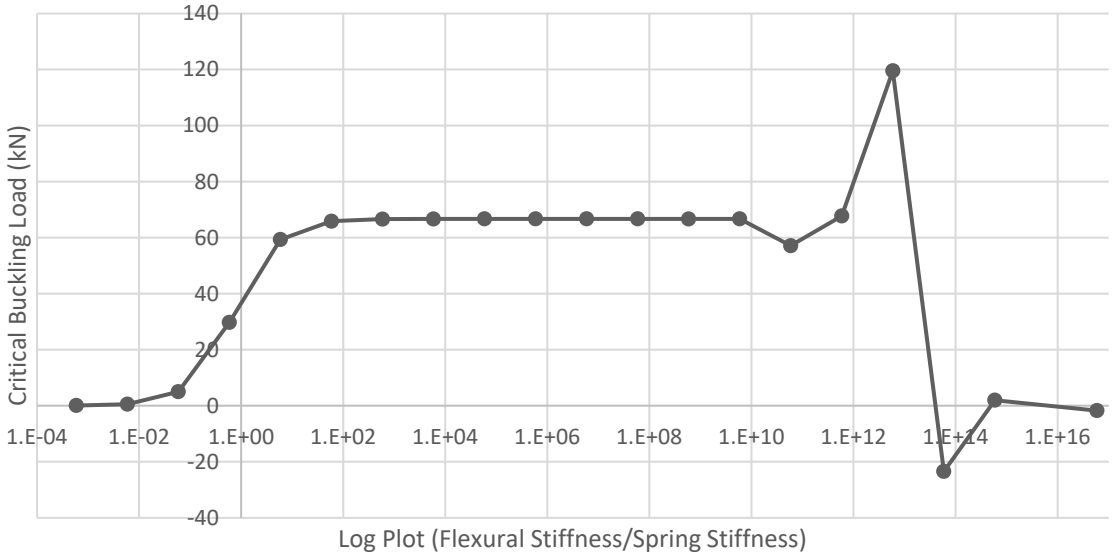


*Figure 4-20 - Log Plot Of Stiffness Ratio Vs Critical Buckling Load For A Single Spring 3m Strut Model.*

This graph shows that there is a sizeable plateau where the ratio is broadly acceptable, and the mode returns sensible results, but as the structural elements become increasingly stiff there comes a point where the model becomes ill-conditioned and the results are no longer reliable.

This process was repeated for the same 3m long strut, for a variety of Young's Modulus values for a range of number of springs, all springs were spaced equally, and the critical buckling loads are shown in the following graphs in Figures 4-27 to 4-33.

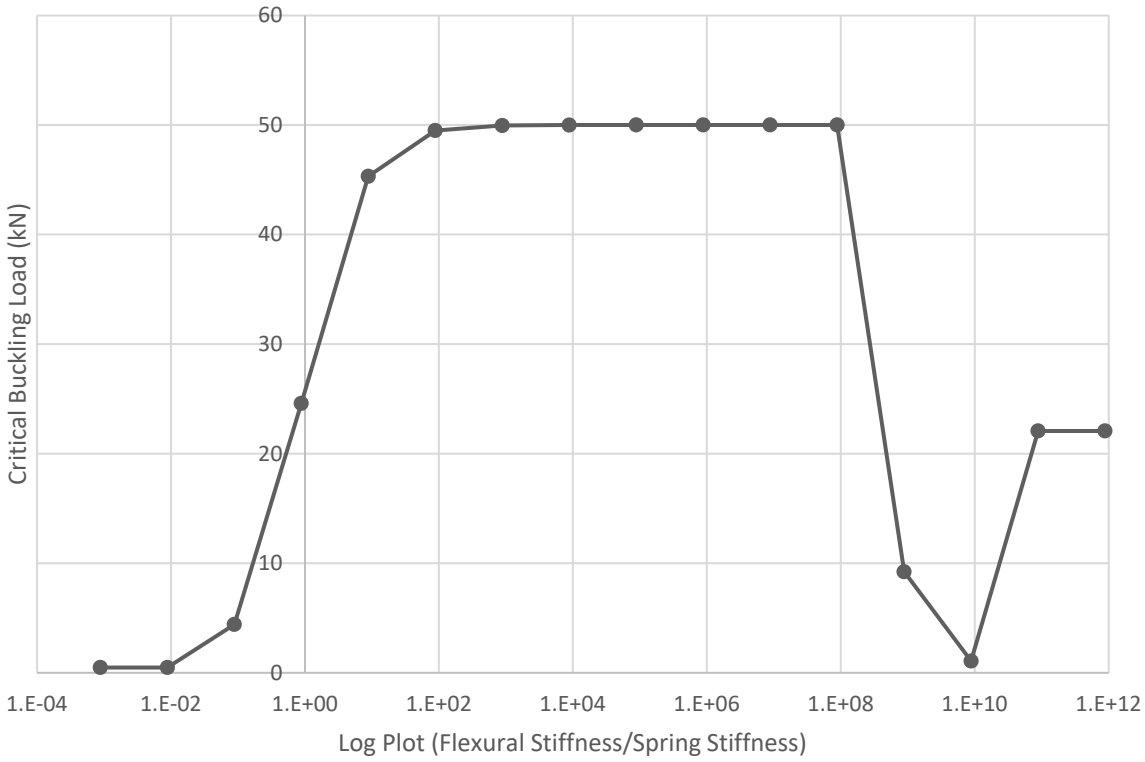


*Figure 4-21 - Log Plot Of Stiffness Ratio Vs Critical Buckling Load For A 2 Spring 3m Strut Model.*

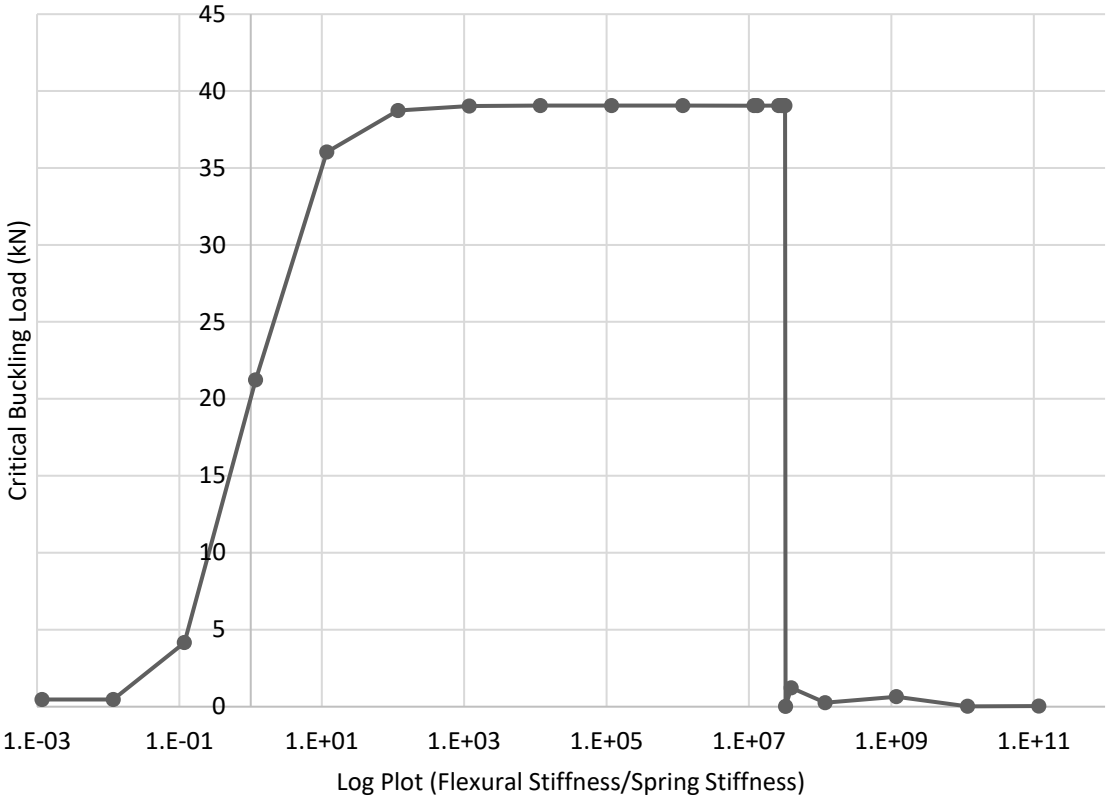


*Figure 4-22 - Log Plot Of Stiffness Ratio Vs Critical Buckling Load For A 3 Spring 3m Strut Model.*

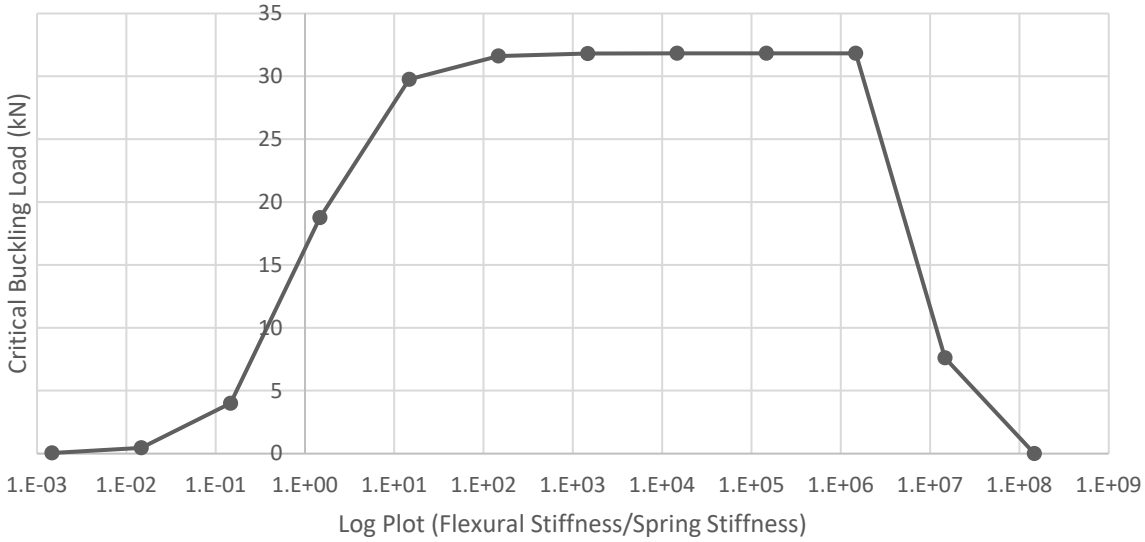


*Figure 4-23 - Log Plot Of Stiffness Ratio Vs Critical Buckling Load For A 4 Spring 3m Strut Model.*

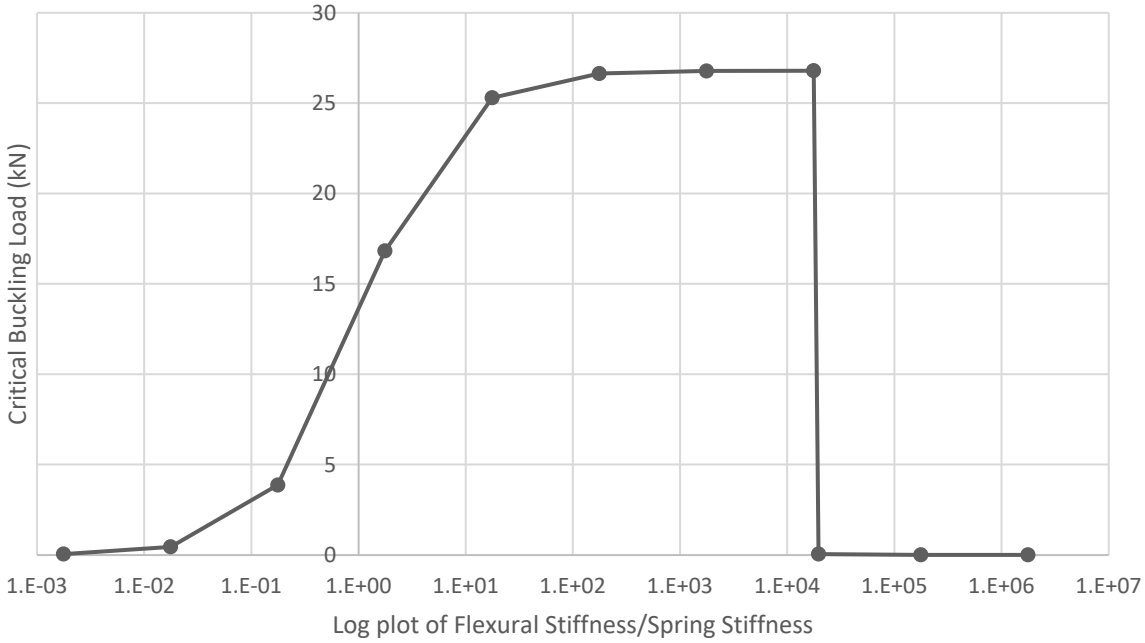


*Figure 4-24 - Log Plot Of Stiffness Ratio Vs Critical Buckling Load For A 5 Spring 3m Strut Model.*

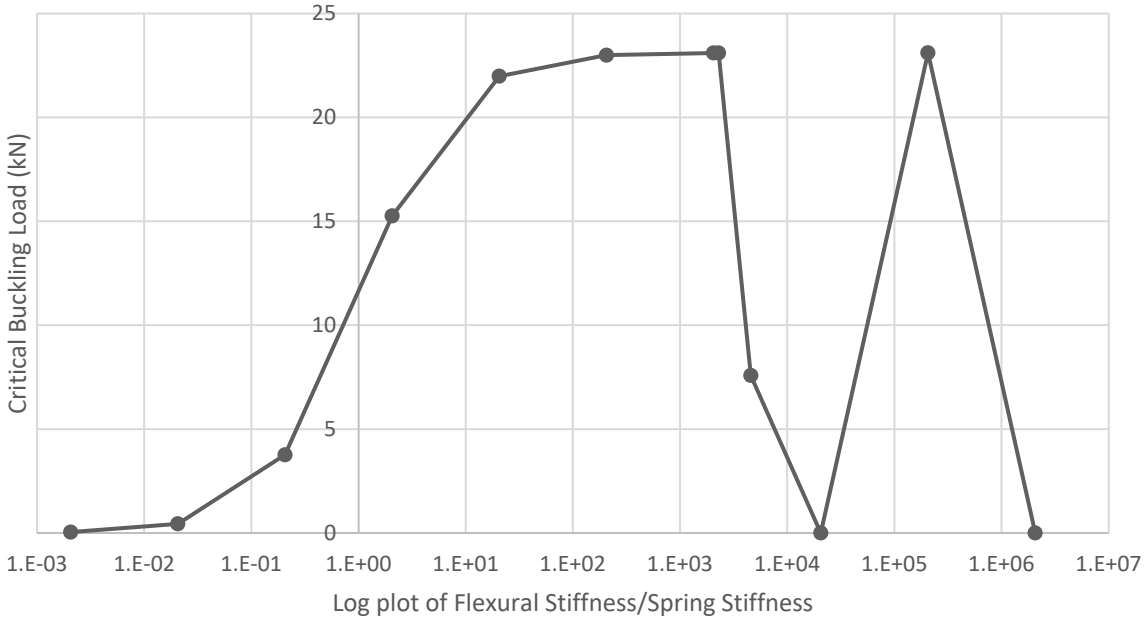


*Figure 4-25 - Log Plot Of Stiffness Ratio Vs Critical Buckling Load For A 6 Spring 3m Strut Model.*

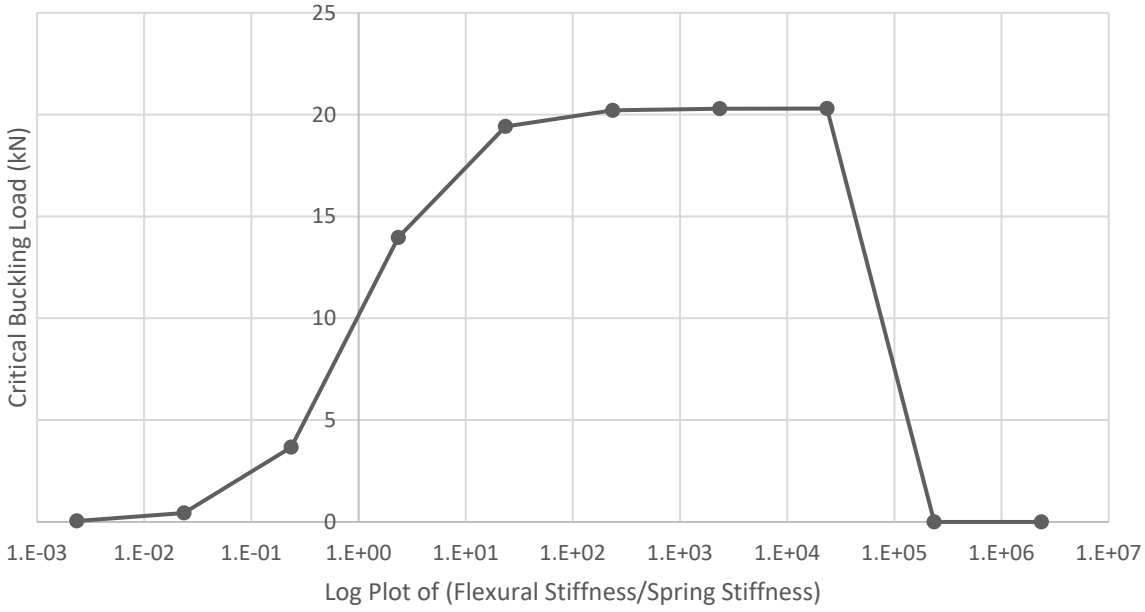


*Figure 4-26 - Log Plot Of Stiffness Ratio Vs Critical Buckling Load For A 7 Spring 3m Strut Model.*

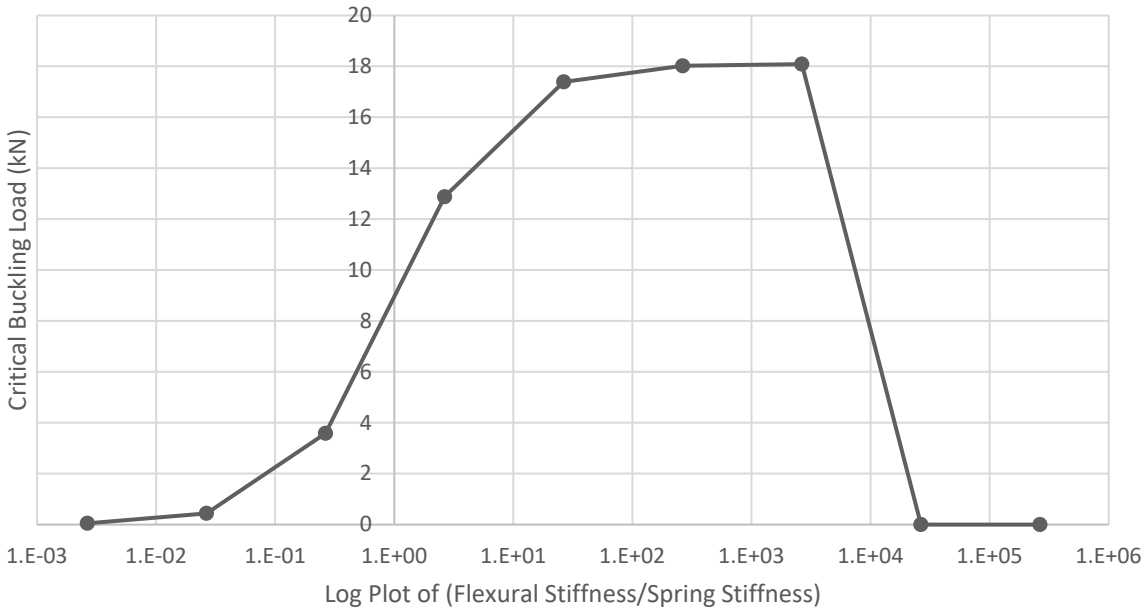


*Figure 4-27 - Log Plot Of Stiffness Ratio Vs Critical Buckling Load For An 8 Spring 3m Strut Model.*

One of the quickest checks that can be undertaken when modelling is to investigate the shapes of the various modes extracted from the buckling analysis. Considering an example from the 3-spring model shows that when the model is well-conditioned, the first three modes are as expected and their displaced forms are demonstrated in Figure 4-28.

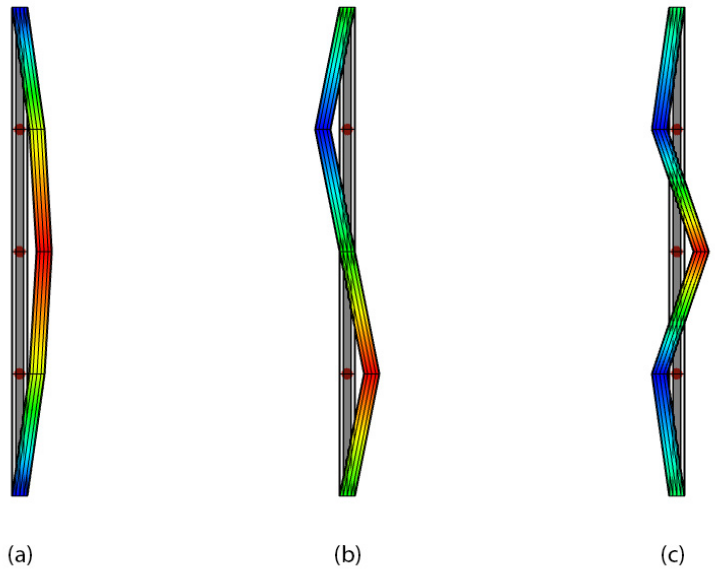


*Figure 4-28 - 3 Spring Strut Buckling Modes of a Well-Conditioned Model- (a) Mode 1 (b) Mode 2 (c) Mode 3.*

However, when the model starts to become ill-conditioned then the modes no longer correctly

solve (see Figure 4-29) with modal shapes being visibly incorrect as well as the critical buckling loads varying.

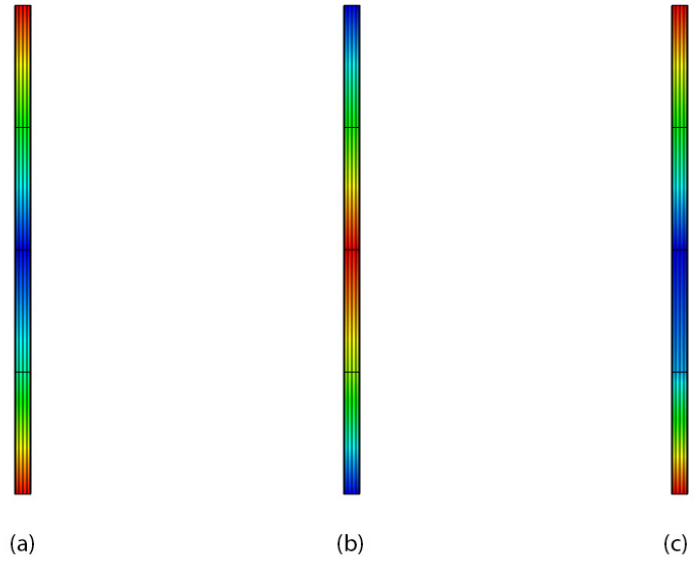


*Figure 4-29 - 3 Spring Strut Buckling Modes of an Ill-conditioned Model - (a) Mode 1 (b) Mode 2 (c) Mode 3.*

Interestingly where the concern is raised regarding the critical buckling loads being extracted, as the beams are typically only meshed as single elements, displaced buckled forms can be used taking a Young's Modulus that may give results that are influenced by the flexural rigidity. The first mode may then be used to deform the mesh on a forced displacement model (say with a 1mm max deformation), with the Youngs Modulus also adjusted to be mega-stiff and sensible results still being determined.

## 4.6 Ill-Conditioning.

Generally, the greater the number of springs or the segments, then the more likely that there will be unexpected behaviours within the modelling and caution should be exercised when reviewing the results. This is not entirely unexpected given the breadth of stiffnesses being considered within the model (MacLeod, 2005).

Whilst not the same, an interesting investigation can be undertaken by looking at numerical limits for the finite difference calculations performed within Mathematica. A rule of thumb that can be used to evaluate the potential for matrices to become ill-conditioned can be to review the ratio between the minimum and the maximum values of the eigenvalues obtained. A value of zero for an eigenvalue for the modelling being considered within this chapter is a clear indicator

that the analysis has become ill-conditioned. This can be expressed as a numerical value using the syntax below.

*Mathematica Snippet 20*

```
eigenratio = Min[gvals]/Max[gvals] // N
```

As a simplification, the order of the value returned is a helpful indicator as to how many decimal places of accuracy are likely to have been sacrificed from the ill-conditioning of the matrices.

As an example, should the Eigen ratio be equal to $1.2504 \times 10^{7}$ then the last 7 decimal places would be suggested as being vulnerable from the ill-conditioning. Typically, Mathematica works in 'Machine Precision' or 16 decimal places, which can be validated within workbooks using the following command.

*Mathematica Snippet 21*

```
$MachinePrecision
```

As more hinges are added to the system, the critical buckling loads will become smaller, reducing the Eigen ratio, this would perhaps go some way in demonstrating that the more flexible the system, the lower the critical buckling loads, the smaller the window of acceptable solutions within the analysis or the more susceptible to ill-conditioning the system becomes. This will eventually arrive at the point where the first eigenvalue becomes zero inferring that the matrix is singular.

Most notebooks return an accuracy of 15.9546 which would suggest that calculations are typically worked to 16 decimal places, with the Eigen ratio above sacrificing the last 7 decimal places, this would give an approximate accuracy of 9 decimal places.

Equally as important as the number of decimal places being sacrificed is the limits with which Mathematica and the associated hardware can reliably store large numbers in the RAM without loss of accuracy. The maximum number that can be stored without being subject to loss of accuracy can be determined by the following command.

*Mathematica Snippet 22*

```
$MaxMachineNumber
```

A typical sheet on the laptop used for the modelling within this thesis returns a $MachinePrecision of 15.9546 and a $MaxMachineNumber of $1.79769 \times 10^{308}$ which will be considered as general limits within the analysis.

Through linear analysis, the susceptibility of matrices to be vulnerable to ill-conditioning can be identified via the conditioning number, which whilst not absolute, can help with identifying potential issues arising from ill-conditioning.

Another rule of thumb that can be used to determine how vulnerable a matrix can be to ill-conditioning is to review the scale of the determinant of the square matrix, where this exceeds the magnitude of the number that can be accurately stored within the memory then results should be considered carefully.

Mathematica has various routines integrated that can be helpful with identifying the structure within matrices, particularly where ill-conditioning may start to occur. Essentially looking for errors or strange values within the diagonalization of the matrices and how this may limit the success of the analysis. One of these routines helpfully identifies the diagonal structure of the upper and lower elements of the matrix, the vector specifying rows used for pivoting, and most usefully the final variable extracted is the conditioning number.

*Mathematica Snippet 23*

```
{lu,p,c}=LUDecomposition[matrix]
```

When the above routine is applied to a square matrix there are two opportunities for errors to be highlighted, the first is via the general processing checks within the routine that flags that Mathematica has struggled with the calculation and raises concern that the matrix may be ill-conditioned and that the results may contain significant numerical errors.

```
{lu2, p2, c2} = LUDecomposition[u.v.Transpose[w]];
```

LUDecomposition: Result for LUDecomposition of badly conditioned matrix $\{\{6.07526 \times 10^{8}, -4.86021 \times 10^{8}, 1.21505 \times 10^{8}, 2.18316 \times 10^{-7}, 6.4917 \times 10^{-7}, \ll 42 \gg, -1.26401 \times 10^{-7}, 1.11741 \times 10^{-7}, -1.09099 \times 10^{-7}, \ll 353 \gg\}, \{\ll 1 \gg\}, \ll 47 \gg, \{\ll 1 \gg\}, \ll 353 \gg\}$ may contain significant numerical errors.

*Figure 4-30 - LUDecomposition Error.*

The other helpful measure is the conditioning number which the routine expressly calculates (in the above example this would be stored as variable c2). The conditioning number is similar in some ways to the Eigen ratio in that it can be used as an indicator as to the decimal places that have potentially been sacrificed from an accuracy perspective.

Interestingly though, a high conditioning number is not an absolute indication that there will be errors within the numerical process. With several of the Mathematica sheets found to result in high conditioning numbers, large determinants that were more than the maximum number that could be stored and with high Eigen ratios but still produced accurate results that were satisfactory for the determination of the buckling loads. Although, further small increases in either the Young's Modulus or the number of segments being considered resulted in numerical instabilities showing that there is an element of resilience within the model and that the warnings are helpful as an early warning system for imminent instabilities.

CivilFEM does not offer this same level of insight during the analysis process with regards providing the conditioning numbers and so on, but there needs to remain an awareness of the potential for these kinds of errors to be evident within the models and confidence can be brought about through several methods, such as visually inspecting the mode shapes, plotting graphs of the critical buckling loads with varying values of the Young's Modulus, applying a forced displacement with a small deformity applied or if possible an alternative analysis method such as finite difference.

Through discussions with technical support at CivilFEM, the eigenvalues are extracted in numerical order when undertaking modal analysis as a Sturm sequence checking algorithm is applied in these instances, however, for buckling analysis a Lanczos method is utilised without a Sturm checking process and therefore it is not assured that the eigenvalues are returned in order for buckling analysis.

As was evident in some of the analysis output where ill-conditioning was evident, the lower modes returned a critical buckling load of zero, but with the expected buckling value being present in one of the higher modes, perhaps suggesting that the eigenvalues were simply extracted out of numeric sequence. However, reviewing the mode shapes visually would infer that this may not always be the case and it may be better to apply the review processes identified previously as it is not currently possible to influence or apply Sturm checking within CivilFEM and it remains a closed system with no adjustable API or ability to extract the matrices used within the calculations.

## 4.7 Higher Modes.

Following the validation of the struts with a uniform distribution of equal stiffness springs, there may be an opportunity to force the sprung struts to buckle into a higher mode through manipulating or varying the spring stiffnesses. For example, taking a strut with three hinges, the system may be forced into the second mode by locking the central hinge, see Figure 4-31.

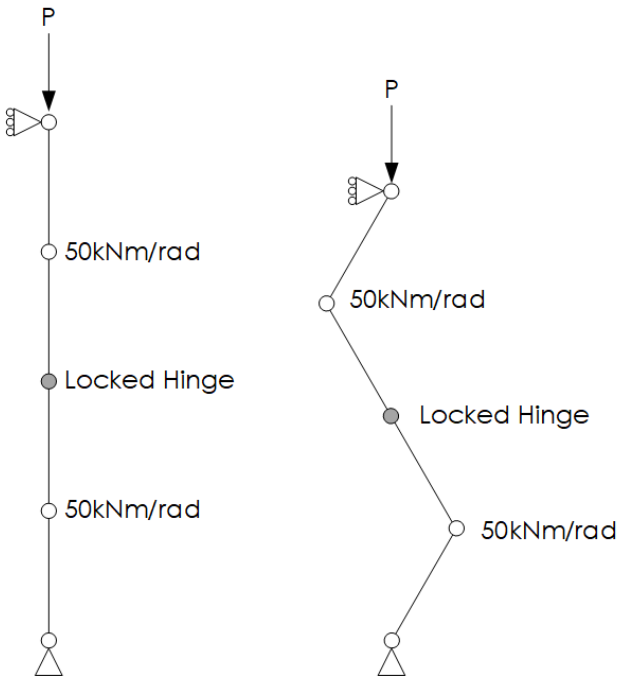


*Figure 4-31 - Spring Stiffnesses Adjusted To Force Mode 2.*

Locking the spring to essentially be infinitely stiff, is achieved by altering the coupled nodes from a spring relationship to be rotationally rigid within CivilFEM, see Figure 4-32.

| **Middle Locked** | |
|---|---|
| Name | Middle Locked |
| Master node | 4 |
| Coord. System | Global Cartesian |
| **Ux** | |
| Type Ux | Rigid |
| **Uy** | |
| Type Uy | Rigid |
| **Rotz** | |
| Type Rotz | Rigid |
| Tied nodes | (1) |
| | 5 |

*Figure 4-32 - Central Spring Fully Locked.*

With the central hinge now able to fully transfer its rotational motion via the coupled nodes, the behaviour is now governed entirely via the upper and lower springs, which will be defined with a rotational stiffness of 50kNm/rad as per the original system, see Figure 4-33.

For this analysis, the springs have been defined as non-linear elements with a directional stiffness to encourage the correct direction of motion (section 5.8 investigates non-linear springs in more detail).

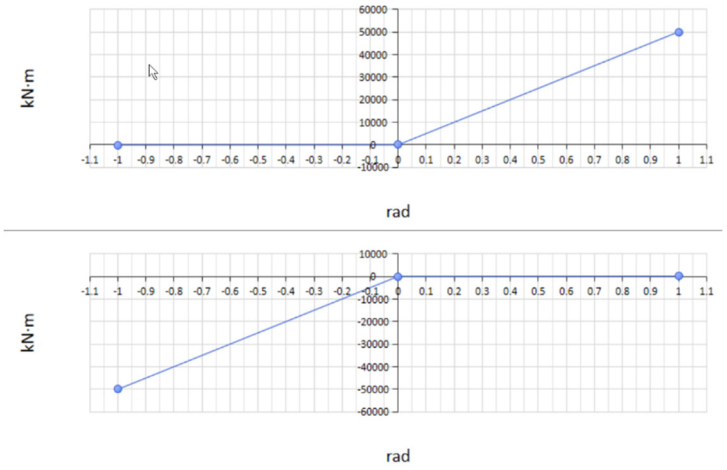


*Figure 4-33 - Upper and Lower Spring Stiffness Definition.*

Using forced displacement to engage the motion of the strut with an applied vertical load will require the mesh to be locally deformed with the second modes displaced form to allow the non-linear analysis to complete. This could equally as well be applied to the chain of springs with uniform stiffness, however, there will be a propensity for the strut to revert to mode 1 in certain instances and the locking of the central hinge will guarantee in this instance that a buckled form that matches the shape of mode 2 will be achieved.

Following the completion of the forced displacement non-linear analysis, the displaced form is as expected, see Figure 4-34.

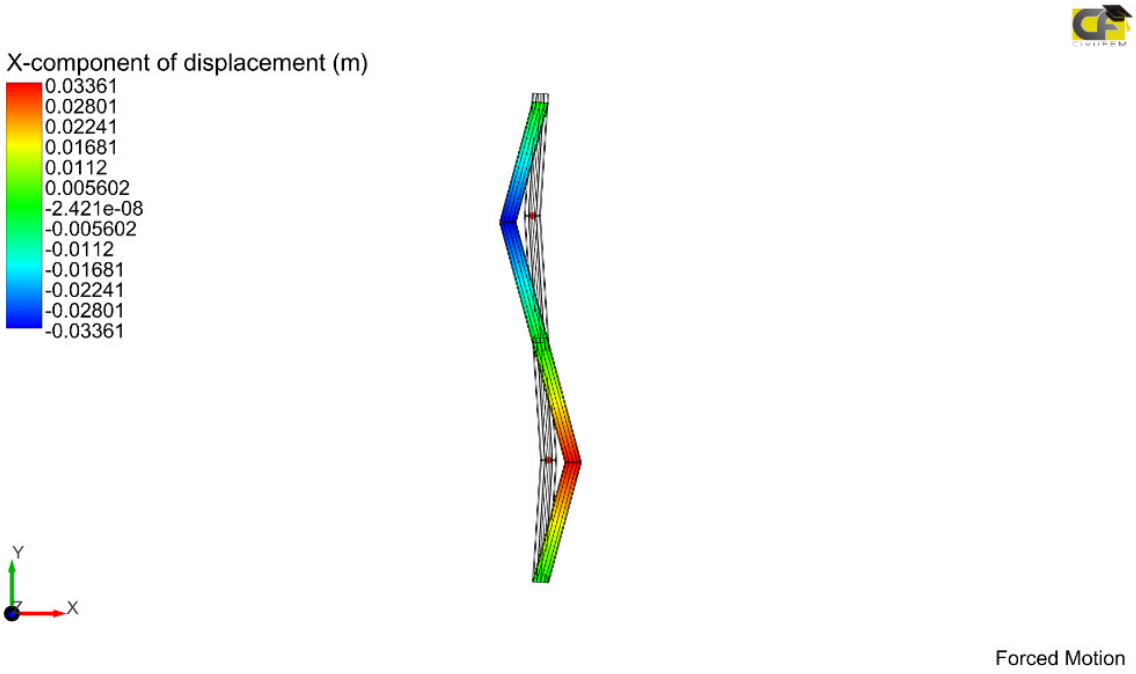


*Figure 4-34 - Spring Stiffness Adjusted To Develop Mode 2 As The Primary Buckling Mode.*

Extracting the history plot from CivilFEM shows that axial force varies (in the lower strut) as the displacement increases (at the top of the system) in a non-linear manner and reaches a peak value before decreasing again as the displacements become truly gross whilst retaining an appreciable reserve of load-carrying capacity.

Given that the springs are elastic, once the forced motion is removed the system would be expected to fully recover. This form of behaviour may prove beneficial for adaptive structures that are required to grossly deform whilst retaining a reserve of strength to support loads.

Unlike where the structure deforms in a non-linear manner because of the material yielding, although motion and behaviour of the structure may on the first inspection appear to be similar, plastic yielding of the structure will not allow the structure to recover fully to its initial position once the load has been removed thus presenting a significant limitation for an adaptive structure.

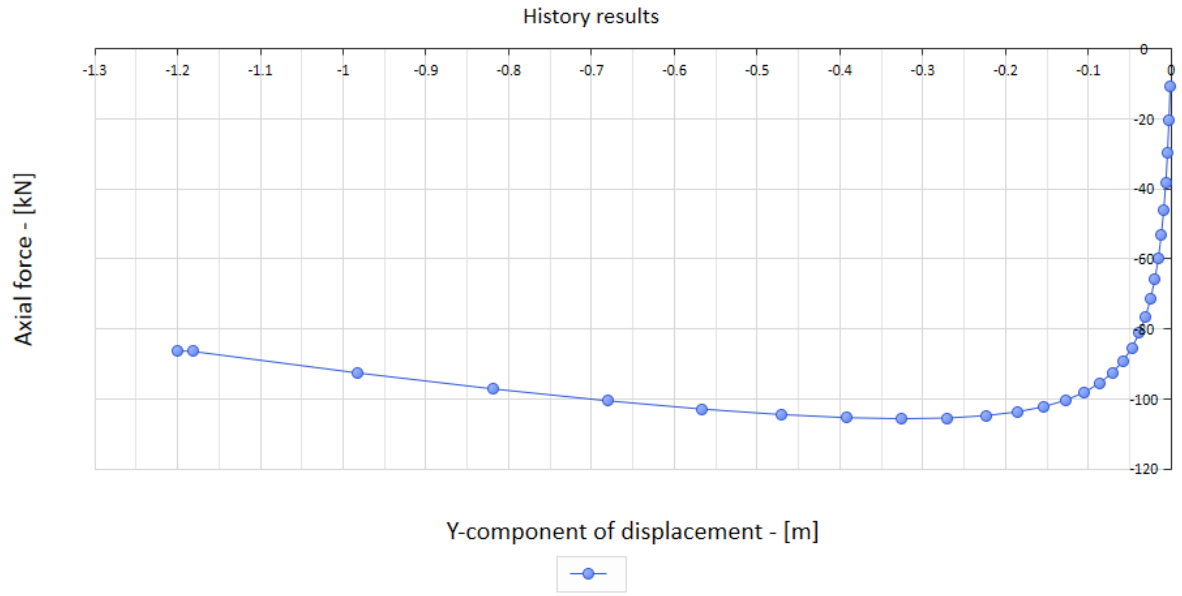


*Figure 4-35 - History Plot from CivilFEM Showing Axial Load-carrying Capacity Post Buckling.*

The critical buckling load (based on extracting the Eigen buckling loads) for a chain of uniform springs for the second mode was 133.325kN (133.33kN from finite difference). For the displacement controlled non-linear analysis shown in Figure 4-35 (with an initial deformation of 5mm scaled from the mode 2 shape), the peak axial force is 105.6kN which is appreciably lower than predicted by the Eigen buckling load for mode 2. As previously discussed though, this is to be expected as the eigenvalues are based on 'perfect' geometry and even small deformations or initial displacements can vastly reduce the buckling capacity as illustrated in Figure 4-2 (page 4-130) and discussed widely with reference to Perry's rule (Bazant & Cedolin, 2010, pp23), general imperfections and their factors of safety (Timoshenko & Gere, 2009, pp193), and axial load with nominal eccentricities reducing the buckling capacity (Allen & Bulson, 1980, pp76).

## 4.8 Summary.

Determining the critical buckling load for a strut with a single central hinge was demonstrated as being straightforward using either geometrical or energy-based methods. However, determining the critical buckling load may become challenging for systems with numerous springs (each additional spring increases the number of degrees of freedom by 1) or with a chain of springs of differing stiffnesses. Alternative computer-based methods will be explored in subsequent chapters, with the merits of each being compared.

3 further methods have been applied to determine the critical buckling loads associated with a hinged strut, including:

1. Finite Difference Methods.
2. Finite Element Methods.
3. Non-linear forced displacement analysis.

Generally, for the simple struts considered with a single spring all of these methods are adequate for determining the effects of a perfectly straight strut with a single central spring, neglecting the effect of self-weight.

Determining the critical buckling loads for sprung struts is a complex process and for the buckling to be entirely governed by the spring stiffnesses, the struts were initially defined as having an infinite flexural stiffness through manipulation of the Young's Modulus.

The novel application of the finite difference method has been used with great effect on solving various forms of differential equations and is well documented with buckling problems of struts with a varying cross-section for example.

However, the application of finite difference methods to strut buckling for struts with rotational springs is undocumented, although there are similarities with the work of Hencky, and a novel approach of manipulating the matrices to reflect the introduction of rotational springs based on specific rotational spring stiffnesses was outlined and shown to have a high level of accuracy even with coarse meshes.

For a large number of springs (1-8 in this investigation) the novel finite difference method has been successfully applied to determine the critical buckling loads.

Finite Element analysis was completed for a variety of sprung struts with several springs ranging from 1 to 8 springs total, with the critical buckling load being determined successfully through the artificial stiffening effect controlled by increasing the Young's modulus of the strut material to ensure that the buckling load was entirely dictated by the rotational spring stiffnesses.

Forced displacement non-linear analysis was also undertaken using CivilFEM with an initial imperfection being added to the geometry by locally deforming the analysis mesh using the modal geometry of the buckling mode obtained during the Finite Element analysis. Instead of applying a unit load to the top of the structure, a displacement was applied at the top that was incrementally applied. A displacement can be selected that could extend the buckled form far beyond the initial critical buckling load to determine to determine the post-buckled failure behaviour. By applying a forced displacement instead of a force the post-buckling behaviour can be determined even when the buckling would become gross or catastrophic as it gently lowers

the structure into the new collapsed form whilst providing usable data from the analysis engine.

The forcing of motion on the structure using a controlled displacement also provided the corresponding forces in the elements during the motion, this could be a useful tool for not only determining the paths of deployable structures during their deployment but also evaluating the forces and stresses developed during deployment which was highlighted in chapter 2 is an area often neglected by deployable structures research.

The introduction of the deformed geometry reduced the critical buckling load noticeably, as expected when introducing imperfections, but was able to identify post-buckled behaviour in a meaningful manner.

For all three numerical solutions (finite difference, finite element, and forced displacement) the effects of ill-conditioning were identified during the analysis process.

Whilst CivilFEM does not allow the matrices and computational output to be interrogated and investigated in depth, the finite difference method was hand-coded within Mathematica and this allowed the matrices to be inspected and assessed to determine if ill-conditioning could be present. These methods of assessing the potential for ill-conditioning included:

- Determining the ratio of the minimum to maximum eigenvalue and comparing this to the precision of numbers stored in the memory.
- The magnitude of the determinant in comparison to the maximum allowable number that could be accurately stored could be used to identify where the matrix was becoming singular.
- The conditioning number calculated using the LUDecomposition routine which could be compared to the precision of numbers stored in the memory.
- Warning messages from LUDecomposition were obtained, warning of numerical accuracy.

Whilst none of the above methods could be applied to CivilFEM or even directly applied as a comparison given the different nature of modelling between the Finite Element and Finite Difference methods, they gave a strong indication that ill-conditioning could be likely in the types of problems being investigated in this chapter and caution should be exercised during the modelling and analysis process.

Within CivilFEM visually inspecting the modal shapes after the extraction of the eigenvalues demonstrated an acceptable method of visually determining if the structure was ill-conditioned

and incorrect numerical results were presented.

However, visually inspecting the modal shapes was not quite as effective for where the Young's Modulus was not stiff enough to ensure that the buckling response was entirely governed by the spring stiffnesses. Where a Young's Modulus that was too low was selected then the flexural stiffness of the struts was seen to influence the critical buckling load and reduce the critical buckling load compared to a rigid strut where the buckling load is governed solely by the spring.

Equally, if a Young's Modulus that was too high was selected, numerical instability was observed with critical buckling loads being returned as zero for the first mode. Incrementing the Young's Modulus by an order of magnitude showed that a single spring strut has a large range of variability of acceptable Young's Modulus and as the number of springs increases, the structure becomes more susceptible to numerical instability and caution must be exercised to validate the value chosen is suitable through undertaking a sensitivity study of the flexural vs rotational stiffnesses.

Some of the higher modes presented interesting forms and shapes that could be used within adaptable structures and an investigation was undertaken to see if spring stiffnesses could be manipulated to achieve these higher-order shapes.

Taking inspiration from the higher buckling modes, the forced displacement analysis was modified through the manipulation of the spring stiffnesses to force the structural system to adopt a shape inspired by a higher mode for buckling, in the example presented the structure was forced into a shape similar to mode 2 through the locking of the central spring. This principle shows the potential for spring stiffnesses to be tuned to either achieve increased post-buckled capacity or to adopt shapes that may be beneficial when considering adaptive, deployable or metamorphic structures.

Both methods outlined for use within CivilFEM appear to be valid from the preliminary modelling, with the modelling process generally offering greater control compared to ROBOT, particularly with regards the forced displacement analysis methods, and CivilFEM will be the software that is used for finite element modelling for the rest of the models being created although investigations that attempted to use Wolfram SystemModeler will be included in the next chapter to highlight the challenges with form finding arched geometry.

Reassuringly, accurate and validated results were obtained for systems with considerable degrees of freedom being integrated (1 degree of freedom per spring) showing the overall robustness of the analysis process.

This chapter has established a workflow for reliably determining the buckled shape and buckling loads for sprung struts, including guidance to allow engineers to mindfully assess the correctness of this analysis with respect to ill-conditioning.

The following chapter will look at applying these principles to sprung arches to determine if the introduction of rotationally sprung hinges can offer benefits to forms identified in Chapter 3 on cable-chain structures by exchanging the internal cables and free pins for rotational springs.

# Chapter 5

# 5 Sprung Frames.

## 5.1 Introduction.

Chapter 4 considered light rods connected with rotational springs and demonstrated that the critical buckling load of these sprung struts could be accurately determined using CivilFEM, with the output from the CivilFEM analysis being validated. In addition to the critical buckling load, the post-buckling behaviour could also be developed far in excess of the initial critical buckling loads. This also demonstrated that the buckling of these types of struts is not catastrophic and that a reserve of load-carrying capacity remains post-buckling.

The analysis undertaken was complex and still had several shortcomings with regards numerical instability, but with care the results were reliable, and the effects of numerical instability could be identified and managed. It was also seen that through the variation of spring stiffnesses and the distribution of the springs through the strut that specific modes of buckling could be developed to generate asymmetrical or tailored buckled shapes.

This chapter expands on the analysis methods established in chapter 4 by applying them to develop an initial stable equilibrium form for arches (before the application of external loadings such as wind) using buckling analysis and forced displacement methods. The development of an initial equilibrium state is important for lightweight structures and without being established can lead to instability during the application of external loading.

The creation of a stable arched form using springs may provide an alternative to the inclusion of cables in arches on a cable-chain structure. Generating a similar type of segmented arch to a cable-chain arch using springs instead of cables may reduce the risk of snap-through on shallow sided arches and other vulnerable geometries whilst still enabling a deployable structure to be realised.

Determining the equilibrium form of an arch can be a challenging analytical problem and several methods were investigated before refining the approach outlined using CivilFEM. This chapter contains a short example of a method that was investigated and eventually abandoned in section 5.4 where Wolfram SystemModeler was adopted to create a multi-physics approach. Whilst this method was robust in determining an equilibrium form, it was ultimately limited by being unable to undertake appropriate structural analysis using this balanced form and demonstrates that analysing sprung struts is a non-trivial problem.

## 5.2 Symmetrical Sprung Arches.

Arches formed with linear springs and uniform length light rods will typically form regular curved arches when buckled from a straight element into the arched shape, or when subjected to a uniformly distributed load and thus remain symmetrical. This matches the geometries generated by sprung struts when buckled into their first mode of buckling as shown in chapter 4. This geometry can be determined for uniformly distributed springs and struts in a relatively straightforward manner, however, this symmetry can be disturbed or unbalanced creating asymmetrical arches when displaced by external forces. The disturbance in symmetry may be as the result of uneven loads, different stiffnesses of linear springs distributed across the chain, non-linear springs in the chain (see section 5.8), or by creating arches with segments of different lengths.

Depending on the stiffnesses chosen for the springs and struts in relation to the loads applied, the deformations may be gross and thus the arch must find an initial balanced self-stress form before the application of external loading to ensure that the structure is indeed stable in its initial state before further applied loads generate potential instability. This initial stable form and the relationship between the distribution and stiffness of the springs is similar to the rigidity ratios explored for self-stress in tensegrity prisms in section 2.9.2, except that it is the relationship between the spring and strut stiffnesses rather than the cable pretension and strut stiffnesses.

Determining the initial self-stabilised condition for deformable structures (as outlined in section 2.9) may require of methods similar to form-finding of fabric structures, by allowing the initial model to balance and settle under a self-weight or initial load case. The buckling analysis and forced displacement methodology developed within chapter 4 can enable the forms to be developed but alternative methods may also be appropriate. This may be a combination of extracting and deforming a structure with one of the modal forms from the buckling analysis, or through the tactical movement of a support as in the forced displacement methodology to

achieve a stable form that can be locked into position to have external loads applied.

Establishing initial equilibrium forms using force-density or dynamic relaxation could be viable methods for determining the initial geometries, with the author having experience in form-finding using inTens software which makes use of dynamic relaxation in an industrial setting. However, software that makes use of these methods is not widely available, beyond the financial limits of the university to purchase, and time consuming to generate a custom a script in Mathematica. The author's experience from industry on the application of these packages show that whilst they are powerful, something as straightforward as a 2D arch could comfortably be modelled using more widely accessible finite element packages with similar results and indeed the more common software packages such as CivilFEM will present benefits such as maturity of non-linear materials and complex stress combinations compared to the likes of inTens.

It would be impractical to include form-finding software within this research to determine the initial form and for the reasons outlined above neither force density or dynamic relaxation will be adopted within the research here explicitly as for the type of structure it is the experience of the author that there are no direct advantages to be gained for such large expenditures of effort. However, the principles and techniques behind the application of both of these form-finding methods will be explored using multi-physics modelling (Wolfram SystemModeler) in section 5.4 where light rods connected with masses will be allowed to freely move until the kinetic energy is dissipated from the system and a stable form developed. This principle of allowing the arch to settle from an initial assumed form into a final equilibrium state will also be explored using CivilFEM in section 5.5.2.

## 5.3 Asymmetrical Arches.

The potential to fundamentally adjust the curvature of an arch beyond a simple symmetrical configuration by refining the number of hinges (Trometer & Krupna, 2006) may present exciting opportunities. Through adjusting the geometry of the arch (Sunguroglu Hensel & Baraut Bover, 2013) via the application of a load or dynamic adjustment of spring stiffnesses it may allow the arch to adopt a more favourable shape aerodynamically, or to enable it to deflect into a specific shape under certain circumstances which could be valuable when looking at smaller scale structures used in Micro-Electro-Mechanical Systems (MEMS) and electronics for switches.

For example, a symmetrical twin chord arch could be encouraged to lose its symmetry by applying uneven loading to the arch such as seen in Figure 5-1 which shows the top chord of the arch swaying under unevenly distributed loads whilst the bottom chord adopts a more complex

wave form to indicate the complexity of shapes that can be generated. This change in symmetry and the associated change in the internal angles between the inter-connected struts, if engineered carefully, could prove positive if specifically engineered or detrimental if not considered and left unchecked. For example, from a positive perspective allowing an arch to adopt a more aerodynamic shape by flattening the leading windward edge under wind loading could aid with the structure being less vulnerable to storm damage providing that the building was able to accommodate such gross deformations. Likely opportunites for a practical application could be lightweight agricultural tunnels used for growing salads and vegetables, although care should be taken to ensure that as the structure becomes more aerodynamic the wind pressures will adjust from those assumed at the undeformed stage and may require adjustment. The balancing of these pressures as the structure flexes between the states and gusts of wind may require an iterative approach to the analysis to ensure that the envelope of loadings can be considered fully.

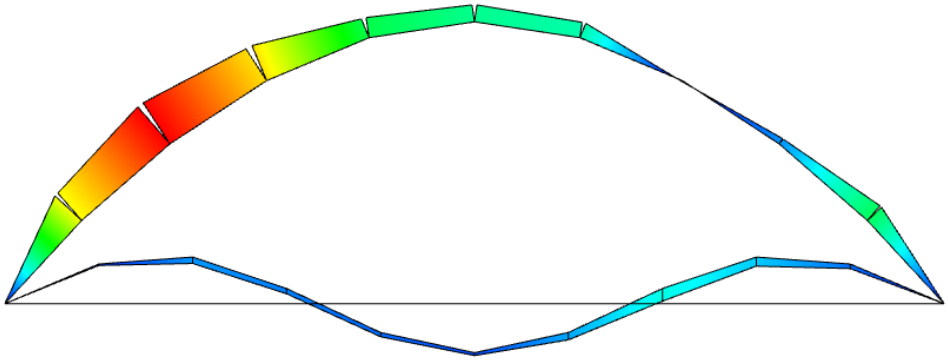

*Figure 5-1 – Deflected Shape of an Asymmetrically Loaded Arch Showing Simple and Complex Deflected Forms.*

Whilst snap-through behaviour was shown to be detrimental for cable-chain structures the introduction of non-linear springs will allow hinges to lock at specific applied loads and consequently could enable an arch to shift between two distinct stable forms. For example, the structure may possess one distinct form under a gravity-based loading (say self-weight) and a different form for a specific applied lateral wind loading or a lateral air pressure loading to create a valve or mechanical sensor to show when a flow has reached a certain speed in a pipe with the structure being a visible indicator in a clear pipe or through displacing to complete an electrical circuit under specific loading criteria as in MEMS.

Flexibility at key positions in an arch, if designed well, can be used to develop a dynamic structure that changes its shape in response to the environment or a deployable arch (Gengnagel

& Burford, 2006). Through varying of the linkage lengths or spring stiffnesses along the chain the form and structural nature of the arch can be developed to allow wind to flow more smoothly over the surface with associated reduced wind pressures. An adaptable arch that is designed to soften its form and modify its curvature under specific wind loading could make use of ellipses or Bezier curves to smooth the transition between regions of wind loading to soften any sharp corners or edges that may develop; through having a combination of longer straight-edged struts and clusters of springs to create smooth rounded transitions to minimalize vortex shedding and associated eddies, similar to the work of Peraza Hernandez, Hu, Kung, Hartl, and Akleman (2013).

The analysis process of such flexible structures presents some similarities to the form-finding and analysis of tensile fabric structures (Wakefield, 1999), requiring that an equilibrium position is found before additional loadings being applied to the arch to ensure that it is stable. Fundamentally, the arch needs to find a balanced geometry where the arch is in a stable equilibrium position before further loads are applied, this may require gross deformations from the initial first guess for the analytical geometry and can often be a challenging process, particularly if the initially assumed geometry is grossly different from the final equilibrium position due to the large displacements involved.

There are a variety of methods that can be adopted for form-finding structural forms including Dynamic Relaxation (which the author has used broadly whilst working at TENSYS) and Force Density to name two. Whilst both methods could be adapted to find the shape of such an arch, the integration of the rotational springs in the structural analysis, specifically with regards buckling can be challenging and so the work from the buckling chapters within this thesis will be adopted as these methods can not only find equilibrium forms but also extend to determine any post-buckled behaviour of the structural forms which will allow the arches to develop multiple stable forms in response to changing load criteria.

Whilst the final method adopted for the establishment of the arch geometry and the post-buckling analysis is based on the CivilFEM buckling analysis methodology established in the previous chapter, several other methods have been considered whilst investigating the behaviour of the structures and these alternative methods will be briefly outlined initially below to show the challenges encountered.

## 5.4 Wolfram SystemModeler Approach.

Considering the sprung arch to be a series of springs with discreet masses and interlinked massless rigid links presents a linkage similar in some ways to a pendulum which can be allowed to find its stable position under self-weight using traditional multi-physics software. One of the initially proposed approaches used Wolfram System Modeler as a graphical interface to control the multiphysics Modelica library components. Whilst ultimately this method was able to find a stable equilibrium form, it was not progressed as it was unable to provide robust bending moment diagrams or other basic structural analysis output. However, using Wolfram SystemModeler enables a linkage chain to be defined using massless links, nodal masses, rotational springs with associated dampers, and pinned supports that are allowed to drape downwards in a fashion similar to hanging chains or the form-finding of the Sagrada Familia in Barcelona, albeit digitally. Some of the lessons learned from these initial modelling assessments proved helpful in refining the methodology further within CivilFEM and they are included for completeness and to demonstrate that various analytical paths were followed before developing the methodology ultimately adopted.

Modelica is an object-oriented and open-source programming language used for modelling complex physical systems either using single or multi-domain physics. Modelica is ordinarily a text-based language and the use of Wolfram SystemModeler[66] has the benefits of creating a graphical library of reusable components that can be linked together procedurally. In theory, this should present a drag and drop environment providing that the components can be connected efficiently, but despite the shape coding of the connectors (flanges) on the elements, the language is poorly documented and can be challenging at times, with even simple models often requiring the use of undocumented features identified by the developers in public forums to complete models. As an example, the model outlined below has generated considerable 'reputation' on programming sharing platforms such as StackExchange through helping other engineers how to model similar, relatively simple structures.

The creation of an arched structure using only spring-loaded hinges with dampers is illustrated within Figure 5-2 where Wolfram SystemModeler has been used to program the mechanism

[66] http://www.wolfram.com/system-modeler/

using Modelica[67]. The model shown in Figure 5-2 makes use of the mechanical components' library, but for example, if, the amount of heat generated in the revolute joints through friction was to be determined this could be modelled through the inclusion of the thermal library.

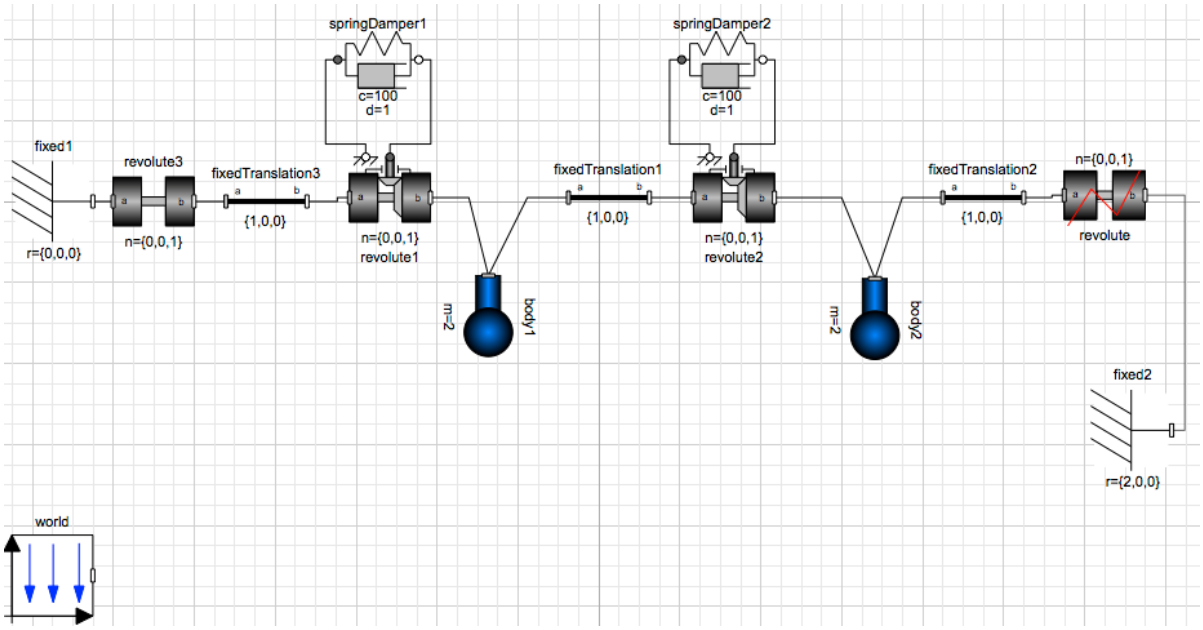


*Figure 5-2 - SystemModeler Arrangement Of A Sprung Dampened Arch.*

The simple 3 element sprung model under consideration has several crucial components to enable the physics needed to determine a stable equilibrium position. The arch is inverted to hang under gravity (similar to form-finding principles used with catenary chains) but with two-point masses being allocated to the internal revolute joints that are in turn connected with massless rigid links. As the masses swing freely and hang under gravity, it is important that the model is anchored within the World to enable support for the hinge anchors and to enable gravity and this is illustrated within the bottom left corner of Figure 5-2. The starting geometry for the arch is intentionally offset (Figure 5-3a) from the equilibrium position (Figure 5-3c) as a starting point to assess SystemModeler's form-finding potential.

[67] https://www.modelica.org/

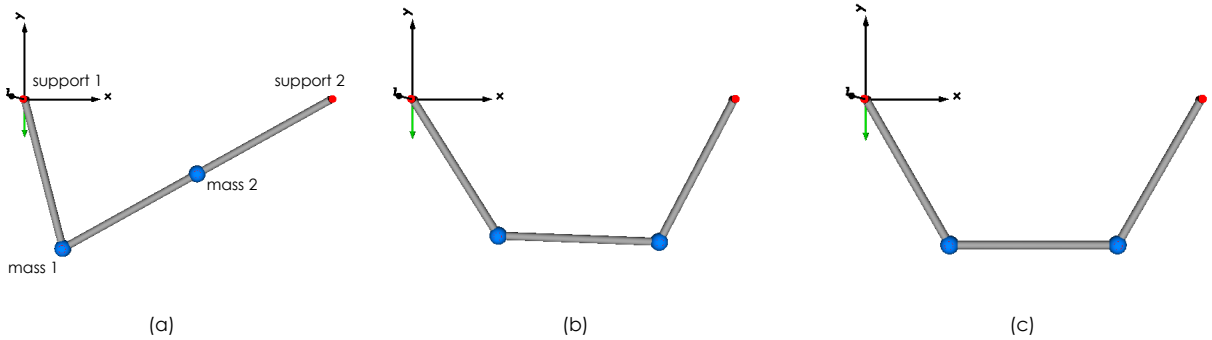


*Figure 5-3 - Animation Of Sprung Arch Within SystemModeler.*

Figure 5-3 shows the 3D visualisation of the digital model of the cable-chain which is constrained to move only within the X-Y plane during the form-finding process by the revolute joints. The inclusion of the dampers has the benefit of dissipating the energy from the system and bringing the system to a standstill in an equilibrium position, otherwise, the model would continue to swing freely. A graph showing the angular velocity of mass 1 (see Figure 5-4) is shown below where it is clear that the structure ceases to move under its self-weight after approximately 5 seconds, showing equilibrium has been reached.

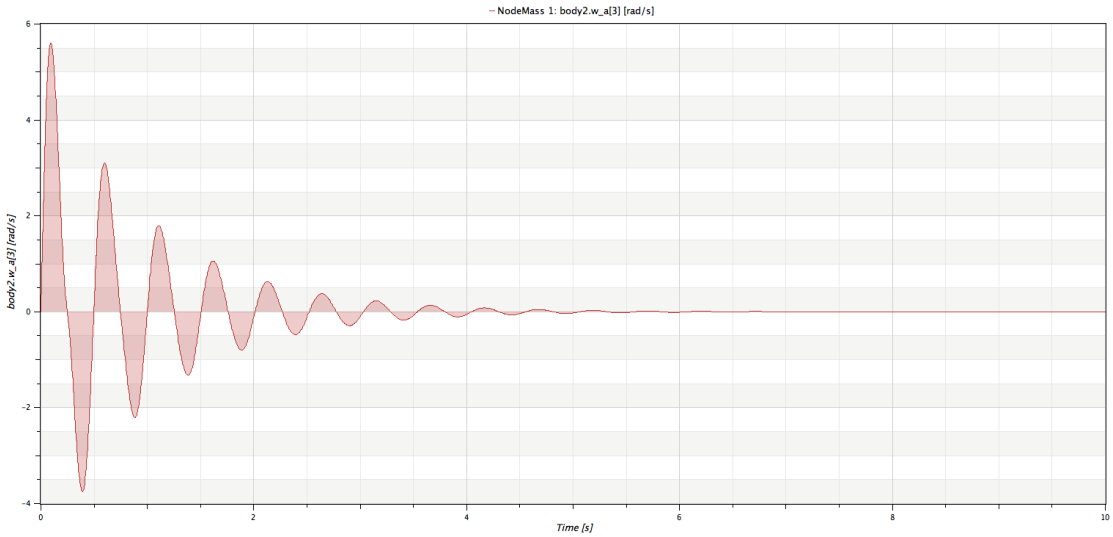


*Figure 5-4 - Angular Velocity Of Joint On Sprung/Dampened Arch.*

Wolfram Systemodeler is aimed at two key markets, Mechanical Engineering and Biomedical Science and it is clear that from the initial model outlined above that it is more than capable of obtaining stable forms that are in an equilibrium state using rotational springs. This is a distinct advantage compared to traditional matrix-based products such as Autodesk ROBOT which struggle with large displacements of such models and can often lack the complex elements required to capture such motion.

However, whilst System Modeler is comfortable generating balanced geometries for kinematic models, it does not provide the level of structural analysis required for the effective assessment of sprung arched structures, such as applying complex loadings or developing bending moment diagrams.

Whilst software based on stiffness matrix methods are generally unable to determine an initial equilibrium state efficiently, they are more than capable of completing the analysis required to determine the structural performance of the structure that starts in an equilibrium position and perhaps a viable methodology would be to inherit the geometry from the form found model and then import this through to a programme such as ROBOT to complete the structural analysis.

However, being able to establish a form-finding routine along with the subsequent follow on analysis within a single piece of software would present a clear benefit in ensuring that the geometry and associated engineering properties are handed over efficiently between each stage of the analysis with no additional entering of information.

Whilst a hybrid method outlined above could be functional it is not perhaps optimal and an approach using the methodology outlined in chapter 4 could be expanded to develop a stable arch form and conduct structural analysis after the form has been found.

## 5.5 Finite Element Approach.

Taking a finite element approach within CivilFEM will have much in common with the method outlined using Wolfram SystemModeler, using very similar type analysis elements. This sub-section will outline two distinct methods within CivilFEM that build upon the methods set out in Chapter 4.

The first method is the spring stiffness equilibrium method which enables a structure to inherit a displaced stable form from a buckling analysis of a linear chain of springs which determines the critical buckling loads and the corresponding modal shapes. These modal shapes are then re-introduced to distort the geometry into a form that can be analysed under more typical static loadings (see section 4.3.2). The second method allows the engineer to make an initial engineering estimate of a geometrical stable form and then allowing the structure to 'settle' under gravity to achieve a stable form, this method requires greater experience from the engineer to obtain a close first guess to the final balanced form (see section 5.5.2).

### 5.5.1 Spring Stiffness Equilibrium.

Taking a similar approach to the forced displacement non-uniform analysis set out in the previous chapter, a linear chain of springs is defined with the end roller being physically displaced to encourage the chain of springs to adopt the desired shape. This could be used to determine a compatible span/depth ratio to aid with determining the final arched geometries proportions approximately. This method at its heart is the same as a displacement control analysis, except that the displacements are gross and the final displaced form is then re-introduced as a zero-stress position to reset the structure into a new form ready to analyse under different loading conditions.

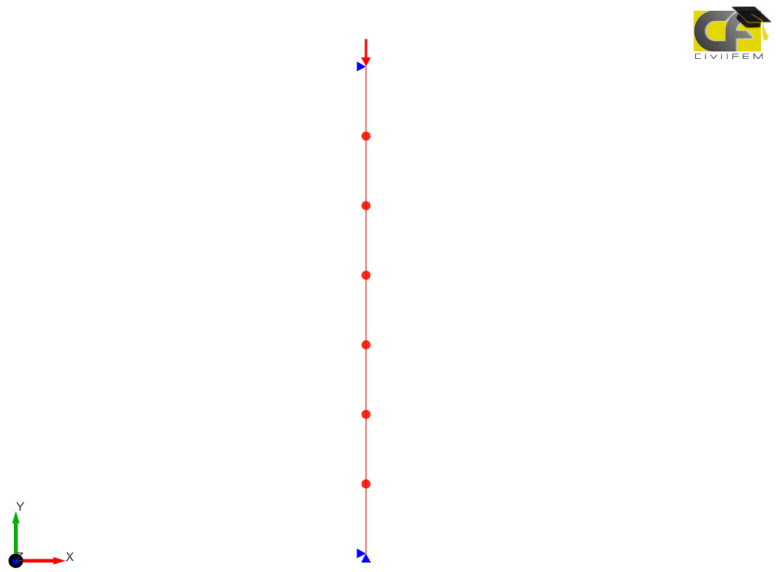


*Figure 5-5 – Initial Arch Geometry Ready to be Deformed.*

The desired shape is entirely governed by the spring stiffnesses as typically the struts will be defined as being massless, although rods with mass could be used but would require greater control to negate self-weight effects during the initial form-finding. Each spring is of equal stiffness in Figure 5-5 and does not require masses to be added (or damping) to allow the curved nature of the catenary to be developed as it is typically governed by spring stiffnesses alone which are far less than the stiffnesses of the rods in this particular example.

Without the introduction of a small imperfection to the flattened arch, the chain will not 'buckle' and deform into the arched shape desired. This imperfection can be integrated into the model in a wide variety of methods but often leads to more predictable behaviour if either the results from the buckling or modal analysis are fed back through as mesh deformations although small lateral

loads would also be functional. The magnitude of these scaled displacements is important to generate reliable behaviours and is typically between 5 and 20mm as a global deformation depending on the number of springs introduced, the greater the degrees of freedom the larger the initial deformation needs to be.

Certainly, where large numbers of degrees of freedom systems are analysed, such as 18 degrees this can require amplifying further, with the imperfection needing to be of the order of 50mm to ensure that the model is well behaved.

When a support is laterally displaced this does not occur as a single one-piece motion within CivilFEM and is instead applied as sub-increments which are defined by the engineer. Experience from the modelling undertaken within this research has shown that smaller increments take longer to solve but are often needed to control the motion on complex structural arrangements to ensure a smooth transition is maintained. By varying the lateral displacement at the end supports (or through adopting an incremental load step as a result of the non-linear analysis which is triggered through the activation of large displacements) it is possible to create a series of arch forms between the zero (flat) and fully displaced forms.

This presents a benefit that any of the incremental geometries may be extracted and adopted as the analysis models initial geometry should it prove more compatible with the engineer's requirements and also that a load/displacement history is generated which can provide valuable insights into the structures overall behaviour. Typically the increment used in many of the analysis models contained within this report have approximately more than 200 incremental stages which help with identifying any peculiarities in the structural behaviour, highlighting specific points where hinges have locked or engaged, and for allowing extraction of specific deflected form geometry. The negative side of such refinement are the associated increased solution times and whilst a typical model file will only be a few kilobytes, the associated results files can easily run into hundreds of megabytes which can prove challenging if adopting a cloud-based storage solution.

The deformed geometry for the final load iteration can be reintroduced to a new model (providing the meshing and numbering of elements are identical) through mesh deformations that can be scaled either by maximum displacement (if the buckling model shows a 1m displacement, this can be substituted back into the model and scaled to be any value, such as 20mm) or through relative scaling of the displaced form being introduced (as a percentage of the total displaced form).

CivilFEM has a limitation in that geometry cannot be extracted explicitly from the deflected form and should this geometry be required to be shared with a BIM or CAD package then an additional step is required to trick CivilFEM to export the deflected form geometry. Essentially CivilFEM is only able to export the nodal geometry for the initial starting position of a model before the load cases are applied, so to allow the final deformed geometry to be extracted a false analysis step is required to distort the mesh by the required load case. This step takes the original model albeit with the end supports changed to pinned supports and the desired load step being applied as a mesh deformation. With no loadings defined, the model can be analysed again which will not displace any further but lock in the new geometry to allow the final equilibrium balanced nodal coordinates to be extracted for the construction of a new model to allow external loads to be applied as shown in Figure 5-6.

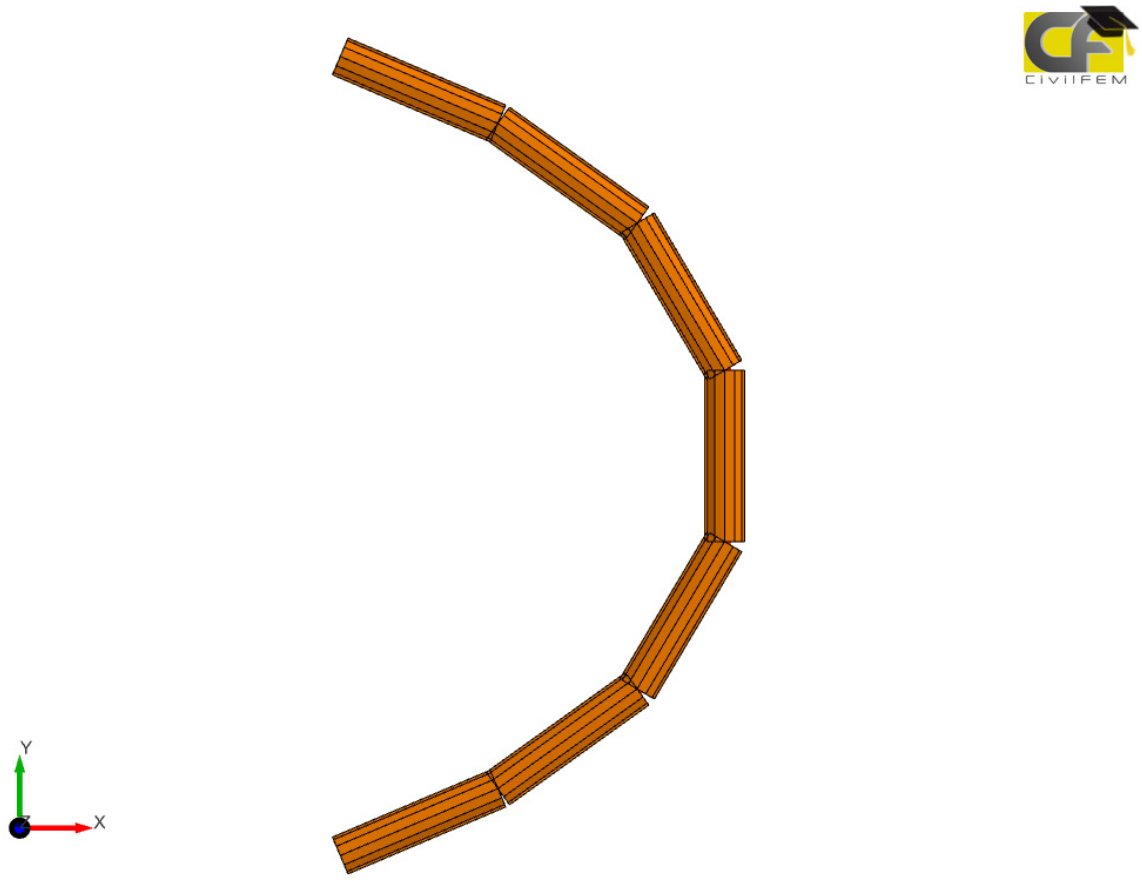


*Figure 5-6 - Mesh Locally Deformed Into An Arch.*

This final analysis step is used predominantly because CivilFEM does not allow the extraction of final deformed geometry, and whilst this can be iterated through by the creation of Python scripting, this hack of solving with no applied loads was found to be quicker and generally more convenient. A similar approach is noted in the investigation of flexible arches by (Phocas &

Alexandrou, 2017) where the controlled displacement at supports are utilised to fold a ribbon into a variety of arched forms, see Figure 5-7.

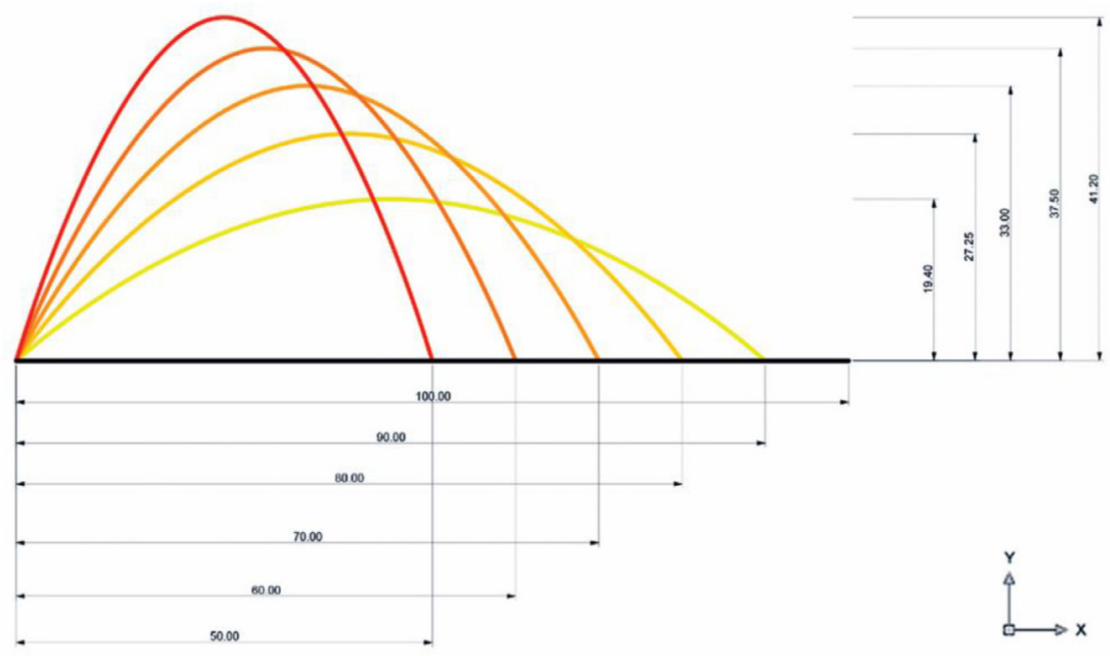


*Figure 5-7 - Form Found Curvatures.*[68]

This process of developing the deformed geometry can be used for any combination of spring stiffnesses to obtain both symmetrical and asymmetrical chains. The example presented shows how the arch orientated as a vertical strut would buckle, but the geometry can easily be transformed with minimal post-processing to align as a horizontal arch.

### 5.5.2 Self-Weight Equilibrium.

An alternative method to forcing a strut into an arch shape is to allow a structure to settle into an equilibrium form through the application of gravity and masses. This is similar in principle to the Wolfram SystemModeler method, although rotational damping cannot yet be applied to the nodal joints due to a software limitation and so a reasonable first guess at the geometry of the arch will increase the chances of success. This method requires CivilFEM to enable the large displacements option within the analysis engine settings and starting the analysis with an assumed initial geometry, perhaps for example, based on a parabola or arc and then allowing the

[68] Phocas, M. C., & Alexandrou, K. C. (2017). Adaptive Structures – Soft Mechanical Approach. *International Journal of Computational Methods and Experimental Measurements, 5*(4), 421-431.

system to settle under its self-weight. Depending on how close to the final geometry the first guess was there may not be a need to enable the large displacements mode in the analysis.

This method, however, requires that there is an inherent mass within the system (just as the Wolfram System Modeler analysis did) but does not require the application of damping as the system is not truly mechanical and is instead intended to find a balance using static analysis.

For particularly lively structures damping can naturally be integrated to the structure via the integration of Rayleigh Damping applied to the material, but is not essential for determining the equilibrium geometry, however, it may present benefits under dynamic loading conditions (see further work where transient analysis has been considered). Through the development of this methodology, it was discovered that CivilFEM was unable to apply rotational spring damping as of the current version (2018 SP1 and 2019 SP1) but that following discussions with the developers in Spain that the omission of this element type was an oversight and it will be integrated within CivilFEM 2019 SP2.

As per all the other methods, once the balanced geometry has been determined then external loadings can be applied and these can be solved and designed for in the same manner as any ordinary type of structure although equilibrium must always be respected and the choice of spring stiffnesses may not always be compatible with the applied loadings.

The forced displacement analysis method was found to give finer control over the final geometry of the chain of springs compared to the self-weight equilibrium method, particularly where gross changes in geometry were integrated within the arch form and it will be this approach that is adopted through the remainder of this thesis.

## 5.6 Flexible Arch and Spring Arch Comparison.

Whilst single arches can be solved, to test the robustness of this approach a comparison in the processing time between an arch formed from a flexible strut of uniform sectional properties (such as the adaptive structures proposed by Knippers or a polymer ruler flexed into a curved form) and a chained link of springs was undertaken.

To make any computational differences more pronounced a relatively complex to solve model was selected to test the ability of the proposed methodologies for form-finding and analysing. Considering two nested arches, geometrically defined as two curves stacked upon each other with pinned supports at either end, these can be forced into more dramatic curved geometries through laterally displacing one of the supports horizontally towards the other support and

essentially reducing the span and pushing the arches upwards, similar in principle to the process outlined by Phocas and Alexandrou (2017).

Consider the form-finding of an arch based on a homogenous elastic material, formed into a uniform cross-section rod held in place by two supports, by displacing the a support the rod is forced into an arch shape and this behaviour is relatively trivial to analyse within CivilFEM. This model is primarily concerned with establishing an equilibrium driven form with the initial starting geometry being geometrically validated as compatible with being deformed into an arch using a form-finding approach and is not concerned with specific material choices with regards stress management. Selection of suitable materials to limit the stress would typically evolve at the later stages of the design process.

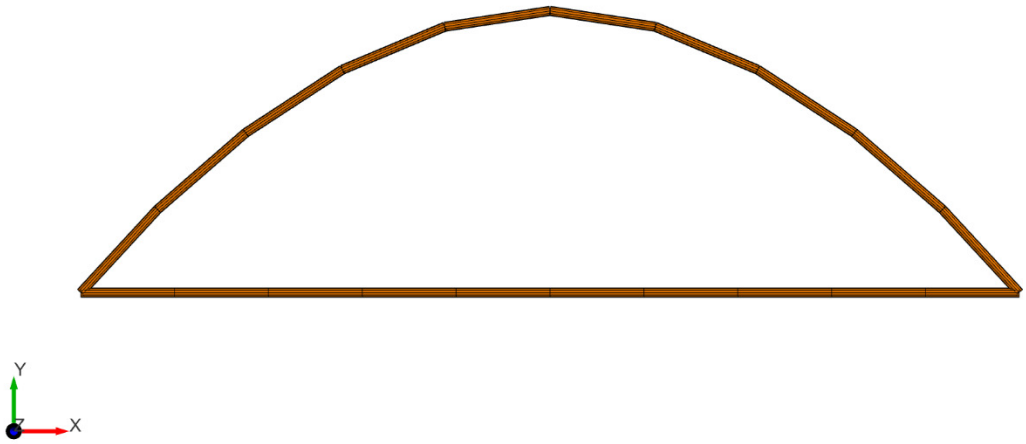


*Figure 5-8 - Initial Starting Geometry.*

Starting with a radial arch defined within CivilFEM as a spline curve and a straight section connecting the supports of the arch (see Figure 5-8), the right-hand support can be forcibly displaced in the negative x-direction and the buckled forms determined accordingly.

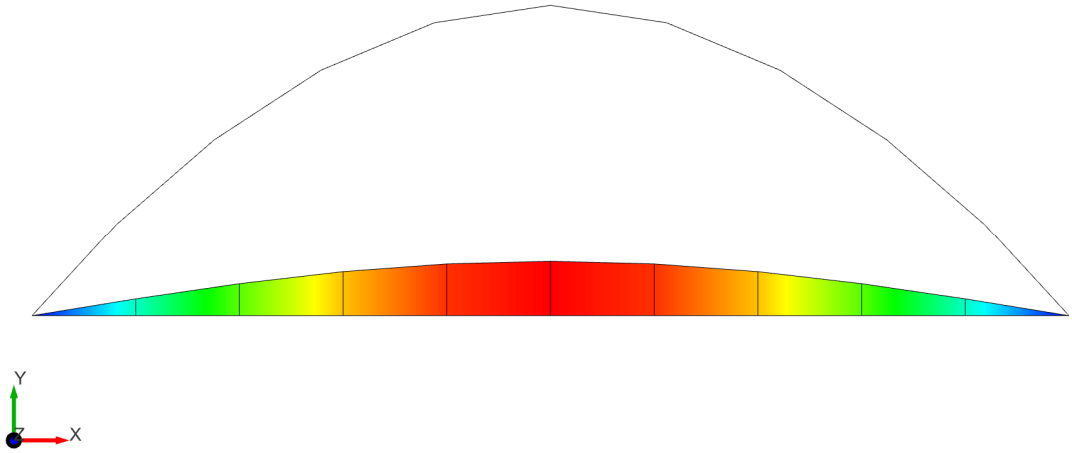


*Figure 5-9 - First Buckling Mode (Y-Axis Displacement).*

As can be seen in Figure 5-9 the bottom segments buckle as expected (mode 1, the top arch buckles in higher modes) and develop a geometry that can be used to deform the mesh for subsequent large displacement analyses.

By using the first buckling mode as a template to deform the mesh locally, encouraging the bottom arch to deform upwards, it is possible to then repeat the analysis using a non-linear methodology to create a balanced arch.

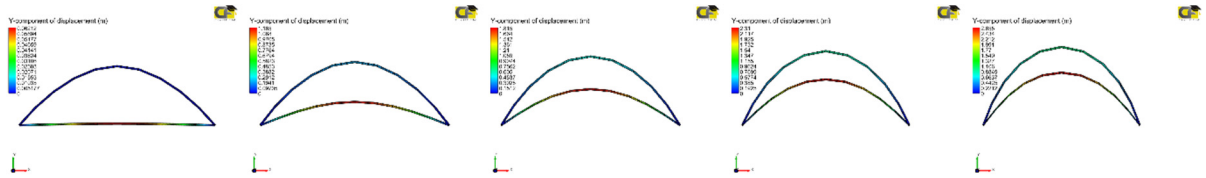

*Figure 5-10 - Stepped Output from the Forced Displacement Analysis.*

Undertaking a large displacement analysis with the right-hand support grossly deformed gives a more pronounced arch form as can be seen in Figure 5-10 which shows 5 of the 207 incremental displaced forms until the final displaced form has been developed.

This exercise is a relatively trivial model to solve for a homogenous rod, solving quickly and with minimal computational strain. However, whilst these type of structure have been used to great effect by Lienhard and Knippers (2013) where they have made flexible fibreglass blades that can flex and rotate as adaptive structures, there are potential weaknesses with the materials typically used to create compliant mechanisms such as fatigue and impact resistance or where flexible composites may develop security issues through vandalism for example.

It is proposed that a comparable structure could be developed using rigid links interconnected with rotational springs by segmenting the geometry. For the example considered within this thesis straight linear segments are used, but curved sections for the struts between springs could equally as easily be integrated should a true curved form be desired. By integrating several springs into the chain, the flexible behaviour of a compliant mechanism could be replicated using springs and links to allow the arch to be delivered in sections and then connected on the ground ahead of being erected, which would be a significant benefit with regards transportation costs and general logistics compared to delivering a long span flexible single piece arch.

It may be that depending on the spring stiffnesses that an arch could be 'rolled' up and placed in a shipping container or wrapped on a pallet ready for delivery, or more practically each link or segment of the arch could be split down and delivered and then re-connected on site to increase the volume of parts that can be delivered at a time. This would be especially helpful for creating very long elements that would ordinarily require an escort to be delivered on UK highways through the subdivision of these longer elements into shorter lengths that can fit on a standard trailer.

However, the workflow to create the initial starting geometry is slightly convoluted, but a functional method is outlined below. To ensure that both the flexible rod model and the sprung model have identical geometries the flexible CivilFEM model is exported as a DXF file, which allows the manipulation through AutoCAD to segment and subdivide the curved geometry into 10 segments for each arch, 20 segments in total. CSV data is created of each nodal point connecting the segments and manipulated within Excel to clean up and remove duplicated points.

With a clean set of (x,y) data points filtered, the geometrical construction can begin as per the previous models using stiff link elements and rotation springs, although making use of Python scripting for speed of data entry simplifies the coupling of nodes and reduces data entry errors. The final model results in the forming of two arched chains of rigid lightweight links connected with springs of known stiffness with each segment being of the same length. The primary difference is that each spring integrated into the system develops a degree of freedom, essentially generating 18 additional degrees of freedom (compared to the flexible rod model) within the model below in Figure 5-11.

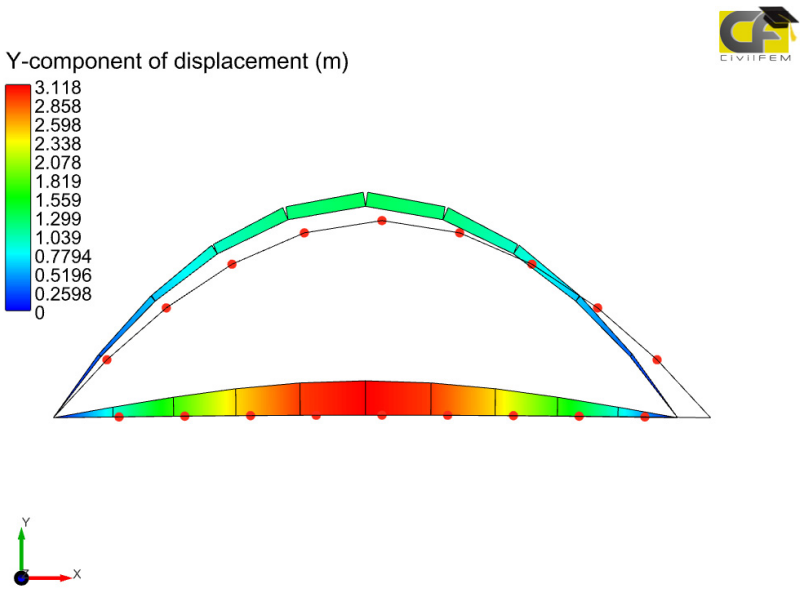


*Figure 5-11 - Vertical Displacements for the 18 Degree of Freedom Arch.*

With so many degrees of freedom to solve this presents challenges with ill-conditioning and several attempts were required to develop suitable stiffnesses and eccentricities to remove the effects of ill-conditioning. As previously highlighted, the greater the number of degrees of freedom the more challenging it can be to make a model well-conditioned. But, with experience and patience, the model can be encouraged to generate the same buckling modes as the uniform cross-section model, which in turn can be used to develop a displaced form as can be seen within Figure 5-11.

In contrast to the uniform struts, the integration of so many additional degrees of freedom not only increases the challenge with regards ill-conditioning but also significantly increases the computation time, with fine-grained iterative models taking roughly half an hour to solve compared to several seconds for flexible arches on a high specification computer intended to model buildings for virtual reality environments.

Effectively this approach can generate a flexible structure that is robust and resilient to puncture damage and develops a clear methodology for generating deployable arch structures whereby the rotational spring stiffness can be locked at certain angles if required to ensure that the structure is correctly deployed (non-linear springs are discussed in more length later in this chapter).

## 5.7 Arches With Different Spring Stiffnesses.

Section 4.7 showed that varying spring stiffnesses within a strut can develop alternative shapes and could be used to mimic higher buckling modes by forcing the struts to change shape during buckling. A similar approach by Knippers et al. (2016) has shown that adaptable structures using varying geometry and material stiffness can adapt and correspondingly modify their behaviour. It may be that specific behaviour can be more accurately controlled and calibrated using springs at key points in the structure to allow the structure to change the form and alignment at specific hinge positions and sharper angles of flexure.

Figure 5-12 shows that varying the springs along a strut can enable the strut to adopt asymmetrical shapes if springs of equal stiffness are distributed, but with a change in the distribution of spring stiffnesses to make some of them stiffer the strut can be used to create asymmetrical arches. In this instance making the bottom half of the strut more flexible and encouraging it to 'yield' before the upper much stiffer section to create a profile similar to a mono-pitch roof.

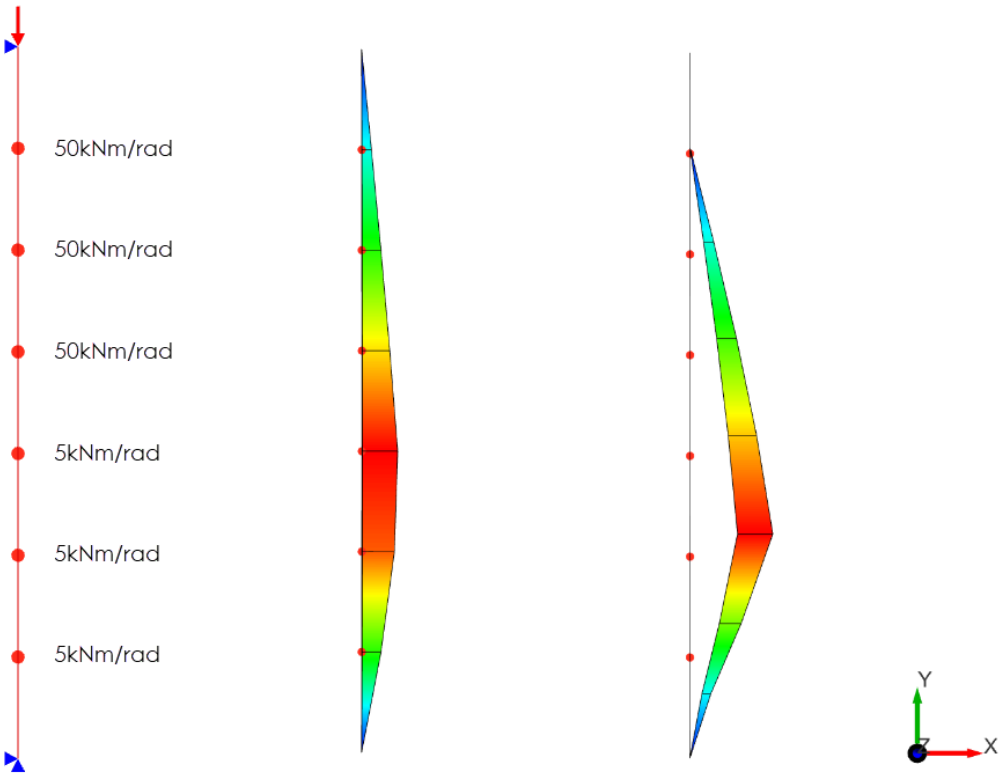


*Figure 5-12 - Non-Uniformly Distributed Springs Displaced Form.*

The distribution of the spring stiffnesses can be adjusted and tailored to encourage pop up arches to adopt desirable shapes, for example in chapter 3 it was noted that the flatter form of

parabolic arches can be used to increase habitable areas within arches but were susceptible to snap-through behaviour. An alternative to an arch based structure could be a portal frame shape that can be encouraged by unevenly distributing the spring stiffnesses along the length of a strut as shown in Figure 5-13, effectively creating a stiffer section in the middle of the chain with weaker springs at the eaves which will result in a profile similar in many ways to a portal frame with a flattened rafter.

This new form will reduce the risk of snap-through whilst retaining an appropriate amount of structural rigidity.

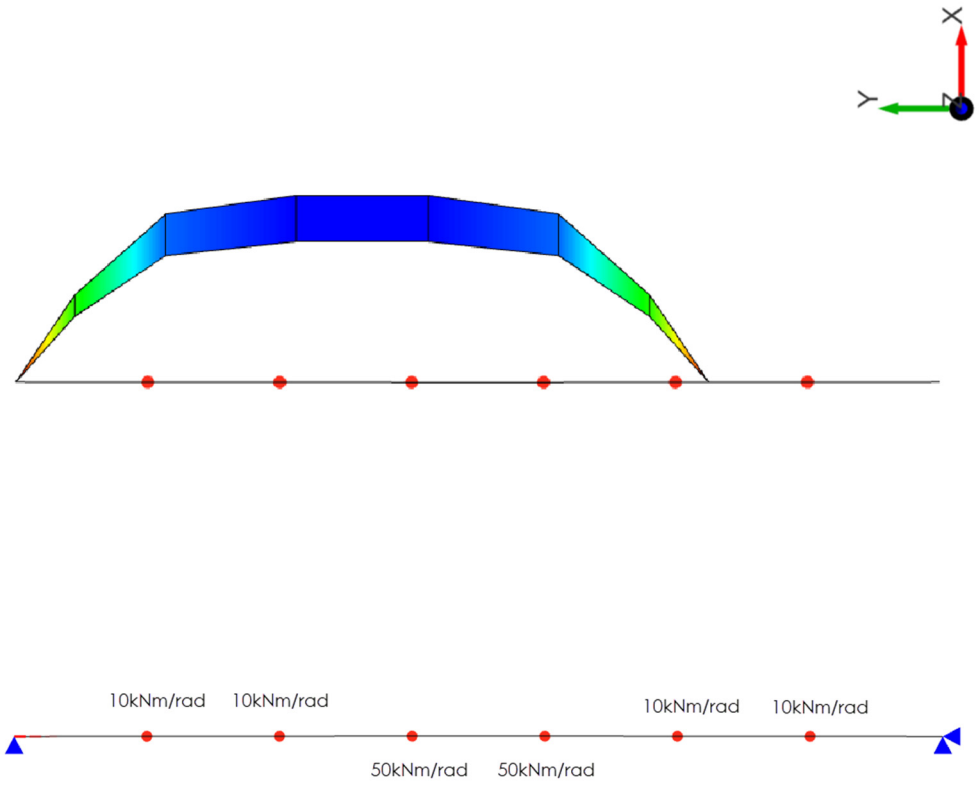


*Figure 5-13 - Flattened Arch Formed with Different Spring Stiffnesses.*

This manipulation of springs to create specific structural forms is an interesting proposition but suffers a shortcoming in that during erection the final desired geometry is defined through the precise location of the supports and any error on this distance directly affects the final deployed geometry.

To overcome this, it would be beneficial to have the hinges lock at specific angles to prevent the arch being over deployed or the joints hyper-extending. This could be achieved by increasing

the rotational stiffness to infinity at some predetermined angle to ensure the geometry is locked at the correct angle. It could be that the segments are formed with non-uniform sectional properties that reflect the bending moment diagram of the in-service structure, perhaps with larger deeper sections at the eaves to reflect the traditional form of a haunch on a portal frame. These segments could have a nominal stiffness in the springs to aid with erection, but once the required geometry has been reached they could be locked in position, perhaps through the insertion of a locking pin or a variable stiffness spring.

To accomplish this in practice is relatively straightforward and makes use of some of the principles established within thick origami, but computationally requires the definition of non-linear hinges which will be the focus of the next section.

## 5.8 Non-Linear Rotational Springs.

A non-linear rotational spring can have a variety of different configurations and behaviours, but the defining factor is that the relationship between the angle the spring rotates through and the associated moment is not a linear relationship.

Non-linear relationships can be as complex or simple as required, but as examples, they can either be a composite of different linear gradients with stiffnesses changing at specific angles (Figure 5-14a), a curved stiffness relationship where the spring can gradually stiffen or soften as the angle subtended increases (Figure 5-14b), or a direction-specific spring where a clockwise rotation generates a different moment compared to an anti-clockwise rotation (Figure 5-14c).

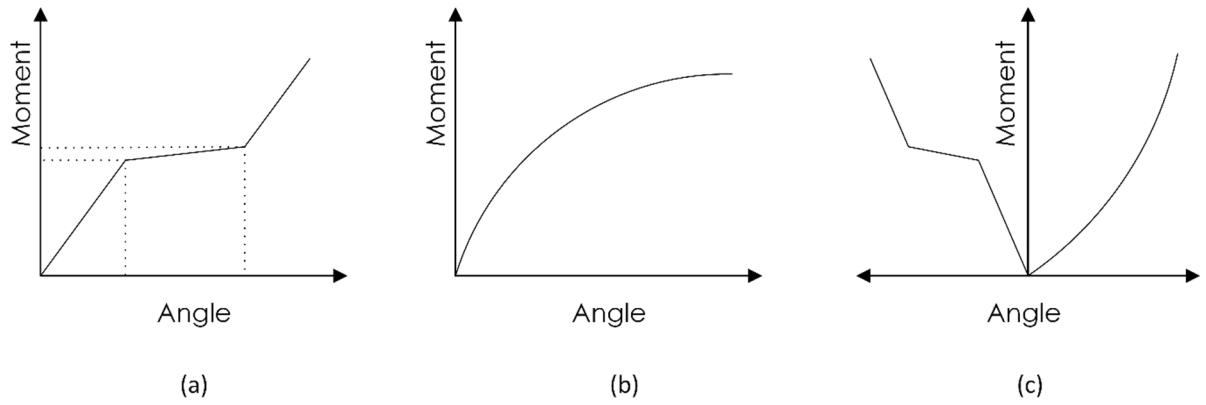


*Figure 5-14 - Example Non-Linear Spring Graphs.*

A non-linear spring within a beaded chain would bring the potential for various changes in the behaviour of a structure to occur at predetermined angles or during the general movement of the structure. Consider the portal frame example of the previous section, each haunch or hinge

could be defined to fully lock at a particular angle to prevent over deployment or hyperextension by locking the moment into a rigid position at a specific angle.

It is proposed that, through the variation of spring stiffnesses (non-linear springs), a beaded chain structure could be developed that behaves as a metamorphic/adaptive structure under applied loads or through the application of external displacements. This change in structural form could either be mobilised through the application of the wind loading or through the change in the prestress state of a central tendon to create a deformed geometry (Hover & Triantafyllou, 1999). Although the inclusion of a tendon with increased prestress would increase the friction forces between beads in much the same way as it does for post-tensioned concrete or even the pantographic structures of Tan and Pellegrino (2008) which may create secondary stiffening forces between the beads. However, the introduction of pretension should also bring about structural benefits in structural performance compared to a simple interlocking arch of compression beads/stone in the same way as would be expected for compressive arches. The beads outlined by Beatini (2013) show curved surfaces rolling over each other, with the tendon extending by a non-linear amount whilst the hinge opens up. The amount that the hinge opens up is controlled by the curvature, type of curve between the two beads, and the positioning of the tendon location.

Considering each bead within Beatini's arches as an infinitely stiff strut with a weaker connecting spring formed by the rolling surfaces and tendons shows similarities to the linked struts considered in previous chapters although with a need for a non-linear spring to be present to model the complexity of the two curved surfaces. Indeed, as was seen in Figure 4-2, the struts will have a residual capacity axial beyond the critical buckling loads which may be beneficial in preventing sudden and catastrophic failure or if engineered carefully generating a second stable geometrical form through controlled displacement at a specific loading. The connection of stiff, thick elements that still allow a metamorphic process to happen is analogous to the principles used within the formation of thick origami (Tachi, 2009b) as shown in Figure 5-15 and the controlling of segmental panels (Wang-Iverson, Lang, & Yim, 2011) similar to the binary springs described in section 5.8.1. These hinges however typically have no moment rotation capacity, but this could easily be introduced through the use of either rotation springs at the hinge positions, or through the introduction of a compressible material in the surfaces between the hinges in a similar manner to the vertebrae in a spine.

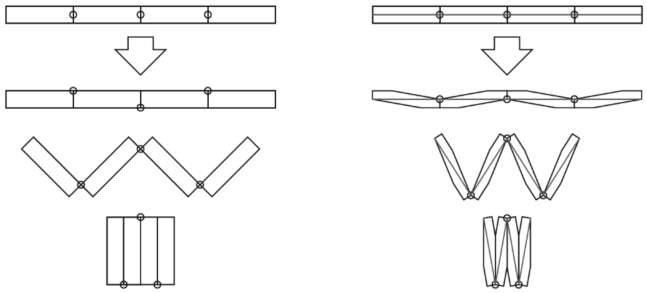

*Figure 5-15 – Thick Foldable Origami By Tachi.*[69]

The behaviour of the joint between stiff elements of origami can be further manipulated to specific values by adding non-linear springs, either with curved parameters or with sharp steps that essentially cause a rotational joint to lock and to become moment transferring through the direct distribution of contact stresses. Some potential spring stiffnesses for consideration are outlined as follows in the following sections.

### 5.8.1 Binary Stiffness.

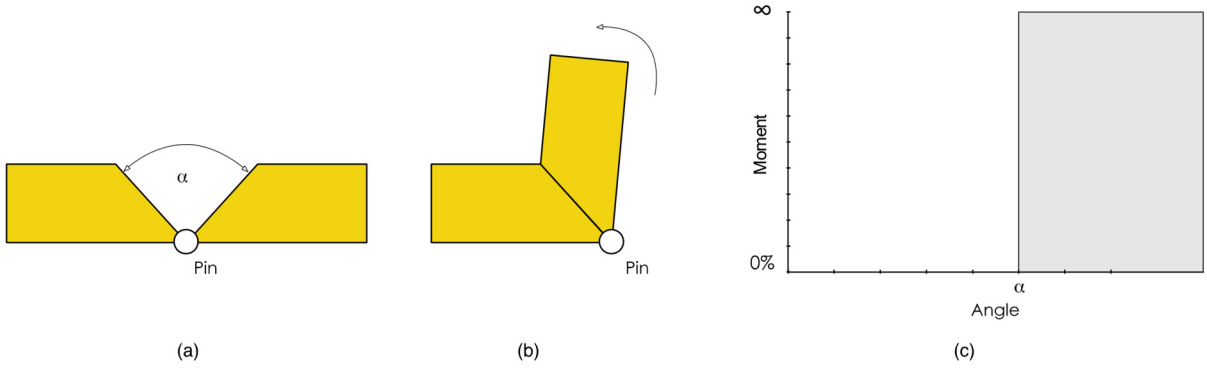


*Figure 5-16 - Change In Stiffness Of Connection Through Rotation.*

For example, by taking a frictionless pin between two elements as shown in Figure 5-16, as one element rotates it has no rotational stiffness. It still can transfer shear and consequently, they are translationally connected, but rotationally independent. If the angle between the two connected faces is taken as being alpha, then once this angle is closed fully and the two adjacent surfaces come into contact the rotation stiffness immediately rises to be fully engaged as shown in Figure 5-16c. This is similar to the connection types proposed by Hernandez (1996) for his segmental

[69] Wang-Iverson, P., Lang, R. J., & Yim, M. (2011). *Origami*[5] (First ed.). Boca Raton: CRC Press.

deployable arched structure and is more commonly seen in the behaviour of a door hinge which is limited when the door closes.

However, through the introduction of a rotational spring of stiffness k (see Figure 5-17a), an intermediate transitional stiffness can be introduced through the range of movement as seen below (see Figure 5-17c).

### 5.8.2 Linear Step With Lock.

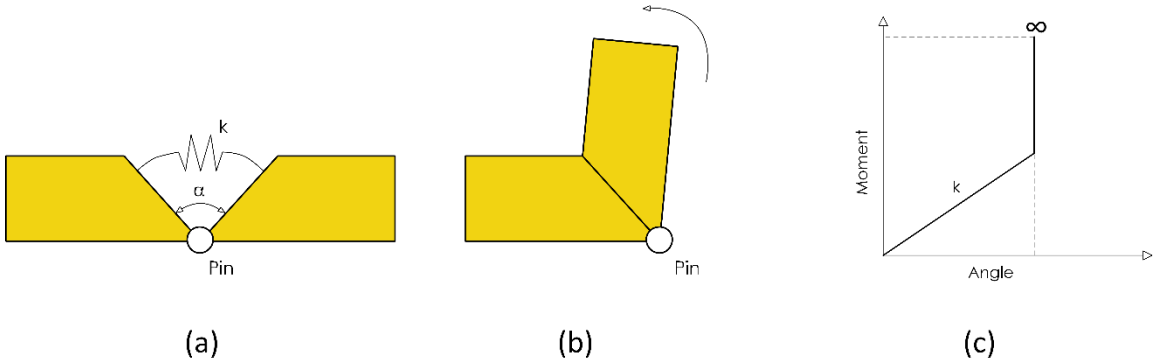


*Figure 5-17 - Pinned Joint With Rotation Stiffness.*

Through the introduction of a rotational spring that can provide ramped stiffness proportional to the angle subtended just as in a traditional rotational spring the joint can behave the same as the spring struts identified earlier within this thesis. Indeed, this intermediate stiffness is arguably more useful to a structural engineer than a free pin on a deployable structure as it will provide the structure with a stiffness at the joints to help limit the structure reverting to a mechanism by maintaining transitional rigidity of the structure. Alternatively, the joint could be provided with a compressible filler of known mechanical properties to adjust the rotational stiffness rather than a spring, this may be preferable for environments where mechanical springs would be vulnerable to damage; such as through the ingress of sand contamination for example.

### 5.8.3 Bidirectional Linear Step With Lock.

One element to consider with regards these types of joints is the influence of the direction of rotation, where the joints in Figure 5-16 and Figure 5-17 cannot hyper-extend back on themselves, the joint could be double-chamfered to allow this, with different properties on the reverse spring if required.

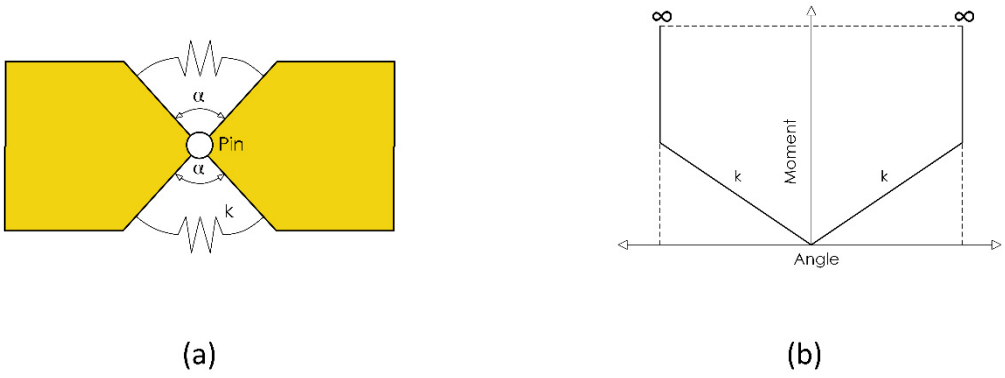


*Figure 5-18 - Pinned Joint With Double Rotational Springs.*

Whilst the spring shown in Figure 5-18 is symmetrical, it could easily be manufactured with different spring stiffnesses in either direction to encourage certain shapes or modes to be developed under certain load conditions. For example, to behave stiffly under gravity-based loads but to be flexible under wind uplift.

### 5.8.4 Beaded Chains With Tendons.

However, the hinges do not have to be straight-edged and two curved surfaces with a central tendon running through them create a different relationship, firstly the curved geometry creates a non-linear path for the tendon exit points on the beads as the two surfaces roll along each other, see Figure 5-19. This creates a difference in length in the cable as it extends which is directly related to the non-linear tension force in the tendon. The lever arm as the curved surfaces roll over each other is also non-linear, which in turn creates an increasingly non-linear moment when multiplied by the non-linear tension force in the tendon, generating the profile as seen in Figure 5-22 which is derived as follows.

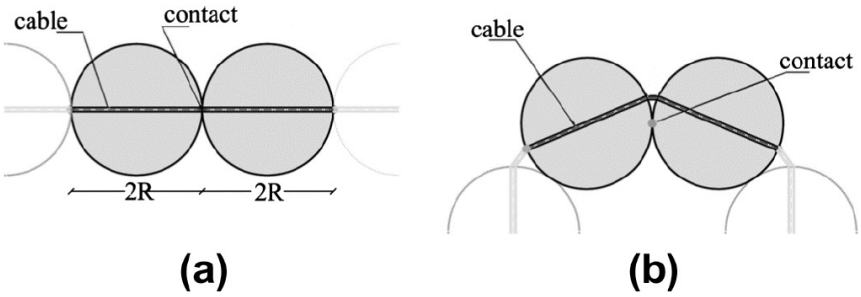


*Figure 5-19 – Cable Stiffened Elastica As A Beaded Chain Structure.*[70]

Consider only two circular surfaces in contact, of radius r. As they rotate through an angle θ the relative distance between them is defined as d, which would be the increase in the tendons length if the tendon was threaded through the beads as shown in Figure 5-20.

As the two surfaces rotate against each other, the points where the tendon exits the beads will no longer remain co-incident (see Figure 5-19) and the distance between these two points will increase as the circles rotate, thus increasing the length of the tendon by d, see Figure 5-20.

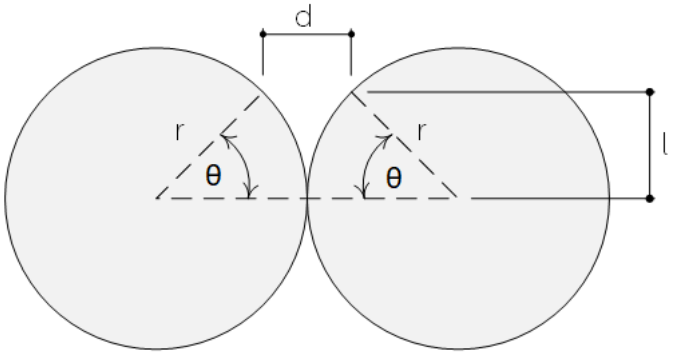


*Figure 5-20 - Relative Geometry Of Two Circles Rolling Against Each Other.*

The increase in tendon length running between the beads will be 'd' as defined below.

$$d = 2\left(r - r\,\mathrm{Cos}\,\theta\right) \tag{5.1}$$

Taking the extension of the cable to be 'd', this will have a relationship directly proportional to the Elastic modulus providing the cable is kept within its elastic range. Assume the tendon to be

[70] Beatini, V., & Royer-Carfagni, G. (2013). Cable-stiffened foldable elastica for movable structures. *Engineering Structures, 56*, 126-136.

a true circle for illustrative purposes (although a real tendon would more likely be a spiral strand) with a diameter of $\phi$.

$$area = \frac{\pi\phi^2}{4} \tag{5.2}$$

Considering the basic relationship between stress and strain over the elastic region, with L being the original length of the element being considered and E being the Young's Modulus.

$$E = \frac{stress}{strain} = \frac{force/area}{\Delta L/L} \tag{5.3}$$

But taking ΔL = d and substituting into (5.3) and then solving for the force in the cable 'f', assuming no pretension and no other beads in the system, gives.

$$f = -\frac{1}{4} E\pi\phi^2 \left(-1 + \mathrm{Cos}(\theta)\right) \tag{5.4}$$

As the two circles will be in a common contact point, the lever arm to where the cables spring from each circle will also vary in a non-linear fashion, with the tension in the tendon 'f' being in a horizontal plane, the lever arm 'l' is taken in the vertical plane as shown in Figure 5-21.

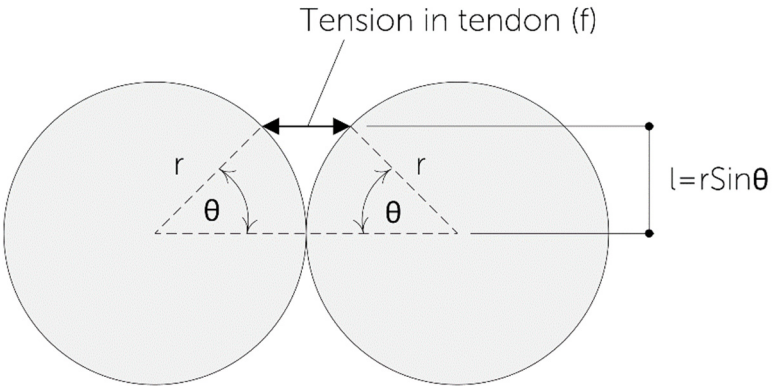


*Figure 5-21 - Lever Arm 'l' for Tendon and Beads*

$$l = r\,\mathrm{Sin}\,\theta \tag{5.5}$$

Resolving the force in the cable through theta to match with the corresponding lever arm will give the function that can be used to generate the pure moment-rotation curve.

$$M = f\,l \tag{5.6}$$

$$M = -\frac{1}{4} E\pi r\phi^2 \left(-1 + \mathrm{Cos}(\theta)\right)\mathrm{Sin}(\theta) \tag{5.7}$$

Taking some initial parameters as E=160,000 N/mm², r=120mm, $\phi$=3mm gives the moment-rotation curve as shown in Figure 5-22.

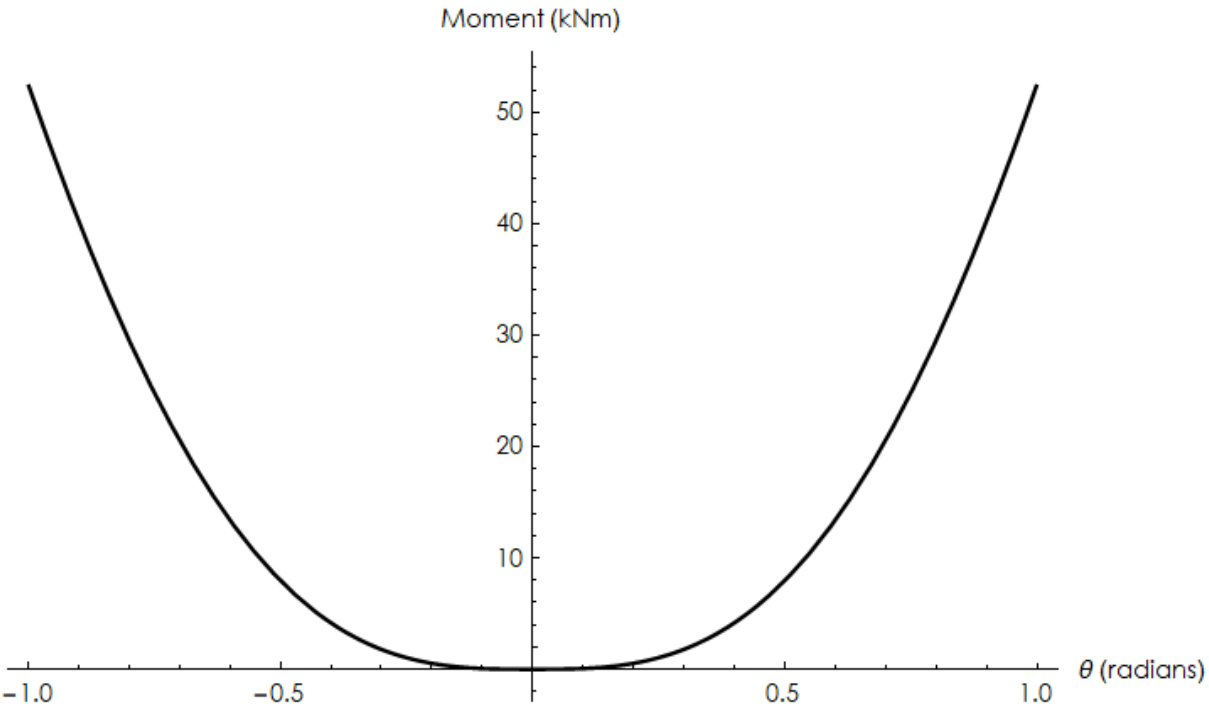


*Figure 5-22 - Tensioned Beaded Chain Moment-Rotation Curve.*

The general shape of the moment/rotation curve is interesting as it clearly shows a non-linear behaviour with a sharp increase in stiffness (general stiffening of the structure) as the rotations become gross. As the rotations become more exaggerated the edges of the graph show a more linear behaviour. This behaviour can be further amplified, by combining beads of different curvatures or profiles to control the stiffness. A key point to consider when developing these curve profiles is that springs within the analytical models could be integrated for bead dimensions that would be problematic or impractical to develop in reality, such as a bead diameter of 5m. A key challenge to be overcome moving between the analytical models and transferring these to a real-world application would be the development of rotational springs of a similar scale and this will require significant development in manufacturing techniques. There is also the risk that this detail is unable to suitably transfer shear at the contact point.

### 5.8.5 Negative Stiffness Springs.

Introducing more complex spring stiffnesses, for example, those associated with the tape spring hinges (Seffen et al., 2000), can encourage a different form of behaviour that enables certain structural forms to snap into new stable states, see Figure 5-23.

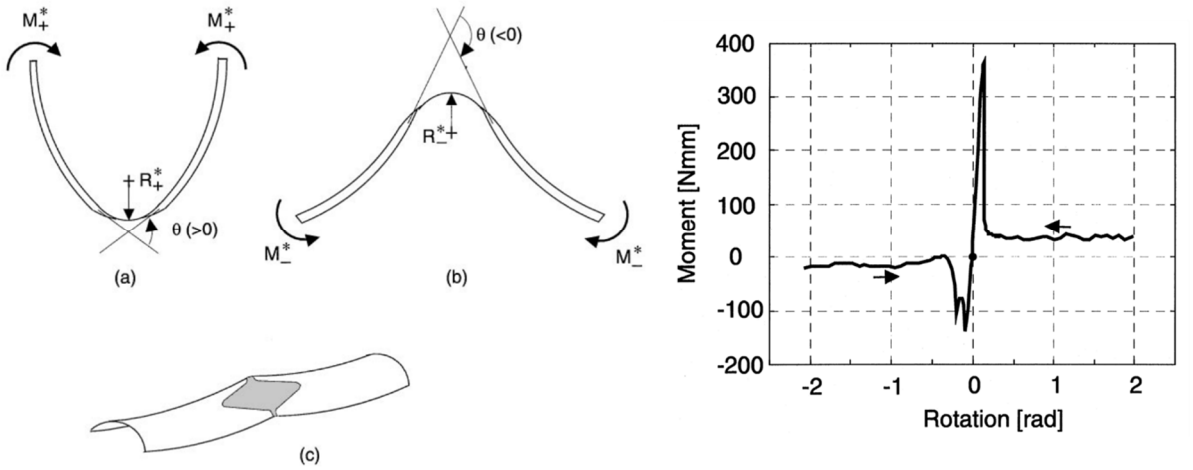


*Figure 5-23 - Taped Hinge Spring Moment Rotation Curve on Contraction Portion of Movement.*[71]

Negative-stiffness springs allow the generation of multi-stable structures through controlled motion. This may be beneficial where structures are required to generate gross changes in shapes to exhibit new forms of behaviour, for example allowing a structure to be stable until the moment at the spring location exceeds the designed capacity and then allowing the hinge to 'pop' into a new state. Typically these forms of spring have been created using steel tapes with curvature across their breadth to generate the change in behaviour, through the local buckling of these tapes the potential energy is stored within them when asymmetrical see Figure 5-24(b).

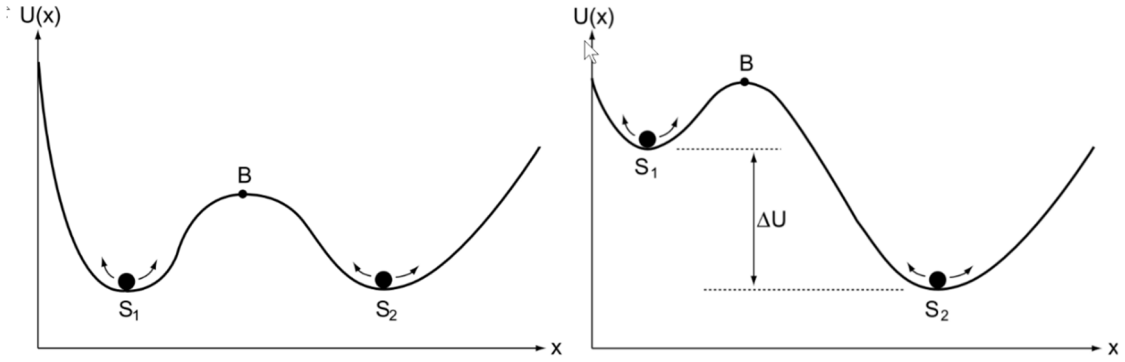


*Figure 5-24 - Multi-Stable Structures (Symmetrical and Non-Symmetrical).*[72]

[71] Seffen, K. A., You, Z., & Pellegrino, S. (2000). Folding and deployment of curved tape springs. *International Journal of Mechanical Sciences, 42*(10), 2055-2073. doi:10.1016/s0020-7403(99)00056-9

[72] Santer, M., & Pellegrino, S. (2008). Compliant multistable structural elements. *International Journal of Solids and Structures, 45*(24), 6190-6204. doi:10.1016/j.ijsolstr.2008.07.014

The use of negative stiffness springs at a structural level is not commonplace given the scale of the forces required are prohibitive with regards the manufacturing of tape springs, although their use at a micro-electronics scale is a developing area of research (Smith & Chase, 2001) particularly with regards using the generation of energy via the buckling modes for remote sensor monitoring. Anecdotally at the 2018 Henderson Colloquium at Cambridge University, the use of doubly curved surfaces to develop interesting alternative buckled forms was mooted as a common area of interest between many attendees over the coming decade with early prototypes making use of sections of curved soft-drink bottles to illustrate principles.

### 5.8.6 Introduction Of Non-Linear Springs Within CivilFEM.

Whereas linear springs can be introduced through a simple connection element within CivilFEM, this element type is limited to purely linear springs and an alternative approach needs to be taken when modelling non-linear springs regardless of being defined as symmetrical, asymmetrical, or with negative stiffness.

The connection element is still used as per previous models to ensure that connectivity is maintained for translations between the two nodes, but the rotational link between the nodes being considered is instead set to be free with an additional rotational spring element needing to be integrated to provide the rotational coupling between nodes.

As the methodology for the integration of linear springs has been validated within this thesis, the development of a comparable model with a non-linear spring (although defined with linear stiffness) has been undertaken to determine if the workflow and the assessment of the forces being generated are still valid.

| **Spring** | |
|---|---|
| Name | Spring |
| Type | Rotational Spring |
| Spring type | Fixed DOF |
| Coord. System | Global Cartesian |
| Structural element 1 | Beam (2) |
| Point1 | (0, 1.5) m |
| Point1 projected | (0, 1.5) m |
| First node | 2 |
| Structural element 2 | Beam |
| Point2 | (0, 1.5) m |
| Point2 projected | (0, 1.5) m |
| Second node | 3 |
| Z | ☑ |
| K | 50000 N·m/rad |
| NonLinear spring | ☐ |

*Figure 5-25 - Additional Rotation Spring.*

A comparison process was undertaken to validate the new elements to ensure that no untoward

effects were generated as part of the new modelling process. To compare this against previous analysis undertaken, an independent spring element was integrated to replace the original connected elements. The new spring was defined as a linear rotational spring to determine that the modelling process was correct with the rotational properties as shown in Figure 5-25, essentially a hinge set at 50kNm/rad.

As in previous analyses, the critical buckling load was correctly identified as 66.6kN showing that the rotational spring added has behaved correctly in the model and that it is compatible with the connection element that has been introduced, providing that the rotational element within the connection is defined as 'unconnected' so that the rotational spring stiffness is only developed by the non-linear spring element.

With the integration of independent springs validated, the next level of complexity is brought about by enabling the NonLinear spring option in the control dialog box. This allows the introduction of a non-linear spring, that can either be defined through the creation of a table for the stiffness or through the creation of a chart (see Figure 5-26).

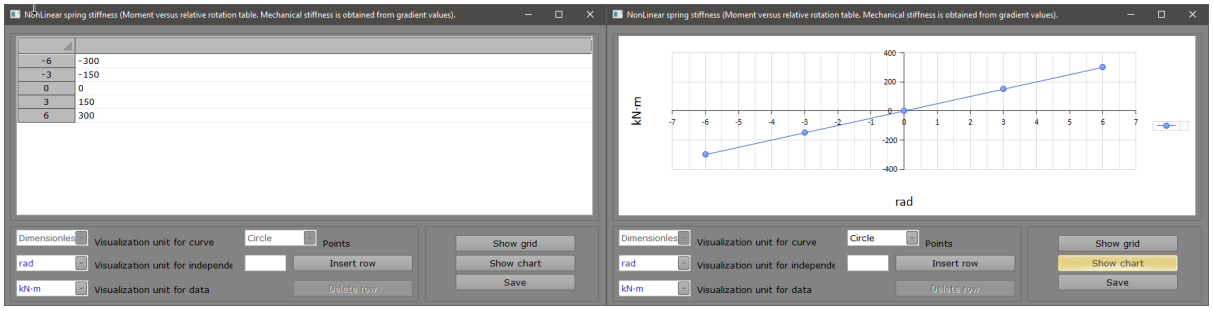


*Figure 5-26 - Non-Linear Spring Stiffness Definition.*

Whilst the non-linear spring stiffness has been enabled, this does not necessarily mean that the model **must** have a non-linear spring relationship defined, rather it means that a more complex relationship for the spring can be defined other than just a linear relationship between moment and rotation, however, a linear relationship can still be defined if desired.

As part of the validation, a linear spring was defined (see Figure 5-26) which gives an equivalent linear spring stiffness of 50kNm/rad as in previous examples although the spring has been declared as being non-linear within CivilFEM.

With the rotational spring stiffness defined as being 50kNm/rad the expected buckling capacity for a 3m strut would be 66.6kN, but as can be seen in Figure 5-27 the buckling load returned is far more than the anticipated critical buckling load.

| | Buckling m | Buckling lo... | File |
|---|---|---|---|
| | | Dimensionless | |
| | 1 | 530.218 | Test#6_1.rcf |
| | 2 | 537511488. | Test#6_2.rcf |
| | 3 | 537516416. | Test#6_3.rcf |
| | 4 | 608594558... | Test#6_4.rcf |
| | 5 | 225179981... | Test#6_5.rcf |
| | 6 | -22517998... | Test#6_6.rcf |
| | 7 | -45035996... | Test#6_7.rcf |

*Figure 5-27 - Critical Buckling Loads for Non-linear spring set to 50kNm/rad uniform stiffness.*

The buckling load for the first mode of 530kN is far greater than the predicted 66.6kN, although as can be seen in Figure 5-28 below the overall behaviour in terms of the modal shape would appear to be correct.

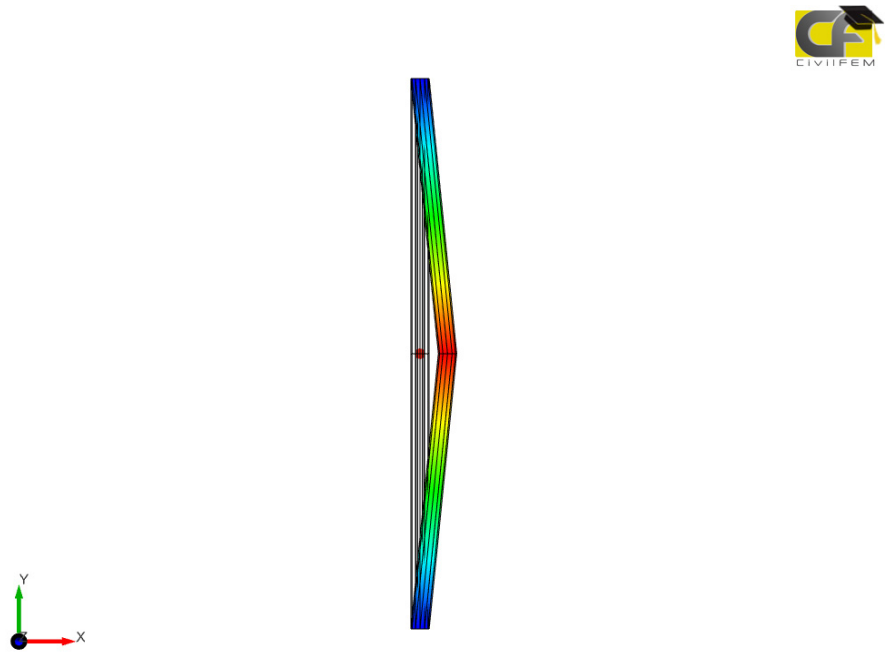


*Figure 5-28 - Buckled Form for Mode 1 with Uniform Non-Linear Spring.*

Through discussions with the support team at CivilFEM and further independent investigations, there is a subtle difference at play when the non-linear spring element is selected in that the non-linear engine solves the model with incremental loads (it is this behaviour explicitly that generates the history plots when forcing displacements at supports) and the buckling load is based upon the last load increment solved, rather than the total load applied.

In this instance, the final loading increment is identified by reviewing the output from the solution engine during the solving process (in the output screen, see Figure 5-29) and

determining the last increment that was solved (this is irrelevant for the linear solutions, only for the non-linear engine).

>>>>>> Summary solve process <<<<<<

| case # | inc # | cycl # | sepa # | cut # | cycl # | separ # | cut # | rmesh # | time step of the inc | total time of the job | min | displ-mag max |
|---|---|---|---|---|---|---|---|---|---|---|---|---|
| | | |--of the inc--| | |------of the analysis------| | | | | | |
| 0 | 0 | 0 | 0 | 0 | 0 | 0 | 0 | 0 | 0.0000E+00 | 0.0000E+00 | 0.0000E+00 | 0.0000E+00 |
| 1 | 1 | 1 | 0 | 0 | 1 | 0 | 0 | 0 | 1.0000E-02 | 1.0000E-02 | 0.0000E+00 | 4.4444E-10 |
| 1 | 2 | 1 | 0 | 0 | 2 | 0 | 0 | 0 | 1.2000E-02 | 2.2000E-02 | 0.0000E+00 | 9.7778E-10 |
| 1 | 3 | 1 | 0 | 0 | 3 | 0 | 0 | 0 | 1.4400E-02 | 3.6400E-02 | 0.0000E+00 | 1.6178E-09 |
| 1 | 4 | 1 | 0 | 0 | 4 | 0 | 0 | 0 | 1.7280E-02 | 5.3680E-02 | 0.0000E+00 | 2.3858E-09 |
| 1 | 5 | 1 | 0 | 0 | 5 | 0 | 0 | 0 | 2.0736E-02 | 7.4416E-02 | 0.0000E+00 | 3.3074E-09 |
| 1 | 6 | 1 | 0 | 0 | 6 | 0 | 0 | 0 | 2.4883E-02 | 9.9299E-02 | 0.0000E+00 | 4.4133E-09 |
| 1 | 7 | 1 | 0 | 0 | 7 | 0 | 0 | 0 | 2.9860E-02 | 1.2916E-01 | 0.0000E+00 | 5.7404E-09 |
| 1 | 8 | 1 | 0 | 0 | 8 | 0 | 0 | 0 | 3.5832E-02 | 1.6499E-01 | 0.0000E+00 | 7.3329E-09 |
| 1 | 9 | 1 | 0 | 0 | 9 | 0 | 0 | 0 | 4.2998E-02 | 2.0799E-01 | 0.0000E+00 | 9.2440E-09 |
| 1 | 10 | 1 | 0 | 0 | 10 | 0 | 0 | 0 | 5.1598E-02 | 2.5959E-01 | 0.0000E+00 | 1.1537E-08 |
| 1 | 11 | 1 | 0 | 0 | 11 | 0 | 0 | 0 | 6.1917E-02 | 3.2150E-01 | 0.0000E+00 | 1.4289E-08 |
| 1 | 12 | 1 | 0 | 0 | 12 | 0 | 0 | 0 | 7.4301E-02 | 3.9581E-01 | 0.0000E+00 | 1.7591E-08 |
| 1 | 13 | 1 | 0 | 0 | 13 | 0 | 0 | 0 | 8.9161E-02 | 4.8497E-01 | 0.0000E+00 | 2.1554E-08 |
| 1 | 14 | 1 | 0 | 0 | 14 | 0 | 0 | 0 | 1.0699E-01 | 5.9196E-01 | 0.0000E+00 | 2.6309E-08 |
| 1 | 15 | 1 | 0 | 0 | 15 | 0 | 0 | 0 | 1.2839E-01 | 7.2035E-01 | 0.0000E+00 | 3.2016E-08 |
| 1 | 16 | 1 | 0 | 0 | 16 | 0 | 0 | 0 | 1.5407E-01 | 8.7442E-01 | 0.0000E+00 | 3.8863E-08 |
| 1 | 17 | 1 | 0 | 0 | 17 | 0 | 0 | 0 | 1.2558E-01 | 1.0000E+00 | 0.0000E+00 | 4.4444E-08 |

*Figure 5-29 - Solution Output for Non-Linear Engine.*

As can be seen above, which is an extract of the analysis engine output, the penultimate load increment that solved was at $8.7442 \times 10^{-1}$ kN. This can be used to modify to the buckling load of 530.218kN to give an appropriately scaled buckling load of:

$$530.218 \times (1 - 0.87442) = 66.585kN$$

This is a very close approximation of the 66.667kN, this discrepancy can be overcome by adopting a slightly higher value for the Young's Modulus (there are flexural contributions to the buckling mode in this example). Increasing the Young's Modulus allows the results to correlate perfectly with the theoretical buckling load.

| | |
|---|---|
| Init. step fraction | 0.001 |
| Min. step fraction | 0.001 |
| Max. step fraction | 0.5 |

*Figure 5-30 - Solution Engine Settings for Forced Displacement.*

Typically when generating forced displacement models, the solver engine requires a fine step fraction setting defined for the solution engine (see Figure 5-30 for higher step settings), typically subdividing the results into over 200 increments for a detailed assessment of the behaviour being

generated and the creation of smooth animations.

As it is often more convenient to retain finer control of the step model in the buckling analysis to ease the reuse of the model between the various analysis domains such as buckling, static, modal, and transient it consequently requires a different method for interpreting the buckling capacity.

An alternative approach to prevent the need for modification of the buckling loads by the load increment, a coarse step function of unity could be defined meaning that the analysis completes only a single step for the buckling analysis and a result that is close to the expected buckling value is returned (see Figure 5-31 for unity load step settings). However, this has a disadvantage in that the same model cannot be easily re-used for post-buckling behaviour.

| | |
|---|---|
| Init. step fraction | 1 |
| Min. step fraction | 1 |
| Max. step fraction | 1 |

*Figure 5-31 - Single Step Increment for Buckling Analysis With Non-Linear Springs.*

Taking the step fractions set to unity solves the model and gives a reasonable approximation of the buckling load again of being 66.584kN (matching the load increment method with a finer load step, with the difference between the theoretical value being as a consequent of the choice in Youngs Modulus) with the step output within the Solution Output being taken as 1.0, therefore with the load being based on the entirety of the applied loading for the buckling behaviour, see Figure 5-32.

| case # | inc # | cycl # | sepa # | cut # | cycl # | separ # | cut # | rmesh # | time step of the inc | total time of the job | min displ-mag | max displ-mag |
|---|---|---|---|---|---|---|---|---|---|---|---|---|
| | | \|--of the inc--\| | | | \|------of the analysis------\| | | | | | |
| 0 | 0 | 0 | 0 | 0 | 0 | 0 | 0 | 0 | 0.0000E+00 | 0.0000E+00 | 0.0000E+00 | 0.0000E+00 |
| 1 | 1 | 1 | 0 | 0 | 1 | 0 | 0 | 0 | 1.0000E+00 | 1.0000E+00 | 0.0000E+00 | 4.4444E-08 |
| | | 0 | 0 | 0 | 1 | 0 | 0 | 0 | 1.0000E+00 | 1.0000E+00 | 0.0000E+00 | 4.4444E-08 |
| | | 0 | 0 | 0 | 1 | 0 | 0 | 0 | 0.0000E+00 | 1.0000E+00 | 0.0000E+00 | 3.3313E-03 |
| | | 0 | 0 | 0 | 1 | 0 | 0 | 0 | 0.0000E+00 | 1.0000E+00 | 0.0000E+00 | 4.6999E-06 |
| | | 0 | 0 | 0 | 1 | 0 | 0 | 0 | 0.0000E+00 | 1.0000E+00 | 0.0000E+00 | 4.7281E-06 |
| | | 0 | 0 | 0 | 1 | 0 | 0 | 0 | 0.0000E+00 | 1.0000E+00 | 0.0000E+00 | 1.4068E-08 |
| | | 0 | 0 | 0 | 1 | 0 | 0 | 0 | 0.0000E+00 | 1.0000E+00 | 0.0000E+00 | 1.8750E-13 |
| | | 0 | 0 | 0 | 1 | 0 | 0 | 0 | 0.0000E+00 | 1.0000E+00 | 0.0000E+00 | 7.2745E-15 |
| 2 | 1 | 0 | 0 | 0 | 1 | 0 | 0 | 0 | 0.0000E+00 | 1.0000E+00 | 0.0000E+00 | 3.5037E-14 |

*Figure 5-32 - Solution Output showing load increment based on unity for the full application of load.*

## 5.9 Non-Linear Springs In A Chain.

Different configurations of non-linear springs can be arranged in a chain to allow the chain to fold/buckle into a predictable and tailored shape. This could be defined in such a manner that the structure can activate certain springs only when loadings have exceeded the initial spring stiffnesses capacity.

As an example, non-linear springs can be used to control angles in chains of springs to ensure that the nodal locations are locked into a particular shape. Taking a chain of springs as defined in Figure 5-33 with springs set to become rigid at particular angles (defined as having infinite moment rigidity at a particular angle) applying a linear displacement at the roller end of the strut will develop a buckled form as shown in Figure 5-35.

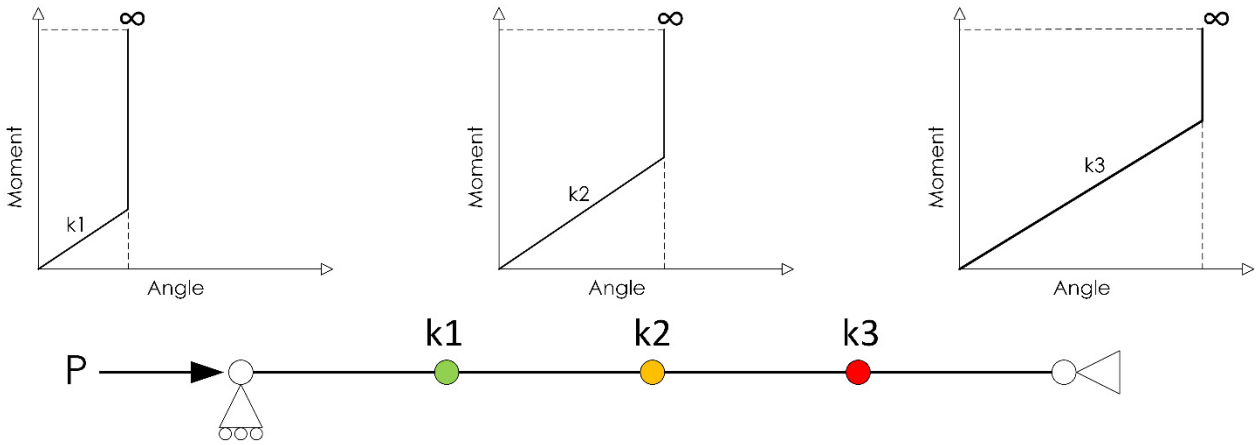


*Figure 5-33 - Chain of Springs with Non-Linear Springs.*

Figure 5-34 illustrates that the hinge K1 has an initial moment-rotation curve of 10kNm/10° but after 10° the hinge has a relative stiffness of infinity (numerically represented as 1000kNm/0.1°) (see Figure 5-34a) and the hinge at K2 has a moment-rotation curve of 40kNm/20° and beyond 20° the stiffness also approaches infinity (see Figure 5-34b). The hinge K3 has been set to have an angle that cannot lock and engage during deployment to demonstrate the free behaviour is also mobilising.

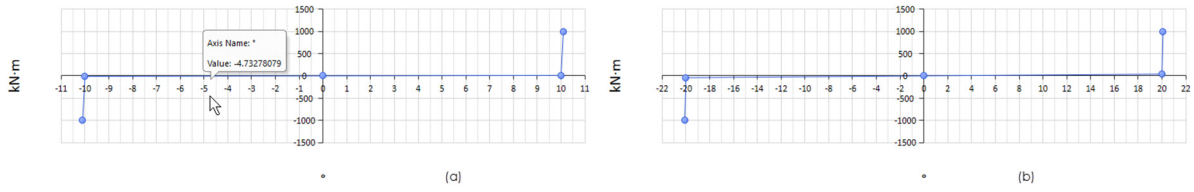


*Figure 5-34 - Non-linear Spring Stiffnesses for K1 (a) and K2 (b).*

When a chain of springs is ordinarily displaced the arc formed has a uniformly distributed curvature, as can be seen, within Figure 5-35 an asymmetrical shape has been developed demonstrating that a change in stiffness has been developed and redistributed up the chain.

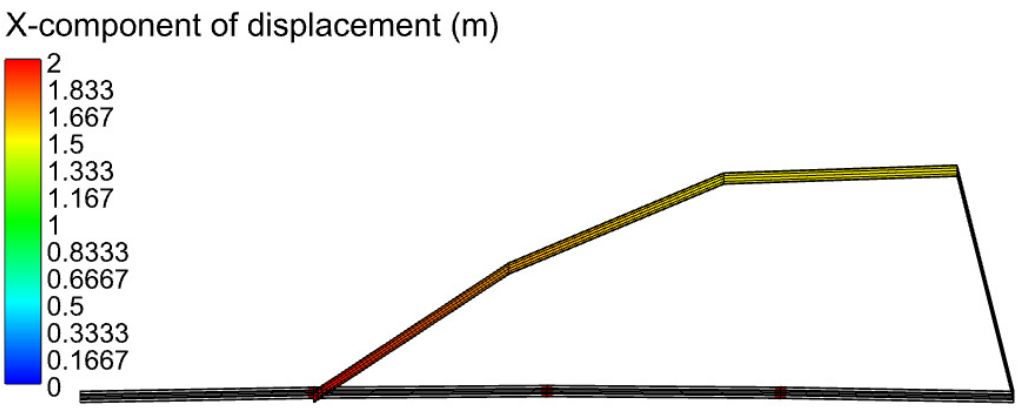


*Figure 5-35 - Chain Of Non-Linear Locking Springs Folded Into Arch.*

With a 2m displacement introduced on a system with an overall flat length of 8m, the relative internal angles defined within the springs will be exceeded, thus demonstrating their compliance. One of the challenges within CivilFEM, however, is that plotting the change in relative angles is not straightforward and requires the extraction of over 200 individual load cases to be post-processed or the development of bespoke Python scripting to enable the relative angles to be extracted, see Figure 5-36.

```python
# Python script to create a new user result: actual angle of the hinge
# To create or modified any result the number of results to set has to be the same number of
# results saved in the result file. All nodes will have same result


nfin = 37  # Total number of results (plus one)
for i in range(1,nfin):
    res = getResults("Displaced_" + str(i) + ".rcf")            # Name of results file
    AngleValues = []                                          # List of angle values
    Ang3 = Double(0.0)                                        # Angle of node 3
    res.getNodeResult(Ang3,"URz",3)
    Ang2 = Double(0.0)                                        # Angle of node 2
    res.getNodeResult(Ang2,"URz",2)
    val = Ang3 - Ang2
    AngleValues1 = []
    Ang4 = Double(0.0)                                        # Angle of node 4
    res.getNodeResult(Ang4,"URz",4)
    Ang5 = Double(0.0)                                        # Angle of node 5
    res.getNodeResult(Ang5,"URz",5)
    val1 = Ang5 - Ang4
    AngleValues2 = []                                         # Hinge Angle
    Ang7 = Double(0.0)                                        # Angle of node 7
    res.getNodeResult(Ang7,"URz",7)
    Ang6 = Double(0.0)                                        # Angle of node 6
    res.getNodeResult(Ang6,"URz",6)
    val2 = Ang7 - Ang6
    for i in range(8):                                        # Loop on total of nodes
        AngleValues.append(val)
    res.addNodeResult("AngleHinge", "Deg", AngleValues)       # New result name will appear on Node Result combo list
    for i in range(8):                                        # Loop on total of nodes
        AngleValues1.append(val1)
    res.addNodeResult("AngleHinge1", "Deg", AngleValues1)
    for i in range(8):                                        # Loop on total of nodes
        AngleValues2.append(val2)
    res.addNodeResult("AngleHinge2", "Deg", AngleValues2)
```

*Figure 5-36 - Python Script to Determine the Internal Relative Angle Between Two Elements.*

The above script modifies the load files to add in three new load result types, AngleValues (left-hand hinge, K1), AngleValues1 (central hinge, K2), and AngleValues2 (right-hand hinge, K3) that can then be plotted using the history plot function, see Figure 5-37.

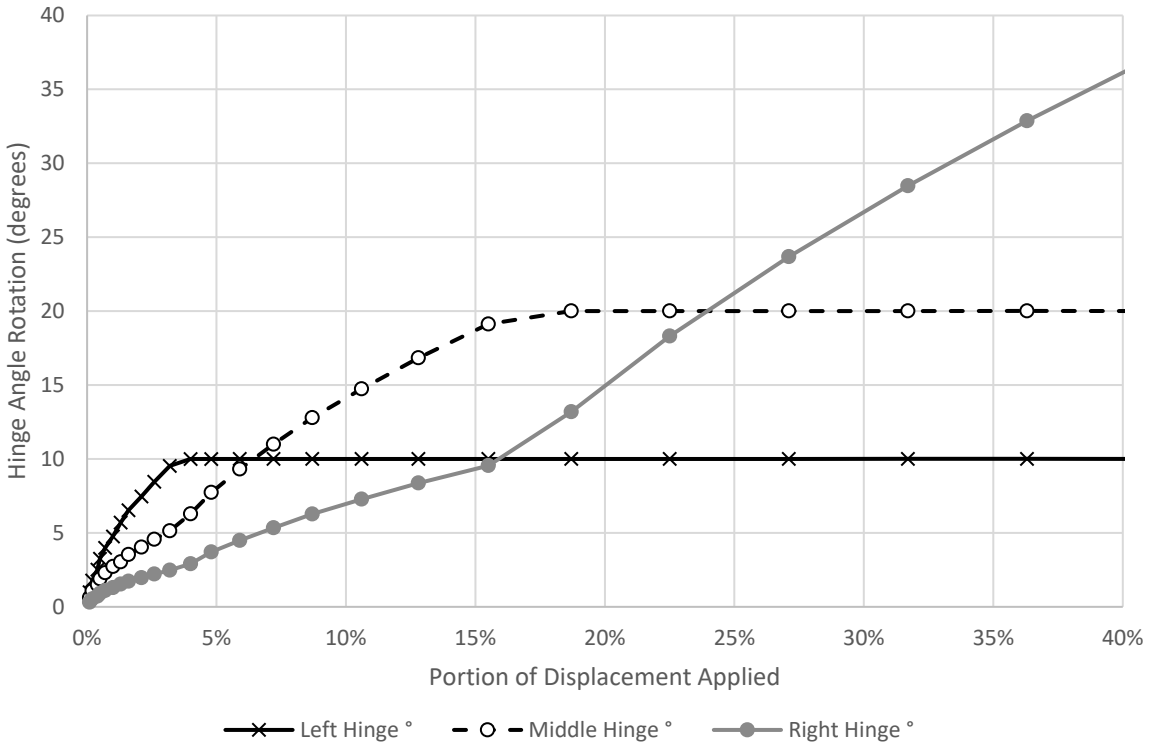


*Figure 5-37 - Relative Rotation Angle At Hinge Locations limited to 40% deployment.*

Plotting the deployment sequence initially to only 40% of the deployment helps to limit the plot scale and show more clearly the change in angles as the hinges lock. Figure 5-37 shows that as each hinge locks at the limiting angle, that the remaining hinges engage. This is evident from the change in the gradient of the curve at the same timestep position as a hinge locks up at with a pronounced kink in the Hinge Rotation Angle showing the change in the overall behaviour of the structure. As can be seen above, the hinges lock at the intended angles, with hinge K1 locking first at 10 degrees, followed by hinge K2 at 20 degrees, with K3 continuing to flex without having reached its limiting angle by 40% of deployment (or even by full deployment as shown within Figure 5-38).

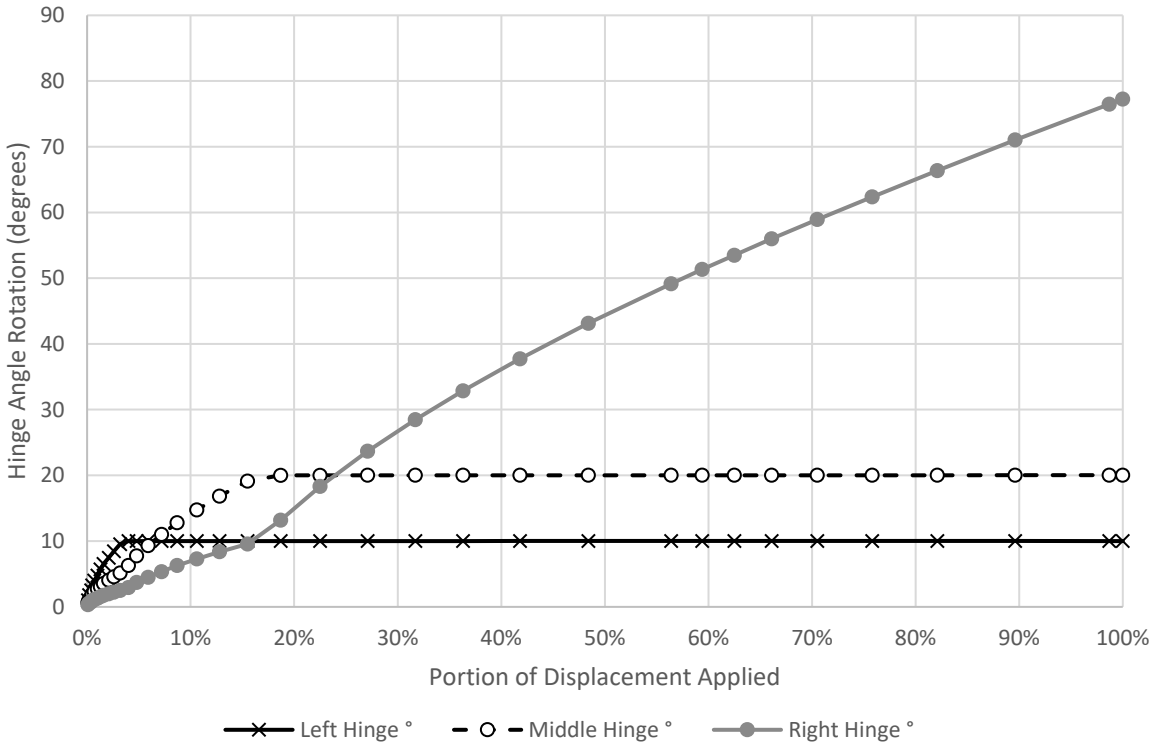


*Figure 5-38 - Relative Rotation Angle At Hinge Locations For Full Deployment.*

With K3 specified to never fully lock during the range of this deployment sequence, the behaviour is as expected within Figure 5-38, with K1 and K2 remaining fully locked at the pre-determined angles but with K3 continuing to flex and rotate.

This principle of locking a structure into different shapes through the displacement of supports could be achieved in practice by linking the feet of an arch together using a cable (or tirfor) that can adjust the relative distance between the supports by connecting a motor to lock a structure into different positions.

Each of these positions could have a different structural response, this response could be adjusted and determined via a bending active approach (Phocas & Alexandrou, 2017) although by integrating springs and controlling the 'weak' points within the structure the structural form can make use of the benefits of stiffer elements similar to thick origami with the hinges providing the articulation and control to the structure.

This could be used to develop a building that could be delivered in parts and assembled into a chain with the deployment sequence pulling the chain into a predetermined shape such as an arch, a portal frame, or a pitched roof. Or even a structure that was able to change its shape to expand or contract if required for uses such as disaster relief shelters or an aircraft hangar that

alters its shape to wrap around a specific aircraft to prevent dust blowing through to the engines in the middle of a sandstorm, or a small device that physically exhibits a particular pattern when the axial load is at a specific value.

## 5.10 Physical Springs.

To this point, the discussion has been about the analytical properties of springs, with potential applications drifting between macro and micro applications. However, it should be noted that the forces associated with a building in comparison to an off the shelf spring are largely incompatible.

Enquiries with large spring manufacturers show that typically torsional springs have limited rotational capacity, even the larger springs such as the LesFjors spring 8607 only have a capacity of 867Nmm/degree which is too low for a practical application for a building.

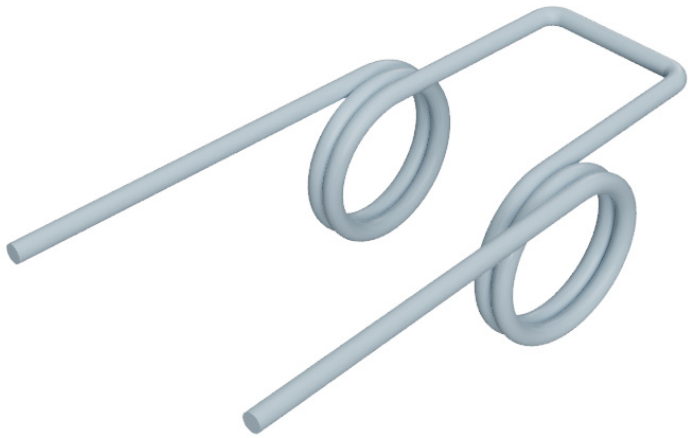

*Figure 5-39 - Typical Torsional Spring*

European Springs manufactures torsional springs using up to 26mm diameter wire, which may provide a larger stiffness than the LesFjors spring 8607 although these are currently special-order items and the actual stiffness would not be confirmed from the manufacturer until a physical order was placed.

Springs are usually defined as linear elements by manufacturers, although this is rarely the case in production and perfectly linear springs are often more expensive than their standard counterparts, with limitations on the range to which linearity can be guaranteed. Translational springs are often defined within their product catalogues with two defined forces, the first is the separation force and the second is the rate of extension. Where the coils of springs are in

contact with each other, there will be an initial force required to peel apart these coils, this initial mobilising force is the separation force. Once the coils have opened, then the typical force per length rate of extension governs as defined by Hook's Law over a defined length. Although for particularly sensitive applications it must be re-iterated that strictly defined linear springs require precise calibration and are more expensive than their more normal counterparts.

Whilst purchasing large capacity torsional springs in theory may be feasible, from discussions with manufacturers springs of the capacity needed for integrating into a building are a special-order item and obtaining information with regards their operational stiffnesses difficult to extract.

Given that linear torsional springs may be difficult to manufacture without specialist equipment to a scale required for a building, it may be feasible to develop a non-linear spring that enables a recoverable and rotational hinge to form within a structure; initial thoughts on potential connections will be developed as below.

A rotationally sprung hinge within an axial or a flexural element needs to provide a single degree of freedom purely for rotation at a specific point within the element, but the hinge location will require to be coupled translationally to prevent any shear deformations across the hinge. A shear connection in a typical structural element could be provided using a single pin and this would provide a rotational degree of freedom in a single axis, but without the inclusion of a spring, this degree of freedom would remain completely free and uncontrolled. Development of initial models within the laboratory has shown that whilst a torsional spring is ideally what is required that linear springs if carefully positioned can develop a non-linear rotational spring as a hinge, see Figure 5-40.

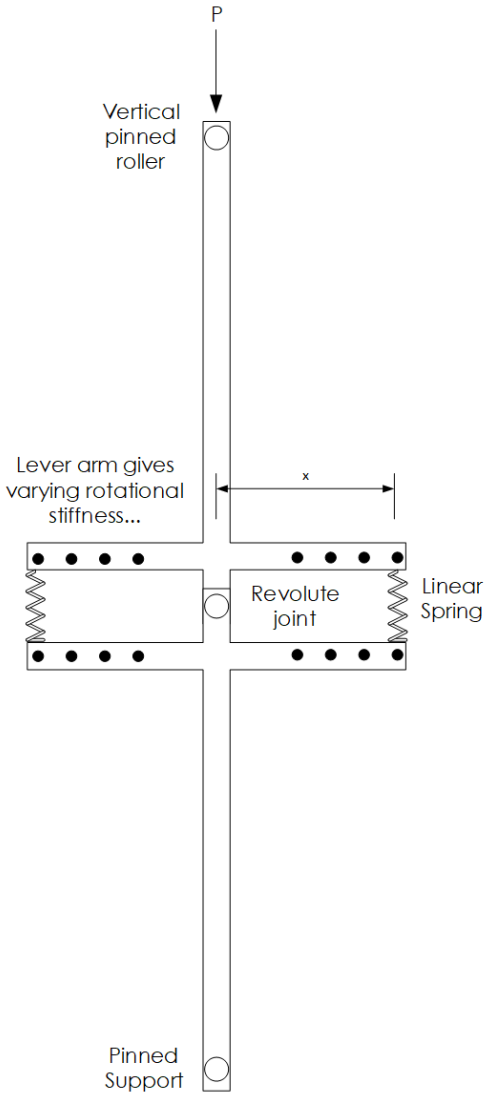


*Figure 5-40 - Initial Concept For Non-Linear Rotational Spring Formed From Linear Translational Springs.*

The initial concept was developed for a strut with a central pin, which makes use of linear translational springs offset from the centreline at various distances (x) to alter and adjust the rotational spring stiffness. Early prototypes were constructed using lengths of Unistrut but found to be difficult to balance due to small imperfections within the fabrication of the holes and subtle differences in the linear springs stiffnesses and initial lengths. No instrumented testing was undertaken from this initial physical model, although the concept could be developed further by integrating a similar connection into a Universal Beam section as seen in Figure 5-41.

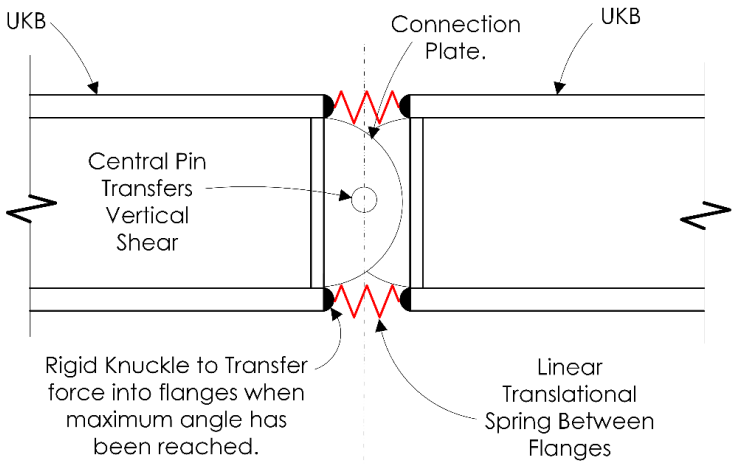


**(a) Neutral Position of Sprung Hinge.**

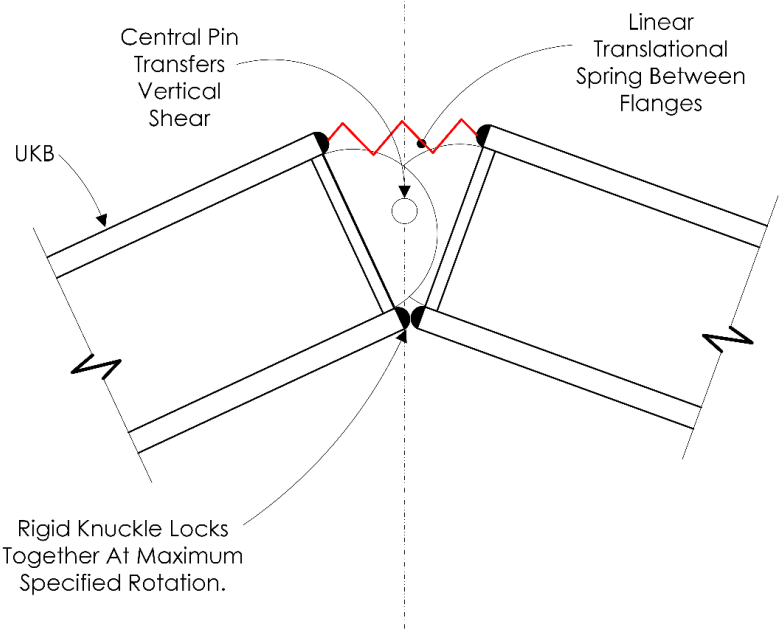


**(b) Locked Position of Sprung Hinge.**

*Figure 5-41 - Non-Linear Rotational Spring Formed in UKB With Linear Translational Springs.*

The above figure has additions compared to the initial cruciform, in that hardened steel 'knuckles' have been integrated that after specific angles will come into bearing and lock. For this to happen freely then it may be better to locate the springs clear of the knuckles to allow the springs to fold more cleanly.

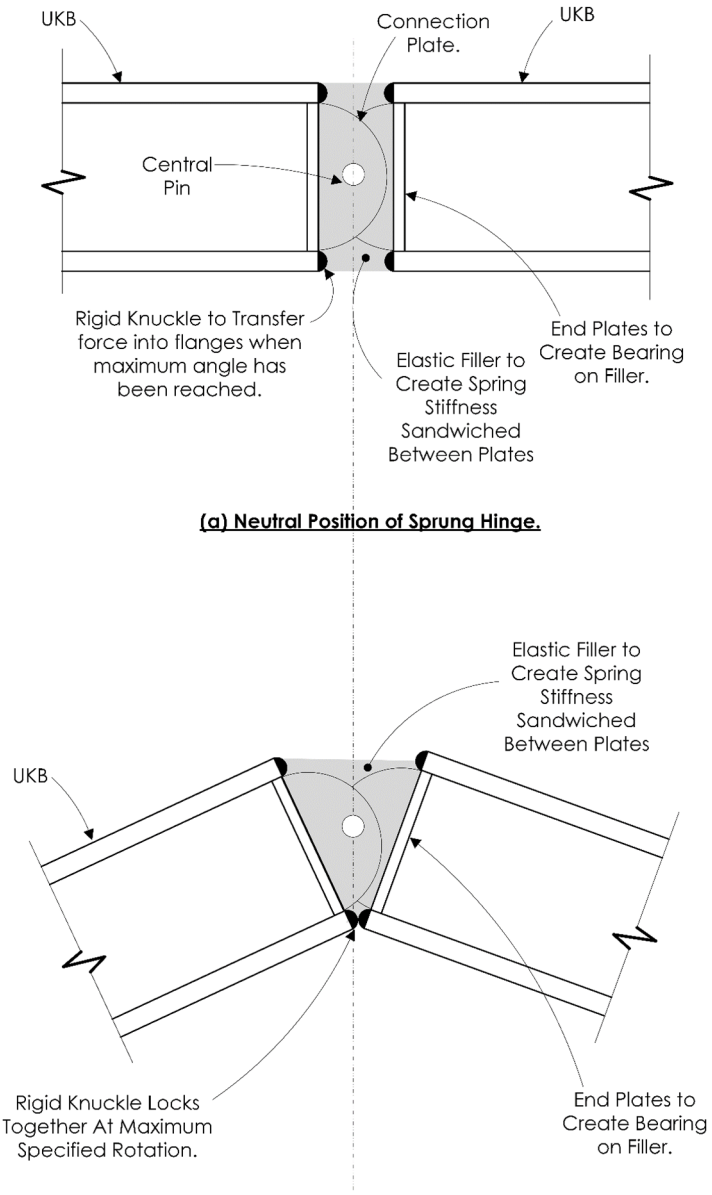


*Figure 5-42 - Alternative Hinge Formed in UKB.*

An alternative to using translational springs would be to replace them with a compressible form of polymer that compresses (or extends) between flat plates as shown in Figure 5-42 as the grey shaded area. This will require adequate bonding to the plates to prevent the material from peeling away from the plates under repeated cycling of the connection but could provide an interesting proposition for a hinged structure. The introduction of tailored springs, dampers, or polymers at hinge locations could potentially be used to increase the damping of structures in catastrophic events, but budgetary constraints and time have meant that the connections outlined in this sub-section are largely theoretical and physical testing is needed to prove the concept and

to determine in-service spring stiffness curves. This will need to be carried out as further work after the submission of this thesis but is anticipated that creating a non-linear spring for a structural use will likely be far more straightforward than creating a linear spring which emphasises the importance of being able to appropriately analyse non-linear springs.

## 5.11 Integration of Springs into a Frame.

To illustrate the behaviour of kinked struts to limit the axial force in struts, the behaviour of a theoretical braced bay will be considered. There may be benefits to limiting the axial forces within the braced bays, for example, to limit the shear across a single pin connection in the event of an accidental loading event to increase the structural robustness of the system thus reducing the associated risk with disproportionate collapse. This section will also demonstrate that whilst the axial force in the element may be restricted as a result of the spring buckling, a second mechanism is developed using the rotational spring which is through the introduction of bending at the location of the spring.

### 5.11.1 Single Hinged Strut Frame.

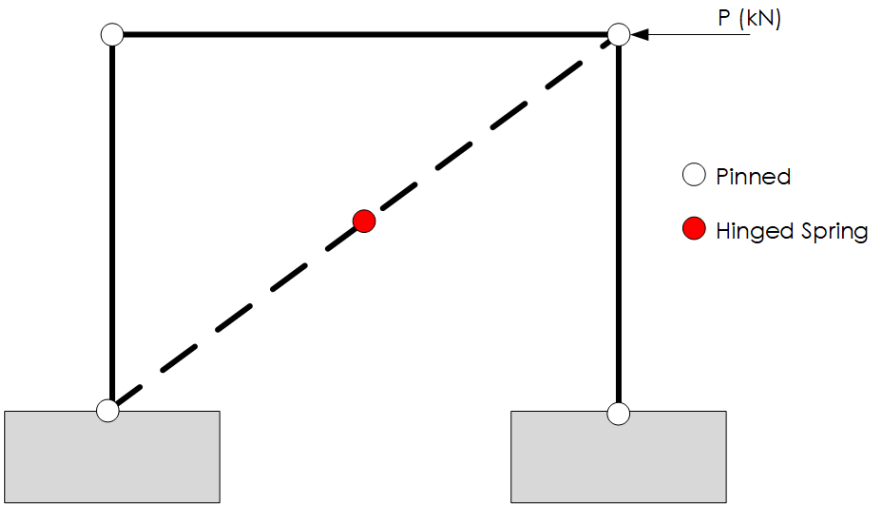


*Figure 5-43 - Proposed Frame Arrangement.*

Taking the frame as shown in Figure 5-43, with the height of 4m and width of 5m, a proposed lateral point load of 10kN gives a compressive force in the diagonal brace of 12.806kN based on simply resolving the applied lateral force. This can also be seen on a quick validation model as shown in Figure 5-44 (where the bracing has no central hinge).

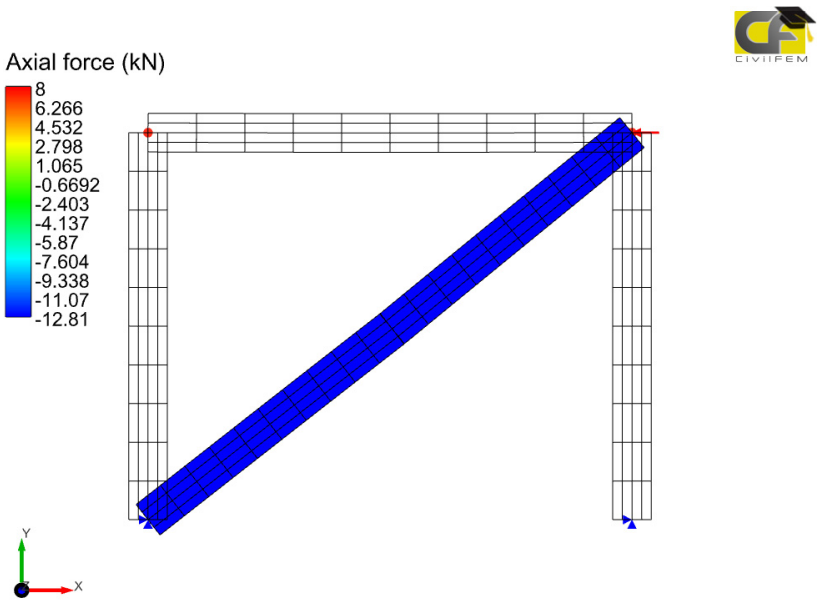


*Figure 5-44 - Axial Force in Bracing (Clipped Plot Range).*

However, say that for example on this frame there was a desire to limit the axial force in the bracing to approximately 6kN, a central uniform spring of stiffness of 10kNm/rad would achieve this based on the models and theory established earlier in this thesis.

The strut is 6.403m long and a central spring hinge of 10kNm/rad would give a critical buckling load of 6.4kN, however, allowing an initial imperfection of 5mm to account for tolerance and potential self-weight displacements would drop this buckling load below 6kN. The precise self-weight deflections have not been defined for this structure, instead, the material has been defined as a light and infinitely stiff material so to demonstrate the influence of introducing the hinge, but an initial displacement has been introduced to encourage buckling to occur.

Applying the 10kN force to the head of the frame will require an initial eccentricity introducing to the bracing to encourage a buckling failure mode within the bracing. In this instance, an initial buckling analysis was undertaken, and the first buckling mode has been applied to the structure as a mesh deformation with the maximum mesh deformation scaled to be 5mm. With a fine load step defined and large deflections enabled in the solver engine, the analysis solves in a well-conditioned manner despite the gross deformations.

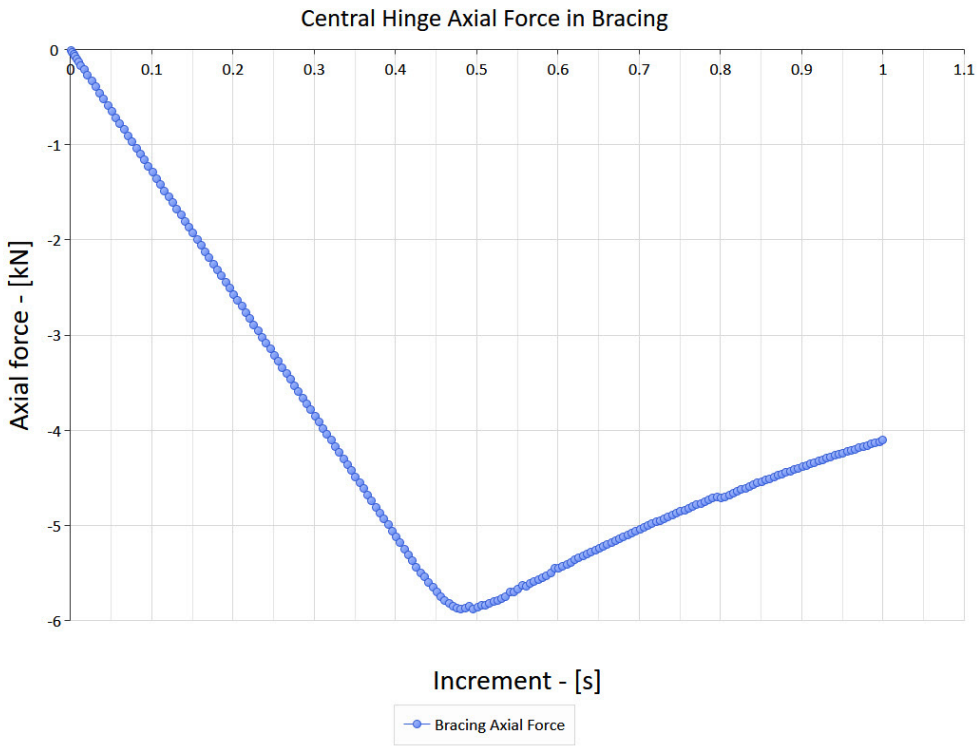


*Figure 5-45 - History Plot from CivilFEM showing Axial Force in Bracing.*

As can be seen clearly within Figure 5-45 the axial force in the bracing (and consequently the shear in the connection bolt assuming a single pin) has been restricted to 6kN, yet the structure has maintained a stable form and continues to resist the lateral load safely. The horizontal axis within the history plotting function in CivilFEM is slightly misleading as it is not time per se, but instead with fine increments and large deflections enabled, the non-linear geometric engine subdivides the load application incrementally into steps ranging from 0 to 1 in this instance. Therefore, at 1 second (on the horizontal graph axis) the load has been 100% applied.

Whilst limiting the axial force in the bracing would perhaps infer that more economical and leaner structures can be designed, it must be remembered that the structure has not failed and therefore whilst it has limited the axial force in the element, it has developed another behaviour to resist the applied lateral force whilst maintaining structural integrity.

The additional behaviour that has been generated is the associated bending moment at the central hinge, as the hinge rotates to limit the axial force, the moment in the connecting sections is developed creating a non-linear behaviour, see Figure 5-46. With the bending moment diagram at the final loading stage shown in Figure 5-47.

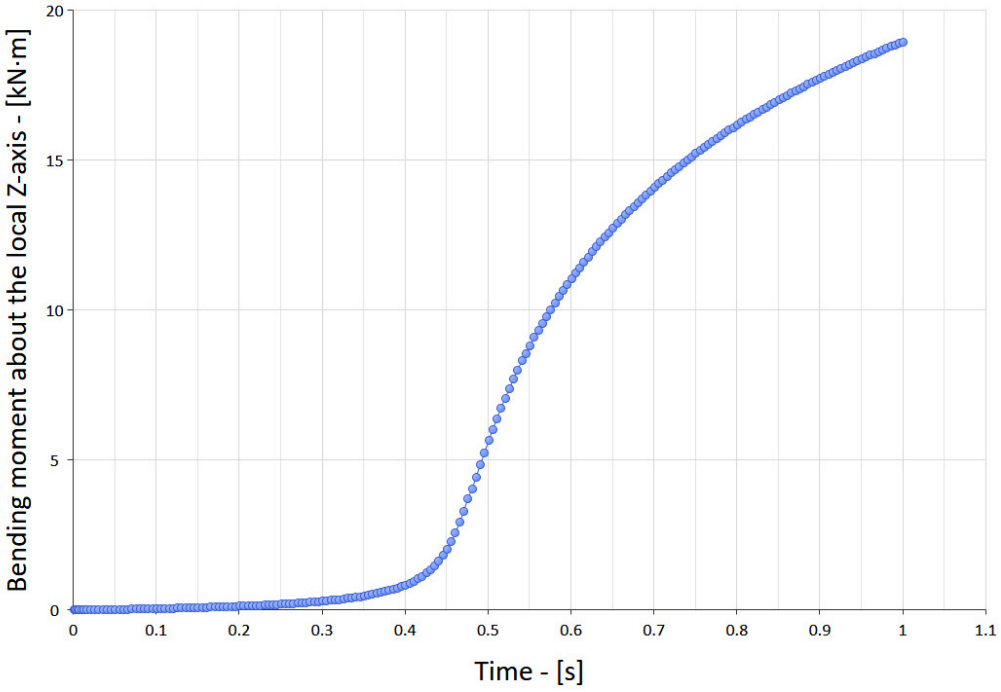


*Figure 5-46 - History Plot from CivilFEM showing Bending Moment Within the Bracing.*

From a material stress perspective for the structural element around the central hinge, the combination of the axial and bending stresses may require the increase in the size of the structural element to resist the combined effects of the axial and the bending moment.

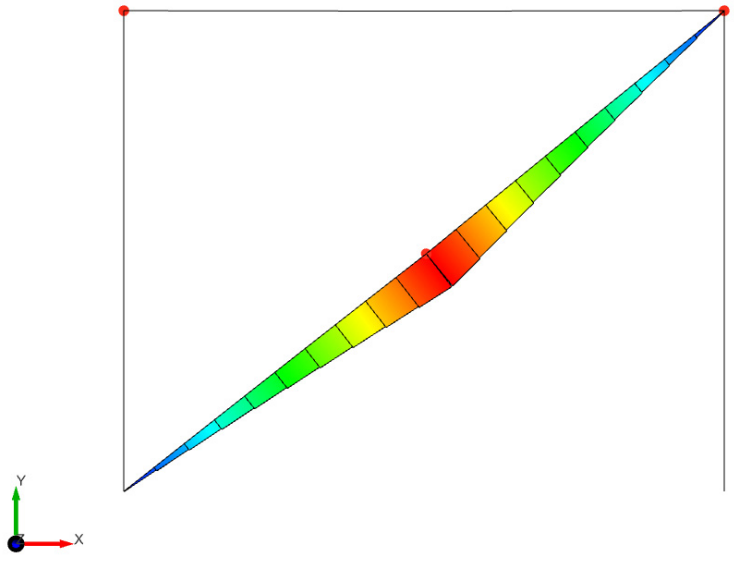


*Figure 5-47 - Bending Moment Diagram at Full Load (Shape only).*

The combined stress block is likely to lead to a bracing section that is wider at the central hinge location (sized for bending) and narrower at the pinned ends (sized for axial force). Such tapered sections are historically quite expensive to fabricate but with the development of increasingly more sophisticated and complex 3D printers, it is not inconceivable that these types of non-uniform structures will soon be printed rather than plate fabricated or cast, placing material only where it is needed at a molecular level with any waste powder being recycled.

4D printing is also becoming more commonplace, with the 4$^{th}$ dimension being time which allows a 3D printed structure to change its properties over time. This change in formation or composition as a result of a change in external parameters is useful when carefully designing structures so that they're able to demonstrate when they've been overloaded or mistreated acting as a form of tell-tale.

Indeed, initial models for 4D printed elements have been undertaken at the University of Salford. These structures are printed as static solid structural elements, but it is possible to fracture the supporting structure around mechanisms and hinges within the structure to drastically alter the permanent stiffness of the element through the application of specific loading regimes.

For example, the spring could be held in place by a lightweight scaffold which remains intact until the bracing load exceeds 6kN at which point the scaffold can fracture and mobilise the spring. This would make a visual inspection of the element to determine if the loads have been exceeded straightforward and aid things such as landlord and due diligence inspections. As a rotation would be generated at the central hinge sensors could be integrated. Either a circuit could be completed to signal an alarm (Figure 5-48a) or a logger could be attached to measure rotations/accelerations (Figure 5-48b) that could be uploaded via the 'Industrial Internet of Things' directly using low powered networks such as LORA or a local Wi-Fi.

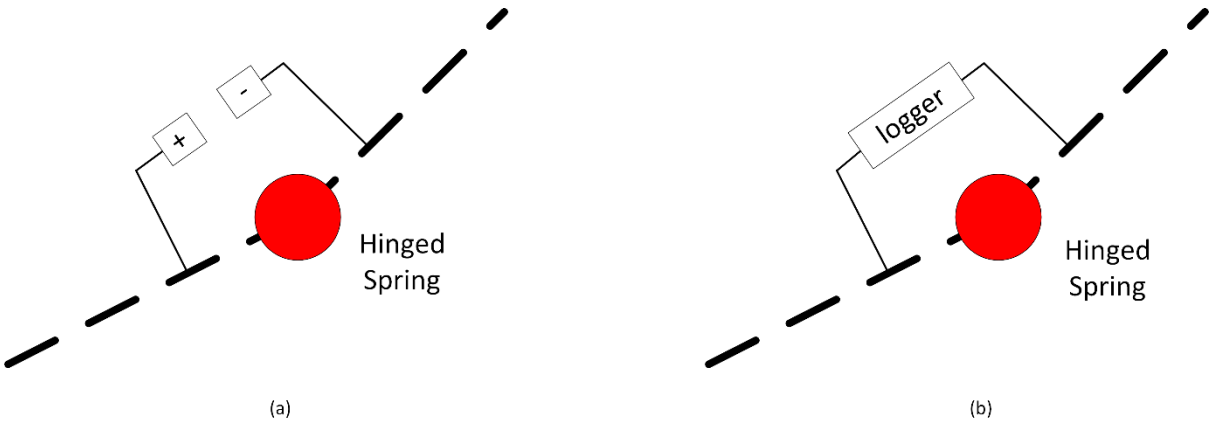


*Figure 5-48 - Intelligent Spring Configurations.*

At the University of Salford, prototypes have been successfully undertaken for 4D printed spherical ball joints and spring type structures, although formed in polymer to allow them to be printed as a single piece, ensuring a perfect fit and creating joints that would be impossible using traditional manufacturing techniques.

Similarly, small low powered devices are being developed integrating accelerometers with ADALoggers that can record vibration data up to 300Hz, these could be easily updated or adjusted to take specific measurements when a threshold has been exceeded. These devices are less than £50 to manufacture, and with the growth in the Maker Space and Industry 4.0 movement, the speed and cost of these types of devices will only make their use more widespread.

The final element of concern for this structure where the axial load is limited would be the lateral displacement at the eaves, as the structure becomes more dependent on the rotational stiffness of the hinge to control displacement it will behave more like a sway frame. As can be seen from the displaced form in Figure 5-49 with a relatively soft spring and under extreme loads the lateral deflections can be excessive although generally for life safety large deflections are acceptable whilst evacuating the building/structure, providing a truly catastrophic failure mechanism has not been mobilised.

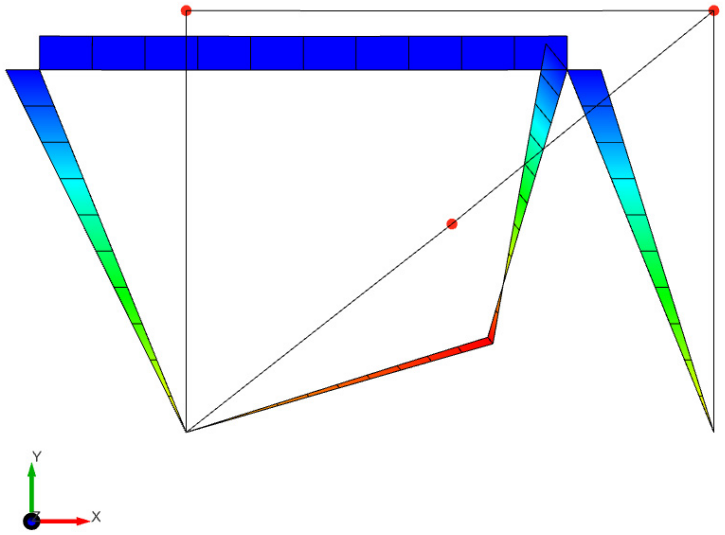


*Figure 5-49 - Deflected Form After Full Lateral Load Applied (Half Scale).*

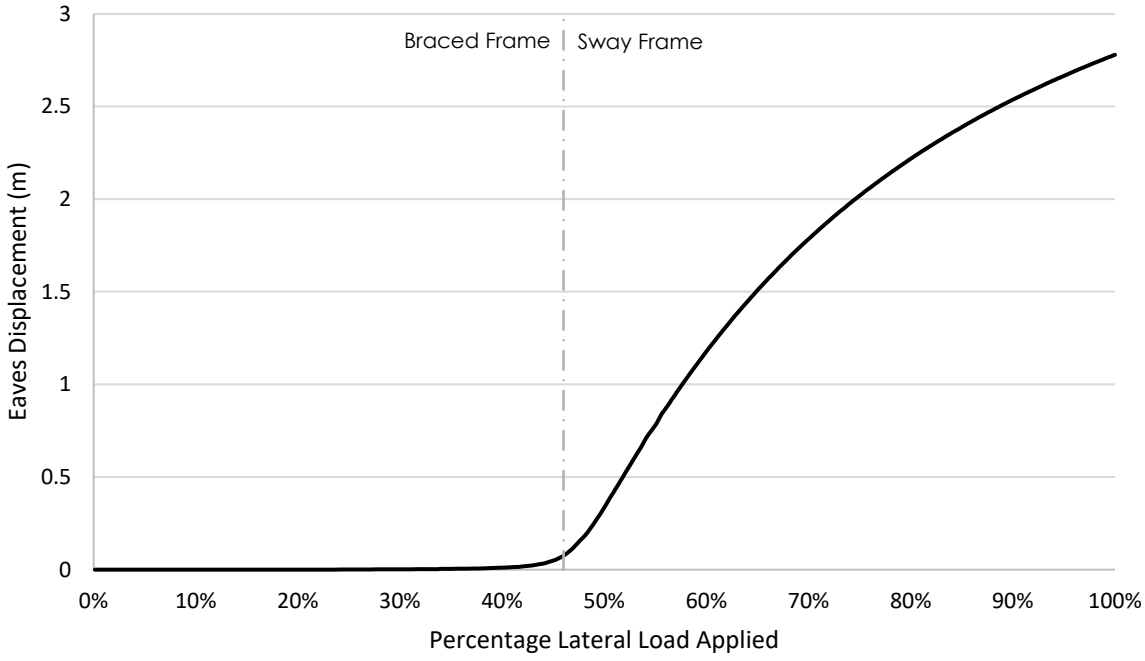


*Figure 5-50 – Eaves Deflection as Lateral Load is Developed to Full Lateral Force.*

When considering the lateral deflection, there is a transition between behaviours as the lateral deflection increases significantly once the strut has buckled which illustrates the change in

behaviour between a braced frame and a sway frame, see Figure 5-50.

Clearly for the rotational spring to generate resistance there needs to be a lateral movement at the eaves to create a corresponding change in angle at the central spring which in turn creates a rotational moment of resistance.

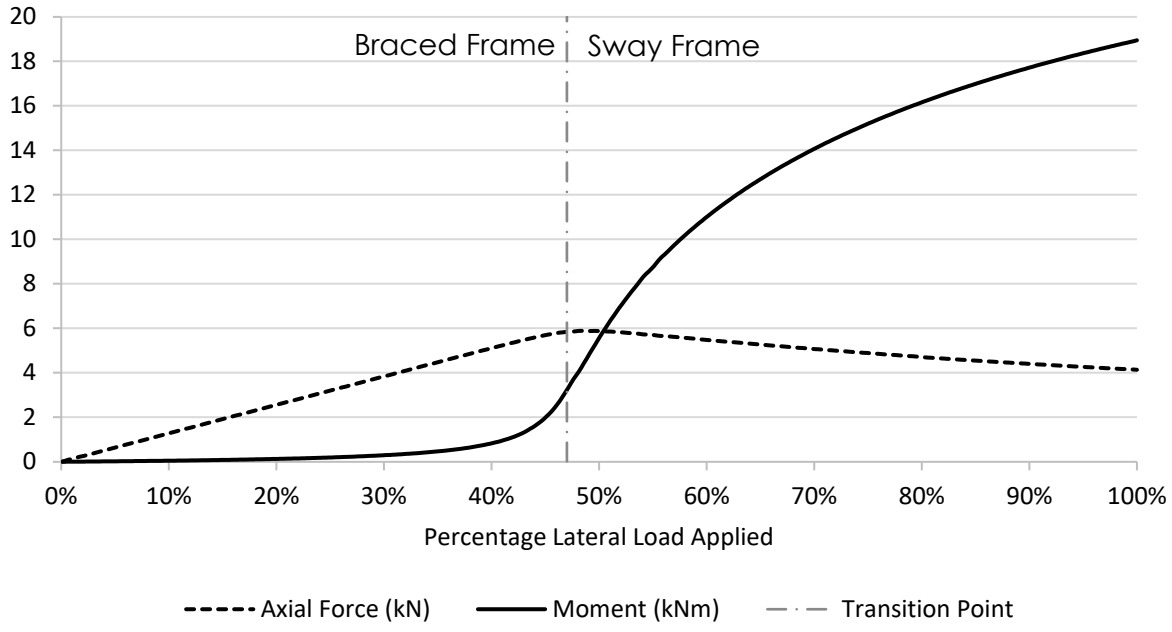


*Figure 5-51 - Moment vs Axial Force in the Bracing.*

This relationship is illustrated clearly in Figure 5-51 where the moment can be seen to be starting to develop just ahead of the bracing reaching its critical buckling load at which point the axial force starts to diminish as the moment grows. The two elements do not perfectly align in this example due to the nominal eccentricity applied to the system as part of the non-linear analysis.

### 5.11.2 Twin Hinged Strut Frame.

Introducing one more spring into the compression bracing should allow the frame to be tuned more subtly (see Figure 5-52) with regards the shape that the compression bracing will make post-buckling. With more springs the spring stiffnesses will need to be adjusted to approach the limiting axial force of 6kN and for speed, the finite difference Mathematica notebook has been used to aid with the preliminary sizing of the springs, giving a spring stiffness of 13kNm/rad although an iterative approach could also have been taken using CivilFEM.

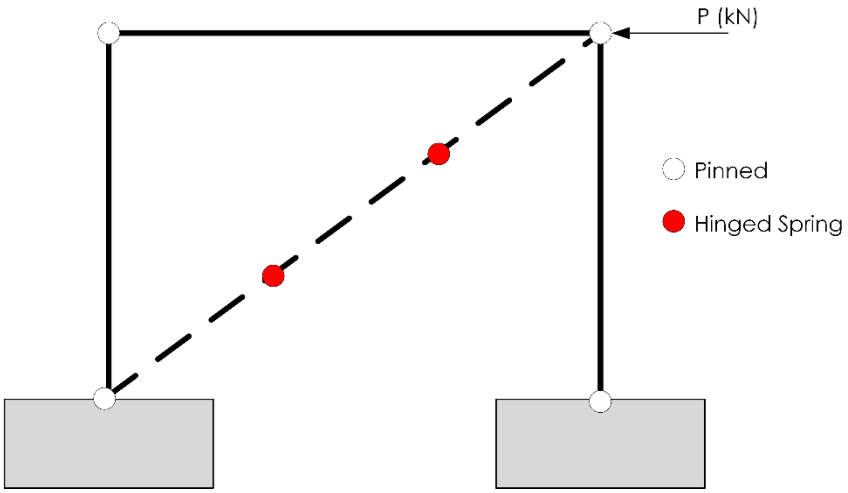


*Figure 5-52 - Twin Sprung Strut-Braced Bay.*

Integrating the pair of springs into a non-linear analysis with a fine load step shows that the lateral displacement under a 10kN is only marginally reduced, from 2.623m to 2.771m, given the extreme displacements being mobilised this is as a result of the slight differences in the buckling loads for the springs (Single 5.884kN vs Twin 5.949kN). However, the deflected forms are largely similar, see Figure 5-53.

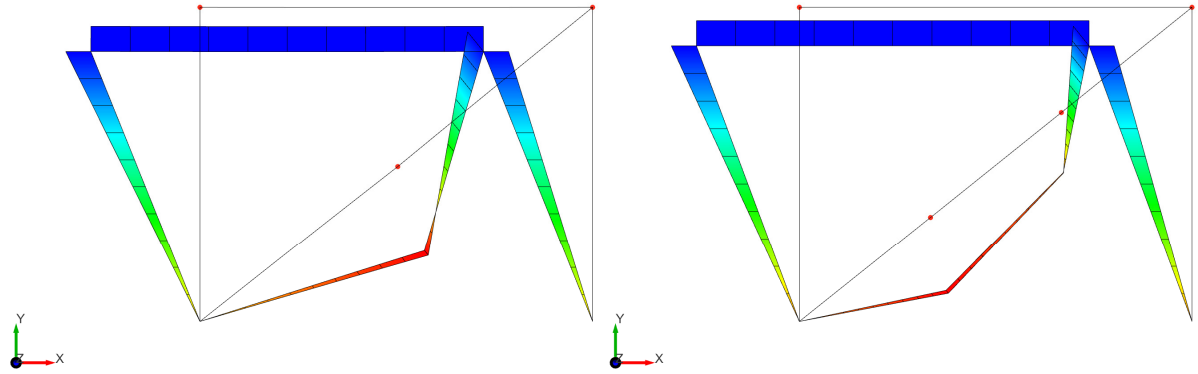

*Figure 5-53 - Deflected Forms of Single vs Double Sprung Struts (Half Scale X-Axis Deformation).*

Whilst a single spring strut will limit the axial forces to the designed force, once more than a single spring is introduced, only the outer elements will be limited to the desired axial force with the central portion increasing due to the geometry (see Figure 5-54). Essentially, the central portion of the sprung strut will start to increase its axial force as the deformations become increasingly gross as a result of the relative angle between the top and middle strut decreasing (see Figure 5-55).

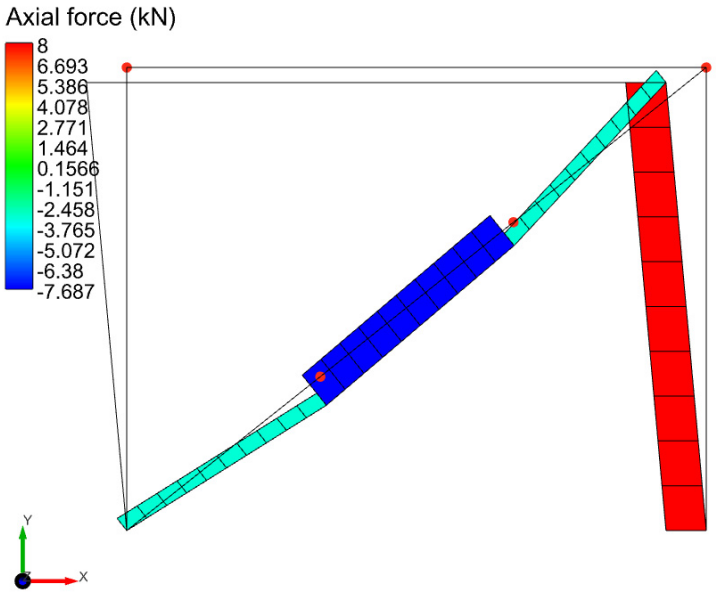


*Figure 5-54 - Axial Force in a Twin Spring Frame.*

Essentially as more springs are introduced the strut will begin to resemble a continuous strut with a stiffness proportionate to the rotational stiffness of the springs. With enough springs in the system, the curvature will smooth and the force in the strut will resemble a more traditional bracing strut.

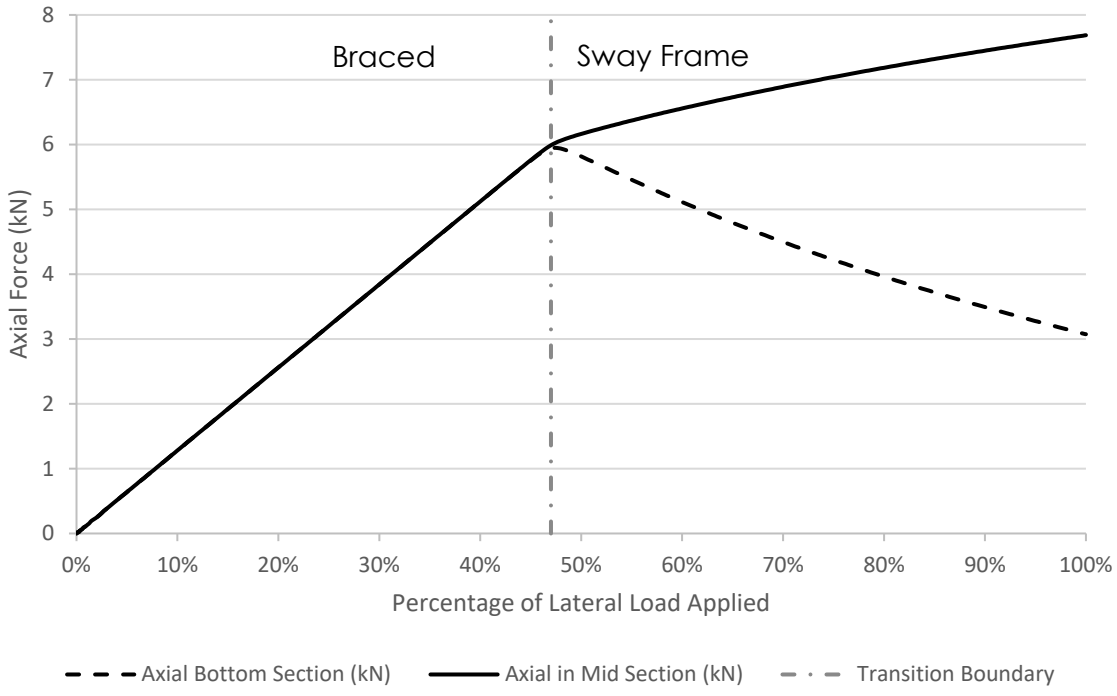


*Figure 5-55 - Axial Force in Bottom and Middle Section of Bracing.*

Whilst the axial force in the central portion of the bracing has increased compared to a single spring strut, it is still considerably lower than the 12.8kN of an ordinary braced section showing that the axial forces can still be manipulated within other sections of the kinked strut.

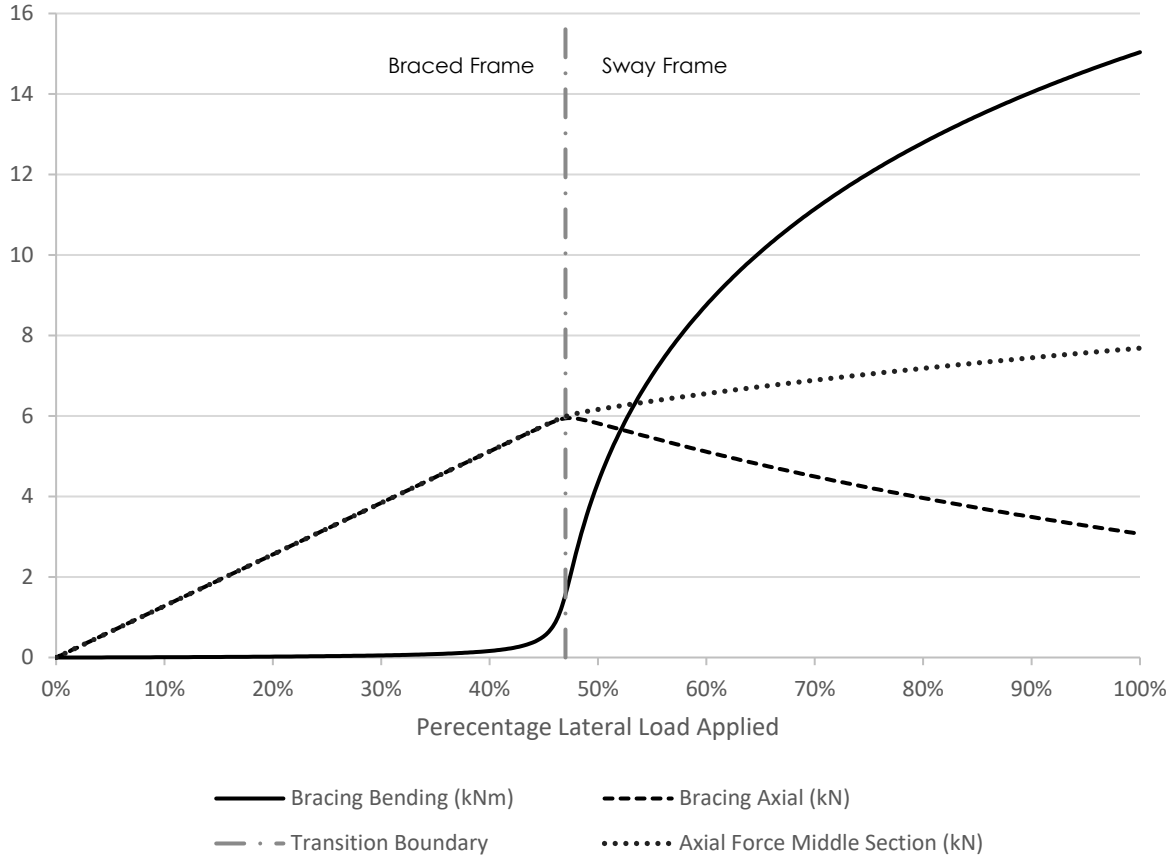


*Figure 5-56 - Forces Within the Bracing Elements.*

Whilst the axial load in the central section has increased compared to the single sprung strut, the associated moment has decreased (see Figure 5-56) which may lead to a reduction in resultant stresses given that design sections to resist bending generally creates larger elements than those designed to resist axial forces alone.

### 5.11.3 Higher Mode Twin Sprung Struts.

Both the single spring and the twin spring bracing struts have a common issue in that the bracing makes contact with the floor after gross lateral displacements have taken place, surprisingly even though the lateral movement of the bracing element is smaller for the two-hinge strut, it fouls the ground earlier than the single spring strut due to the distance between the floor and the spring being smaller.

There are many ways that the deflection can be limited: either by limiting the applied load,

increasing the axial limit that bracing works to by increasing the spring stiffness, adding additional nominal stiffness to the pinned hinges within the frame, or introducing a non-linear hinge that stiffens at a certain point.

Another method to overcome the bracing fouling the ground is an alternative configuration for the springs in the two-spring bracing element which will be investigated in this section. With the springs adjusted to take advantage of the 2nd mode of buckling form from the buckling analysis, see Figure 5-57. By forcing the two-spring bracing to develop a higher buckling mode the deformations could be adjusted to stay within the bays envelope using the principles set out in section 4.7.

Previously the struts have been allowed to buckle into their primary buckling mode shape, but as outlined in section 4.7 it is possible to engage higher buckling modes through the locking of springs or careful application of eccentricities.

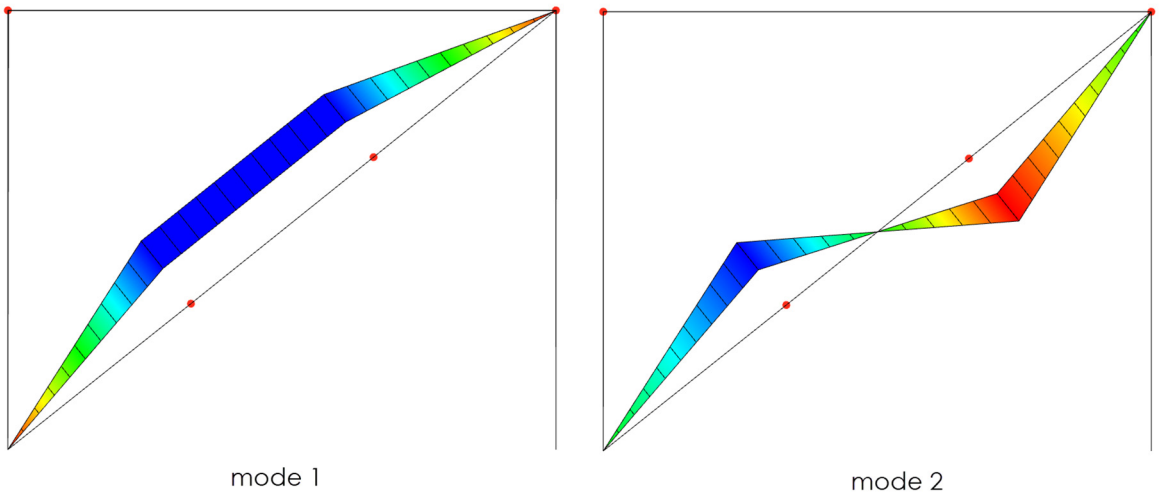


*Figure 5-57 - Twin Hinged Bay First Two Buckling Modes.*

It is proposed that through the introduction of deformed meshes that the second mode of buckling (see Figure 5-57) can be encouraged and that this can be used to encourage the frame to adopt a specific shape when it begins to mobilise the sway frame behaviour.

Whilst deforming a strut behaves well in the previous models, this is not the case when the strut is contained within a braced bay. There is a propensity for all the nodes in the frame to receive an amplified deformation when the mesh is deformed and when lateral forces are applied these small eccentricities encourage the upper spring to displace downwards, creating a straightening effect on the overall frame, resulting in the braced bay behaving as mode 1 as the geometry straightens.

Even with large (500mm) amplifications the structure eventually adopts the default twin spring failure mechanism. This is due to the small subtle differences in the displaced forms, with the displacements at the eaves also being integrated via mesh deformations. As the eaves displace laterally under loads, the upper spring rotates, and the corresponding node displaces downwards. This change in angle between the upper and middle bracing strut pushes the lower spring downwards too, creating a straightening effect which subsequently unfolds the bracing, drawing it back into the original mode 1 form, see Figure 5-58.

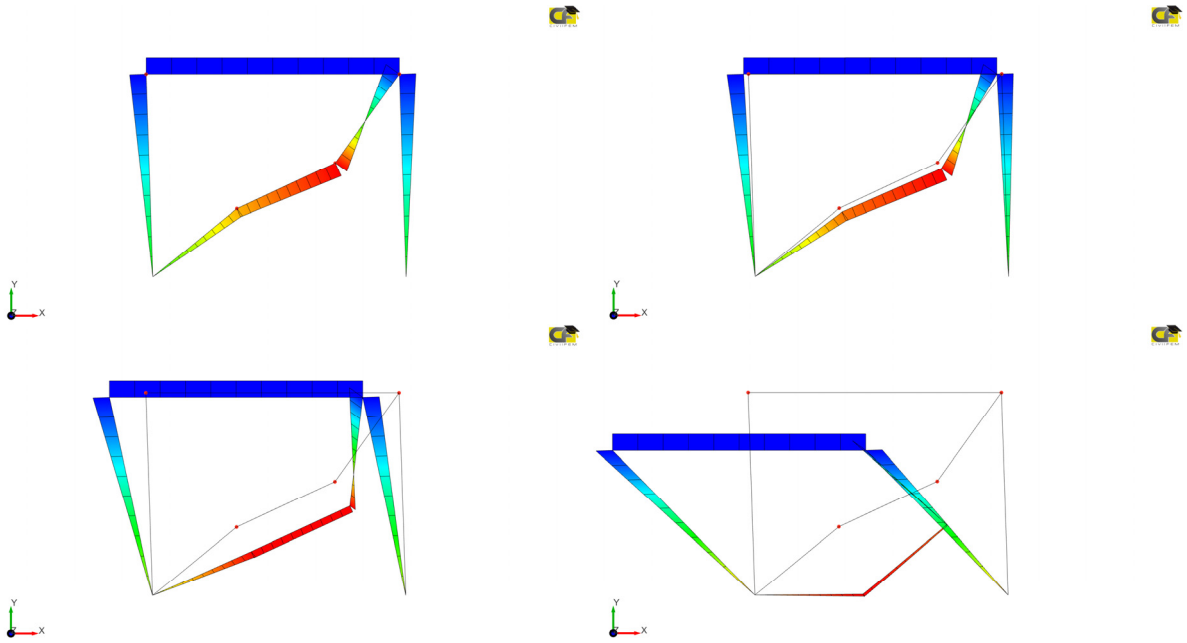

*Figure 5-58 - Braced Frame Deflections with 500mm Initial Deformation and 10kN Lateral Load.*

Through introducing deformations only to the bracing (modifying the spring coordinates manually before meshing) the higher second mode can be induced although this requires the spring stiffnesses to be considerably reduced as a function of the structure adopting the second mode of buckling load (with its increased buckling load compared to mode 1) to stay close to the 6kN axial force limit (6.1kN in reality).

Whilst the bracing now stays contained within the braced bay whilst under gross deformations and no longer fouls the ground, there is an unexpected mechanism that develops. Effectively the central portion of bracing 'flips' and develops tension, allowing the bracing to relatively shorten its overall length to stay contained within the braced bay (see Figure 5-59).

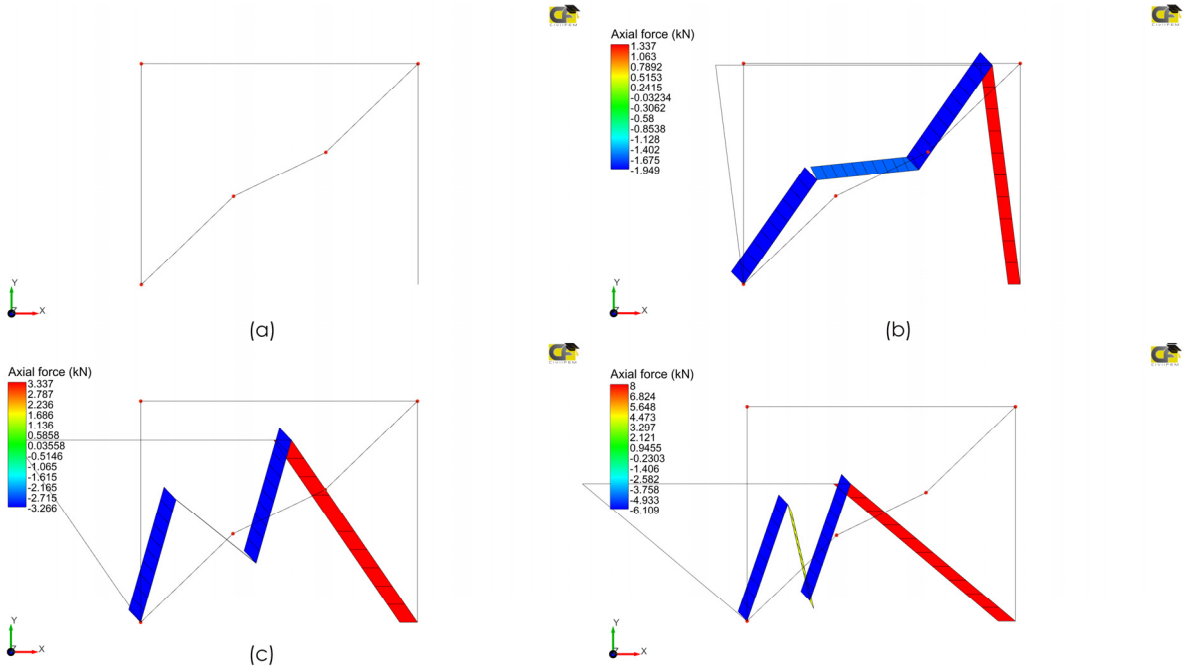


*Figure 5-59 - 2kNm/rad Springs with Mode 2.*

This provides an interesting development where the bracing adopts an additional third transition, starting as a compression-based braced element, then buckling and creating a sway type of behaviour where the bracing is driven by the rotational stiffness of the springs until the deformations become so gross that the central portion flips and becomes a tension element.

The ability to transition between more than two distinct states has typically required the use of non-linear springs, but it is clear from this example that with some careful geometrical manipulation that elements can be forced to change their geometrical alignment so extremely that they can also change their structural behaviour.

As the spring and the materials have not yielded, all the deformations applied are fully elastic and once the load has been removed the structure should in theory fully restore. Although in practice the restoring load case will need to be verified to ensure that there is adequate restoring spring stiffness to return the frame into its starting position as the mass may have displaced over the centre of stiffness.

This is like the pantographic arches, where the initial part of the deployment sequence is a lifting operation as the mass of the frame is lifted from the stowed positions, however as the structure extends the centre of mass also relocates until a critical point where the deployment is no longer a lifting motion, but rather a lowering motion as the end support is lowered into place.

### 5.11.4 Non-Linear Hinged Frame.

Whilst the structure in section 5.11.1 managed to successfully limit the axial force within the bracing, it is noticeable that once the buckling force has been achieved then the axial force in the bracing element drops to approximately 4kN post-buckling, see Figure 5-45.

However, it is proposed that a non-linear spring could be developed that still limited the axial force to be less than 6kN, but with its post-buckled behaviour being modified through a non-linear stiffness to hold a higher axial load post-buckling.

Figure 5-60 shows that even a subtle adjustment to a spring stiffness to gradually increase the stiffness of the spring (taking care to do so at a rotation angle that is clearly post-buckled) can be used to balance the axial force in the bracing member.

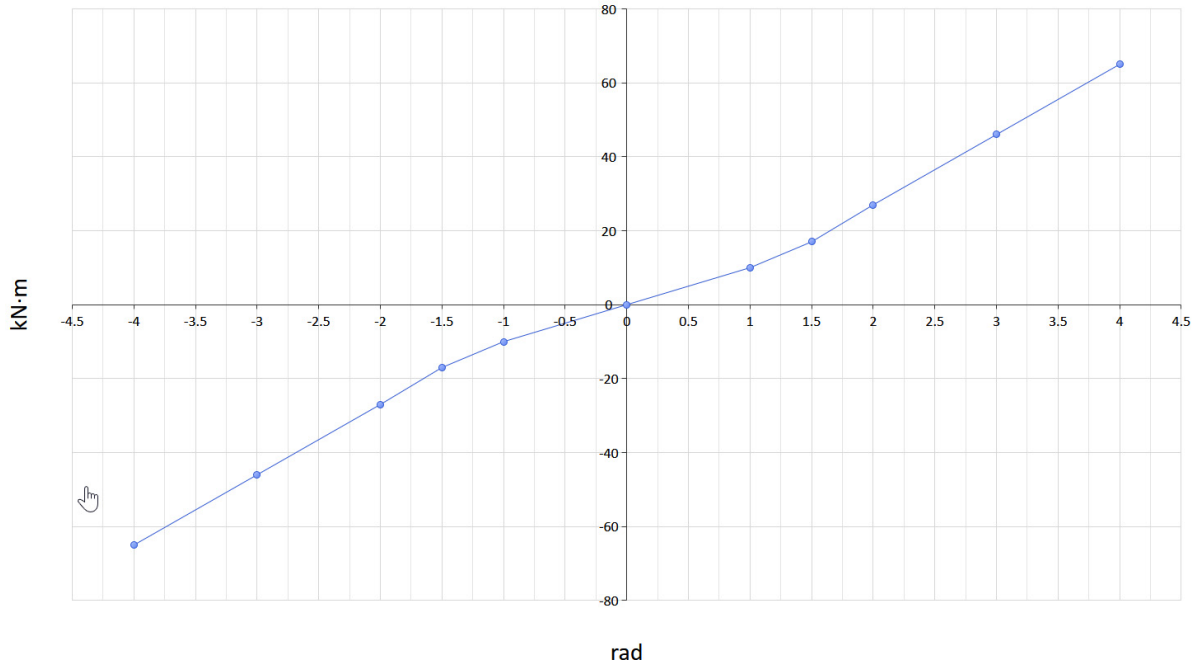


*Figure 5-60 - Non-Linear Spring Stiffness Defined For Bracing.*

Figure 5-61 shows a comparison between the linear and the non-linear spring, both displayed as history plots from CivilFEM with no post-processing. By subtly adjusting the spring stiffness it is possible to develop a strut which holds much closer to the buckling load.

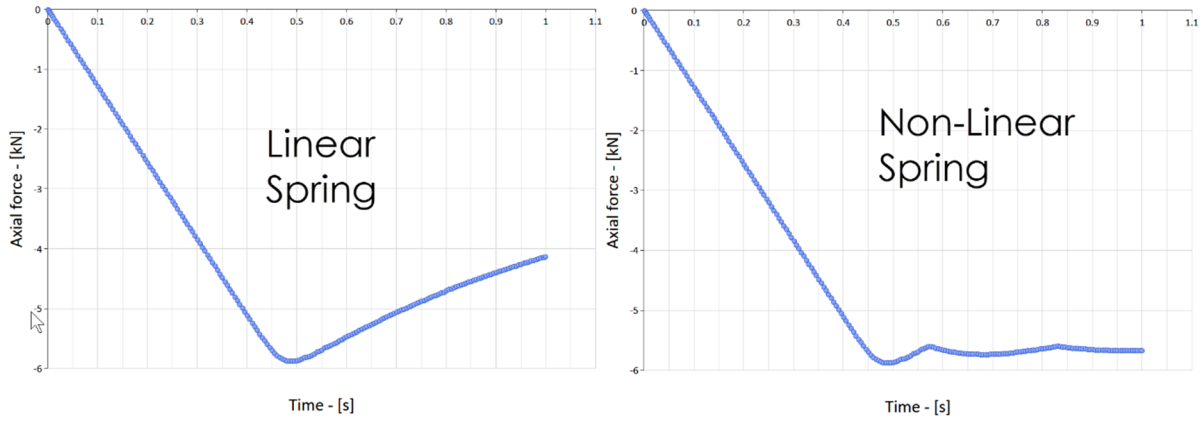


*Figure 5-61 - History Plots From CivilFEM Showing Axial Force In Bracing Struts.*

A strut that can balance the vertical reaction regardless of the amount of axial load applied would be useful in a structure integrated into a process such as a printing press for example where a constant pressure needs to be applied and controlled. Whilst passive control could be developed with a finely tuned spring, the ability to vary and adjust a spring stiffness to maintain a constant reaction on the fly is an interesting proposition and in theory could be developed through the application of a brake drum, although this would naturally attract additional maintenance costs to replace the pads as they wear.

## 5.12 Summary.

This chapter has looked at the challenges with introducing rotational springs linked in a chain to form an arched structure similar in many ways to the buckled form of the struts considered in Chapter 4.

One of the challenges with linking numerous springs within a large structure is finding a form where the structure is in equilibrium from the springs before applying any additional loads. This is similar in many ways to the form-finding approach adopted in the analysis of tensile fabric structures despite there being a significant difference in stiffnesses between the two types of structures.

Wolfram System-Modeler was considered initially for the development of a stable geometrical form given the inbuilt multi-physics engine provided by the Modelica libraries. However, whilst the form-finding capabilities were strong and energy was dissipated efficiently in the initial models, the structural analysis capabilities were weak and this approach was subsequently abandoned.

A single environment that could share the form-finding and the structural analysis modelling

would present benefits in terms of consistency of modelling environment and a considered approach using CivilFEM has been established based upon the methods developed within chapter 4.

While a stable equilibrium form is important to establish before applying the loads, the final form once loads have been applied equally needs to settle into a balanced equilibrium position otherwise the structure may collapse if an inappropriate spring stiffness or element stiffness is selected. This is a key consideration when maintaining the stability of the arches.

A comparison was undertaken looking at the relatively simple process of form-finding the geometry for a flexible arch comprised from a single homogenous rod that is forced into a buckled shape through forced displacement compared to a model containing 18 springs linked in a chain to create a similar arched shape.

Whilst the solution of a homogenous rod was relatively trivial and solved quickly, the large number of degrees of freedom present in the sprung model required numerous attempts before suitable stiffnesses and deformities could be integrated into the model to remove issues associated with ill-conditioning.

Considering the difficulties that the models in previous chapters had determining the buckled form and loads associated with a single degree of freedom, the matured approach developed in Chapter 4 has coped well with a large number of degrees of freedom, and whilst the model was computationally demanding, it was solved, demonstrating that the method is generally robust when appropriate stiffnesses have been selected.

The ability to form long chains of sprung struts is interesting as an alternative to more traditional compliant mechanisms where typically a flexible single element has been used. The introduction of the springs facilitates the packability of the struts into shipping containers or even for them to be delivered to a construction site in sections.

Having rigid and robust linear sections between the springs also increases the overall usefulness of the structure and prevents degradation and attack from the elements (such as wind-borne debris that can puncture flexible materials) and vandalism in comparison to thinner more flexible alternatives which can be vulnerable to puncture attacks.

Whilst the modelling process outlined performed well, the increased number of degrees of freedom was challenging and ill-conditioning of the structure during the large scale forced displacements was an issue. Fortunately, the techniques and observations of Chapter 4 helped to

define an appropriate eccentricity and Youngs Modulus to help the arch settle into a balanced form. Without the development of the understanding of the sorts of ill-conditioning issues associated with these chains from the previous chapter, the creation of such a flexible structure would have been problematic.

The distribution of different linear springs along the chain was briefly discussed to demonstrate that flexible arches formed of different geometries could be developed that resemble more traditional forms of structures such as portal frames. Indeed, the springs could be linked with differing segment forms too, perhaps to resemble a traditional haunch.

Symmetrical structures are more common generally in the built environment to aid with the repeatability for design and construction purposes, this does not have to be the case and asymmetrical structures can be created through the uneven distribution of spring stiffnesses or the uneven distribution of segment lengths.

The linear spring structures considered have demonstrated that the structure can move from a stable rigid form and once buckled can adopt another form (section 5.9) which is an interesting proposition, as typically, engineers design their structures to be of a single form and to not transition into alternate configurations.

There are endless varieties of non-linear springs which can be tailored to suit the desired behaviour, some such as the binary stiffness springs allow free movement until an angle has been subtended and then create an infinite stiffness through being locked. These types of connections are used widely in thick origami and are akin to a door hinge in their structural behaviour.

The springs, however, do not have to be symmetrical and may have different behaviours for either a positive or negative angle of rotation, this may help define different structural responses for different loadings. For example, a stronger wind force moving in from the sea may be dominant and require a stiffer response to a subtler wind in the opposite direction coming in from the land.

One of the inspirations for this research was the cable-stiffened elastica for movable structures of Beatini and Royer-Carfagni (2013). Beatini's work looks at using voussoirs of different curvatures and tendon profiles to create articulation at specific points and the 'springiness' of these connections is something that the author has found interesting. A study of the geometrical arrangement of a pair of round voussoirs was developed in section 5.8.4 that has shown that theoretical spring property curves could be generated ready for use in CivilFEM as an exercise to illustrate that complex spring configurations can be developed analytically.

Concept designs for physical non-linear rotational springs were presented that broadly feel feasible, with the vertical shear transferred through the single pin that also facilitates rotation. Although physical testing and development of the connections is still required to determine not only their absolute behaviour but to validate their durability and long-term performance.

A singly braced frame was modelled in section 5.11 which highlighted a key behaviour of structures with springs inserted within them. Essentially once a strut with a spring has buckled its continued ability to support axial loads is developed through the rotation of the spring and this, in turn, generates an associated bending moment around the spring. This additional moment is important when considering the design of the bracing element as typically elements require more material to resist flexural forces compared to axial forces.

Equally, the initial position setting of the springs was shown to be important when integrating several springs within a framed element. In the example considered it was shown that if the bracing element was not controlled it would deflect and clash with the ground, but, if a higher modal pattern was encouraged through the pre-setting of the geometry then the bracing could fold neatly without fouling the ground. This principle could be further expanded to encourage deployable structures to create repeatable and compact folding forms when using springs.

It was also shown that through the introduction of non-linear springs into a strut it was possible not only control the axial force at the end of the strut at the point of buckling but to then continue to hold this end reaction as a constant force through the post-buckling deformed stage.

Some of the benefits identified by the inclusion of springs and spring like behaviour will be examined in more detail in the next chapter, where the application of kinked structures and rotational springs will be applied to high-level conceptual structures to demonstrate in more detail the benefits that they may bring.

# Chapter 6

# 6 Novel Applications.

## 6.1 Introduction.

This penultimate section of this thesis will apply a selection of the analytical methods established within this research to two distinct scenarios. Each scenario has been selected specifically to demonstrate how the analysis techniques developed for CivilFEM could be combined and applied.

However, it is important to re-iterate that the primary aim of this thesis was to develop an appropriate method for the analysis and modelling of structures (static and deployable) with integral rotational springs with regards to their structural behaviour, performance, and ability to adapt the structure and not to establish a working prototype or a design that could be immediately implemented.

The development of a design to a level of detail equivalent to RIBA Stage 4 or 5 would require considerable further design, development, and testing of a prototype rotational spring for the magnitudes of forces typical for a building which would be a substantial independent area of research within itself. However some initial thoughts regarding how the development of such a connection could be started as a high level concept is outlined in section 5.10. Equally, the development of such a bespoke connection would require the detailing and the analysis process to be an iterative process after each prototype as the designs mature.

The two examples presented in this chapter draw upon the metamorphic properties that the introduction of springs to a structure can facilitate the geometrical changes needed to develop a load relieving form or provide control of during deployment of a deployable structure.

The control of structures such as these is not commonplace within construction currently and an emerging field of design research, primarily due to the limitations associated with the magnitude

of the forces involved and the difficulty in manufacturing the springs at this scale.

## 6.2 Metamorphic Arches.

The proposed analytical case study within this section will make use of the principles set out earlier in the thesis to facilitate the gross displacements of an arch that behaves as a metamorphic structure. The case study will integrate rotational springs that enable the arch to change shape under anticipated wind loadings to a form which is generally more aerodynamic along the windward edge. The wind loadings have been defined using the current Eurocode code of practice and applied as a static load case to demonstrate that, in principle, the analysis methods established thus far in the thesis are capable of appropriately modelling gross displacements with integral rotational springs and that the inclusion of springs can enable gross displacements without suffering the effects of snap-through. Determining the stiffnesses of the springs for an arch needs to be established using an iterative process as it is highly dependent on the form of the arch, number of segments, the anticipated loading conditions, and the required deformed geometry. The stiffnesses for the arch considered within this chapter were adjusted iteratively until a flatter, more aerodynamic, profile was established along the windward edge.

The example considered within this section combines several concepts that have been established through the work thus far and combines them into a single example. These concepts include establishing a simple analysis model of a structure that can adapt to the external force system (section 2.10 - Adaptive Structures.) without suffering the effects of snap-through (section 3.10.2 - Snap-Through Behaviour.). This process includes the principles used to model the behaviour of sprung arches (section 5.2 - Symmetrical Sprung Arches.) by integrating the modelling process in CivilFEM as defined in section 5.7 (Arches With Different Spring Stiffnesses.) in order to establish the structural form and assess the post-buckling behaviour.

Through integrating different spring stiffnesses at each hinge location a tailored, more aerodynamic, deflected shape will be formed under an applied wind loading. Finally, the arch will be re-modelled with glue-laminated beam elements connected with sprung hinges based on the principles shown in section 5.10 (Physical Springs.) to give an example of scale.

The introduction of a spring within a structure provides the ability for the structure to significantly alter its shape or structural behaviour as a result of an external load whilst maintaining structural integrity. Large deflections in cable-chain arches were shown to be detrimental due to snap-through effects and a method to mitigate this in a lightweight arch form was to introduce rotational springs at the pin positions and for the cables to be removed which

will result in a structure that can grossly deflect whilst maintaining stability under loading. It is proposed that by carefully controlling the position and stiffness of these springs the resulting form can be controlled to change shape predictably under specific loadings.

For an arch, this behaviour could be utilised to make the shape of the arch more aerodynamic and consequently reduce the amount of load that the structure attracts. Similar concepts of softening structures with hinges or springs have been shown by Tibbits (2014) to enable structures to change their shape in specific environmental conditions, typically, being immersed in water but passive adaptable behaviour under loading should equally be feasible. The ability for a structure to change shape in response to an applied loading (either passively or actively) to become more aerodynamic and then to return to its neutral position once that loading is removed may be helpful for certain forms of structure such as agricultural poly-tunnels which are by nature lightweight and not subject to the same strict deflection criteria of other forms of structure.

This principle of adapting curved surfaces to adjust airflow is well understood in aircraft wing design (Wagg, Bond, Weaver, & Friswell, 2007, pp116) where the airflow over wings is intentionally altered through the manipulation of the internal struts on belt ribs changing the profile shape of the wing, see Figure 6-1.

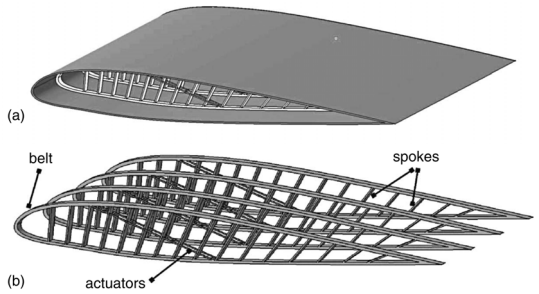


*Figure 6-1 - Cross Section of Belt Ribs with Actuators.*[73]

If the top surface of the wing was represented by an arch formed of springs this could be controlled with an active system, such as the actuators shown in Figure 6-1, or with the careful selection of rotational spring stiffnesses perhaps the profile could be designed to adapt its shape passively.

[73] Wagg, D., Bond, I., Weaver, P., & Friswell, M. (2007). *Adaptive Structures Engineering Applications*. Chichester: Wiley.

The precise profile and shape of an arch will determine the loading regime for a crosswind. Generally the windward edge is a positive pressure, with the leeward face developing a negative pressure (see Figure 6-2), and the top of the arch under suction (negative) pressure. Each of these pressures will be applied normal to the arch surface and create a pressure distribution as shown in Figure 6-2. Frequently, the skin friction component is ignored for the lateral case with the pressures normal to the surface governing the design.

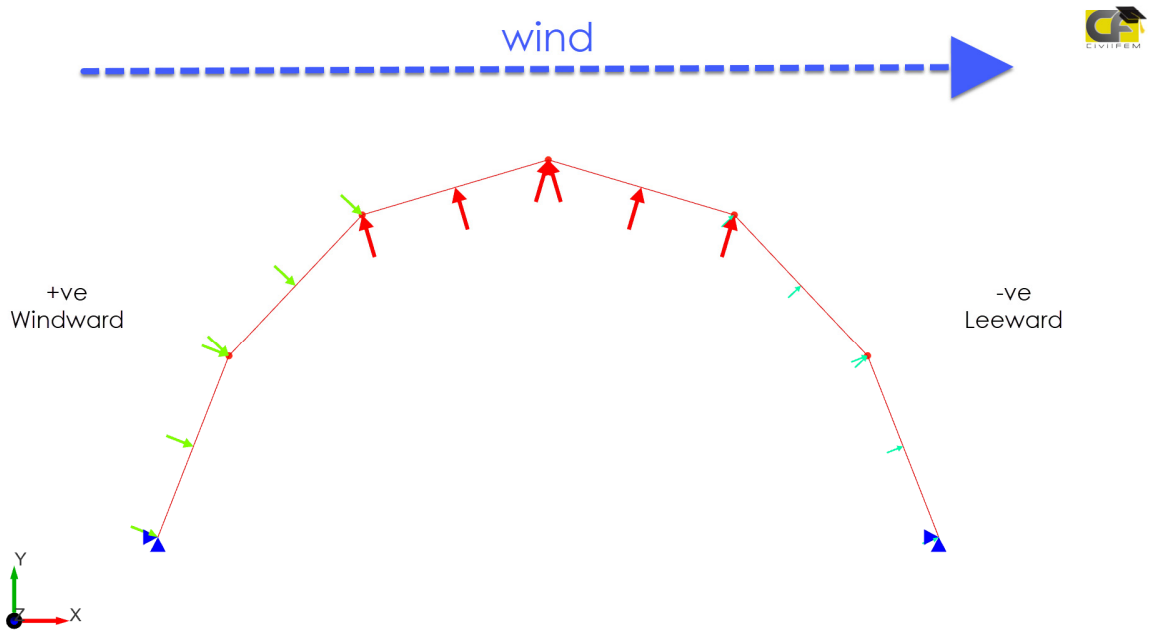


*Figure 6-2 - General Pressure Distribution for an Arch Under Cross Wind.*

Based on this initial pressure distribution it is proposed that a minimum of 5 springs distributed across the arch is suggested to create effective zoning of the structure, and given the potential for the wind direction to be reversed (moving right to left in the figure) the spring stiffnesses are made symmetrical about the centreline and the supports taken as free pins (see Figure 6-3). To develop a flatter, more aerodynamic, surface under wind loading the relative spring stiffness relationship between the springs should be distributed so that spring k1 is the softest and spring k3 be the stiffest spring, see Figure 6-3.

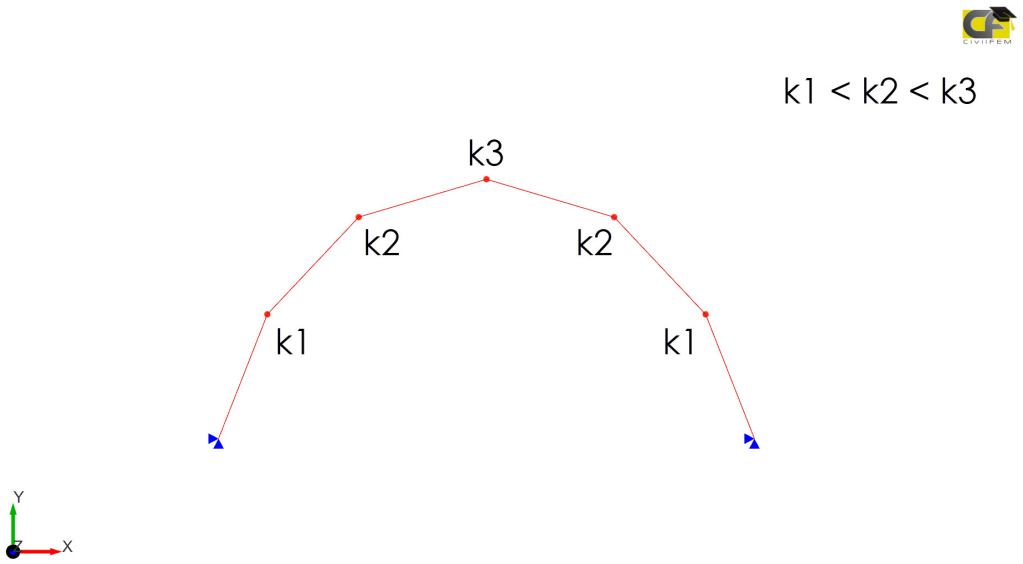


*Figure 6-3 - Spring Distribution For Load Relieving Arch Under Wind.*

Through applying a simple symmetrical load case as a test regime, the arch will laterally sway in the windward direction with the windward edge becoming flatter and visibly more aerodynamic, see Figure 6-4.

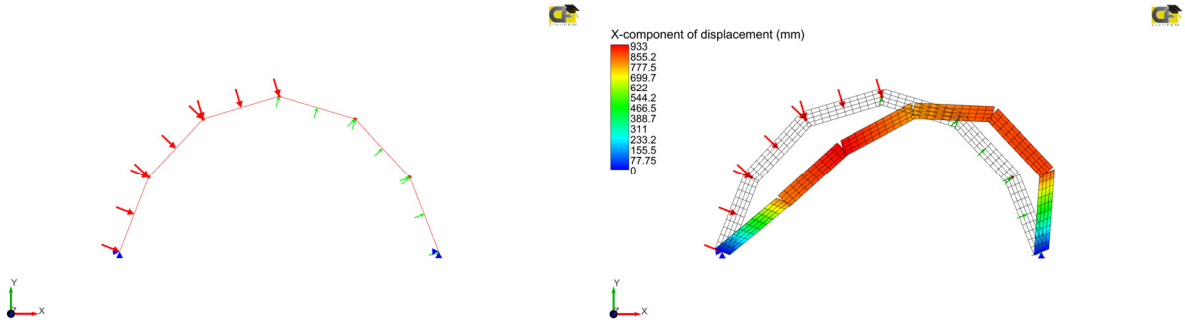


*Figure 6-4 - Softened Arch Adopting a more Aerodynamic Arrangement.*

The inclusion of the springs to soften the arch allows for the stiffer interconnecting elements to provide overall robustness for the occupants if the motions are controlled. Effectively creating a flexible arch behaviour through stiff elements, this has the benefit of increasing the overall robustness and reducing concerns with disaster relief shelters, for example, associated with accidental damage through debris moving in the wind damaging the panels or through intentional slashing with knives of flexible sheeting from thieves to gain access. The arch could be subdivided in such a manner that the stiff panels between the springs could be sized to fit within a shipping container for ease of shipping then erected with springs connected once in-situ. It is not inconceivable that future prototypes could make use of living hinges cut into

plywood panels (González et al., 2008) with the pattern and stiffness adjusted to suit the location and orientation of the arch to increase its flexural compliance (Santer & Pellegrino, 2008), or to lock the hinge at given angles (Estrada, Hawkes, Christensen, & Cutkosky, 2014), see Figure 6-5 which has a living hinge cut into the black material to create a hinge but as shown in the lower part of the figure it has constraints that lock it a pre-determined angle.

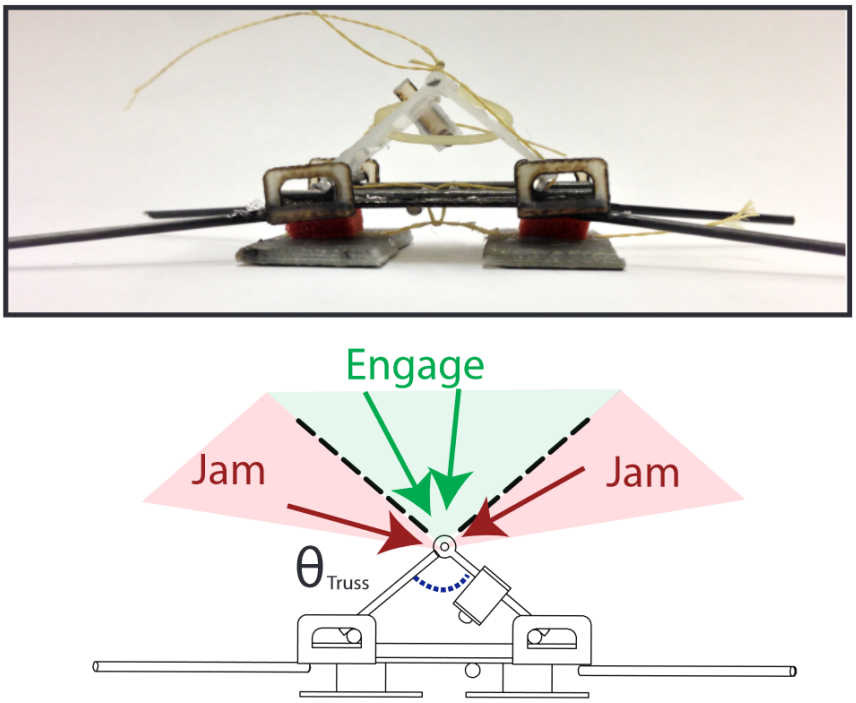


*Figure 6-5 - Living Hinge with Locked Angles.*[74]

It should be noted that currently living hinges are only used on a small scale or by makers for crafting purposes. However, initial prototypes made at the University of Salford have shown potential and it may be that these could be used to form load relieving structures from a single piece of plywood, but they may require further strengthening. No physical testing at the University has been undertaken yet to determine capacities and moment/rotation curves for further analysis.

Considering a specific arrangement for the arch with an 8m span and a rise of 3.872m (see Figure 6-6) it can be seen that the flatter front edge attracts a larger positive pressure coefficient

[74] Estrada, M. A., Hawkes, E. W., Christensen, D. L., & Cutkosky, M. R. (2014). *Perching and vertical climbing: Design of a multimodal robot.* Paper presented at the 2014 IEEE International Conference on Robotics and Automation (ICRA).

on the windward edge (Zone A). The shallower the arch, the lower the corresponding pressure coefficient, as the structure forms a more aerodynamic profile. The same relationship can be seen with regards Zone B on the arch with a flatter arch also having a corresponding reduction in wind uplift.

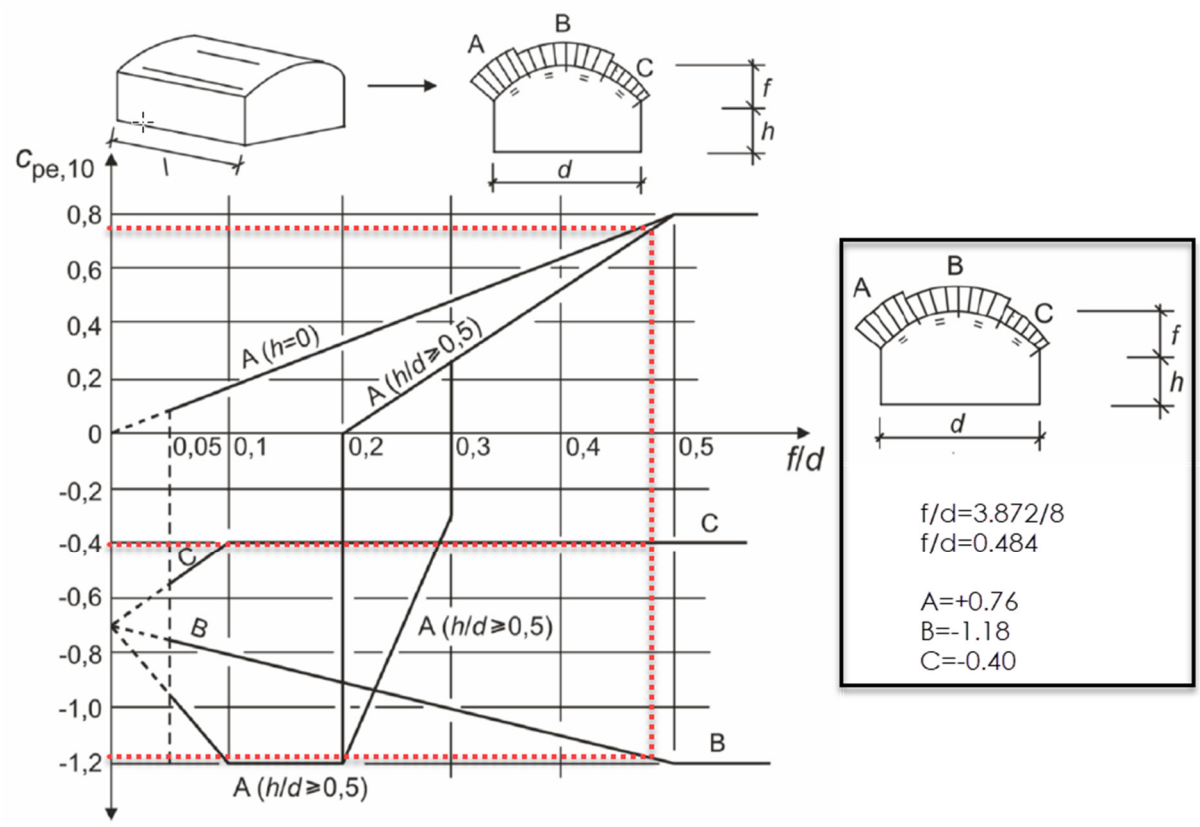


*Figure 6-6 - Pressure Distribution Across the Arch.*[75]

Applying the determined wind pressures with a unit load at the ratios calculated in Figure 6-6 shows that a more aerodynamic form can be developed which in turn will reduce the forces on the structure.

[75] British Standards. (2011). BS EN 1991-1-4:2005 +A1:2010 *Eurocode 1: Actions on structures - Part 1-4: General actions — Wind actions*. London: BSI.

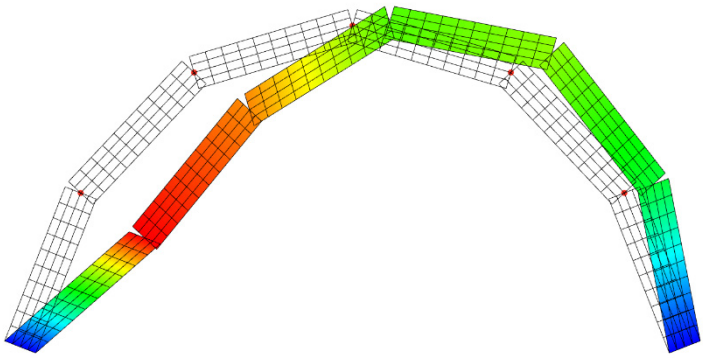

*Figure 6-7 - Displaced Arch Form Under Lateral Loading from Wind.*

As the structure has been designed to grossly deform under wind loading to develop an aerodynamic form (see Figure 6-7) it must be remembered that the external pressure coefficients will also change as a result of the change in shape which is likely to restore the structure to an intermediate stage. More advanced methods of determining the pressure co-efficients will need to be developed for such flexible buildings as the pressures will change over time as the building changes shape, this work sits outside the scope of this thesis however but may take the form of aero-elastic wind tunnel testing or CFD with flexible surfaces.

By integrating non-linear springs it is possible to control the deflected form even more precisely, effectively ensuring that the structure 'snaps' into a more rigid and predictable form than the simple arch outlined above. For example, it could be possible to set spring stiffnesses to a quarter of the desired load to allow the structure to adopt the more aerodynamic profile, but to stop the arch collapsing the stiffness of the spring could be set to reach infinity (essentially locking) at a predetermined angle to maintain structural integrity.

The application of arches that can change shape, particularly with snap-through behaviour that captures energy is of particular interest in the generation of energy in MEMs (Smith & Chase, 2001), with the development of new quantum devices requiring less energy to power them during remote monitoring, the integration of energy-generating micro-devices is likely to become even more desirable.

### 6.2.1 Timber Arch.

As an indicative case study, consider the same 8m span outlined above but placed at 5m longitudinal centres, formed using a relatively lightweight glulam say, a rectangular 400mmx200mm deep, grade GL28c Glu-laminated Timber section. The applied loading for a typical arch of these proportions is outlined below in Figure 6-8 taking a generic base pressure of 0.8kN/m² and using standard coefficients of pressure from the Eurocodes as shown in Figure 6-6 and calculated below.

$$Zone\,A = 5m \times \underbrace{0.76}_{C_p} \times \underbrace{0.8}_{q} = 3.0kN/m$$

$$Zone\,B = 5m \times \underbrace{1.18}_{C_p} \times \underbrace{0.8}_{q} = 4.8kN/m$$

$$Zone\,C = 5m \times \underbrace{0.40}_{C_p} \times \underbrace{0.8}_{q} = 1.6kN/m$$

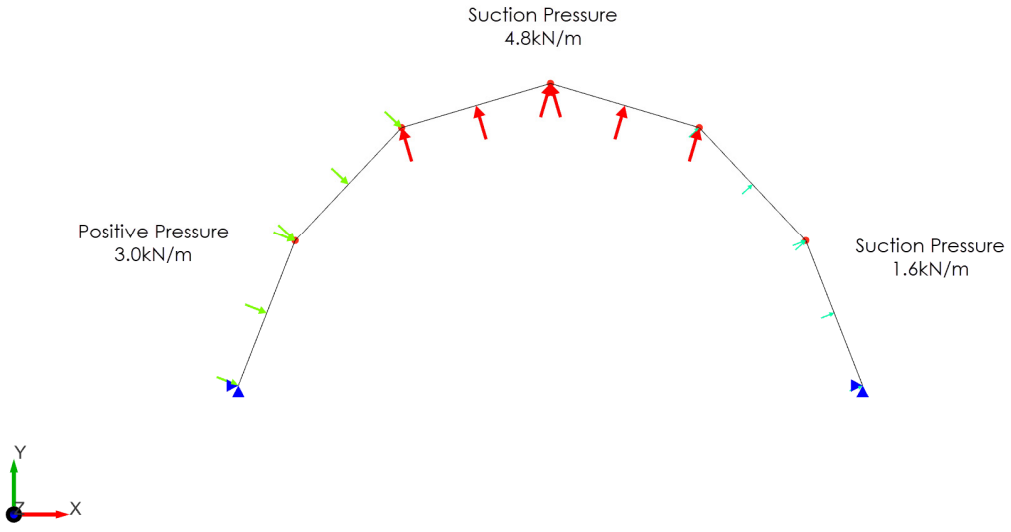


*Figure 6-8 - Typical Load Distribution for Glulam Frame at 5m Centres.*

Taking the material properties for the Glulam is outlined below. E=10,200 MPa, with a density of 430 kg/m³ an arch has been modelled with the spring stiffnesses as shown in Figure 6-9. These linear spring stiffnesses have been generated by adopting an iterative process to obtain a shape that has a more aerodynamic shape once deformed under the above loading.

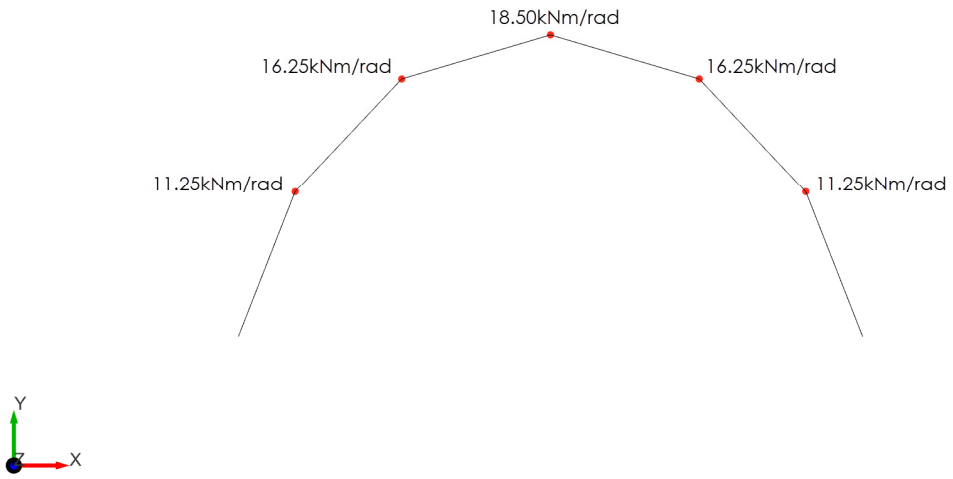


*Figure 6-9 - Rotational Spring Stiffnesses in Glulam Frame.*

Performing the analysis shows that the deflected form under the proposed loadings (Figure 6-8) with the spring stiffnesses (Figure 6-9), the deflected form developed has a shallower leading edge as per the previous theoretical example (Figure 6-7), with bending moments sitting comfortably within the working range of the glulam sections (Figure 6-10).

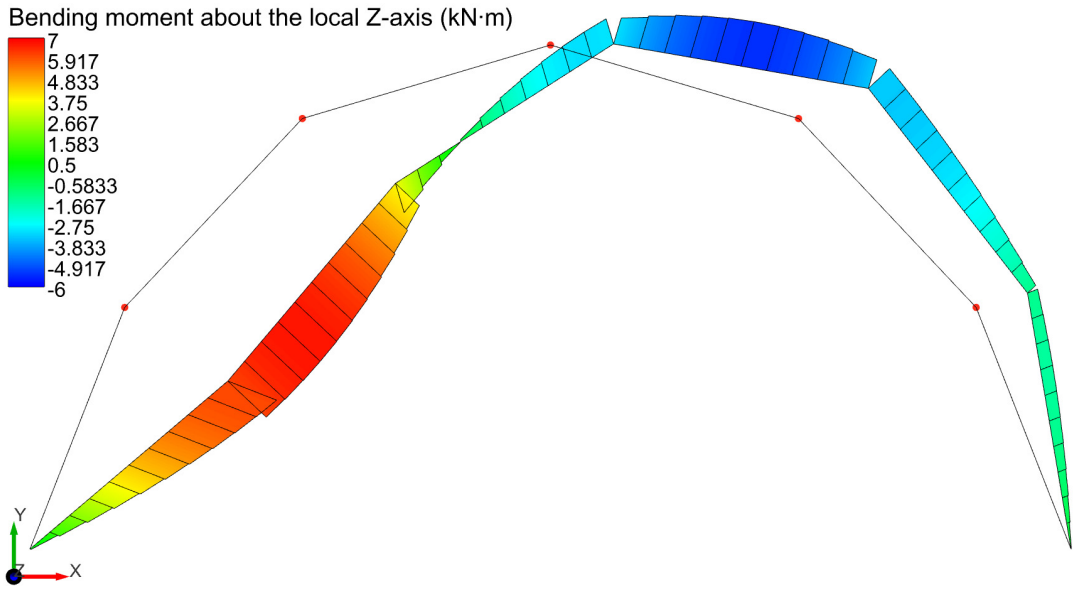


*Figure 6-10 - Bending Moment Diagram For Glulam Frame.*

Whilst the bending moments are relatively small for the structural elements specified it could be argued that they're over-designed, but to develop the spring stiffnesses required there is a need to have a reasonable structural depth for the initial concepts presented earlier in Figure 5-42 to allow the lever arm to be developed in the compressible filler. Initial calculations show that a material with a Young's Modulus of the order of 2MPa may be required, although a softer material introduces issues with shear which could be overcome with a steel pinned detail as shown in Figure 5-42 - Alternative Hinge Formed in UKB. on page 5-222. The development of a multi-material hinge though would require considerable design development and is something that will be undertaken as further research.

By way of comparison between a frame with and without hinges, an equivalent frame has been modelled with the springs removed to form a continuous glulam arch, the bending moment diagram shape between the two forms is similar, but with subtle differences in the magnitude of the bending moments see Figure 6-11.

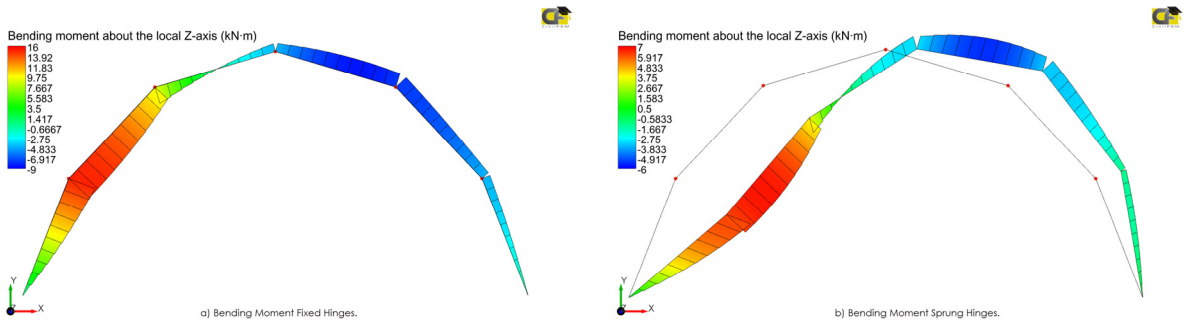


*Figure 6-11 - Comparison Between Bending Moment Diagrams of Fixed and Sprung Hinges.*

The introduction of the sprung hinges has approximately halved the magnitude of bending moment within the frame on the windward edge, with only a nominal difference on the leeward edge.

The reduction in bending moment on the windward side, however, has an associated large deflection compared to the rigid arch which shows less lateral movement, which is as expected. With the overall magnitude of deflections between the two arches also being significant as can be seen in Figure 6-12 with the flexible arch deflecting approximately 150 times more than the rigid arch.

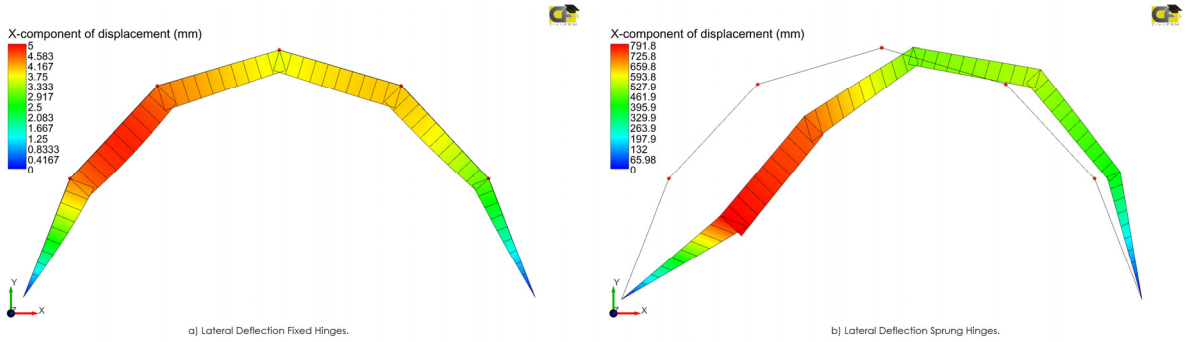


*Figure 6-12 - Comparison Between Lateral Deflection Diagrams of Fixed and Sprung Hinges.*

A structure such as presented above may prove useful for agricultural buildings where deflection criteria are often more relaxed in the design codes and where reductions in section size (due to reduced bending moments) may offer savings associated with material costs. Equally, agricultural poly-tunnels are often clad in flexible sheeting which may be more compatible with the significant deflections experienced as a result of the introduction of the hinges.

### 6.2.2 Alternative Applications.

Other potential applications may include a flexible arch that could be placed along the leading edges of slender bridges to aid with the reduction of vortex shedding by the arch moving under the wind loadings and consequently removing sharp continual edges along the edge of the bridge and potentially generating subsequent reductions in the wind effects through the 'fluttering' of the flexible arches, this concept would require additional CFD modelling to validate further.

On an even grander scale a flexible arch of proportions suitable to encapsulate an aircraft, such as those developed by Rubb Building Solutions, could be created that could adapt its form through the integration of a tendon that could pull the arch inwards and enable the arch to adopt a more complex form that could tightly wrap around specific aircraft to protect their engines during a sandstorm for example. This would require further development and could be undertaken as further development of this concept.

## 6.3 Kinematic Façade.

The case study above considers the metamorphic behaviour of a structure under a specific loading criteria and establishes that the analysis method developed is capable of successfully analysing sizeable arched structures with timber glulam elements. The inclusion of springs was also identified as being of potential benefit for deployable structures.

The case study defined in this section considers the development of a thick origami (section

5.8.1 - Binary Stiffness.) deployable structure (section 2.4 - Deployable Structures.) as a kinematic façade element similar to the adaptive façade elements discussed in section 2.10 (Adaptive Structures.). Whilst the proposed structure doesn't make use of a specifically defined spring element, it does make use of one of the key concepts utilised within the analytical modelling in section 4.1 where the Young's Modulus was varied within an element to mimic the behaviour of a spring using the finite difference method.

The integration of hinges and enabling controlled motion is not limited to 2D structures comprised of 1D elements which have been the focus of the structures considered thus far. As outlined within section 5.8 (Non-Linear Rotational Springs.), thick origami hinges can also be represented by varying spring stiffnesses, including non-linear springs and this section will investigate the potential integration of the analysis method developed to assess a kinematic façade element formed from 2D elements.

Buckling of thin sheets into origami patterns has been documented by Yoshimura (1955) with regards the simplification of analysis of buckling of thin sheets for aircraft design in a design guide published for NASA and his pattern is still used decoratively today. The principles of origami were later used by Miura (2009) to create a single degree of freedom motion structure folded initially from paper that has been successfully used in the generation of deployable surfaces and map folding. The Miura-Ori fold has been observed in nature as occurring naturally on hornbeam leaves (Tachi, 2009a) and has been used for deployable structures for folding sails in satellites where the solar panels are thin and able to fold without the complications of thick origami.

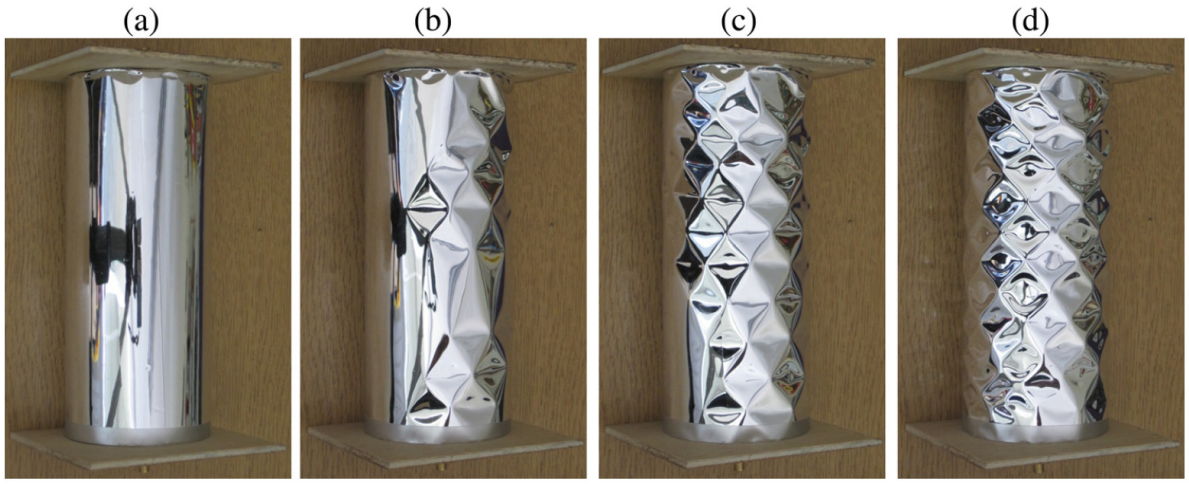


*Figure 6-13 - Yoshimura Fold Patterns in Thin Sheet Metal Formed Cylinders.*[76]

It is proposed that through the application of a panel inspired by the Miura-Ori fold a kinematic façade that can intelligently alter the amount of shading provided to a building in direct response to the amount of sunshine or thermal gain being applied to the elevation could be developed. The conceptual analysis makes use of the principles established throughout this thesis by combining stiff panels with rotationally softer joints.

Typically, facades may be shaded from solar gains using passive shading methods such as brise soleils, integrated blinds, double skinned facades with integrated buffer zones, or corridors placed on the outside of buildings to create natural shading to rooms on the inside line. However, active solutions integrating kinetic or adaptive facades have been used to create a dynamic control to solar gains on specific elevations to provide shading during bright parts of the day whilst allowing higher levels of natural light when the elevation is not placed in the path of direct sunshine.

Buildings with adaptive or kinetic facades are becoming more commonplace as technologies mature (Knaack, 2014), with examples such as the Al-Bahr tower (Fortmeyer & Linn, 2014, pp176) in the United Arab Emirates (see Figure 6-14) integrating a folding façade designed to aid with reducing solar gains and subsequently reduce the amount of energy consumed for cooling the building.

[76] Seffen, K. A., & Stott, S. V. (2014). Surface Texturing Through Cylinder Buckling. *Journal of Applied Mechanics, 81*(6). doi:10.1115/1.4026331

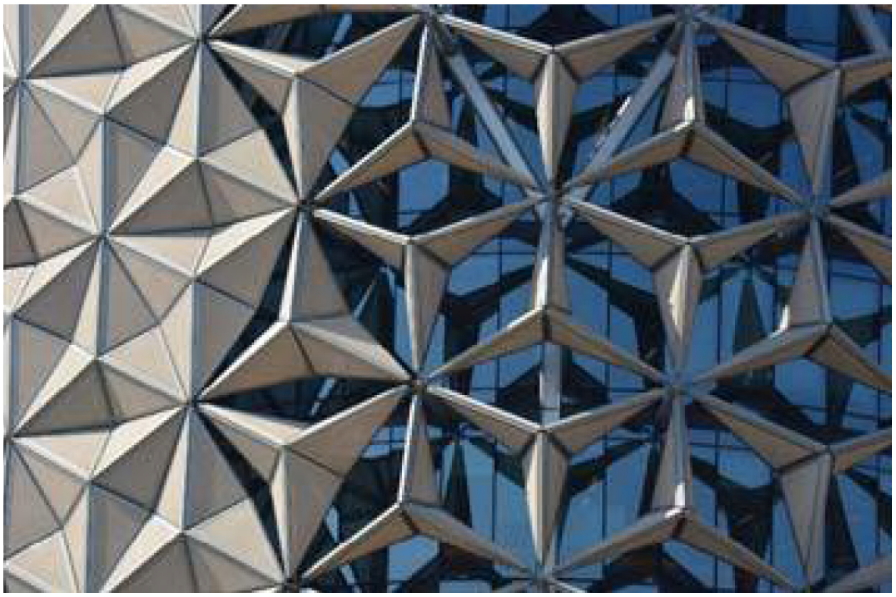

*Figure 6-14 - Al-Bahr Tower Adaptive Facade Showing Open and Closed Units.*[77]

Given the aggressive environment and difficulty with access for maintenance of the articulated façade units on such a tall building, extensive design and testing of the elements was undertaken in a controlled environment intended to mimic the desert-like conditions (Attia, 2018) with prototype panels being subjected to approximately 30,000 cycles before the manufacture of the full façade. Other less dramatic examples of actively controlled solar gains include the 'Gardens By the Bay' Building in Singapore (Davey, Bellew, Er, Kwek, & Lim, 2010) which has active solar shading integrated that responds to the sunlight levels to aid with protecting against solar shading through the integration of roller blinds that are controlled through motors.

### 6.3.1 Kinematic Façade Concept.

It is proposed that the modelling process outlined within this thesis could be applied to a kinematic structure inspired by the Miura-Ori fold from origami. Paper is a thin material and folding it when developing origami forms imparts a crease deep into the sheet, but the thinness of the paper is generally compatible with being folded and this is why paper and foils are good choices for origami. Paper and foil, however, may not be good choices for external elements in a façade design as whilst their thinness and ability to be folded are ideal properties for origami they are poor choices for a structural element and a thicker, more rigid material may be required to

[77] Attia, S. (2018). Evaluation of adaptive facades: The case study of Al Bahr Towers in the UAE. *QScience Connect, Special Issue on Shaping Qatar's Sustainable Built Environment, 2017*(2), 6-18.

deal with the stresses and general wear and tear. Thicker more rigid materials however, struggle with being folded and can often result in the material snapping unless an intervention or amendment along the fold line can be integrated. Tachi (2011) identified several challenges when detailing the joints between thick origami and looked at offsetting hinge positions from the centre-line (Figure 5-15 page 5-202) or locally altering thicknesses of material panels along the fold lines to make the folding action easier. There may be an alternative method to those proposed by Tachi through forming these panels using multi-material 3D printers to form panels of different thicknesses plus combining materials with very different properties along the hinges/valleys at the fold lines.

The mixing of materials with notably different Youngs Moduli to create tailored buckling forms with predictable buckling loads was established as a principle in section 4.1 where the Youngs Modulus of a material was manipulated in the finite difference method to mimic the stiffness of a rotational spring.

It is proposed that a similar logic could be used to create an analysis model for a Miura-Ora folded leaf made from two materials, with distinctly different properties. The hinged veins will be formed as thinner sections of structure in a more flexible material, whilst the primary panels will be formed in a stronger material and generally thicker than the hinges. The softening of the structure along predetermined paths combined with the geometry of a Miura-Ori fold would enable a complex shape to maintain a single degree of freedom and to fold in a repeatable and predictable manner which is a key criterion for the design of a deployable structure as outlined in section 2.4 (Deployable Structures.) of this thesis.

Figure 6-16 shows an initial analysis test model for a generic Miura-Ori folding pattern. In this application, the geometry has been simplified into a leaf pattern rather than a full square to simplify deployment. This also presents a modelling benefit with regards the definition of the supports due to the central line of symmetry. This triangulated leaf geometry, with stiff rigid panels interwoven with thinner bands of more flexible material, is shown in Figure 6-16, with the thinner veins of softer material set at angles close to 30 degrees (on plan) to give a neat folding pattern.

Each of the panels has been modelled using shell elements within CivilFEM with a thickness of 2mm initially to develop a model to investigate the motion study with nodes connecting panels being merged to model an equivalent sheet comprised of different materials. The plate is of a constant thickness, but the Young's Modulus for the panel and the folding vein has been

selected to create flexibility along the veins by having a relative difference between the two stiffnesses of an order of $10^5$ to develop a naturally folding line between the more rigid panels. Similar orders of magnitude for the difference in stiffnesses were demonstrated earlier in the research to illustrate that the flexural behaviour of the system during deployment was typically limited to the flexural behaviour of hinges rather than the flexing of the panels. The Youngs modulus for the panels has been selected as $9x10^9$ MPa and for the veins as $9x10^4$ MPa.

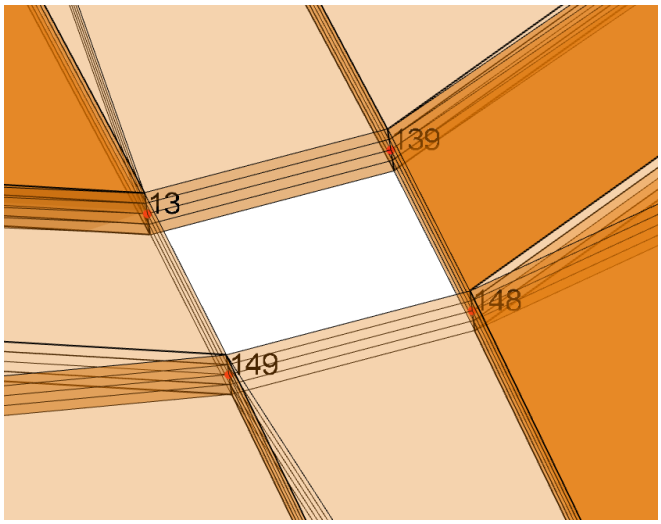


*Figure 6-15 - Panel Connections on CivilFEM model.*

Small open voids were left where the vertices met to aid with the folding of the panels to prevent the material 'bunching up' during the folding operation, this rationale also made it more straightforward when creating physical prototype structures, see Figure 6-15 and Figure 6-16 where the square voids can be seen running up the centreline of the leaf.

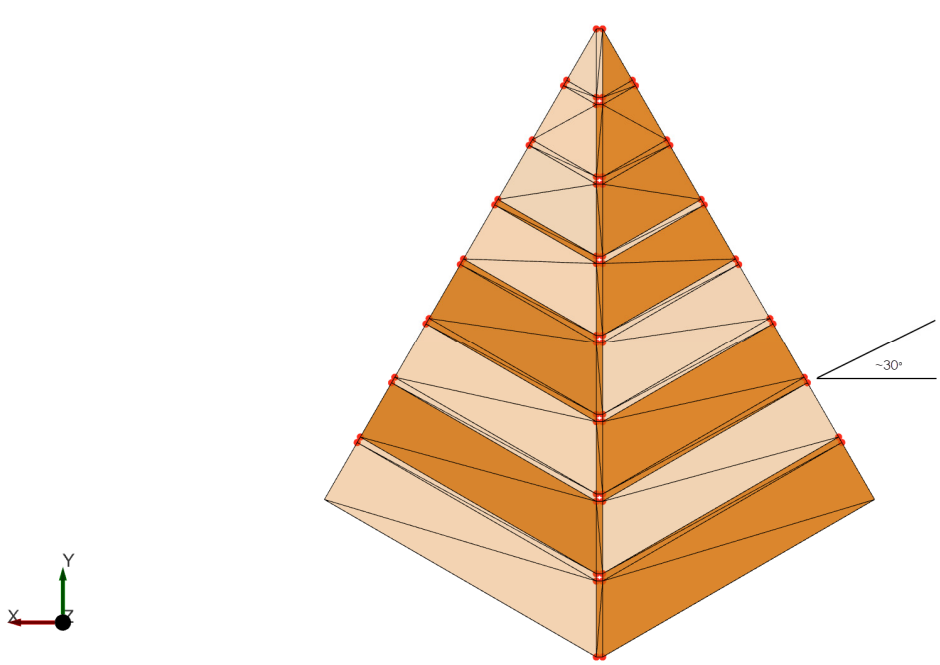


*Figure 6-16 - Initial Miura-Ora Geometry.*

When a small hand-held physical Miura-Ora leaf model is folded (say, made from stiff paper) and then manipulated through hand control it is common for a person to grip the base of the leaf and pinch the bottom parts together to cause the leaf to fold. If this was a cladding panel however and a similar folding principle was used, this would require the driving mechanism to follow a curved path (if the stem is held locked in position) which may complicate the use of actuators or further linkages to convert a linear motion for the required curved path. The scale of the initial leaf used in this investigation is 1000mm long in the Y axis and 900mm wide in the X axis, with the panels subdivided into a notional 8 equal width regions with the lateral veins running at 30 degrees to the central spine as is typical for a Miura Ora fold.

Each vein is taken as assumed to be 10mm wide within the initial model, which is approximately $1/10^{th}$ of the width of the stiff connecting panels. In reality the thickness of this vein will be dictated by the bend radius and the overall stiffness of the final material selected and the relative thickness of the connecting panels.

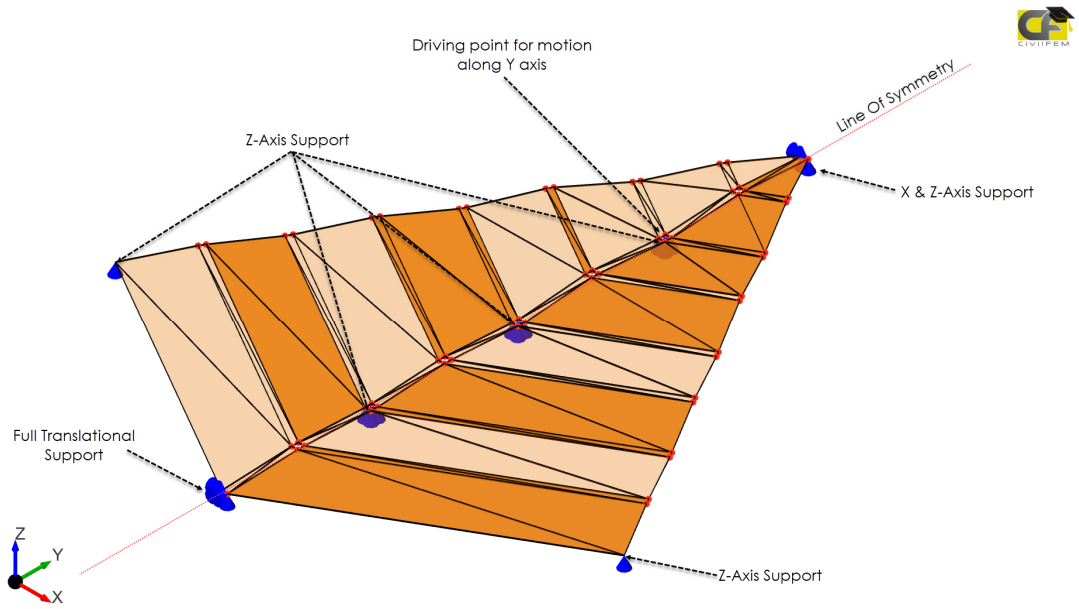


*Figure 6-17 - Boundary Conditions for Typical Miura-Ora Leaf.*

A more practical method for controlling deployment is to displace a group of spine nodes (located along the axis of symmetry) in the Y-axis along the central line of symmetry to activate the folding mechanism, this could be generated in practice through a cable pulling along a track in the Y-axis (with a linear spring for restoring the leaf to its unfolded geometry) or a hydraulic ram. It is this central actuated spine principle that has been modelled in Figure 6-17 which shows a single driving node along the central spine which will be able to both drive and control the leaf during deployment due to the single degree of freedom nature of a Miura Ora fold. The outer elements of the wings running on free-floating Z-Axis supports which in practice would be pre-formed radial tracks set the sweeping angle of the panel to prevent the wings lifting and peeling away from a façade, but these tracks would be guides and not required to drive the deployment and so have been modelled as simple Z-Axis supports as no horizontal reactions will be required initially.

The selected driving point for the folding mechanism was initially set to the be the tip of the Miura-Ora leaf in early attempts at modelling, but given the reduced width of the profile towards the tip of the leaf and the associated reduction in stiffness the tip often buckled prematurely and collapsed the leaf before activating the mechanism. So a driving point deeper into the leaf pattern was chosen to create a predictable folding pattern, the driving point for motion along the Y-axis is shown on Figure 6-17.

With the geometry of the leaf and the boundary conditions defined, a buckling analysis was

undertaken to determine the required buckled modal shape for the leaf to re-introduce a deformation as part of the forced displacement analysis. This initial buckling analysis is important to establish the folding pattern of the plate as an initial imperfection needs to be introduced to the structure to ensure that the structure folds predictably and in a repeatable manner ahead of the forced displacement analysis method. In practical terms the structure would never be allowed to be perfectly flat and would remain pre-loaded with a minor imperfection to ensure the folding process to be repeatable. Such preloading is often observed in paper origami structures as they naturally unfold along their crease lines to a neutral condition. As outlined previously structures with large degrees of freedom require a significant eccentricity to enable the analysis model to solve efficiently but the deformed mesh settings are often established using an iterative approach. However, the proposed leaf structure is a single degree of freedom system and for the example a 5mm deformation was found to be appropriate to generate a repeatable motion during the forced displacement of the analysis.

The model building and analysis steps for this particular case study follow the forced displacement method as developed within this thesis and in general terms are as follows:

Construct initial geometry and define panels, apply material stiffnesses, establish boundary conditions and loading criteria with a unit load along a central node along the Y axis, solve initially as a modal buckling analysis and review critical buckling loads and deformed shapes to check for ill-conditioning, extract the preferred modal shape (mode 1 for this example), re-assign analysis engine from buckling to structural analysis, deform mesh with mode 1 buckled displaced geometry with a scaled maximum deformation of 5mm, exchange unit load along the Y-axis with Y-Axis forced displacement, adjust engine solution settings as previous chapters in order to give refined intermediate steps (200 plus) to aid with highlighting any 'judders' or irregularities in solving that would hint at an ill-conditioned/constructed model, and finally extract results.

It could be seen that a well behaved and controlled deployable structure could be developed with fictional materials of stiffnesses of $9x10^9$ MPa for the stiff panels and $9x10^4$MPa for the more flexible hinges. Extracts from the displacement models can be seen in Figure 6-18 which show the leaf folding from an almost flat position (notionally distorted to develop a repeatable folding pattern) into a more compact folded position.

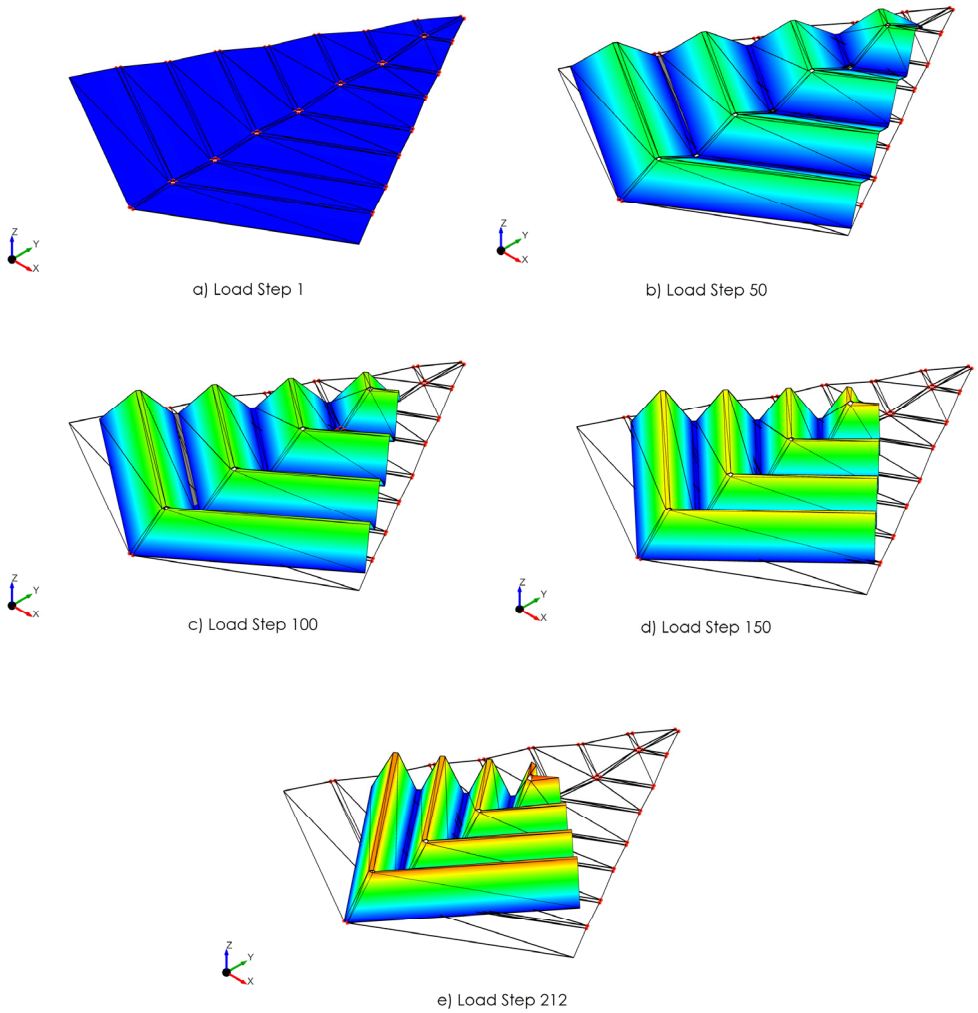


*Figure 6-18 - Deployment Stages of Miura-Ora CivilFEM Model (Showing Z-Axis Displacement)*

From these early digital models, it quickly became apparent that the analysis methodology was confidently modelling the movement and behaviour of a Miura-Ora fold with an articulated folding pattern in a similar manner to the arches from previous chapters. The concept of introducing a mixed material structural element as shown in the earlier finite difference methodology could have a practical application when developing a structure that could be encouraged to kink and buckle into a folded state. However, the material choices thus far are for a fictitious material with a significant relative difference in magnitude between the stiff panels and the more flexible veins to establish the overall feasibility of the analysis approach on a more complex structure. How this difference in stiffness may be developed in a physical model is investigated for an initial small-scale study in the following pages.

### 6.3.2 3D Printed Prototype Miura-Ori Leaf.

Whilst the above analysis was undertaken with fictional materials to establish if the motion of a complex structure could be established, an attempt to construct physical models was undertaken making use the University of Salford's Maker Space's MarkForged 3D printers and integrating the lessons learned with regards to stiffness ratios for the elements from the above model. These printers can print models in two materials, with the base material being Onyx which is the brand name for the general printing material with a second nozzle being able to lay down lengths of carbon fibre filament to create stiffer/stronger panels. The material properties for each are shown below in figures Figure 6-19 and Figure 6-20 and extracted from the MarkForged Technical Website.

| Property | Test Standard | Onyx | Nylon |
|---|---|---|---|
| Tensile Strength (MPa) | ASTM D638 | **36** | **54** |
| Tensile Modulus (GPa) | ASTM D638 | **1.4** | **0.94** |
| Tensile Strain at Break (%) | ASTM D638 | **58** | **260** |
| Flexural Strength (MPa) | ASTM D790* | **81** | **32** |
| Flexural Modulus (GPa) | ASTM D790* | **2.9** | **0.84** |
| Flexural Strain at Break (%) | ASTM D790* | **N/A**** | **N/A**** |
| Heat Deflection Temperature (°Celcius) | ASTM D648 Method B | **145** | **44-50** |
| Density (g/cm^3) | N/A | **1.18** | **1.10** |

*Figure 6-19 - MarkForged Data Sheet Onyx & Nylon Materials.*

| Property | Test Standard | Carbon Fiber |
|---|---|---|
| Tensile Strength (MPa) | ASTM D3039 | **700** |
| Tensile Modulus (GPa) | ASTM D30309 | **54** |
| Tensile Strain at Break (%) | ASTM D3039 | **1.5** |
| Flexural Strength (MPa) | ASTM D790* | **470** |
| Flexural Modulus (GPa) | ASTM D790* | **51** |
| Flexural Strain at Break (%) | ASTM D790* | **1.2** |
| Compressive Strength (MPa) | ASTM D6641 | **320** |
| Compressive Modulus (GPa) | ASTM D6641 | **54** |
| Compressive Strain at Break (%) | ASTM D6641 | **0.7** |
| Heat Deflection Temperature (°Celcius) | ASTM D648 Method B | **105** |
| Density (g/cm^3) | N/A | **1.4** |

*Figure 6-20 - Mark Forged Material Properties for Carbon Fibre.*

Whilst the relative difference between the two materials flexural modulus is nowhere near the same magnitude as the fictional materials (shown to be of the order of $10^5$ through iterative testing with the fictitious material and with similar magnitudes being shown in the earlier finite difference buckling analysis), there is still a notable difference with the Onyx having a lower flexural modulus. However, whilst the CivilFEM model was formed using a constant thickness, the 3D printed model can print different thicknesses of material as well as flexurally softer materials to create the step change in relative stiffness required to form a hinge.

Given the blended nature of the stiffer panels being formed with carbon fibre interwoven into

the Onyx material, the above data sheets cannot be taken at face value as the path followed for the carbon fibre can vary between prints depending on the pathing of the printing head and the slicing of the model. That said, the introduction of carbon fibre into the Onyx blend will give a stronger, stiffer panel on a like for like basis.

The relative thickness across the hinge is approximately $1/10^{th}$ of the thickness of the stiffer panels and flexural modulus of the Onyx being approximately 5% of the carbon fibre there is a relative EI value of $x10^4$ difference in rough magnitude (see below) which is similar to the change in stiffnesses shown in the CivilFEM models.

$$EI_{Onyx} = \frac{bd^3}{12}.E = \frac{1\times1^3}{12}2.9 = 0.24$$

$$EI_{Carbon} = \frac{bd^3}{12}.E = \frac{1\times10^3}{12}51 = 4250$$

The flat sheets are printed as one continuous piece, with valleys integrated into their surface along the pre-determined folding lines ahead of being folded. As the folding pattern for a Miura-Ori leaf pattern has an alternating valley and ridge patterns, the printed elements have the thinner notches alternated within the top and bottom side during printing to suit the face in which the valley fold is formed to encourage a specific folding pattern, see Figure 6-21.

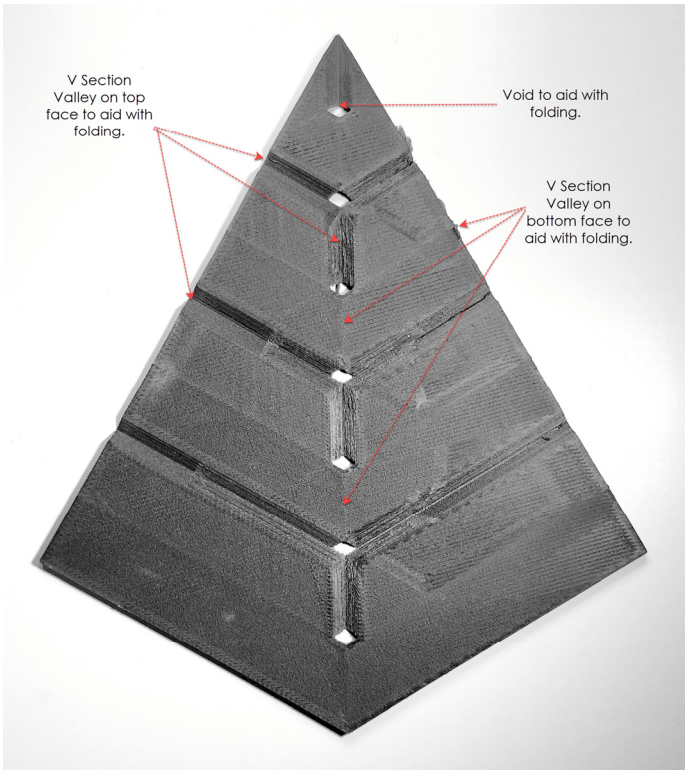


*Figure 6-21 - 3D Printed Miura-Ora Leaf Sheet, not yet folded.*

As the sheets are printed flat, the 'vee' on the bottom face of the sheet requires material support as part of the printing process which is manually removed with a scalpel or dentists scraping tool to create the contoured sheet. However, even following the removal of the support material from the underside of the sheets it was observed that the sheets still hold flat and true under their self-weight until the hinges are 'cracked' and the initial defect is introduced into the sheet. This forcing of the creases into a Miura-Ori pattern requires careful manipulation of the sheets even though they are pre-defined with the thinner notched channels which encourage the correct folding pattern to obtain the folded pattern shown in Figure 6-22.

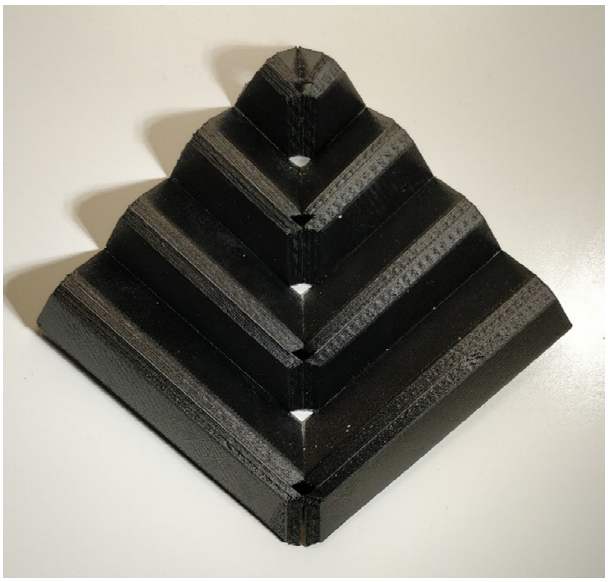

*Figure 6-22 - 3D Printed Miura-Ora Leaf Folded.*

Once folded into the Miura-Ori pattern the materials chosen had a natural resting point halfway between being fully folded and completely flat. Whilst the sheet could be unfolded and laid flat on a surface the same could not be said if the sheet was fully folded and placed on a surface where the stored energy within the leaf pushed the hinges apart making the leaf open. This release of energy reflected the stresses observed in the form-found analysis model which showed that the folded state increased the stresses and the tighter the folding achieved, the higher the stresses. A CivilFEM model was attempted to exactly replicate the printed physical model using the correct materials and section properties, however, the thinning of the hinges proved to be problematic with the analysis and this caused convergence issues due to the relative thicknesses. This could be overcome as the design concept develops through the inclusion of similar thickness materials or the modelling of equivalent stiffnesses through the manipulation of the Youngs modulus in a similar fashion to the finite difference and finite element models contained within this thesis.

The model printed for Figure 6-22, was used as a demonstration model for many months in various workshops and meetings and used regularly to appreciate and understand the modelling process within CivilFEM and was folded many times without any signs of distress or cause for concern. However, as noted in the design of the Al Bahr tower, fatigue and overworking of the hinges did prove to be an area of concern which resulted ultimately in the bottom central hinge splitting. This is an interesting point to consider with regards the future design of a more robust prototype as whilst the motion and the initial performance was satisfactory for the leaf, there is a longevity issue associated with the performance and working of the hinges from a fatigue perspective.

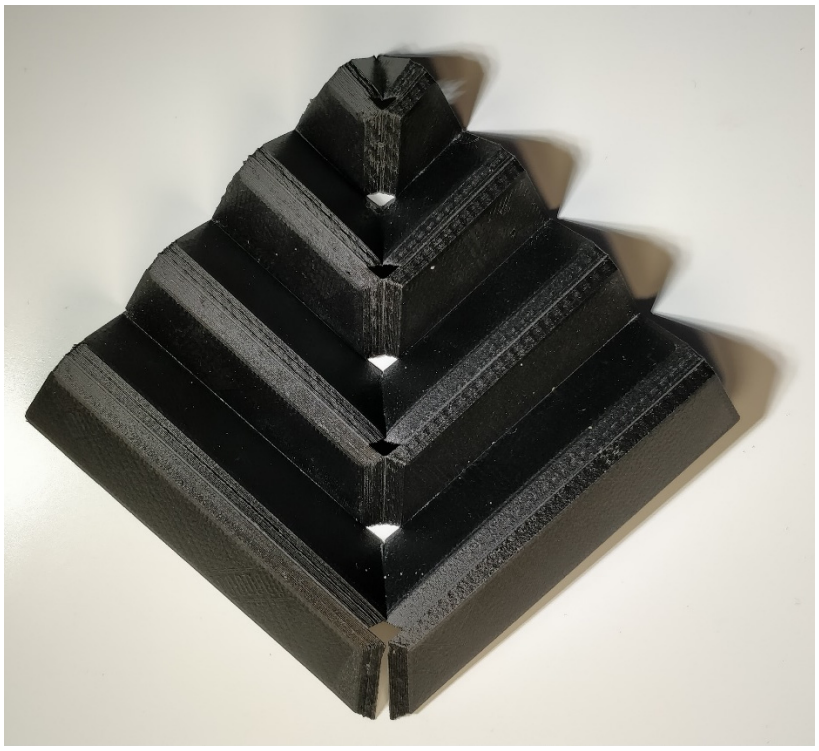

*Figure 6-23 - Fatigue Defect Evident On The Bottom Edge.*

The small scale test model highlighted that the analysis model and form-finding processes gave similar haptic and intuitive findings with regards the structural behaviours observed, with the force required to close the structure increasing as the structure became more tightly packed, as can be seen in Figure 6-24 which shows the distribution of stresses during folding using similar material properties.

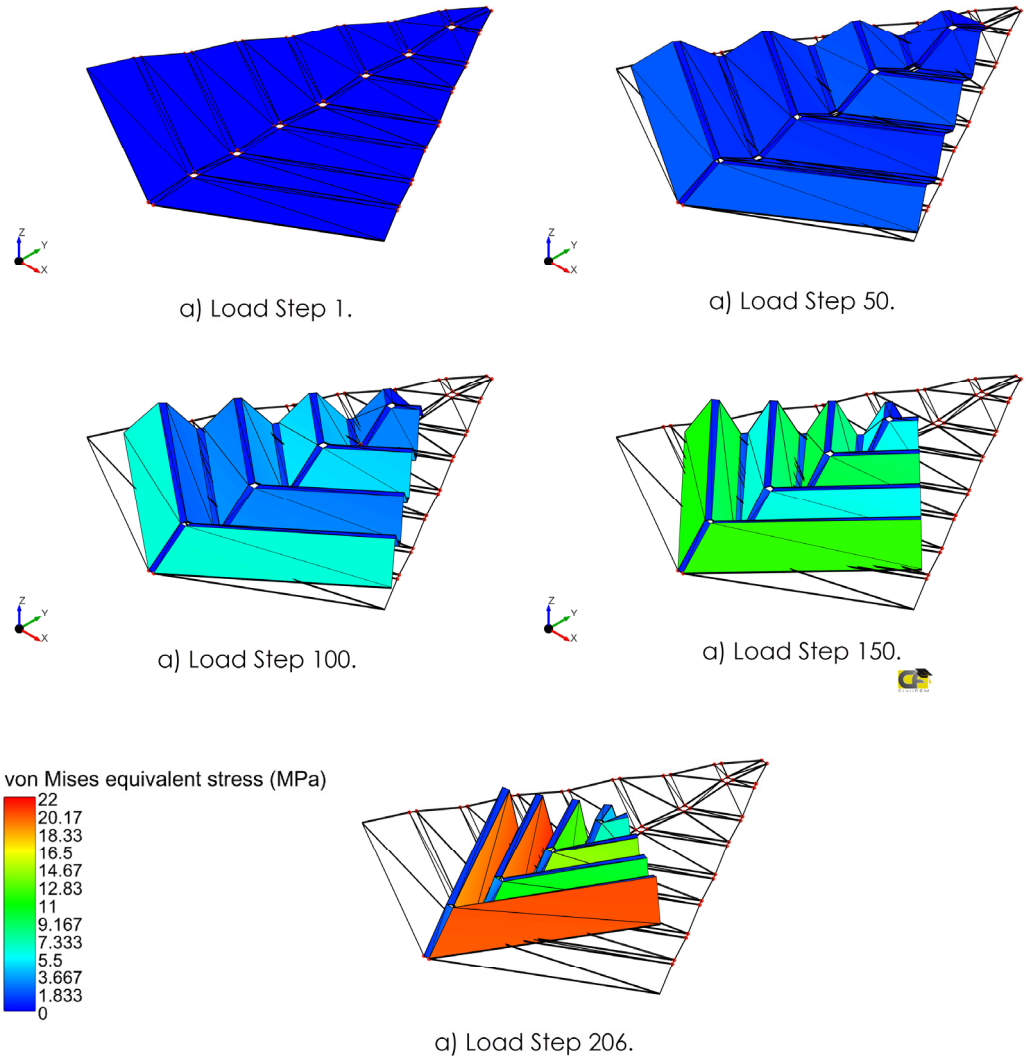


*Figure 6-24 - Increase in Element Stress During Folding.*

Although due to the small scale of the models the actual values of forces required for deployment the associated stresses could not be fully validated and this is something that should be developed further as part of this ongoing research. The calibration of the digital and physical testing should also be used to determine the reason behind the splitting of materials along the joint lines and perhaps a more careful selection of materials may be able to overcome this failure mechanism.

For example, perhaps the solid stiff panels could be formed from a lightweight aluminium composite panel with the hinged elements formed from natural rubber or similar material that is not prone to being 'worked' due to continuous folding as this could cause splitting as observed in the smaller model, or potential loss of elasticity in the hinges as the material becomes either

worked or potentially stiffens through exposure to the environment.

## 6.4 Summary.

The integration of rotational springs has been shown to provide an arch with the ability to passively change its shape and form to adopt a more aerodynamic profile to reduce the applied loading. A careful balance needs to be maintained though to ensure that the gross change in internal profiles does not negatively affect the internal habitable area.

The introduction of sprung hinges was shown to give benefits with regards to the reduction of bending moment along the windward edge of an arched structure, with nominal reductions along the leeward edge. The reduction in bending moments, however, comes at the cost of an increased lateral deflection which would be problematic potentially for buildings with sensitive facades such as glass but would present the potential for more flexible agricultural buildings such as poly-tunnels.

More work is required to develop a fully working and practical spring of a size needed for such a structure, but initial concepts contained within this thesis (section 5.10) show potential ways forward.

The development of a controlled kinematic façade element that makes use of the analytical methodology defined within this thesis was shown to be feasible making use of fictitious materials. With stiffer panels connected with softer hinged joints, a digital model was developed that demonstrated a clear motion path inspired by the Miura-Ori origami fold. This was achieved by modifying the Youngs Modulus for a specific sub-regions of a constant thickness sheet of material.

The relative difference in stiffness of the two regions, combined with an initial geometrical pre-set allowed the structure to fold neatly in a predictable manner. Whilst constructing a full-size panel of this nature will require considerable design development and is beyond the scope of this thesis, a smaller physical model was 4D printed using the University of Salford Maker Space. Using multi-material 3D printing techniques, a 4D element was able to be printed with the relative difference in stiffnesses between the elements being of a similar order of magnitude to the initial digital model. Whilst the model performed well in terms of general motion it eventually split and failed at a hinge position through fatigue along the lines of flexure and this should be considered in more detail in the development of a larger prototype.

Whilst the small printed model helped demonstrate that a physical prototype would be feasible

and that the resistance within the elements in terms of the forces felt broadly correct during folding, a larger instrumented model would be beneficial to develop the design further and to help validate the analysis model.

A larger model is unlikely to be 3D printed due to the size and scale of the elements being beyond that of most commercially available printers. It is more likely that the stiff panels would be constructed using a form of an aluminium clad panel, with the hinges made from a softer more flexible material such as natural rubber to aid with reducing the risk associated with working the hinges.

# Chapter 7

# 7 Conclusions.

To aid the examiners whilst reading this work, the aim and objectives are reposted below to reduce the amount of time flicking back and forth with fingers lodged within this thesis, they are contained within boxes to ensure they stand out from the rest of the text.

## 7.1 Concluding Against The Aim.

The thesis aims to develop an appropriate method for the analysis and modelling of structures (static and deployable) with integral rotational springs with regards to their structural behaviour, performance, and ability to adapt the structure.

### 7.1.1 Deployable Structures.

The literature review introduced the concept that certain structural forms such as deployable structures and adaptable structures are designed by engineers to grossly displace or change form under certain predetermined conditions.

It was outlined that certain types of lightweight and deployable structures that make use of cables, under particular loading conditions, can become unstable and suffer the effects of snap-through which may lead to structural instabilities and/or collapse. Snap-through was found to be of a concern for lightweight strut and cable structures where the angle between the cable and the strut is small, with limited evidence of this phenomenon being presented in the literature review. Due to the lack of literature associated with cable-chain arches and snap through the analysis of cable-chain arches was undertaken in chapter 3 which demonstrated that snap-through was indeed of concern.

An alternative configuration to a cable-chain arch was proposed to overcome the effects of snap-through, by removing the free pins and the cables and replacing them with a rotational spring.

To investigate this intervention further it was necessary to develop a suitable methodology to analyse sprung structures as traditional matrix-based software such as ROBOT (section 4.2.1) or physics-based software such as SystemModeler (section 5.4) were found to be lacking in the ability to analyse these forms of structure adequately.

It was proposed that the introduction of rotational springs to replace free pins could be beneficial for a deployable structure and could be introduced to a structure to have the following potential positive effects:

- Reduction of risk due to disproportionate collapse due to increased structural redundancy. *(Not explicitly checked but demonstrated by the nature that springs can limit the uncontrolled rotations of a free pin in section 2.7)*
- Controlling motion during deployment. *(Demonstrated by the Miura-Ori leaf in section 6.3.1)*
- Mimicking the behaviour of a flexible rod such as those used in adaptive facades. *(Demonstrated by the comparison analysis in section 5.6)*
- Remove risk associated with snap-through. *(Demonstrated through gross displacements being accommodated in various models without analytical collapse)*
- Forcing a deployable structure to hold a specific position in the event of a mechanical failure or a power cut. *(Demonstrated through various models being stable in the self-weight condition)*

### 7.1.2 Springs and Buckling.

Determining the critical buckling load of a sprung strut is relatively trivial to solve for a single linear spring, with this example being widely used in undergraduate teaching to introduce the concept of strut buckling (section 4). However, the post-buckling behaviour for this same structure requires a different approach to analyse which is further complicated in that for each additional spring added to the system, there is an additional degree of freedom introduced which consequently increases the complexity of determining the buckling loads of these sprung struts.

A reliable methodology was developed for determining both the critical buckling load, the post-buckled behaviour, and associated deformations of spring linked struts using CivilFEM. The proposed methodology was validated against various techniques including a novel adaptation of the Finite Difference Method plus Finite Element analysis with comparative studies up to 8 degrees of freedom being completed.

The integration of springs into structures and finding compatible structural forms that are in

equilibrium using the buckled shape was established as a workflow with up to 18 degrees of freedom. These form-found balanced geometries were able to be successfully reintroduced back into forced displacement models to determine their post-buckled behaviour reliably.

The post-buckled behaviour was shown to have practical applications with benefits particularly aligned to the creation of adaptive structures for both passive and actively controlled structures with investigations in a metamorphic arch (section 6.2) and an origami-inspired leaf (section 6.3) modelled as case studies.

### 7.1.3 Ill Conditioning.

Due to the significant differences between the relative stiffnesses of the springs and the struts, ill-conditioning was noted as being a major concern in the generation of sensible analysis models. Ill-conditioned models were shown to either provide no solutions or incorrect solutions both in terms of the critical buckling loads and the associated modal shapes. Due to no modal shapes being generated post-buckling behaviour could not be investigated for the examples considered.

Methods for identifying the effects of ill-conditioning and for adapting the relative stiffnesses of the structure to allow the models to over-come and solve were established to help reduce the effects of ill-conditioning. These methods made use primarily of visual assessments of the buckled form combined with inspection of the analysis results. Where uncertainty lies, the Young's Modulus could be incremented by an order of magnitude to look for sharp changes in behaviour as shown in the graphs within section 4.5. Several different check methods were proposed using the Finite Difference Mathematica sheet, but the sealed box nature of CivilFEM prevents the matrices to be extracted and interrogated explicitly.

The case study models for the arch and the leaf in chapter 6 both relied on rotational spring stiffnesses that were several orders of magnitude smaller than the relative stiffness of the struts. As ill-conditioning was noted as being an issue driven by large relative differences in stiffness this behaviour should be at the back of practicing engineers' minds when designing structures with springs as the relatively large difference in stiffness may still be an issue.

### 7.1.4 Post-Buckling Behaviour.

The behaviour of sprung struts is complex, they present linear behavioural traits until the struts buckle, at which point a non-linear behaviour is developed through a combination of the rotational stiffness of the spring and the strut changing angle at the mid-point. Sprung struts differ from traditional struts in that they can continue to support increased applied axial loads

with a post-buckling reserve whereas a traditional strut would buckle and lose its stability under increased loading with no post-buckled strength.

The additional load-carrying capacity was noted in Figure 4-2 in the work undertaken by Walker (1975). What is not obvious from Walker's work though is the mechanism by which the additional load-carrying capacity is developed and this is due to the additional bending moments developed in the strut, changing the behaviour from a purely axial element (pre-buckling) to a combined axial and bending element (post-buckling). The transition of this behaviour was shown clearly in the frame analysis undertaken in section 5.11, particularly in Figure 5-51 where the moment can be seen to increase at the hinge position once buckling occurs for the strut.

Providing additional post-buckling resistance for an element by simply introducing a rotational spring may initially appear appealing, but the generation of the additional bending moment should not be neglected as this may require additional material to be introduced to the element when designing to resist the additional moments at the hinge locations.

The increased post-buckling capacity of struts with rotational springs is governed by the stiffness of the rotational spring providing that the struts are considerably stiffer than the rotational springs. If this is not the case then the struts will start to buckle and overly flex and will not be able to mobilise the spring effectively. Increases in applied load realized in the post buckling stage result in a corresponding increase in rotation at the spring position and an increase in system deflections. These post-buckled deflections for the strut can become gross under extreme loadings and are likely to be greater than the allowable deflections limits for a real building. Assuming that the sections are designed to resist the moments generated by the springs, and that the rest of the connections within the frame are able to accommodate this magnitude of rotation, this deflection could continue until the frame was flat and/or touching the floor and the case study in Chapter 6 noted that this may limit its application to uses that are not governed by strict deflection limiting criteria such as agricultural storage sheds.

One potential application for a sprung strut could be the introduction of a spring with an integrated damper to absorb the energy from a blast as this design criteria is about life safety and it is acceptable that gross deflections occur, within reason. However, this hypothesis could not be evaluated in this research as CivilFEM has a limitation in that whilst it is capable of undertaking dynamic analysis, damping cannot yet be applied to rotational springs.

### 7.1.5 Metamorphic abilities.

As the first mode of buckling typically occurs at the lowest axial load, this first buckling mode is usually developed by the struts when in service and the critical buckling load is reached.

But, it was shown to be possible to bypass this first buckling mode and to develop the shapes derived from higher modes through either introducing specific geometrical eccentricities that encourage the structure to transform into a higher modal shape or by adjusting spring stiffnesses to strengthen the struts in such a manner that a higher mode shape is developed.

This principle was shown to be beneficial for encouraging struts to fold into more compact forms, for example, the compressive bracing in section 5.11.3 which allowed greater eaves deflection before steelwork fouled the ground.

### 7.1.6 Snap-Through Mitigation.

It was shown that structures that may be vulnerable to snap-through, such as shallow angled cable-chain uniplets, could benefit from the introduction of rotational springs to remove the instabilities associated with gross deflections. The arch example in Chapter 6 was comprised as springs and able to act as a metamorphic structure to alter its aerodynamic properties whilst maintaining a stable structural form with no snap-through issues despite the large deflections (almost 800mm).

The creation of physical springs with rotational stiffnesses appropriate for use in a building however will require significant development and design work before this principle can be reliably built and implemented.

### 7.1.7 Practical Applications.

It was shown that the introduction of springs into a lightweight arch if designed carefully, could allow the arch to displace into a more aerodynamic shape and that change in shape also enabled a reduction in the associated bending moments, see section 6.2.1. However, the introduction of these springs comes at a cost of correspondingly greater lateral deflections which may compromise the performance of the internal space although it was proposed that this may be acceptable for some agricultural buildings for example.

An origami-inspired leaf was developed as a prototype model (digital and physical) to show the principles of softening parts of the structure to create a single degree of freedom structure. This mobility could be achieved through the combination of different materials and the reduction in cross-sectional area to develop the shift in relative stiffness between the stiff panels and the more

flexible hinges. This process could be modelled well digitally and a working 4D printed model was created, although a larger model will be required to enable instrumentation for final validation of the FE modelling. However, the behaviour of the hand-held model intuitively aligned with the FE analysis, as greater resistance was observed from the structure as it was pinched together in order for it to fold tighter which reflects the observations in the digital model which showed a corresponding increase in stress during the folding motion.

The small physical model was operated successfully for several months as a concept but eventually, fatigue and working of the hinges have caused the material to split with an associated hinge failure. Future models will need to not only consider the working properties of the material with regards compatible stiffnesses to generate a specifically targeted spring stiffness, but also the impact of repetitive cycling of the hinges and fatigue.

As structures with springs may be able to change their shape and form more easily than traditional structures it may be necessary for more sophisticated methods of determining pressure co-efficients to be developed, perhaps with CFD applied to flexible surfaces or methods of aero-elastic modelling. The inability to determine the precise wind pressure co-efficients for such a flexible structure will increase the complexity of developing accurate analysis models given the changing nature of the loadings.

### 7.1.8 Challenges with Full-Scale Construction.

Whilst fabrication of large hinged structural sections for development of the leaf structure may be prohibitively expensive and beyond the scale of current 3D printing techniques as a single piece, alternatives through the combining of aluminium panels and natural rubbers may provide an option.

In the future though, the development of advanced fabrication techniques such as large scale 3D printing and multi-material 3D printing for metals could also open up exciting new developments for structures that can fail in pre-determined and controlled ways and develop tailored behaviours through 4D printing techniques.

A similar challenge was noted in that the development of a physical connection that could function adequately as a rotational spring in a beam/strut element within a structure of this scale. This would require the manufacture of a bespoke spring as no rotational springs of this scale could be located in the open market that were readily available from commercial suppliers. Suggestions for potential prototypes were outlined in section 5.10 and lessons learned from the leaf case study have highlighted the need to assess the durability of these types of connections.

More research is needed to develop a viable prototype for testing for practical applications generally and this is outlined in further work.

### 7.1.9 Summary.

Ultimately the work contained within this thesis has shown that the introduction of springs into frames can, in certain arrangements, introduce benefits for structures such as the ability to create a predictable failure mechanism that maintains load-carrying capacity beyond the predicted failure load, introducing controlled deployment or articulation during deployment for deployable structures, or creating adaptable structures that can change their form in response to specific loading conditions.

However it is recognised that the whilst the modelling of these types of structures would seem to be reasonably well controlled using the methodology developed in this thesis, they have been applied to somewhat idealised structures and there is a significant amount of research required to take the next step through to a buildable full-scale structure that embraces the introduction of rotational springs.

More research is needed to bring about these concepts to a stage where they can be manufactured cost-effectively and to a scale which is both safe and economically viable for buildings and this development may, in turn, raise additional challenges associated with the form-finding and analysis of sprung structures.

## 7.2 Concluding Against The Objectives.

Each objective will be addressed in sequence to aid with demonstrating that the work has been achieved and towards the end of this chapter the unique contributions will be explicitly outlined. This is a brief overview of each objective to demonstrate that they have been completed rather than a deep critical review which is contained within the primary chapters and the associated summary for each chapter.

### 7.2.1 Objective 1.

| |
|---|
| To undertake a literature review to identify the general forms of deployable, metamorphic and adaptive structures to identify how articulation can influence structures. |

The literature review identified that there are a broad range of deployable, metamorphic and adaptive structures available and that the area of research is still developing.

From the perspective of the introduction of springs, strut and cable/strut forms of deployable

structures were identified as being compatible through having their free pinned connection exchanged for a rotational spring.

The inclusion of the rotational spring, however, would introduce bending to the structural elements which may influence how these deployable structures are designed as they are often designed to reflect the principles from lightweight structures with elements purely in tension or compression, no bending.

It was proposed that the introduction of rotational springs to replace free pins could be beneficial for a deployable structure and could be introduced a structure to have the following potential positive effects:

- Reduction of risk due to disproportionate collapse due to increased structural redundancy.
- Controlling motion during deployment.
- Mimicking the behaviour of a flexible rod such as those used in adaptive facades.
- Remove risk associated with snap-through
- Forcing a deployable structure to hold a specific position in the event of a mechanical failure or a power cut.

Adaptive structures are commonly formed from flexible materials and were deemed to generally already be too flexible for the insertion of springs to be practical. However, the forms created by these flexible structures held potential to be mimicked by chains of springs.

### 7.2.2 Objective 2.

| To investigate the cable-chain structural form and identify shortcomings in this structural form that could be improved upon. |
|---|

Cable-chain structures were investigated in detail in Chapter 3 and were illustrated through the limited available research to have been successfully deployed in service for a shopping mall roof in Russia and for the Rubb aircraft hangars.

The structures were found to be vulnerable when shallow angles were formed between the struts and the cables, which reflected the work undertaken on other similar forms of lightweight structure. ROBOT structural analysis was undertaken to demonstrate that shallow angles could indeed make the structure unstable.

It was proposed that removing the cables and replacing the free pins with a rotational spring may make the arch more stable under significant displacements which would ordinarily cause a cable-chain arch to fail due to snap-through.

### 7.2.3 Objective 3.

| To identify the potential benefits of rotational springs on arched structures and to determine their potential in being integrated to deployable, metamorphic or adaptive structures. |
|---|

The inclusion of rotational springs would allow for a relatively lightweight arch to be formed, with greater available internal area due to the removal of the internal cables and that would also be able to maintain stability even under gross displacements.

The inclusion of the springs will eliminate the risk of snap-through for all but the most extreme of displacements within an arch, such as when an arch loops back on itself.

It must be noted though that the correct spring stiffness must be selected when being integrated into a structure, a spring that is too weak will not be able to support the self-weight of the structure, with a spring that is too stiff resulting in the arch behaving as a continuous element and will transfer moment between the links.

Determining the spring stiffnesses to create a balanced equilibrium state can be challenging and various analysis methods and pieces of software were evaluated but finding a balance between software that could generate a balanced arch form as well as performing structural analysis to calculate the bending moments proved difficult.

Form-finding software was beyond the scope of this thesis and the budget of the University to purchase, an alternative method was proposed that enables equilibrium forms to be developed through determining the buckled shape of a strut, with the first modes typically forming a curved arch structure that has an equilibrium state.

### 7.2.4 Objective 4.

| To identify, implement, and validate methods of determining the buckling capacity of struts formed with lightweight infinitely stiff struts and linear rotational springs. |
|---|

5 different methods have been applied to determine the critical buckling loads associated with a hinged strut, including:

1. Geometrical Methods,
2. Energy Methods,
3. Finite Difference Methods,
4. Finite Element Methods,
5. Non-linear forced displacement analysis.

Generally, for the simple struts considered with a single spring, any of these methods are adequate for determining the buckling behaviour of a perfectly straight strut with a single central spring, neglecting the effect of self-weight.

However, the geometrical method has limitations as once the models become increasingly complex there will be limitations on the assumptions based on the deflected geometry.

The energy method has broader applicability than the geometrical methods with typically lower calculation overheads when undertaken manually but lacks the speed and efficiency of the finite element method given the affordability of modern computing hardware and ability within modern Finite Element software such as CivilFEM.

For a large number of springs, the finite difference method has been used successfully to determine the critical buckling load. The method for application within this thesis was novel and developed specifically for this work.

Finite Element analysis was completed for a variety of sprung struts with several springs ranging from 1 to 8 springs total, with the critical buckling load and modal shapes being determined successfully through the artificial stiffening of the Young's Modulus to ensure that the buckling load was entirely dictated by the rotational spring stiffnesses.

Forced displacement non-linear analysis was also undertaken using CivilFEM with an initial imperfection being added to the geometry by locally deforming the analysis mesh using the modal geometry of the buckling mode obtained during the Finite Element analysis. Instead of

applying a unit load to the top of the structure, a displacement was applied at the top that was incrementally applied which allows the model to solve even where the failure mode would ordinarily be catastrophic had a load, rather than a displacement, been applied. This methodology allowed the post-buckling behaviour of the structure to be analysed.

For all three numerical solutions (Finite Difference, Finite Element, And Forced Displacement) the effects of ill-conditioning were identified during the analysis process and methods for visually identifying the occurrence of this phenomenon were presented.

Both the CivilFEM modelling processes were developed and applied to a wide variety of sprung forms succesfully.

### 7.2.5 Objective 5.

| |
|---|
| To implement linear rotational springs in an arch structure and identify appropriate methods of analysing and determining balanced forms of arch structures. |

An initial study was undertaken for form-finding using Wolfram SystemModeler, which whilst proving to be capable for form finding for arches, was unable to produce structural analysis output for the elements within the model and consequently this methodology was abandoned.

The CivilFEM methodology developed was applied to develop arches in equilibrium through forcing displacement of a chain of sprung struts with an initial deformation by the first mode buckling shape and then undertaking forced displacement analysis to develop the arched form.

Various arches were successfully form-found and a complex arch comprising of 18 degrees of freedom was solved showing that the method of analysis developed within this thesis is robust and able to develop a broad variety of structural forms containing springs.

Ill-conditioning was encountered during the analysis but overcome following the guidance developed in Objective 4.

### 7.2.6 Objective 6.

| To investigate different forms of springs that may be integrated within a spring chained strut/arch and identify potential implementations. |
|---|

A variety of springs were investigated which can be split into two key groups, linear and non-linear. The analysis engine of CivilFEM was tested with non-linear springs and it was identified that the output from the analysis required to be modified by the load increment to determine the critical buckling loads, but that the model was still valid.

A variety of non-linear springs were identified including those that could lock at pre-determined angles to create specific shapes through deployment as well as a spring that could model the connection between voussoirs by Beatini.

Potential implementations were highlighted including a folding portal frame type of structure, and as mentioned above, a spring between elements that could mimic the elastica of Beatini's work.

### 7.2.7 Objective 7.

| Develop novel structures that make use of the principles identified within the sprung struts that have clear and distinct advantages that may be applied to a real-world scenario. |
|---|

Two case studies were identified, the first was an arched structure which was able to displace laterally and become more aerodynamic and subsequently developed smaller bending moments in the elements compared to the equivalent static arch. The model for this structure was successful but it was acknowledged that once the structure had displaced the wind pressures acting upon it would also change and thus the structure may change shape again.

Further development for determining the iterative wind pressures would be an interesting point to develop, but by others.

The second case study was a kinematic façade element inspired by an origami fold that was able to expand and fold in the shape of the leaf. This model did not explicitly use springs, but instead built upon the concept of creating a spring through integrating materials of different elasticities, similar to the novel finite difference approach developed in this thesis. This created a digital model that was able to demonstrate the folding behaviour of the origami leaf and showed that

the stresses in the elements increased as the leaf folded to its most compact form.

A 3D printed, 4D model was created using a multi-material printer and as the model was folded by hand there was increased physical resistance to fold towards its final compact form which echoed the analysis models which showed the highest stresses in the fully folded form.

However, the printed model, after a number of folding cycles, started to show signs of fatigue and eventually split along one of the hinges, highlighting that durability of these kinds of structures is something that will need to be considered.

## 7.3 Unique Contributions.

A summary of some of the unique contributions to knowledge has been created to draw attention to where innovative research and application has been developed.

1) Determining the buckling capacity of sprung struts with more than a single spring.
2) Determining the critical buckling loads of sprung struts using the Finite Difference method, particularly with a large number of degrees of freedom.
3) Development of strategies for identifying and correcting the effects of ill-conditioning in sprung strut analysis.
4) Application of multi-spring hinged struts using buckled forms for deployable struts and adaptive structures.
5) Methodology for solving deployable structures through their deployment with up to 18 degrees of freedom using Finite Element Analysis.
6) The application of hinged struts to limit the axial force within an axial element in a frame.
7) Adaptive structures using rotational linear springs to develop three distinct structural behaviours within the elements. Specifically, the folding struts, where the application of a lateral displacement to a frame enabled the bracing to start as a compressive element, then buckle and become a bending element, then fold and have the central portion become a tension element.
8) The potential to use non-linear springs to hold a force at a constant value through the use of non-linear springs.

Adaptable and deployable structures that can adjust their behaviour are becoming more commonplace as research and the understanding of adaptable structures develops. The ability to integrate springs into a frame has been shown to be analytically challenging, but the methods developed in this thesis demonstrate an appropriate starting point in the development of determining their behaviour.

# Chapter 8

## 8 Further Work.

One of the hardest parts of writing this thesis was knowing when to stop and when enough had been done, several sections of work can be extended further, others that were almost complete but hampered by the limits of the software, and others that were started but were of such a scale they could form a topic for PhD research on their own.

Below is a small selection of many of the parts of research where the ideas contained within this thesis are anticipated to be expanded and developed further over the coming years, either by myself or with other people.

Fundamentally there are two primary strands that remain with respect to the development of the work contained within this thesis through to a proven practical application that I would like to consider. The first strand is the development of a physical rotational spring connection detail that has rotational stiffnesses and robustness that is compatible with a working structure. The broad principle was shown to be feasible with the 4D printed leaf structure, but fatigue and early failure along the creases proved to be a deficiency. Selecting and combining suitable materials in a manner to create weakened channels for plated structures and developing a hinge with compressible filler as shown in Figure 5-41 and Figure 5-42.

The second consideration is more of an opportunity than a barrier per se and relates to the nature that as the physical connection detail develops there is an opportunity that this will include a natural dampening capability. The ability to model the dampening of rotation springs has only just been added to CivilFEM in August 2020 and this presents an opportunity to investigate if rotationally sprung struts may present benefits in energy absorption/dissipation from accidental impact or blast loading situations by allowing structures to simulate yielding whilst remaining fully elastic.

## 8.1 Physical Testing.

Early test models were developed to determine the relationship of the beads and the central tendon when forming beaded chains, these have taken a variety of forms including polystyrene balls used to make Christmas decorations, wooden beads with a hole drilled through them, snooker balls with holes drilled through them, machined brass sections painted white with a red equatorial line to aid with data capture using Mathematica Scripts and cruciform struts to allow linear translational springs to develop an equivalent non-linear rotational spring stiffness. All of these models have been used primarily to aid with the visualisation of the structures to develop an understanding of the motion that is created through the introduction of flexible hinges.

What has become apparent as the research has matured is that there is a significant barrier to the introduction of the hinges in a real scaled structure either through the development of a suitable moment of resistance for the hinges as shown on the glue-laminated arch investigation, or through fatigue issues as identified within the leaf.

Further work will be needed to develop a more detailed, physical understanding of how these hinges may be reliably formed and manufactured to resist the scale of forces and number of cycles that these structures may require particularly given the failure of early 3D printed test models failing as outlined in section 6.3.2 as a result of fatigue.

One of the first proposed elements to be investigated is the development of the detail shown in Figure 5-42, the steel detailing of such a connection is relatively trivial but the integration of the soft infill material is an area that will require significant development.

## 8.2 Transient Analysis.

One of the primary shortfalls identified within CivilFEM during the work undertaken for this thesis is the unfortunate omission for the ability for damping and pre-load to be set for the rotational springs. The work contained within this thesis pushes hard at the capabilities of many of the commercially available Finite Element packages and has been undertaken with an open line of communication between the author and the software developers which has made the process enjoyable even when at its most challenging.

Many months have been spent trying to manipulate the Rayleigh Damping of the material to allow transient analysis to be undertaken to simulate blast analysis with mixed success.

For example, some successful models were developed for buckling and modal analysis which were subsequently adapted to develop a transient analysis. This was developed by determining

the range of modes that were developed that engaged approximately 80% of the mass of the system.

As can be seen in Table 4 most of the mass of the system is mobilised within the first four modes (over 80% of the mass) and consequently, the associated modal frequencies were used to develop the Rayleigh Damping Coefficients within CivilFEM. Sample visual representations of the modal analysis of the sprung strut frame are shown in Figure 8-1 which illustrates clearly that the bracing is the livelier part of the structure due to the introduction of the springs, which is as expected.

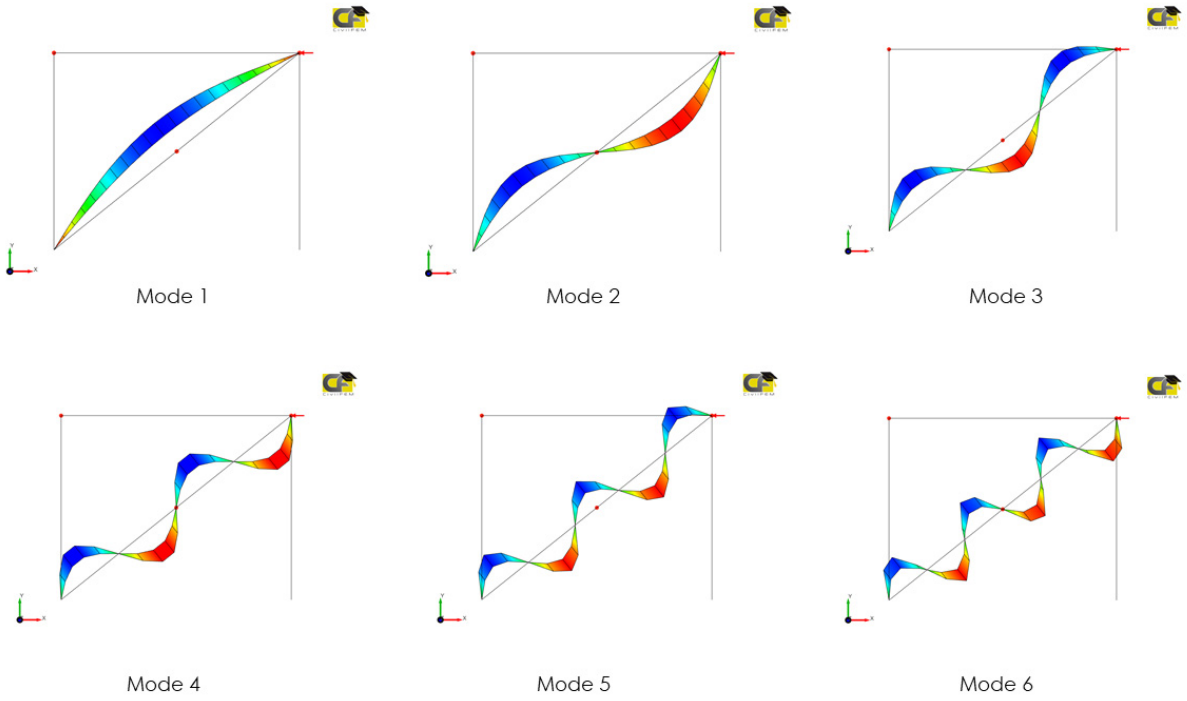


*Figure 8-1 - First 6 Modes of Frame Analysis.*

*Table 4 - Modal Analysis Output from CivilFEM.*

| Mode | Frequency Hz | Period s | ∑ MeffT kg | Mode | Frequency Hz | Period s | ∑ MeffT kg |
|---|---|---|---|---|---|---|---|
| **1** | 32.274 | 0.031 | 32.193 | **11** | 2186.885 | 0 | 0.074 |
| **2** | 136.171 | 0.007 | 0.169 | **12** | 2661.783 | 0 | 0.41 |
| **3** | 291.972 | 0.003 | 3.747 | **13** | 3055.265 | 0 | 0.659 |

| | | | | | | | |
|---|---|---|---|---|---|---|---|
| **4** | 432.51 | 0.002 | 32.201 | **14** | 3422.875 | 0 | 0.001 |
| **5** | 545.523 | 0.002 | 0.001 | **15** | 3958.686 | 0 | 0.399 |
| **6** | 814.617 | 0.001 | 1.331 | **16** | 3999.324 | 0 | 0.274 |
| **7** | 1227.877 | 0 | 0.003 | **17** | 4888.651 | 0 | 0.26 |
| **8** | 1296.319 | 0 | 3.59 | **18** | 4949.4 | 0 | 0.006 |
| **9** | 1603.196 | 0 | 0.68 | **19** | 5621.485 | 0 | 0.195 |
| **10** | 2167.713 | 0 | 1.224 | **20** | 5848.773 | 0 | 0.189 |

The range of frequencies to engage the first four modes range between 32.274Hz and 432.51Hz, which engage the majority of the mass within the system and these frequencies are used to develop the Rayleigh Damping Co-Efficients for the struts using the inbuilt CivilFEM routines.

Conveniently CivilFEM has a Rayleigh Damping calculator integrated as part of the material definition but whilst independently validating the CivilFEM routines using MathCAD sheets it was noted that CivilFEM uses the angular frequencies and subsequently needs multiplying by $2\pi$ before being inputted, see Figure 8-2 where the frequencies have been modified and the Rayleigh coefficients correctly calculated based on 5% damping.

| **S 275** | |
|---|---|
| Name | S 275 |
| Type | Structural steel |
| E | 2.1e+11 Pa |
| ν | 0.3 |
| ρ | 7850 kg/m³ |
| G | 8.07692e+10 Pa |
| α | 1.2e-05 1/ΔK |
| Act. time | 0 day |
| Deact. time | 36500 day |
| Steel type | Non austenitic |
| ⊞ Thickness | (3) |
| ⊞ **Design σ-ε diagram** | |
| ⊞ **Code properties** | |
| ⊟ **Damping** | |
| Automatic | ☑ |
| α | 18.8687 1/s |
| β | 3.42805e-05 s |
| Damping | 5 % |
| ω min. | 202.784 1/s |
| ω max. | 2714.33 1/s |

*Figure 8-2 - Rayleigh Damping Co-Efficient Determined from Modal Analysis.*

With some damping now applied to the frames, a blast loading can be defined (see Figure 8-3) which in this instance mimics a 34kN/m UDL ramped linearly from zero up to 34kN/m over 100ms and which then drops back to zero after 100ms.

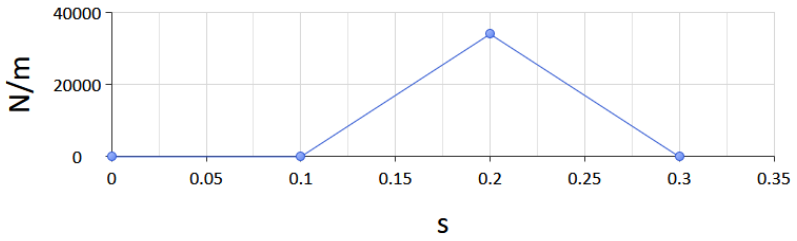


*Figure 8-3 - Indicative Lateral Blast Loading.*

Numerous analysis models were undertaken and generally, the lateral behaviour of the structures seems reasonable with the structure reaching equilibrium positions in a reasonably well-defined manner see Figure 8-4 and Figure 8-5, but there were issues with the structures being able to recover their original position post-blast. This is a result of the mass of the structure holding the frame in position as the springs were not preloaded with a recovery force once rotated out of place. This could be overcome by applying an equivalent restorative moment at the hinge positions which would model a more realistic spring by providing a returning force.

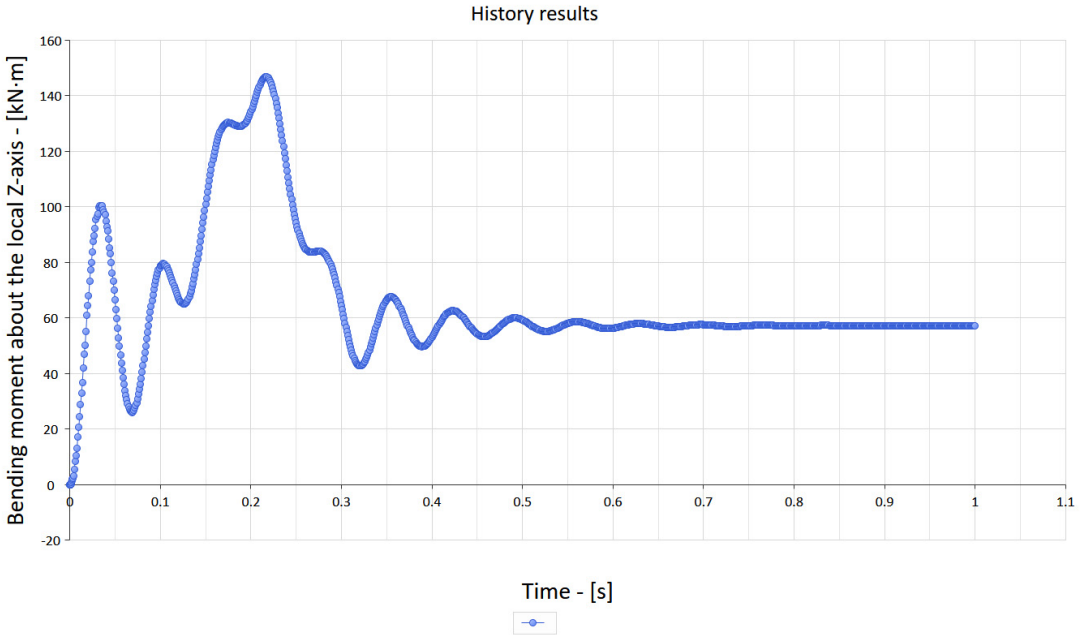


*Figure 8-4 – Bending Moment With Spring.*

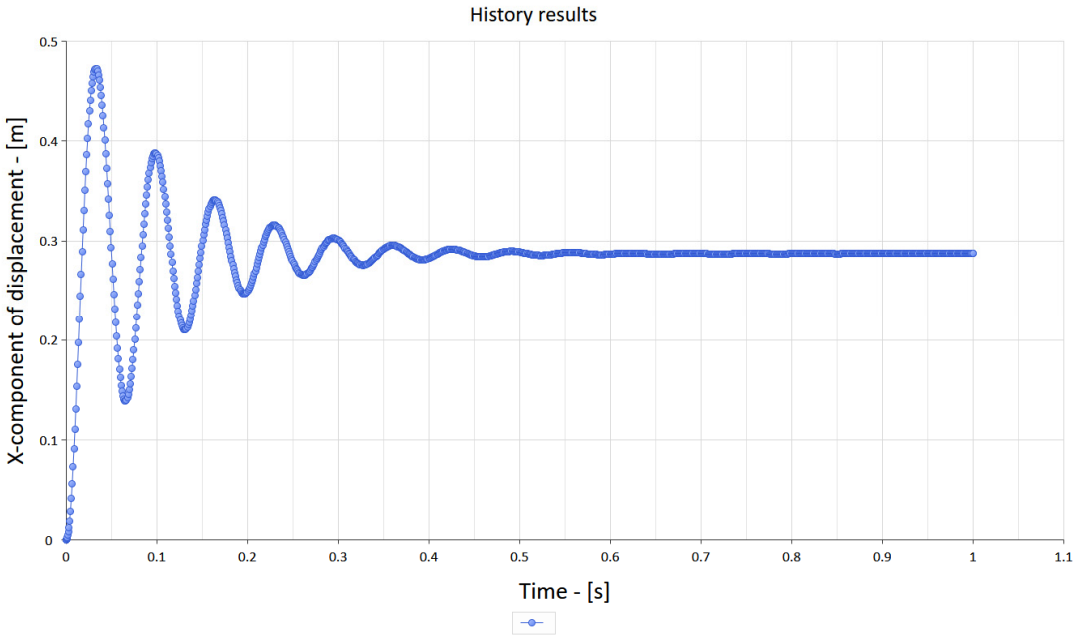


*Figure 8-5 - Eaves Deflection.*

Whilst the above graphs give the illusion of a well-behaved system, the bracing force flips between tension and compression (see Figure 8-6) which is incorrect and brings into doubt the validity of the modelling generally within the transient analysis.

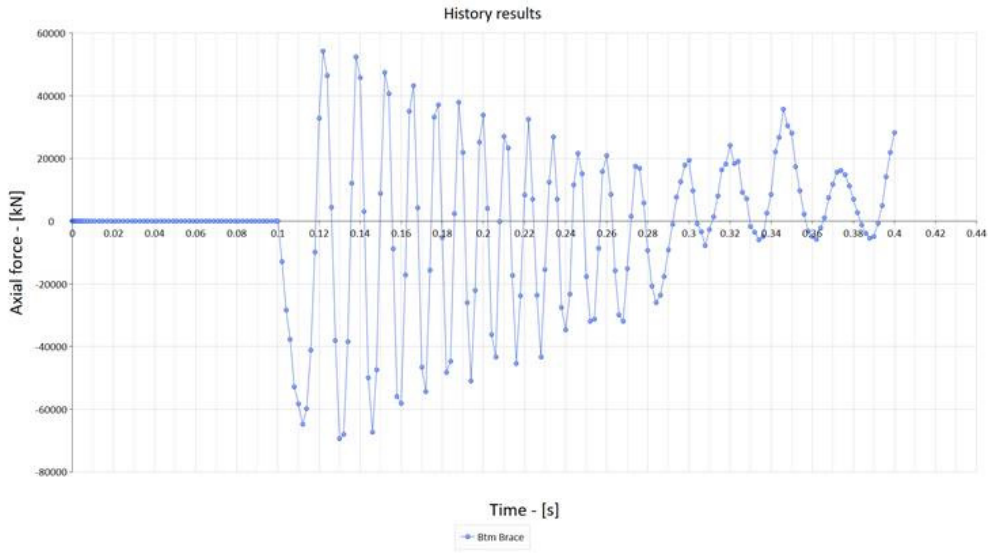


*Figure 8-6 - Axial Force Bottom Section of the Bracing.*

The release of CivilFEM 2019 was intended to have damping enabled for rotational springs, but two patches into the release it has still not been integrated.

# References…


Adriaenssens, S. M. L., & Barnes, M. R. (2001). Tensegrity spline beam and grid shell structures. *Engineering structures, 23*(1), 29-36. doi:10.1016/s0141-0296(00)00019-5

Adrover, E. R. (2015). *Deployable Structures*. London: Laurence King Publishing London.

Akgün, Y., Gantes, C. J., Kalochairetis, K. E., & Kiper, G. k. (2010). A novel concept of convertible roofs with high transformability consisting of planar scissor-hinge structures. *Engineering structures, 32*(9), 2873-2883. doi:10.1016/j.engstruct.2010.05.006

Akgün, Y., Gantes, C. J., Sobek, W., Korkmaz, K., & Kalochairetis, K. (2011). A novel adaptive spatial scissor-hinge structural mechanism for convertible roofs. *Engineering structures, 33*(4), 1365-1376. doi:10.1016/j.engstruct.2011.01.014

Al-Sadder, S., Shatnawi, A. S., & Dado, M. (2007). Exact post-buckling configurations of cantilevered column subjected to forces produced by a tensioned cable. *Mechanics Research Communications, 34*(4), 395-404. doi:10.1016/j.mechrescom.2007.03.001

Alegria Mira, L., Thrall, A. P., & De Temmerman, N. (2014). Deployable scissor arch for transitional shelters. *Automation in Construction, 43*, 123-131. doi:10.1016/j.autcon.2014.03.014

Allen, H. G., & Bulson, P. S. (1980). *Background to Buckling*. London: McGraw Hill Book Company Ltd.

Ario, I., Nakazawa, M., Tanaka, Y., Tanikura, I., & Ono, S. (2013). Development of a prototype deployable bridge based on origami skill. *Automation in Construction, 32*, 104-111. doi:10.1016/j.autcon.2013.01.012

Attia, S. (2018). Evaluation of adaptive facades: The case study of Al Bahr Towers in the UAE. *QScience Connect, Special Issue on Shaping Qatar's Sustainable Built Environment, 2017*(2), 6-18.

Barnes, M., & Dickson, M. (2000). *Widespan Roof Structures*. London: Thomas Telford.

Bazant, Z. P., & Cedolin, L. (2010). *Stability of Structures: Elastic, Inelastic, Fracture and Damage Theories*. Singapore: World Scientific.

Beatini, V., & Royer-Carfagni, G. (2013). Cable-stiffened foldable elastica for movable structures. *Engineering structures, 56*, 126-136.

Bel Hadj Ali, N., Rhode-Barbarigos, L., Pascual Albi, A. A., & Smith, I. F. C. (2010). Design optimization and dynamic analysis of a tensegrity-based footbridge. *Engineering structures, 32*(11), 3650-3659. doi:10.1016/j.engstruct.2010.08.009

Bel Hadj Ali, N., Rhode-Barbarigos, L., & Smith, I. F. C. (2011). Analysis of clustered tensegrity structures using a modified dynamic relaxation algorithm. *International Journal of Solids and Structures, 48*(5), 637-647. doi:10.1016/j.ijsolstr.2010.10.029

Bel Hadj Ali, N., & Smith, I. F. C. (2010). Dynamic behavior and vibration control of a tensegrity structure. *International Journal of Solids and Structures, 47*(9), 1285-1296. doi:10.1016/j.ijsolstr.2010.01.012

Brouwer, G. (2002). Retractable arch will take center stage in Salt Lake. *Civil Engineering, 72*(1),

15.
Bruns, T., Sigmund, O., & Tortorelli, D. A. (2002). Numerical methods for the topology optimization of structures that exhibit snap-through. *International Journal for Numerical Methods in Engineering, 55*(10), 1215-1237.
Cai, J., Deng, X., Feng, J., & Xu, Y. (2014). Mobility analysis of generalized angulated scissor-like elements with the reciprocal screw theory. *Mechanism and Machine Theory, 82*, 256-265. doi:10.1016/j.mechmachtheory.2014.07.011
Calladine, C. R. (1978). Buckminster Fuller's "Tensegrity" structures and Clerk Maxwell's rules for the construction of stiff frames. *International Journal of Solids and Structures, 14*(2), 161-172.
Calladine, C. R., & Pellegrino, S. (1991). First-order infinitesimal mechanisms. *International Journal of Solids and Structures, 27*(4), 505-515. doi:10.1016/0020-7683(91)90137-5
Chen, Y., You, Z., & Tarnai, T. (2005). Threefold-symmetric Bricard linkages for deployable structures. *International Journal of Solids and Structures, 42*(8), 2287-2301. doi:DOI: 10.1016/j.ijsolstr.2004.09.014
Chi Tran, H., & Lee, J. (2010). Advanced form-finding for cable-strut structures. *International Journal of Solids and Structures, 47*(14-15), 1785-1794. doi:10.1016/j.ijsolstr.2010.03.008
Chilton, J. (2000). *Space Grid Structures*. Oxford: Architectural Press.
Coates, R. C., Coutie, M. G., & Kong, F. K. (1988). *Structural Analysis* (3rd ed.). London: Chapman & Hall.
Croll, J. G. A., & Walker, A. C. (1972). *Elements of Structural Stability*. London: MacMillan.
Crosby, A. J. (2010). Why should we care about buckling? *Soft Matter, 6*(22), 5660-5660.
Davey, M., Bellew, P., Er, K., Kwek, A., & Lim, J. (2010). Gardens by the Bay: High performance through design optimization and integration. *Intelligent Buildings International, 2*(2), 140-157.
De Temmerman, N., Alegria Mira, L., & Vergauwen, A. (2012). Feasibility of the Universal Scissor Component (USC): Building a Full-Scale Deployable Dome. *Journal for the International Association for Shell and Spatial Structures, 53*(174), 227-236.
Del Grosso, A. E., & Basso, P. (2010). Adaptive building skin structures. *Smart Materials and Structures, 19*(12), 124011.
Del Grosso, A. E., & Basso, P. (2013). Deployable structures. *Advances in Science and Technology, 83*, 122-131.
Demaine, E. D., & O'Rourke, J. (2007). *Geometric Folding Algorithms: Linkages, Origami, Polyhedra*. Cambridge: Cambridge University Press.
Deng, H., Jiang, Q. F., & Kwan, A. S. K. (2005). Shape finding of incomplete cable-strut assemblies containing slack and prestressed elements. *Computers & Structures, 83*(21-22), 1767-1779. doi:10.1016/j.compstruc.2005.02.022
Deng, H., & Kwan, A. S. K. (2005). Unified classification of stability of pin-jointed bar assemblies. *International Journal of Solids and Structures, 42*(15), 4393-4413. doi:10.1016/j.ijsolstr.2005.01.009
Descamps, B. (2014). *Computational Design of Lightweight Structures*. London: John Wiley & Sons.
Escrig, F. (1984). Estructuras espaciales de barras desplegables. *Informes de la Construcción, 36*(365), 35-46.
Escrig, F., & Valcarcel, J. P. (1993). Geometry of Expandable Space Structures. *International Journal of Space Structures, 8*(1&2), 71-84.
Estrada, M. A., Hawkes, E. W., Christensen, D. L., & Cutkosky, M. R. (2014). *Perching and vertical climbing: Design of a multimodal robot*. Paper presented at the 2014 IEEE International Conference on Robotics and Automation (ICRA).
Fenci, G. E., & Currie, N. G. R. (2017a). Deployable structures classification: A review. *International Journal of Space Structures, 32*(2), 112-130.

Fenci, G. E., & Currie, N. G. R. (2017b). Optimisation Of The Deployment Sequence Of 2 Dof Systems. *International Journal of Computational Methods and Experimental Measurements, 5*(4), 504-513.
Fortmeyer, R., & Linn, C. D. (2014). *Kinetic Architecture: Design for Active Envelopes*. Victoria, Australia: Images Publishing.
Friedman, N., & Ibrahimbegovic, A. (2013). Overview of highly flexible, deployable lattice structures used in architecture and civil engineering undergoing large displacements. *YBL Journal of Built Environment, 1*(1), 85-103.
Frumar, J. A., Zhou, Y. Y., Xie, Y. M., & Burry, M. C. (2009). Tensegrity structures with 3D compressed components: development, assembly and design. *Journal of the International Association of Shell and Spatial Structures, 50*(161), 99-110.
Gantes, C. (1997). An improved analytical model for the prediction of the nonlinear behavior of flat and curved deployable space frames. *Journal of Constructional Steel Research, 44*(1-2), 129-158. doi:10.1016/s0143-974x(97)00042-4
Gantes, C. (2001). *Deployable Structures: Analysis and Design* (First ed.). Southampton: WIT Press.
Gantes, C., Connor, J. J., & Logcher, R. D. (1993). Simple Friction Model for Scissor-Type Mobile Structures. *Journal of Engineering Mechanics, 119*(3), 456-475.
Gantes, C., Connor, J. J., Logcher, R. D., & Rosenfeld, Y. (1989). Structural analysis and design of deployable structures. *Computers & Structures, 32*(3-4), 661-669.
Gantes, C., Giakoumakis, A., & Vousvounis, P. (1997). Symbolic manipulation as a tool for design of deployable domes. *Computers & Structures, 64*(1-4), 865-878. doi:10.1016/s0045-7949(96)00433-6
Gantes, C., & Konitopoulou, E. (2004). Geometric design of arbitrarily curved bi-stable deployable arches with discrete joint size. *International Journal of Solids and Structures, 41*(20), 5517-5540.
Gengnagel, C., & Burford, N. (2006). *Transformable Structures for Mobile Shelters*. Paper presented at the Adaptables 2006 - International Conference on Adaptable Building Structures, Eindhoven.
Gere, J. M., & Goodno, B. J. (2012). *Mechanics of Materials, SI Edition* (8th ed.). Stamford: Cl Engineering - M.U.A.
Gibson, I., Goenka, G., Narasimhan, R., & Bhat, N. (2010). *Design rules for additive manufacture*. Paper presented at the Solid Freeform Fabrication Symposium.
González, N., Kerl, F.-J., & Engineers, A. (2008). EOS Design Rules Design study: living hinge sintering. *EOS*.
Hachem, C., & Hanaor, A. (2005). Deployable applications based on biological organisms. *Journal for the International Association for Shell and Spatial Structures, 46*(148), 95-106.
Hanaor, A., & Levy, R. (2001). Evaluation of deployable structures for space enclosures. *International Journal of Space Structures, 16*(4), 211-229.
Harrhuis, K. J. (2012). Maximally Transparent Barrel-Vaulted Glass Roof. *Journal of the international association for shell and spatial structures, 53*(173), 163-168.
Hencky, H. (1921). Über die angenäherte Lösung von Stabilitätsproblemen im Raum mittels der elastischen Gelenkkette. *Der Eisenbau, 11*, 437-452.
Hernandez, C. H. (1996). New ideas on deployable structures. In F. Escrig & C. A. Brebbia (Eds.), *Mobile and Rapidly Assembled Structures II* (pp. 63-72). Southampton: WIT Press.
Hirst, A. E. (1995). *Vectors in 2 or 3 Dimensions* (First ed.). London: Arnold.
Hoberman, C. (1990). Reversibly expandable doubly-curved truss structure: Google Patents.
Hosozawa, O., Shimamura, K., & Mizutani, T. (1999). The role of cables in large span spatial structures: introduction of recent space structures with cables in Japan. *Engineering structures, 21*(8), 795-804. doi:10.1016/S0141-0296(98)00032-7
Hover, F. S., & Triantafyllou, M. S. (1999). LINEAR DYNAMICS OF CURVED

TENSIONED ELASTIC BEAMS. *Journal of Sound and Vibration, 228*(4), 923-930. doi:10.1006/jsvi.1999.2497
Hu, N., & Burgueño, R. (2015). Buckling-induced smart applications: recent advances and trends. *Smart Materials and Structures, 24*(6), 063001.
Iremonger, M. (1980). Finite difference buckling analysis of non-uniform columns. *Computers & Structures, 12*(5), 741-748.
Ishii, K. (Ed.) (2000). *Structural Design of Retractable Roof Structures*. Southampton: WiT Press.
IStructE. (2007). *Temporary demountable structures: Guidance on procurement, design and use* (Third ed.). London: The Institution of Structural Engineers.
Jazar, R. N. (2010). *Theory of Applied Robotics: Kinematics, Dynamics, and Control*. London: Springer.
Juan, S. H. n., & Mirats Tur, J. M. (2008). Tensegrity frameworks: Static analysis review. *Mechanism and Machine Theory, 43*(7), 859-881. doi:10.1016/j.mechmachtheory.2007.06.010
Kalathur, H., & Lakes, R. (2013). Column dampers with negative stiffness: high damping at small amplitude. *Smart Materials and Structures, 22*(8), 084013.
Kaveh, A., & Davaran, A. (1996). Analysis of pantograph foldable structures. *Computers & Structures, 59*(1), 131-140. doi:10.1016/0045-7949(95)00231-6
Kaveh, A., Jafarvand, A., & Barkhordari, M. A. (1999). Optimal Design of Pantograph Foldable Structures. *International Journal of Space Structures, 14*(4), 295-302.
Kebadze, E., Guest, S. D., & Pellegrino, S. (2004). Bistable prestressed shell structures. *International Journal of Solids and Structures, 41*(11-12), 2801-2820. doi:10.1016/j.ijsolstr.2004.01.028
Kiper, G., Söylemez, E., & Kişisel, A. U. Ö. (2008). A family of deployable polygons and polyhedra. *Mechanism and Machine Theory, 43*(5), 627-640. doi:10.1016/j.mechmachtheory.2007.04.011
Knaack, U. a. (2014). Chapter 6 - Adaptive Facades *Façades : principles of construction* (Second and revised edition. ed., pp. 85-101): Boston : Birkhäuser.
Knippers, J., Cremers, J., Gabler, M., & Lienhard, J. (2011). *Construction manual for polymers+ membranes: materials, semi-finished products, form finding, design*. Munich: Birkhäuser.
Knippers, J., Nickel, K. G., & Speck, T. (2016). *Biomimetic research for architecture and building construction : biological design and integrative structures*: New York, NY : Springer Berlin Heidelberg.
Knippers, J., & Speck, T. (2012). Design and construction principles in nature and architecture. *Bioinspiration & Biomimetics, 7*(1), 1-10.
Korkmaz, K. (2004). *An analytical study of the design potentials in kinetic architecture.* (PhD), İzmir Institute of Technology, İzmir.
Kuribayashi, K., Tsuchiya, K., You, Z., Tomus, D., Umemoto, M., Ito, T., & Sasaki, M. (2006). Self-deployable origami stent grafts as a biomedical application of Ni-rich TiNi shape memory alloy foil. *Materials Science and Engineering: A, 419*(1-2), 131-137. doi:10.1016/j.msea.2005.12.016
Kuznetsov, E. N. (1999). Singular configurations of structural systems. *International Journal of Solids and Structures, 36*(6), 885-897. doi:10.1016/S0020-7683(97)00333-8
Kwan, A. S. K., & Pellegrino, S. (1991). The Pantographic Deployable Mast: design, structural performance, and deployment tests. In P. S. Bulson (Ed.), *Rapidly Assembled Structures* (Vol. 8, pp. 213-224). Chippenham: Computational Mechanics Publications.
Lachenal, X., Daynes, S., & Weaver, P. M. (2014). A non-linear stiffness composite twisting I-beam. *Journal of Intelligent Material Systems and Structures, 25*(6), 744-754.
Laet, L. D., Luchsinger, R. H., Crettol, R., Mollaert, M., & Temmerman, N. D. (2009). Deployable tensairity structures *Journal for the International Association for Shell and Spatial Structures, 50*(161), 121-128.
Langbecker, T., & Albermani, F. (2001). Kinematic and non-linear analysis of foldable barrel

vaults. *Engineering structures, 23*(2), 158-171. doi:10.1016/s0141-0296(00)00033-x
Li, Y., Vu, K. K., & Richard, J. Y. (2011). Deployable Cable-Chain Structures: Morphology, Structural Response And Robustness Study. *Journal for the International Association for Shell and Spatial Structures, 52*(168), 83-96.
Lienhard, J., & Knippers, J. (2013). Considerations on the scaling of bending-active structures. *International Journal of Space Structures, 28*(3-4), 137-148.
Long, A., Kirkpatrick, J., Gupta, A., Nanukuttan, S., & Polin, D. M. (2013). *Rapid Construction of arch bridges using the innovative FlexiArch*. Paper presented at the Proceedings of the Institution of Civil Engineers-Bridge Engineering.
MacLeod, I. A. (2005). *Modern structural analysis: Modelling process and guidance*. London: Thomas Telford.
Masic, M., Skelton, R. E., & Gill, P. E. (2006). Optimization of tensegrity structures. *International Journal of Solids and Structures, 43*(16), 4687-4703. doi:10.1016/j.ijsolstr.2005.07.046
Maurin, B., Motro, R., Raducanu, V., & Pauli, N. (2005). Soft "Tensegrity Like" Panel: Conceptual Design And Form - Finding. *Journal of the International Association of Shell and Spatial Structures, 49*(158), 77-87.
Merchan, C. H. H. (1987). *Deployable structures.* (MSc), Massachusetts Institute of Technology, Dept. of Architecture.
Miura, K. (2009). The Science of Miura-Ori: A Review *Origami⁴* (pp. 99-112). Boca Raton: AK Peters/CRC Press.
Moored, K. W., & Bart-Smith, H. (2009). Investigation of clustered actuation in tensegrity structures. *International Journal of Solids and Structures, 46*(17), 3272-3281. doi:10.1016/j.ijsolstr.2009.04.026
Motro, R. (1992). Tensegrity systems: the state of the art. *International Journal of Space Structures, 7*(2), 75-83.
Motro, R., & Gerardo Oliva, J. S. (2010). Who is the designer? *Journal for the International Association for Shell and Spatial Structures, 51*(165), 207-216.
Nagaraj, B. P., Pandiyan, R., & Ghosal, A. (2010). A constraint Jacobian based approach for static analysis of pantograph masts. *Computers & Structures, 88*(1-2), 95-104. doi:10.1016/j.compstruc.2009.09.007
O'Rourke, J. (2011). *How to fold it: The mathematics of linkages, origami and polyhedra* (First ed.). Cambridge: Cambridge University Press.
Pellegrino, S. (1990). Analysis of prestressed mechanisms. *International Journal of Solids and Structures, 26*(12), 1329-1350.
Pellegrino, S. (1993). Structural computations with the singular value decomposition of the equilibrium matrix. *International Journal of Solids and Structures, 30*(21), 3025-3035. doi:10.1016/0020-7683(93)90210-x
Pellegrino, S. (2001). *Deployable Structures* (First ed. Vol. 412). Udine: SpringerWeinNewYork.
Pellegrino, S., & Calladine, C. R. (1986). Matrix analysis of statically and kinematically indeterminate frameworks. *International Journal of Solids and Structures, 22*(4), 409-428.
Peña, D. M., Llorens, I., Sastre, R., Crespo, D., & Martínez, J. (2011). Application of tensegrity to tensile-textile constructions: formfinding and structural analysis. *Journal for the International Association for Shell and Spatial Structures, 52*(168), 67-81.
Peraza Hernandez, E. A., Hu, S., Kung, H. W., Hartl, D., & Akleman, E. (2013). Towards building smart self-folding structures. *Computers & Graphics, 37*(6), 730-742. doi:10.1016/j.cag.2013.05.022
Perrone, N., & Kao, R. (1975). A general finite difference method for arbitrary meshes. *Computers & Structures, 5*(1), 45-57.
Petroski, H. (2004). Deployable Structures. *American Scientist, 92* (March/April), 122-126.
Phocas, M. C., & Alexandrou, K. C. (2017). Adaptive Structures – Soft Mechanical Approach.

*International Journal of Computational Methods and Experimental Measurements, 5*(4), 421-431.
Piñero , E. P. (1965).
Plaut, R. H., Goh, J. K. S., Kigudde, M., & Hammerand, D. C. (2000). Shell analysis of an inflatable arch subjected to snow and wind loading. *International Journal of Solids and Structures, 37*(31), 4275-4288.
Ramzy, N., & Fayed, H. (2011). Kinetic systems in architecture: New approach for environmental control systems and context-sensitive buildings. *Sustainable Cities and Society, 1*(3), 170-177. doi:10.1016/j.scs.2011.07.004
Raskin, I., & Roorda, J. (1996). Buckling Force for Deployable Pantographic Columns. *Mobile and Rapidly Assembled Structures II, Proc. MARAS, 96*, 305-314.
Rauschenbach, H. S. (2012). *Solar cell array design handbook: the principles and technology of photovoltaic energy conversion*. London: New York: Von Nostrand Reinhold Company.
Rhode-Barbarigos, L., Hadj Ali, N. B., Motro, R., & Smith, I. F. C. (2010). Designing tensegrity modules for pedestrian bridges. *Engineering structures, 32*(4), 1158-1167. doi:10.1016/j.engstruct.2009.12.042
Ruocco, E., Zhang, H., & Wang, C. (2016). Hencky bar-chain model for buckling analysis of non-uniform columns. *Structures, 6*, 73-84.
Saito, D., & Wadee, M. A. (2009). Buckling behaviour of prestressed steel stayed columns with imperfections and stress limitation. *Engineering structures, 31*(1), 1-15. doi:10.1016/j.engstruct.2008.07.006
Saitoh, M., & Okada, A. (1999). The role of string in hybrid string structure. *Engineering structures, 21*(8), 756-769. doi:10.1016/S0141-0296(98)00029-7
Santer, M., & Pellegrino, S. (2008). Compliant multistable structural elements. *International Journal of Solids and Structures, 45*(24), 6190-6204. doi:10.1016/j.ijsolstr.2008.07.014
Schleicher, S., Lienhard, J., Poppinga, S., Speck, T., & Knippers, J. (2015). A methodology for transferring principles of plant movements to elastic systems in architecture. *Computer-Aided Design, 60*, 105-117. doi:10.1016/j.cad.2014.01.005
Seffen, K. A., You, Z., & Pellegrino, S. (2000). Folding and deployment of curved tape springs. *International Journal of Mechanical Sciences, 42*(10), 2055-2073. doi:10.1016/s0020-7403(99)00056-9
Senatore, G. (2018). Designing and Prototyping Adaptive Structures—An Energy-Based Approach Beyond Lightweight Design *Robotic Building* (pp. 169-189). London: Springer.
Senatore, G., Duffour, P., Hanna, S., Labbé, F., & Winslow, P. (2011). Adaptive structures for whole-life energy savings. *Journal of the international association for shell and spatial structures, 52*(4), 233-240.
Senatore, G., Duffour, P., & Winslow, P. (2018a). Energy and Cost Assessment of Adaptive Structures: Case Studies. *Journal of Structural Engineering, 144*(8), 04018107.
Senatore, G., Duffour, P., & Winslow, P. (2018b). Exploring the application domain of adaptive structures. *Engineering structures, 167*, 608-628. doi:10.1016/j.engstruct.2018.03.057
Senatore, G., Duffour, P., Winslow, P., & Wise, C. (2017). Shape control and whole-life energy assessment of an 'infinitely stiff'prototype adaptive structure. *Smart Materials and Structures, 27*(1), 15-22.
Senatore, G., & Piker, D. (2015). Interactive real-time physics: An intuitive approach to form-finding and structural analysis for design and education. *Computer-Aided Design, 61*, 32-41.
Shan, W., & Chen, Z. (2013). Mechanical instability of thin elastic rods. *Journal of Postdoctoral Research February, 1*(2), 1-8.
Shea, K., Fest, E., & Smith, I. F. C. (2002). Developing intelligent tensegrity structures with stochastic search. *Advanced Engineering Informatics, 16*(1), 21-40. doi:10.1016/s1474-0346(02)00003-4
Sinan, K. (2011). A review of active structural control: challenges for engineering informatics.

*Computers & Structures, 89*(23-24), 2113-2132. doi:10.1016/j.compstruc.2011.07.010
Smith, B. W., & Chase, J. G. (2001). Design of MEMS-based Stabilization for Buckling Constrained Structures. *International Journal of Structural Stability and Dynamics, 1*(04), 467-484.
Snelson, K. (1996). Snelson on the tensegrity invention. *International Journal of Space Structures, 11*(1-2), 43-48.
Stevenson, C. (2011). *Morphological Principles: Current Kinetic Architectural Structures*. Paper presented at the International Adaptive Architecture Conference, Building Centre, London.
Sunguroglu Hensel, D., & Baraut Bover, G. (2013). Nested Catenaries. *Journal of the International Association of Shell and Spatial Structures, 54*(175), 39-55.
Tachi, T. (2009a). Generalization of rigid-foldable quadrilateral-mesh origami. *Journal of the international association for shell and spatial structures, 50*(3), 173-179.
Tachi, T. (2009b). Generalization of rigid-foldable quadrilateral-mesh origami. *Journal for the International Association for Shell and Spatial Structures, 50*(162), 173-179.
Tachi, T. (2011). Rigid-foldable thick origami *Origami*$^5$ (First ed., Vol. 5, pp. 253-264). Boca Raton: CRC Press.
Takatsuka, M., & Ohmori, H. (2011). 2D-Deployable Flat-Panel Structure. *Journal for the International Association for Shell and Spatial Structures, 52*(168), 109-120.
Tan, G. E. B., & Pellegrino, S. (2008). Nonlinear vibration of cable-stiffened pantographic deployable structures. *Journal of Sound and Vibration, 314*(3-5), 783-802. doi:10.1016/j.jsv.2008.01.022
Thrall, A. P., & Quaglia, C. P. (2014). Accordion shelters: A historical review of origami-like deployable shelters developed by the US military. *Engineering structures, 59*, 686-692. doi:10.1016/j.engstruct.2013.11.009
Tibbits, S. (2014). 4D Printing: Multi-material shape change. *Architectural Design, 84*(1), 116-121.
Tibert, A., & Pellegrino, S. (2003). Review of form-finding methods for tensegrity structures. *International Journal of Space Structures, 18*(4), 209-223.
Timoshenko, S. P., & Gere, J. M. (2009). *Theory of Elastic Stability* (2nd ed.). New York: Dover.
Trometer, S., & Krupna, M. (2006). Development and Design of Glass Folded Plate Structures. *Journal of the international association for shell and spatial structures, 47*(152), 253-260.
Valcárcel, J. P., & Escrig, F. (1996). Recent advances in the analysis of expandable structures. In F. Escrig & C. A. Brebbia (Eds.), *Mobile and Rapidly Assembled Structures II* (pp. 45-54). Southampton: WIT Press.
Vu, K. K., Richard Liew, J. Y., & Anandasivam, K. (2006). Deployable tension-strut structures: from concept to implementation. *Journal of Constructional Steel Research, 62*(3), 195-209. doi:10.1016/j.jcsr.2005.07.007
Wadee, M. A., Gardner, L., & Osofero, A. I. (2013). Design of prestressed stayed columns. *Journal of Constructional Steel Research, 80*, 287-298. doi:10.1016/j.jcsr.2012.09.021
Wagg, D., Bond, I., Weaver, P., & Friswell, M. (2007). *Adaptive Structures Engineering Applications*. Chichester: Wiley.
Wakefield, D. (1999). Engineering analysis of tension structures: theory and practice. *Engineering structures, 21*(8), 680-690.
Walker, A. C. (Ed.) (1975). *Buckling of Struts*. Edinburgh: Chatto & Windus.
Wang-Iverson, P., Lang, R. J., & Yim, M. (2011). *Origami*$^5$ (First ed.). Boca Raton: CRC Press.
Wang, B.-B. (1998). Cable-strut systems: part I - tensegrity. *Journal of Constructional Steel Research, 45*(3), 281-289. doi:10.1016/s0143-974x(97)00075-8
Wang, C. M., Zhang, H., Gao, R., Duan, W., & Challamel, N. (2015). Hencky bar-chain model for buckling and vibration of beams with elastic end restraints. *International Journal of Structural Stability and Dynamics, 15*(07), 1540007.
Wang, J., & Kong, X. (2018). Deployable mechanisms constructed by connecting orthogonal

Bricard linkages, 8R or 10R single-loop linkages using S joints. *Mechanism and Machine Theory, 120*, 178-191.
Williamson, D., Skelton, R. E., & Han, J. (2003). Equilibrium conditions of a tensegrity structure. *International Journal of Solids and Structures, 40*(23), 6347-6367. doi:10.1016/s0020-7683(03)00400-1
Wohlhart, K. (1993). The two types of the orthogonal Bricard linkage. *Mechanism and Machine Theory, 28*(6), 809-817.
Wu, M. (2008). Analytical method for the lateral buckling of the struts in beam string structures. *Engineering structures, 30*(9), 2301-2310. doi:10.1016/j.engstruct.2008.01.008
Wu, M., & Sasaki, M. (2007). Structural behaviors of an arch stiffened by cables. *Engineering structures, 29*(4), 529-541. doi:10.1016/j.engstruct.2006.05.018
Xue, W., & Liu, S. (2009). Design optimization and experimental study on beam string structures. *Journal of Constructional Steel Research, 65*(1), 70-80. doi:10.1016/j.jcsr.2008.08.009
Yavin, Y. (1998). The control of the motion of a pantograph. *Mathematical and Computer Modelling, 28*(2), 13-23. doi:10.1016/s0895-7177(98)00088-0
Yee, J. C. H., & Pellegrino, S. (2005). Folding of woven composite structures. *Composites Part A: Applied Science and Manufacturing, 36*(2), 273-278. doi:10.1016/j.compositesa.2004.06.017
Yoshiaki, G., Yasuhito, W., Toshihiro, K., & Makoto, O. (1992). Elastic buckling phenomenon applicable to deployable rings. *International Journal of Solids and Structures, 29*(7), 893-909. doi:10.1016/0020-7683(92)90024-n
Yoshimura, Y. (1955). *NACA Technical Memorandum 1390 - On the mechanism of buckling of a circular cylindrical shell under axial compression.* Washington: NACA.
You, Z. (2007). Motion structures extend their reach. *Materials Today, 10*(12), 52-57. doi:10.1016/s1369-7021(07)70308-5
You, Z., & Chan, Y. C. (2012). *Motion Structures.* Abingdon: Spon Press.
You, Z., & Pellegrino, S. (1997). Foldable bar structures. *International Journal of Solids and Structures, 34*(15), 1825-1847. doi:Doi: 10.1016/s0020-7683(96)00125-4
Zhang, H., Wang, C., & Challamel, N. (2016). Buckling and vibration of Hencky bar-chain with internal elastic springs. *International Journal of Mechanical Sciences, 119*, 383-395.
Zhao, J.-S., Chu, F., & Feng, Z.-J. (2009). The mechanism theory and application of deployable structures based on SLE. *Mechanism and Machine Theory, 44*(2), 324-335. doi:10.1016/j.mechmachtheory.2008.03.014
Zhao, J.-S., Feng, Z., Chu, F., & Ma, N. (2014). Chapter 11 - Mechanism Theory and Application of Deployable Structures Based on Scissor-Like Elements. In J. Zhao, Z. Feng, F. Chu, & N. Ma (Eds.), *Advanced Theory of Constraint and Motion Analysis for Robot Mechanisms* (pp. 349-366). Oxford: Academic Press.
Zhao, M., & Guan, F. (2005). Kinematic analysis of deployable toroidal spatial truss structures for large mesh antenna. *Journal for the International Association for Shell and Spatial Structures, 46*(149), 195-204.

# Index

# Appendix 1

This appendix provides a sample of some of the Mathematica Scripts used for developing the geometry of cable-chain arches, both parabolic and circular.

# Split a curve into equal segments...

```
Remove["Global`*"];
```

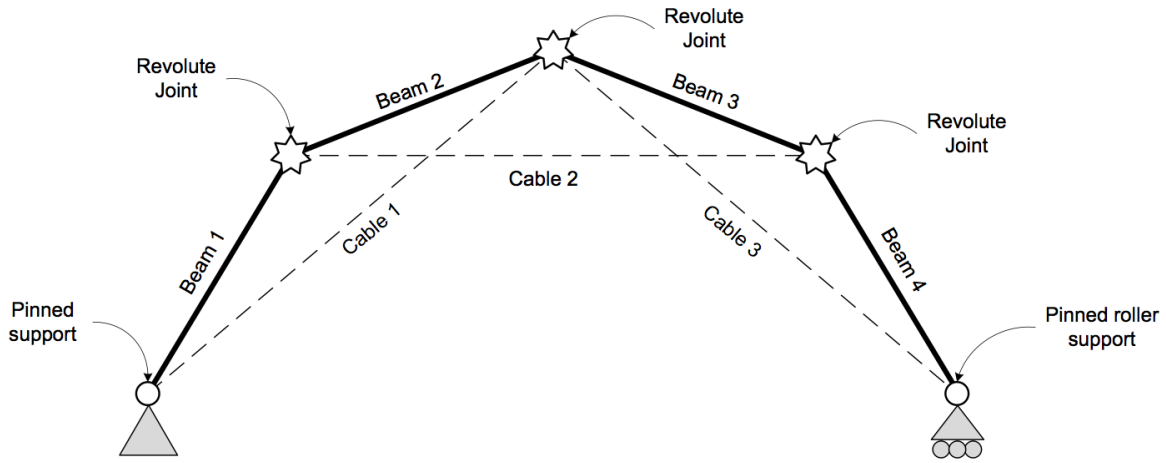


## Define the co-ordinates and the number of segments under consideration...

These are the three points that were used to determine the parabola, effectively a and c are the supports, with b determining the maximum dip of the parabola:

```
a := {0, 0}
```

```
b := {2050, 2500}
```

```
c := {4100, 0}
```

Define the number of segments to subdivide the curve into:

```
nSeg := 7
```

Define the optimum internal height for occupation:

```
intHeight = 700;
```

## Extract the components into key variables to find the equations of the line...

```
x1 := Part[a, 1]

x2 := Part[b, 1]

x3 := Part[c, 1]

y1 := Part[a, 2]

y2 := Part[b, 2]

y3 := Part[c, 2]
```

# Solve the simultaneous equations using vectors.

Solve for the simultaneous equations...

```
curve = Solve[{varA x1^2 + varB x1 + varC == y1,
    varA x2^2 + varB x2 + varC == y2,
    varA x3^2 + varB x3 + varC == y3},
   {varA, varB, varC},
   Reals];

{varA, varB, varC} = {varA, varB, varC} /. curve[[1]];
```

# Define the equation of the line as a function

```
f[x_] := varC + varB x + varA x^2

f[x]
```

$$\frac{100\,x}{41} - \frac{x^2}{1681}$$

Check plot for the point locations...

```
Plot[f[x], {x, x1 - (x2 - x1) / 2, x3 + (x3 - x2) / 2},
 Prolog → {Red, PointSize[0.02], Point[{{x1, y1}, {x2, y2}, {x3, y3}}]}]
```

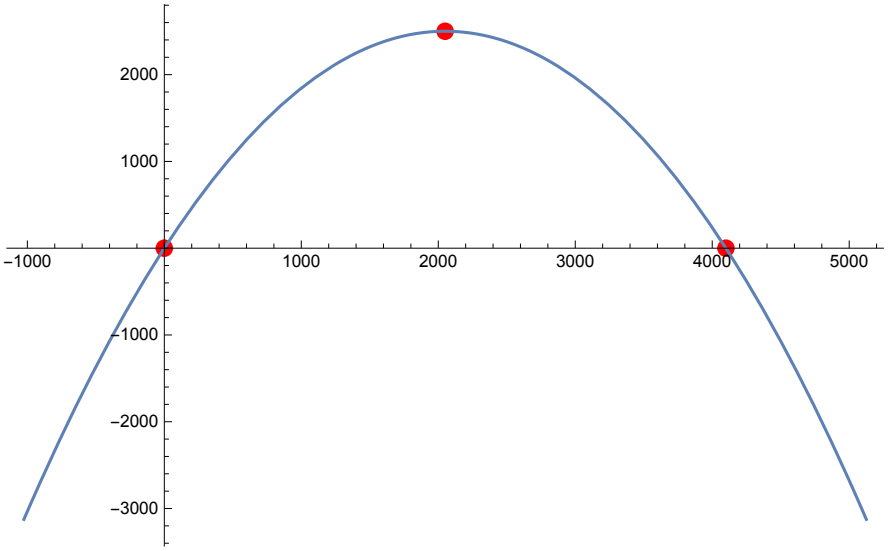


# Then equation for the length of the curve between two points can be determined.

To find the first differential of the expression dy/dx this is found using the term f'[x] in Mathematica...

$$arc = \int_a^b \sqrt{1 + \left(\frac{dy}{dx}\right)^2}\, dx$$

Taken from http://www.mathwords.com/a/arc_length_of_a_curve.htm and http://www.thiel.edu/mathproject/mathematica/L009.pdf

```
f'[x]
```

$$\frac{100}{41} - \frac{2x}{1681}$$

# Determine the curved length based on the function of the curve...

```
curveL = NIntegrate[√(1 + (f'[x])^2),
   {x, x1, x3}] // Simplify
```

```
6769.2
```

# Divide the curve into nSeg number of equal segments ...

```
upVal = Part[c, 1];
chordL = Table[Sqrt[(x_{i+1} - x_i)^2 + (f[x_{i+1}] - f[x_i])^2], {i, 1, nSeg}];
combEqs = # == d & /@ chordL;
ClearAll[vars, x];
vars = Append[{x_#, #, Part[a, 1] + 10^-6, upVal - 10^-6} & /@ Range[2, nSeg], {d, 1}];
```

Define the function and execute the code.

```
x_1 = Part[a, 1];
x_{nSeg+1} = upVal;
sol = {FindRoot[combEqs, vars, MaxIterations → 10 000, AccuracyGoal → Infinity]}
```

FindRoot::lstol :

The line search decreased the step size to within tolerance specified by AccuracyGoal and PrecisionGoal but was unable to find a sufficient decrease in the merit function. You may need more than MachinePrecision digits of working precision to meet these tolerances. ≫

```
{{x_2 → 395.715, x_3 → 886.288, x_4 → 1571.2,
  x_5 → 2528.8, x_6 → 3213.71, x_7 → 3704.29, d → 957.592}}
```

Need to sort how to write the solution back into the variables from a list...

```
vals = Table[x_i, {i, 2, nSeg}, {d, 1}] /. sol[[1]]
```

```
{{395.715}, {886.288}, {1571.2}, {2528.8}, {3213.71}, {3704.29}}
```

```
f[Table[x_i, {i, 2, nSeg}]] /. sol[[1]]
```

```
{872.005, 1694.39, 2363.63, 2363.63, 1694.39, 872.005}
```

# Determine the length of cables.

```
cableL = Table[Sqrt[(x_{i+2} - x_i)^2 + (f[x_{i+2}] - f[x_i])^2],
    {i, 1, nSeg - 1}] /. sol[[1]]
```

```
{1912.19, 1899.13, 1773.61, 1773.61, 1899.13, 1912.19}
```

Double check that the straight lengths are somewhere close to the actual curved length...

```
diffL = (nSeg * d /. sol[[1]]) - curveL
```

```
-66.0493
```

# Determine the points where the cables intersect.

```
intPoints = Table[pᵢ = {xᵢ, f[xᵢ]}, {i, 1, nSeg + 1}] /. sol[[1]];

iPoint = Table[(1 - λᵢ) pᵢ + λᵢ * pᵢ₊₂ == (1 - λᵢ₊₁) pᵢ₊₁ + λᵢ₊₁ * pᵢ₊₃, {i, 1, nSeg - 2}];

Flatten[iPoint];

iVars = Table[λᵢ, {i, 1, nSeg - 1}];

iVarsL = Length[iVars]
6
```

Create a Do[] command to iterate through and solve the equations.

```
Do[
 iSol = Table[Solve[Part[iPoint, n],
    Part[iVars, j ;; j + 1]],
   {n, 1, nSeg - 2},
   {j, 1, iVarsL - 1}]]

iNode = Table[(1 - λᵢ) pᵢ + λᵢ * pᵢ₊₂, {i, 1, nSeg - 2}];

test = Flatten[iSol] /. sol[[1]];
```

Create a variable/list that drops even numbers, but not the last even number...

```
dropVars = If[EvenQ[Length[test]],
  {2, Length[test] - 2},
  {2, Length[test] - 1}
 ]
{2, 8}

test = If[dropVars[[2]] == 0,
  test,
  Drop[test, 2 ;; dropVars[[2]] ;; 2]
 ]
{λ₁ → 0.649176, λ₂ → 0.614716, λ₃ → 0.708497, λ₄ → 0.858741, λ₅ → 0.847177, λ₆ → 0.350824}

iPlot = iNode /. test /. sol[[1]]
{{575.357, 1099.96}, {1118.31, 1788.93},
 {2050., 2168.54}, {2981.69, 1788.93}, {3524.64, 1099.96}}
```

# Calculate the internal area...

```
polyPlot = Append[iPlot, {x_{nSeg+1}, f[x_{nSeg+1}]}];
polyPlot = Prepend[polyPlot, {x_1, f[x_1]}];
```

```
area[n_List] := Abs[Total[Det /@ Partition[n, 2, 1, {1, 1}]] / 2]
```

```
intArea = area[polyPlot]
```

$5.88854 \times 10^6$

# Useable area defined by height...

Making use of winding numbers to determine if a point sits within a polygon.

Based on cables.

```
(* NB the Winding Number function changed in v10 and is still undocumented. *)
(* http://mathematica.stackexchange.com/questions/9405/how-
  to-check-if-a-2d-point-is-in-a-polygon *)
```

```
(* inPolyQ[poly_,pt_]:=Graphics`Mesh`PointWindingNumber[poly,pt]=!=0 *)
```

```
inPolyQ[poly_, pt_] := Graphics`PolygonUtils`PointWindingNumber[poly, pt] =!= 0
```

```
primeArea = Table[inPolyQ[polyPlot, {x, intHeight}], {x, 0, x_{nSeg+1}}];
boxNodes = Flatten[Tally[Boole[primeArea]]];
widthBox = boxNodes[[4]]
```

3367

```
boxArea = widthBox * intHeight
```

2 356 900

Based on struts.

```
primeAreaS = Table[inPolyQ[intPoints, {x, intHeight}], {x, 0, x_{nSeg+1}}];
boxNodesS = Flatten[Tally[Boole[primeAreaS]]];
widthBoxS = boxNodesS[[4]]
```

3465

```
boxAreaS = widthBoxS * intHeight
```

2 425 500

# Visualise the structure...

```
Show[Plot[f[x], {x, Subscript[x, 1], Subscript[x, nSeg + 1]}, PlotStyle → {Dotted}],
 Graphics[{Black, Thick, Line[Table[{{Subscript[x, i], f[Subscript[x, i]]},
       {Subscript[x, i + 1], f[Subscript[x, i + 1]]}}, {i, 3, nSeg - 2}] /. sol[[1]]]}],
 Graphics[{Black, Dashed, Line[Table[{{Subscript[x, i], f[Subscript[x, i]]},
       {Subscript[x, i + 2], f[Subscript[x, i + 2]]}}, {i, 3, nSeg - 3}] /. sol[[1]]]}],
 Graphics[{Red, PointSize[Large], Point[
    Table[{Subscript[x, i], f[Subscript[x, i]]}, {i, 3, nSeg - 1}] /. sol[[1]]]}],
 Graphics[{Black, PointSize[Large], Point[{iPlot[[3]]}]}],
 AspectRatio → Automatic,
 Axes → False]
```

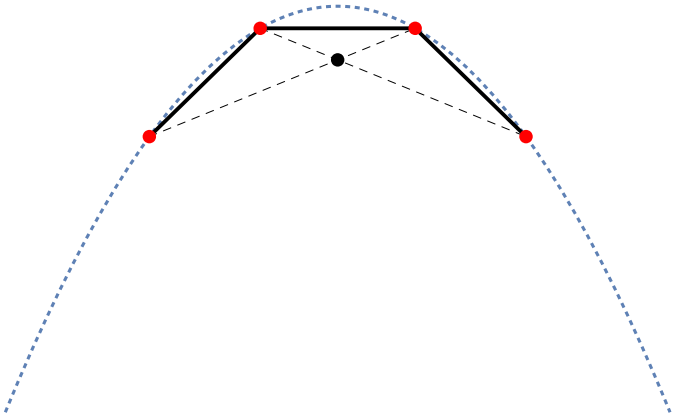

```
Show[Plot[f[x], {x, x1, xnSeg+1}, PlotStyle -> {Dotted}],
 Graphics[{Black, Thick,
   Line[Table[{{xi, f[xi]}, {xi+1, f[xi+1]}}, {i, 1, nSeg}] /. sol[[1]]]}],
 Graphics[{Black, Dashed, Line[
    Table[{{xi, f[xi]}, {xi+2, f[xi+2]}}, {i, 1, nSeg - 1}] /. sol[[1]]]}],
 Graphics[{Red, PointSize[Large], Point[
    Table[{xi, f[xi]}, {i, 1, nSeg + 1}] /. sol[[1]]]}],
 Graphics[{Black, PointSize[Large], Point[iPlot]}],
 AspectRatio → Automatic,
 Axes → False]
```

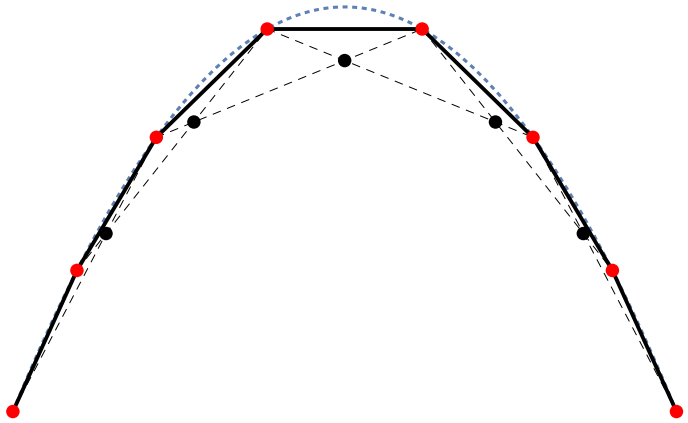

```
Show[Plot[f[x], {x, x1, xnSeg+1}, PlotStyle -> {Dotted}],
 Graphics[{Pink, Opacity[0.3], Polygon[polyPlot]}],
 Graphics[{Black, Thick,
   Line[Table[{{xi, f[xi]}, {xi+1, f[xi+1]}}, {i, 1, nSeg}] /. sol[[1]]]}],
 Graphics[{Black, Dashed, Line[
    Table[{{xi, f[xi]}, {xi+2, f[xi+2]}}, {i, 1, nSeg - 1}] /. sol[[1]]]}],
 Graphics[{Red, PointSize[Large], Point[
    Table[{xi, f[xi]}, {i, 1, nSeg + 1}] /. sol[[1]]]}],
 Graphics[{Black, PointSize[Large], Point[iPlot]}],
 Graphics[{{EdgeForm[Thin], Red, Opacity[0.3], Rectangle[
    {boxNodes[[2]] / 2, 0}, {boxNodes[[2]] / 2 + boxNodes[[4]], intHeight}]}],
 Graphics[{{EdgeForm[Thin], Dashed, Transparent, Rectangle[
    {boxNodesS[[2]] / 2, 0}, {boxNodesS[[2]] / 2 + boxNodesS[[4]], intHeight}]}],
 AspectRatio → Automatic,
 Axes → False]
```

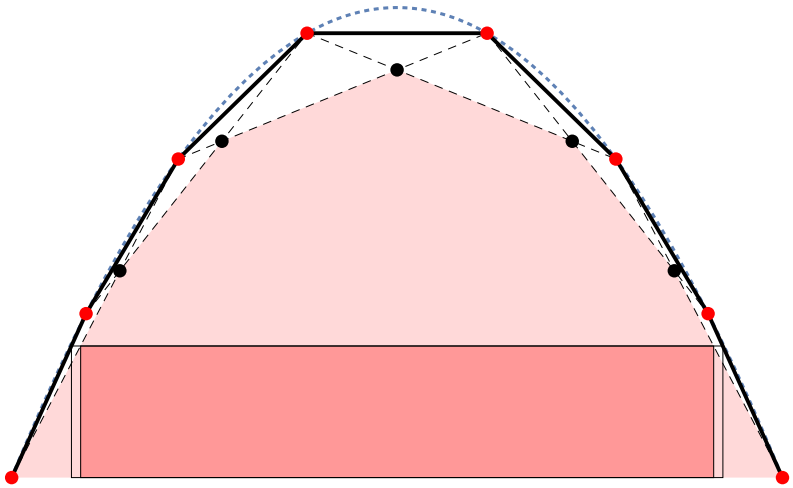

# Determine the internal angles...

```
vector[x_, y_] := {x[[1]] - y[[1]], x[[2]] - y[[2]]}
```

```
intAngles =
 Table[ArcCos[vector[{xi, f[xi]}, {xi-1, f[xi-1]}].vector[{xi, f[xi]}, {xi+1, f[xi+1]}] /
       (Norm[vector[{xi, f[xi]}, {xi-1, f[xi-1]}]]
         Norm[vector[{xi, f[xi]}, {xi+1, f[xi+1]}]])] 180/Pi, {i, 2, nSeg}] /. sol[[1]]
```

```
{173.591, 165.153, 135.664, 135.664, 165.153, 173.591}
```

```
cabAng[x_] := (180 - x) / 2
```

```
cabAngs = cabAng[intAngles]
```

```
{3.20428, 7.42325, 22.1682, 22.1682, 7.42325, 3.20428}
```

# Load up the sub-modules for the analysis...

```
PlaneBar2Stiffness[ncoor_, mprop_, fprop_, opt_] :=
  Module[{x1, x2, y1, y2, x21, y21, Em, Gm, rho, alpha, A, numer, L, LL, LLL, Ke},
   {{x1, y1}, {x2, y2}} = ncoor;
   {x21, y21} = {x2 - x1, y2 - y1};
   {Em, Gm, rho, alpha} = mprop; {A} = fprop; {numer} = opt;
   If[numer, {x21, y21, Em, A} = N[{x21, y21, Em, A}]];
   LL = x21^2 + y21^2;
   L = PowerExpand[Sqrt[LL]];
   LLL = Simplify[LL * L];
   Ke = (Em * A / LLL) * {{x21 * x21, x21 * y21, -x21 * x21, -x21 * y21},
      {y21 * x21, y21 * y21, -y21 * x21, -y21 * y21}, {-x21 * x21, -x21 * y21,
       x21 * x21, x21 * y21}, {-y21 * x21, -y21 * y21, y21 * x21, y21 * y21}};
   Return[
    Ke]];

ModifiedMasterStiffness[pdof_, K_] :=
  Module[{i, j, k, n = Length[K], np = Length[pdof], Kmod}, Kmod = K;
   For[k = 1, k ≤ np, k++, i = pdof[[k]];
    For[j = 1, j ≤ n, j++, Kmod[[i, j]] = Kmod[[j, i]] = 0];
    Kmod[[i, i]] = 1];
   Return[Kmod]];
ModifiedNodeForces[pdof_, f_] := Module[{i, k, np = Length[pdof], fmod}, fmod = f;
   For[k = 1, k ≤ np, k++, i = pdof[[k]]; fmod[[i]] = 0];
   Return[fmod]];

PlaneTrussIntForces[nodcoor_, elenod_, elemat_, elefab_, eleopt_, u_] :=
  Module[{numele = Length[elenod], numnod = Length[nodcoor], e, eNL, eftab,
    ni, nj, i, ncoor, mprop, fprop, opt, ue, p}, p = Table[0, {numele}];
   ue = Table[0, {4}];
   For[e = 1, e ≤ numele, e++, eNL = elenod[[e]]; {ni, nj} = eNL;
    eftab = {2 * ni - 1, 2 * ni, 2 * nj - 1, 2 * nj};
    ncoor = {nodcoor[[ni]], nodcoor[[nj]]};
    mprop = elemat[[e]]; fprop = elefab[[e]]; opt = eleopt;
    For[i = 1, i ≤ 4, i++, ii = eftab[[i]]; ue[[i]] = u[[ii]]];
    p[[e]] = PlaneBar2IntForce[ncoor, mprop, fprop, opt, ue]];
   Return[p]];
```

```
PlaneBar2IntForce[ncoor_, mprop_, fprop_, opt_, ue_] :=
 Module[{x1, x2, y1, y2, x21, y21, Em, Gm, rho, alpha, A, numer, LL, pe},
  {{x1, y1}, {x2, y2}} = ncoor;
  {x21, y21} = {x2 - x1, y2 - y1};
  {Em, Gm, rho, alpha} = mprop; {A} = fprop; {numer} = opt;
  (*If[numer,{x21,y21,Em,A}=N[{x21,y21,Em,A}]];*)
  LL = x21^2 + y21^2;
  pe = Em * A * (x21 * (ue[[3]] - ue[[1]]) + y21 * (ue[[4]] - ue[[2]])) / LL;
  Return[pe]
 ]; ClearAll[];

PlaneTrussMasterStiffness[nodxyz_, elenod_, elemat_, elefab_, eleopt_] :=
  Module[{numele = Length[elenod], numnod = Length[nodxyz], e, ni, nj, eft, i, j, ii,
    jj, ncoor, Em, A, options, Ke, K}, K = Table[0, {2 * numnod}, {2 * numnod}];
   For[e = 1, e ≤ numele, e++, {ni, nj} = elenod[[e]];
    eft = {2 * ni - 1, 2 * ni, 2 * nj - 1, 2 * nj};
    ncoor = {nodxyz[[ni]], nodxyz[[nj]]};
    Em = elemat[[e]]; A = elefab[[e]]; options = eleopt;
    Ke = PlaneBar2Stiffness[ncoor, Em, A, options];
    For[i = 1, i ≤ 4, i++, ii = eft[[i]];
     For[j = i, j ≤ 4, j++, jj = eft[[j]];
      K[[jj, ii]] = K[[ii, jj]] += Ke[[i, j]];];];
   Return[K]];
```

# Input the co-ordinates and define geometry...

```
NodeCoordinates = Table[{xi, f[xi]}, {i, 1, nSeg + 1}] /. sol[[1]];
ElemNodeLists =
  Join[Table[{i, i + 1}, {i, 1, nSeg}], Table[{i, i + 2}, {i, 1, nSeg - 1}]];
numnod = Length[NodeCoordinates];
numele = Length[ElemNodeLists];
numdof = 2 * numnod;
ElemMaterial = Table[{205 000, 0, 0, 0}, {numele}];
Abot = 2; Atop = 10; Abat = 3; Adia = 1;
ElemFabrication = Join[Table[{Abot}, {6}],
   Table[{Atop}, {6}], Table[{Abat}, {5}], Table[{Adia}, {4}]];
ProcessOptions = {True}; aspect = 0;
FreedomTag = FreedomValue = Table[{0, 0}, {numnod}];
FreedomValue[[2]] = {0, -10};
Print["Applied node forces="]; Print[FreedomValue];
FreedomTag[[1]] = {1, 1};(*fixed node 1*)
FreedomTag[[numnod]] = {0, 1}; (*hroller@node nSeg+1*)
```

```
Applied node forces=
{{0, 0}, {0, -10}, {0, 0}, {0, 0}, {0, 0}, {0, 0}, {0, 0}, {0, 0}}
eleopt = {True};
```

# Run the analysis...

```
fMat = Flatten[FreedomValue];
K = PlaneTrussMasterStiffness[NodeCoordinates,
    ElemNodeLists, ElemMaterial, ElemFabrication, ProcessOptions];
pdof = {};
For[n = 1, n ≤ numnod, n++,
  For[j = 1, j ≤ 2, j++, If[FreedomTag[[n, j]] > 0, AppendTo[pdof, 2 * (n - 1) + j]]]];
Kmod = ModifiedMasterStiffness[pdof, K];
fmod = ModifiedNodeForces[pdof, fMat];
u = LinearSolve[Kmod, fmod];
u = Chop[u];
Print["Computed Nodal Displacements:"];
Print[Partition[u, 2]];
Print["Relative Nodal Displacements:"];
defLen[x_] := (x[[1]]^2 + x[[2]]^2)^0.5;
Print[Map[defLen, Partition[u, 2]]];
fMat = Simplify[K.u];
fMat = Chop[fMat];
Print["External Node Forces Including Reactions:"];
Print[Partition[fMat, 2]];
p = PlaneTrussIntForces[NodeCoordinates,
    ElemNodeLists, ElemMaterial, ElemFabrication, eleopt, u];
p = Chop[p];
sigma = Table[p[[i]] / ElemFabrication[[i, 1]], {i, 1, numele}];
Print["Strut Member Forces: (-ve comp, +ve tension)"];
Print[Part[p, 1 ;; nSeg]];
Print["Cable Member Forces: (-ve comp, +ve tension)"];
Print[Part[p, nSeg + 1 ;; Length[ElemNodeLists]]];
```

```
Computed Nodal Displacements:
{{0, 0}, {8.5198, -4.05842}, {9.62254, -4.96296}, {8.91381, -4.33936},
 {8.89013, -3.1499}, {9.79542, -2.18523}, {11.36, -1.21168}, {14.021, 0}}
Relative Nodal Displacements:
{0., 9.43704, 10.827, 9.91394, 9.43166, 10.0362, 11.4244, 14.021}
External Node Forces Including Reactions:
{{0, 9.03484}, {0, -10.}, {0, 0}, {0, 0}, {0, 0}, {0, 0}, {0, 0}, {0, 0.965158}}
Strut Member Forces: (-ve comp, +ve tension)
{-74.9175, -90.722, -30.4417, -10.1422, -11.4174, -14.8093, -8.00315}
Cable Member Forces: (-ve comp, +ve tension)
{66.7946, 25.0708, 6.75481, 4.19693, 6.91412, 7.13541}
```

# Gather the solutions together at the end for exporting ...

```
a; b; c;
nSeg;
f[x];
seg = d /. sol[[1]];
curveL;
segL = nSeg * d;
cableL;
diffL;
points = Table[{xi, f[xi]}, {i, 1, nSeg + 1}] /. sol[[1]]
{{0, 0}, {395.715, 872.005}, {886.288, 1694.39}, {1571.2, 2363.63},
 {2528.8, 2363.63}, {3213.71, 1694.39}, {3704.29, 872.005}, {4100, 0}}
iPlot;
intArea;
intAngles;
cabAngs;
widthBox;
(* Need to add in the forces, reactions, and displacements*)
totStruts;
totCables;
totFrame;
```

# Deflected form, scale factor included..

```
scale = 100;

defpoint = NodeCoordinates + Partition[u, 2];
magdefpoint = NodeCoordinates + scale * Partition[u, 2];

Show[Plot[f[x], {x, x1, First[Last[magdefpoint]]}, PlotStyle -> {Dotted}],
 Graphics[{Pink, Opacity[0.3], Polygon[polyPlot]}],
 Graphics[{Black, Thick,
   Line[Table[{{xi, f[xi]}, {xi+1, f[xi+1]}}, {i, 1, nSeg}] /. sol[[1]]]}],
 Graphics[{Black, Dashed, Line[
    Table[{{xi, f[xi]}, {xi+2, f[xi+2]}}, {i, 1, nSeg - 1}] /. sol[[1]]]}],
 Graphics[{Red, PointSize[Large], Point[
    Table[{xi, f[xi]}, {i, 1, nSeg + 1}] /. sol[[1]]]}],
 Graphics[{Blue, PointSize[Large], Point[magdefpoint]}],
 Graphics[{Blue, Thick, Line[magdefpoint]}],
 Graphics[{Blue, Dashed, Line[Table[magdefpoint[[i]], {i, 1, nSeg + 1, 2}]]}],
 Graphics[{Blue, Dashed, Line[Table[magdefpoint[[i]], {i, 2, nSeg + 1, 2}]]}],
 Graphics[{Black, PointSize[Large], Point[iPlot]}],
 AspectRatio → Automatic,
 Axes → False]
```

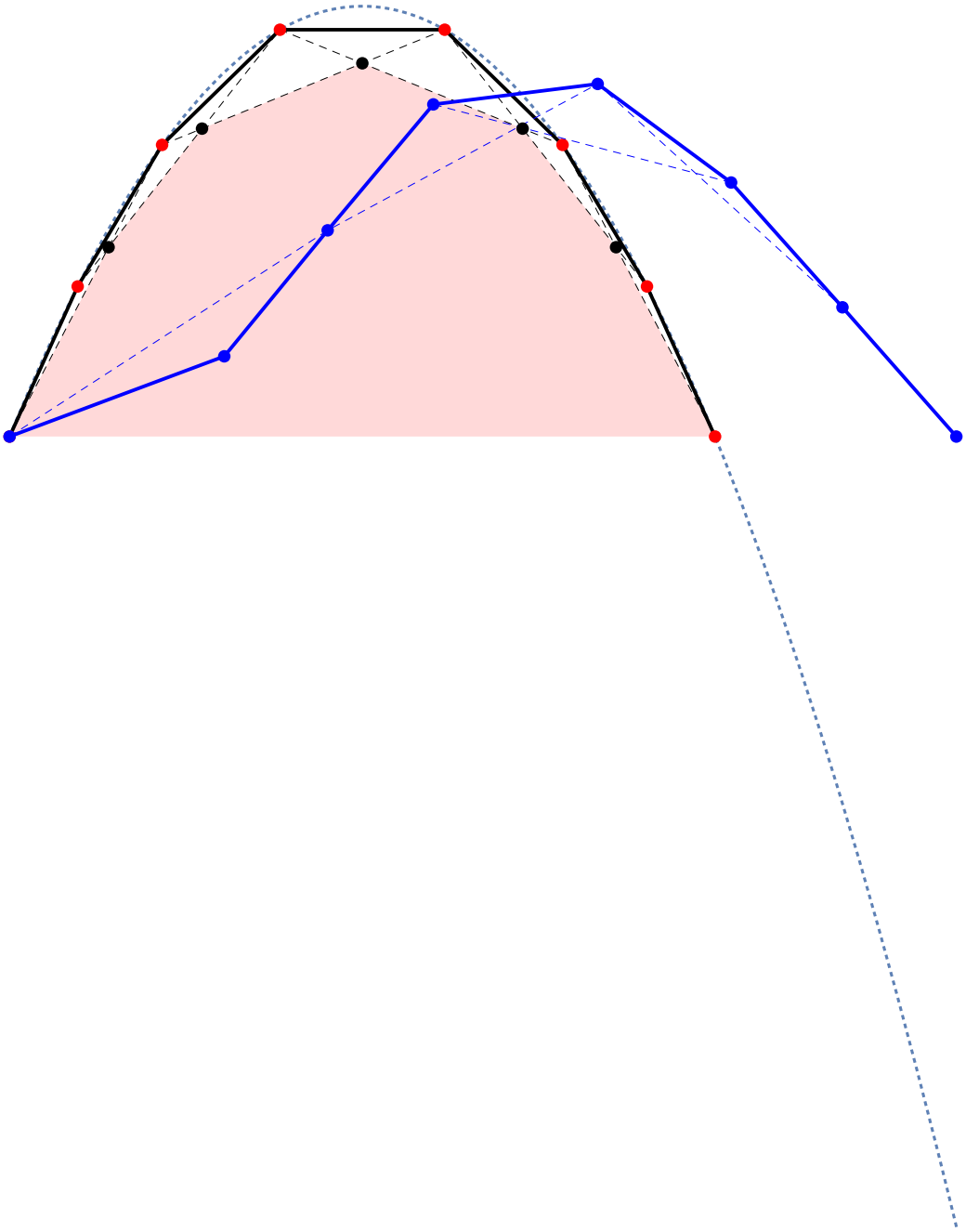

# Determine sections sizes...

```
buckleRad[bF_, bL_] := Sqrt[4, bF * bL^2 * 4 / (Pi^3 * 205 000)]
```

```
struts = buckleRad[Abs[Part[p, 1 ;; nSeg]], d] /. sol[[1]](*units*)
```

```
{2.56419, 2.68988, 2.04725, 1.55538, 1.60212, 1.70977, 1.46595}
```

```
steelW[rad_, len_] := Pi * rad^2 * len * 7850 (*units*)
```

```
totStruts = Total[steelW[struts, d] /. sol[[1]]]
```

$6.62658 \times 10^8$

```
tensionRad[tF_] := Sqrt[tF / (275 Pi)]
```

```
cables = tensionRad[Part[p, nSeg + 1 ;; Length[ElemNodeLists]]](*units*)
```

```
{0.278054, 0.17035, 0.088423, 0.0696987, 0.0894596, 0.09088}
```

```
totCables = Total[steelW[cables, cableL]]
```

$6.32385 \times 10^6$

```
totFrame = totCables + totStruts
```

$6.68982 \times 10^8$

Need to calculate kg/m2 of habitable area? Total area as a comparison measure?

# To Do :

Improve output plots, labels, forces, loads?

Determine element sizes

Calculate overall weight

Add analysis outputs to the output area.

Tension only elements? Do[...] or If[...]?

Any benefit of calculating the gradient at each node position?

Export to a text file.

```
points
```

```
{{0, 0}, {395.715, 872.005}, {886.288, 1694.39}, {1571.2, 2363.63},
 {2528.8, 2363.63}, {3213.71, 1694.39}, {3704.29, 872.005}, {4100, 0}}
```

```
exportPoints = Drop[Riffle[points, points], 1]
```

```
{{0, 0}, {395.715, 872.005}, {395.715, 872.005}, {886.288, 1694.39},
 {886.288, 1694.39}, {1571.2, 2363.63}, {1571.2, 2363.63}, {2528.8, 2363.63},
 {2528.8, 2363.63}, {3213.71, 1694.39}, {3213.71, 1694.39},
 {3704.29, 872.005}, {3704.29, 872.005}, {4100, 0}, {4100, 0}}
```

```
exportPoints = Round[Drop[exportPoints / 1000, -1], 0.0001]
```

```
{{0., 0.}, {0.3957, 0.872}, {0.3957, 0.872}, {0.8863, 1.6944}, {0.8863, 1.6944},
 {1.5712, 2.3636}, {1.5712, 2.3636}, {2.5288, 2.3636}, {2.5288, 2.3636},
 {3.2137, 1.6944}, {3.2137, 1.6944}, {3.7043, 0.872}, {3.7043, 0.872}, {4.1, 0.}}
```

```
Drop
```

```
Drop
```

```
Export["points.xlsx", exportPoints, Overwrite → True]
```

```
points.xlsx
```

```
SystemOpen[DirectoryName[AbsoluteFileName["points.xlsx"]]]
```

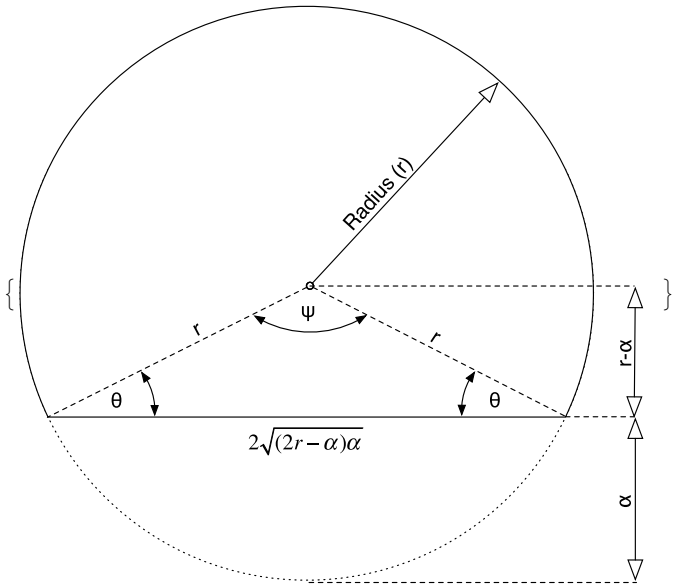


In[53]:=
```
Clear[a, b, c, A, r, θ, α];
FullSimplify[Solve[r^2 == (r - a)^2 + m^2, m]]
```

Out[54]= $\left\{\left\{m \to -\sqrt{-a\,(a-2\,r)}\right\}, \left\{m \to \sqrt{-a\,(a-2\,r)}\right\}\right\}$

In[55]:=
```
θ = ArcTan[(r - α)/Sqrt[(2 r - a) a]] // FullSimplify
```

Out[55]= $\text{ArcTan}\left[\frac{r-\alpha}{\sqrt{-a\,(a-2\,r)}}\right]$

In[56]:=
```
Clear[a, b, c, A]
```

In[57]:=
```
a := (b^2 + c^2 - 2 b c Cos[A])^0.5
```

In[58]:=
```
a
```

Out[58]= $\left(b^2 + c^2 - 2\,b\,c\,\text{Cos}[A]\right)^{0.5}$

In[59]:=
```
b = r; c = r; a = 2 Sqrt[(2 r - α) α];
```

In[60]:=
```
a // Simplify
```

Out[60]= $2\sqrt{(2\,r-\alpha)\,\alpha}$

In[61]:=
```
a
```

Out[61]= $2\sqrt{(2\,r-\alpha)\,\alpha}$

In[62]:=
```
2^0.5
```

Out[62]= 1.41421

In[63]:=
```
A := ArcCos[(a^2 - b^2 - c^2)/(-2 b c)]
```

In[64]:=
```
A // FullSimplify
```

Out[64]= $\text{ArcCos}\left[\frac{r^2 - 4\,r\,\alpha + 2\,\alpha^2}{r^2}\right]$

In[65]:= **angleN := 2 * ArcTan[$\frac{\sqrt{(2\,r-\alpha)\,\alpha}}{r-\alpha}$] // FullSimplify**

In[66]:= **r = 10; α = 10;**

In[67]:= **angleN // N**

Out[67]= Indeterminate

In[68]:= **A // N**

Out[68]= 3.14159

In[69]:= **intAngle = (2 Pi - A) // N**

Out[69]= 3.14159

# Define numbers of segments here.

In[70]:= **nSeg = 5**

Out[70]= 5

In[71]:= **archSeg = intAngle / nSeg**

Out[71]= 0.628319

Distribute the segments via polar co-ordinates?

In[72]:= **convertToCartesian[{r_, theta_}] := {r Cos[theta], r Sin[theta]}**

In[73]:= **convertToCartesian[4, Pi / 2]**

Out[73]= convertToCartesian[4, $\frac{\pi}{2}$]

Angles are determined from 3 o clock and work anti-clockwise, keep angles in radians.

Would the start point be -Pi/2-inAngle/2?

In[74]:= **startAngle = - (A / 2 + Pi / 2) // N**

Out[74]= -3.14159

In[75]:= **endAngle = - (Pi / 2 - A / 2) // N**

Out[75]= 0.

In[76]:= **convertToCartesian[r, startAngle]**

Out[76]= convertToCartesian[10, -3.14159]

In[77]:= **convertToCartesian[r, endAngle]**

Out[77]= convertToCartesian[10, 0.]

In[78]:= **nextAngle = Table[{r, startAngle - i * archSeg}, {i, 1, nSeg}]**

Out[78]= {{10, -3.76991}, {10, -4.39823}, {10, -5.02655}, {10, -5.65487}, {10, -6.28319}}

In[79]:= {nextAngle, f}

Out[79]= {{{10, -3.76991}, {10, -4.39823}, {10, -5.02655}, {10, -5.65487}, {10, -6.28319}}, f}

In[80]:= plotOut = convertToCartesian /@ nextAngle

Out[80]= {{-8.09017, 5.87785}, {-3.09017, 9.51057}, {3.09017, 9.51057}, {8.09017, 5.87785}, {10., 2.44929 × 10^-15}}

In[81]:= plotOut = Prepend[plotOut, convertToCartesian[{r, startAngle}]]

Out[81]= {{-10., -1.22465 × 10^-15}, {-8.09017, 5.87785}, {-3.09017, 9.51057}, {3.09017, 9.51057}, {8.09017, 5.87785}, {10., 2.44929 × 10^-15}}

In[82]:= plotOut = Append[plotOut, convertToCartesian[{r, endAngle}]]

Out[82]= {{-10., -1.22465 × 10^-15}, {-8.09017, 5.87785}, {-3.09017, 9.51057}, {3.09017, 9.51057}, {8.09017, 5.87785}, {10., 2.44929 × 10^-15}, {10., 0.}}

In[83]:= ListPlot[plotOut]

Out[83]=

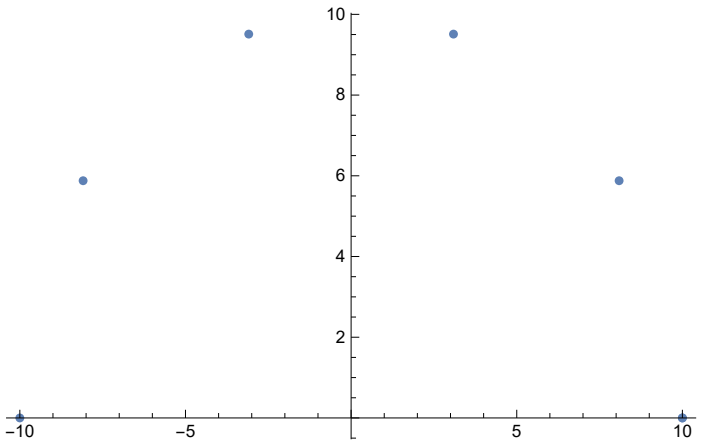


# Determine the points where the cables intersect.

In[84]:= intPoints = plotOut;

In[85]:= plotOut

Out[85]= {{-10., -1.22465 × 10^-15}, {-8.09017, 5.87785}, {-3.09017, 9.51057}, {3.09017, 9.51057}, {8.09017, 5.87785}, {10., 2.44929 × 10^-15}, {10., 0.}}

In[86]:= iPoint = Table[(1 - λ_i) p_i + λ_i * p_i+2 == (1 - λ_i+1) p_i+1 + λ_i+1 * p_i+3, {i, 1, nSeg - 2}] ;

In[87]:= Flatten[iPoint];

In[88]:= iVars = Table[λ_i, {i, 1, nSeg - 1}];

In[89]:= iVarsL = Length[iVars]

Out[89]= 4

Create a Do[] command to iterate through and solve the equations.

In[90]:=
```
Do[
 iSol = Table[Solve[Part[iPoint, n],
    Part[iVars, j ;; j + 1]],
   {n, 1, nSeg - 2},
   {j, 1, iVarsL - 1}]]
```

In[91]:=
```
iSol;
```

In[92]:=
```
iNode = Table[(1 - λi) pi + λi * pi+2, {i, 1, nSeg - 2}] ;
```

In[93]:=
```
test = Flatten[iSol] ;
```

Create a variable/list that drops even numbers, but not the last even number...

In[94]:=
```
dropVars = If[EvenQ[Length[test]],
   {2, Length[test] - 2},
   {2, Length[test] - 1}
  ]
```

Out[94]= {2, 6}

In[95]:=
```
test = If[dropVars[[2]] == 0,
    test,
    Drop[test, 2 ;; dropVars[[2]] ;; 2]
   ];
```

In[96]:=
```
iPlot = iNode  /. test /. sol[[1]];
```

... Part: Part specification sol[[1]] is longer than depth of object.

... ReplaceAll: {sol[[1]]} is neither a list of replacement rules nor a valid dispatch table, and so cannot be used for replacing.

In[97]:=
```
Show[ListPlot[plotOut, PlotStyle -> {Dotted}],
 Graphics[{Black, Thick, Line[plotOut]}],
 Graphics[
  {Black, Dashed, Line[Table[{plotOut[[i]], plotOut[[i + 2]]}, {i, 1, nSeg - 1}]]}],
 Graphics[{Red, PointSize[Large], Point[Table[plotOut[[i]], {i, 1, nSeg + 1}]]}],
 AspectRatio → Automatic,
 Axes → False]
```

Out[97]=

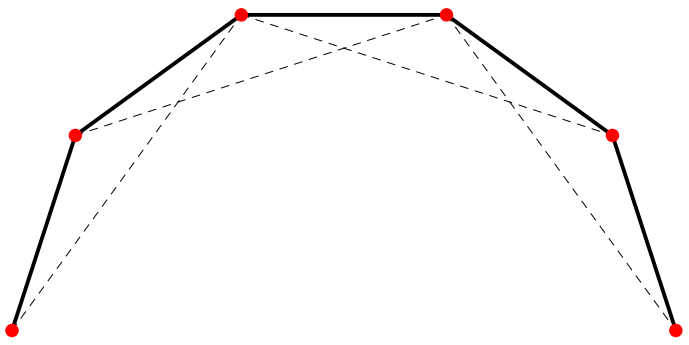

# Determine the internal angles...

Can this be done algebraically based on the nSeg value?

In[98]:=
```
cableL = Table[Norm[plotOut[[i]] - plotOut[[i + 2]]], {i, 1, nSeg - 1}]
```

Out[98]=
```
{11.7557, 11.7557, 11.7557, 11.7557}
```

Out[46]=
```
{11.7557, 11.7557, 11.7557, 11.7557}
```

```
{11.7557, 11.7557, 11.7557, 11.7557}
{12.3944, 12.3944, 12.3944, 12.3944}
{13.0194, 13.0194, 13.0194, 13.0194}
{13.6356, 13.6356, 13.6356, 13.6356}
{14.2482, 14.2482, 14.2482, 14.2482}
{14.8629, 14.8629, 14.8629, 14.8629}
{15.4874, 15.4874, 15.4874, 15.4874}
{16.1332, 16.1332, 16.1332, 16.1332}
{16.8212, 16.8212, 16.8212, 16.8212}
{17.6035, 17.6035, 17.6035, 17.6035}
{14.2482, 14.2482, 14.2482, 14.2482}
{14.8629, 14.8629, 14.8629, 14.8629}
{23.8719, 23.8719, 23.8719, 23.8719}
{23.8719, 23.8719, 23.8719, 23.8719}
{13.3213, 13.3213, 13.3213, 13.3213, 13.3213, 13.3213, 13.3213, 13.3213, 13.3213}
{13.3213, 13.3213, 13.3213, 13.3213, 13.3213, 13.3213, 13.3213, 13.3213, 13.3213}
{13.3213, 13.3213, 13.3213, 13.3213, 13.3213, 13.3213, 13.3213, 13.3213, 13.3213}
{13.3213, 13.3213, 13.3213, 13.3213, 13.3213, 13.3213, 13.3213, 13.3213, 13.3213}
{13.3213, 13.3213, 13.3213, 13.3213, 13.3213, 13.3213, 13.3213, 13.3213, 13.3213}
{13.3213, 13.3213, 13.3213, 13.3213, 13.3213, 13.3213, 13.3213, 13.3213, 13.3213}
{13.3213, 13.3213, 13.3213, 13.3213, 13.3213, 13.3213, 13.3213, 13.3213, 13.3213}
{13.3213, 13.3213, 13.3213, 13.3213, 13.3213, 13.3213, 13.3213, 13.3213, 13.3213}
{13.3213, 13.3213, 13.3213, 13.3213, 13.3213, 13.3213, 13.3213, 13.3213, 13.3213}
{13.3213, 13.3213, 13.3213, 13.3213, 13.3213, 13.3213, 13.3213, 13.3213, 13.3213}
{13.3213, 13.3213, 13.3213, 13.3213, 13.3213, 13.3213, 13.3213, 13.3213, 13.3213}
```

In[99]:=
```
Table[{plotOut[[i]], plotOut[[i + 2]]}, {i, 1, nSeg - 1}]
```

Out[99]=
```
{{{-10., -1.22465 × 10^-15}, {-3.09017, 9.51057}},
 {{-8.09017, 5.87785}, {3.09017, 9.51057}}, {{-3.09017, 9.51057}, {8.09017, 5.87785}},
 {{3.09017, 9.51057}, {10., 2.44929 × 10^-15}}}
```

In[100]:=
```
plotOut
```

Out[100]=
$$\left\{\left\{-10.,\ -1.22465\times10^{-15}\right\},\ \{-8.09017,\ 5.87785\},\ \{-3.09017,\ 9.51057\},\ \{3.09017,\ 9.51057\},\ \{8.09017,\ 5.87785\},\ \left\{10.,\ 2.44929\times10^{-15}\right\},\ \{10.,\ 0.\}\right\}$$

In[101]:=
```
robotPoints = Drop[Riffle[plotOut, plotOut], 1];
```

In[102]:=
```
robotPoints = Round[Drop[robotPoints / 1000, -1], 0.0001]
```

Out[102]=
$$\{\{-0.01,\ 0.\},\ \{-0.0081,\ 0.0059\},\ \{-0.0081,\ 0.0059\},\ \{-0.0031,\ 0.0095\},\ \{-0.0031,\ 0.0095\},\ \{0.0031,\ 0.0095\},\ \{0.0031,\ 0.0095\},\ \{0.0081,\ 0.0059\},\ \{0.0081,\ 0.0059\},\ \{0.01,\ 0.\},\ \{0.01,\ 0.\},\ \{0.01,\ 0.\}\}$$

In[103]:=
```
Export["robotcircpoints.xlsx", robotPoints, Overwrite → True]
```

Out[103]=
```
robotcircpoints.xlsx
```

In[104]:=
```
SystemOpen[DirectoryName[AbsoluteFileName["robotcircpoints.xlsx"]]]
```

# Appendix 2

This appendix contains the Mathematica sheet used to create the graph in Figure 4-2 Buckling Curve Ignoring Secondary Effects.

```
p = 2 * c / l * (theta - theta_init) / Sin[theta]
```

```
50 Csc[theta] (theta - theta_init)
```

```
c = 50
```

```
50
```

```
l = 2
```

```
2
```

```
p
```

```
50 Csc[theta] (theta - theta_init)
```

```
Plot[50 theta Csc[theta], {theta, -Pi/4, Pi/4}, Ticks → {Range[-Pi, π, π/6], None}]
```

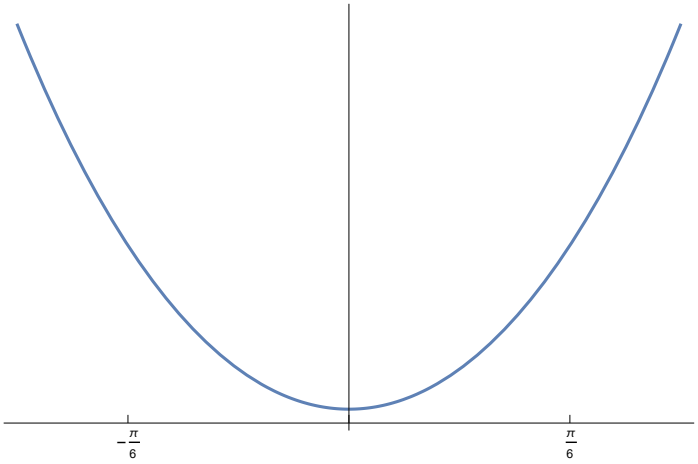


```
Plot[50 theta Csc[theta], {theta, -Pi/4, Pi/4}]
```

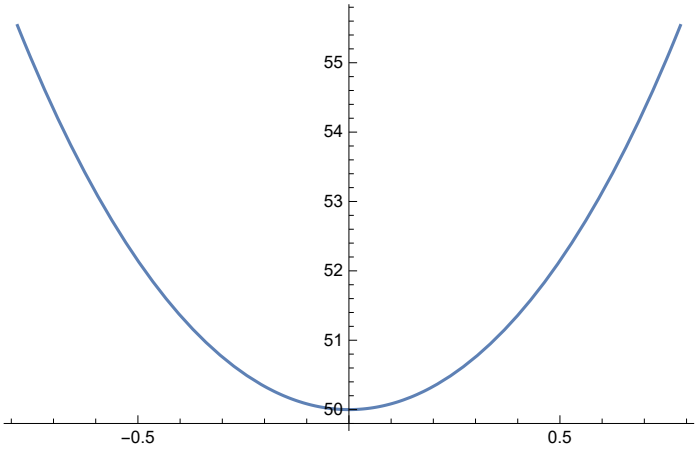


```
Show[%7, AxesLabel → {HoldForm[Angle], HoldForm[Pcr]},
 PlotLabel → None, LabelStyle → {GrayLevel[0]}]
```

$RecursionLimit::reclim2 : Recursion depth of 1024 exceeded during evaluation of %7. >>

```
Hold[%7]
```

```
e = Plot[50 theta Csc[theta], {theta, -Pi/2, Pi/2},
  PlotStyle → {Black, Thin},
  Ticks → {Range[-Pi, π, π/12],
    Range[0, 80, 10]},
  AxesOrigin → {0, 0}
 ]
```

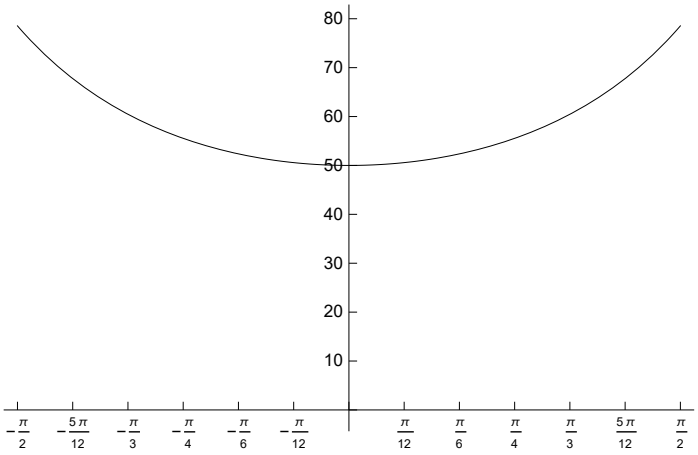


```
a = Plot[2 * c/l * (theta - (1 * 2 * Pi/360))/Sin[theta],
  {theta, 0, Pi/2}, PlotStyle → {Red, Dashed, Thin}, Ticks → None]
```

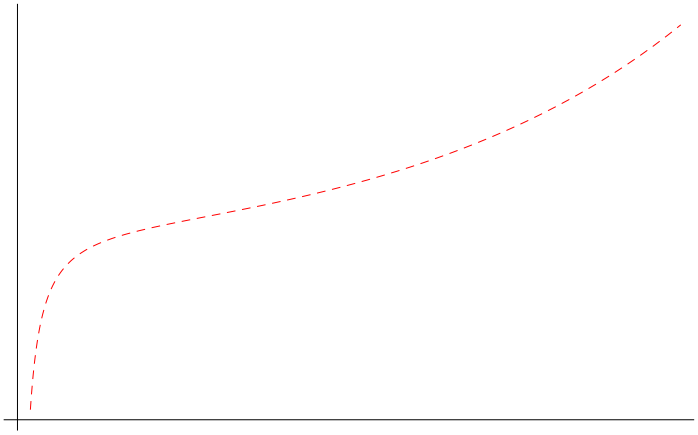

```
b = Plot[(2 * c)/l * (theta - (2 * 2 * Pi/360))/Sin[theta],
  {theta, 0, Pi/2}, PlotStyle → {Orange, Dashed, Thin}, Ticks → None]
```

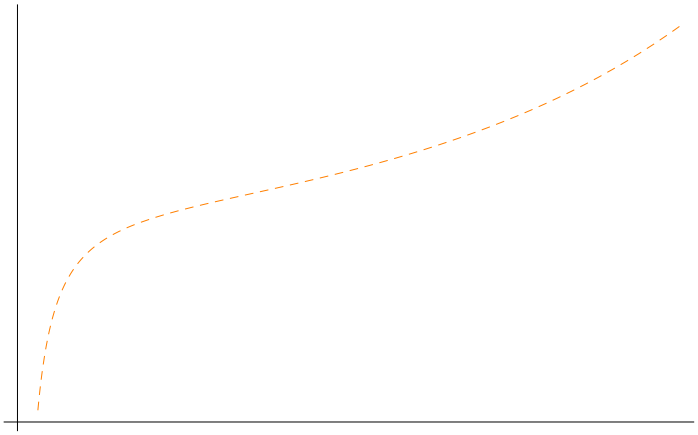

```
cc = Plot[(2 * c)/l * (theta - (3 * 2 * Pi/360))/Sin[theta],
  {theta, 0, Pi/2}, PlotStyle → {Green, Dashed, Thin}, Ticks → None]
```

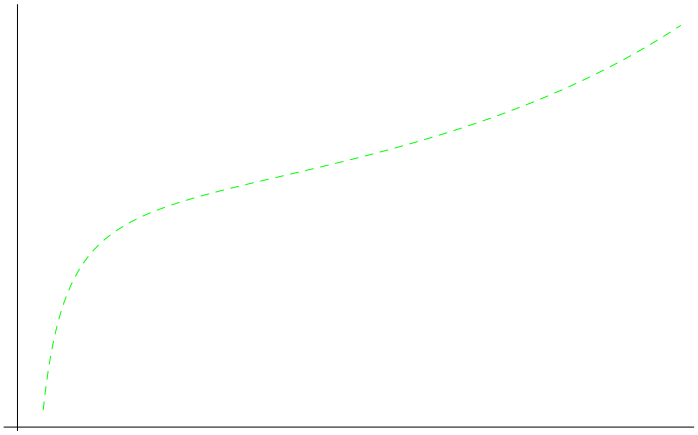

```
d = Plot[(2 * c)/l * (theta - (4 * 2 * Pi/360))/Sin[theta],
  {theta, 0, Pi/2}, PlotStyle → {Dashed, Thin}, Ticks → None]
```

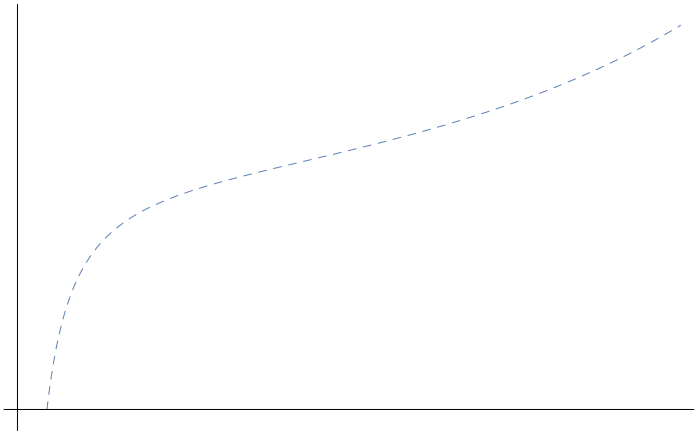

```
f = Plot[(2 * c)/l * (theta - (-1 * (2 * Pi) / 360))/Sin[theta], {theta, 0, Pi / 2}]
```

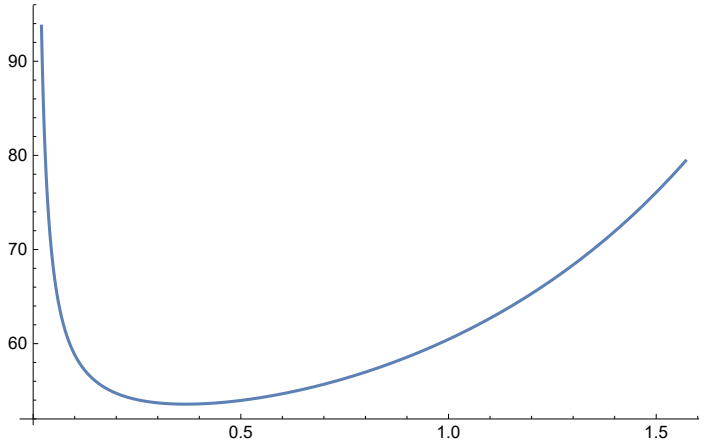


```
Show[e, a, b, cc, d, PlotRange → All]
```

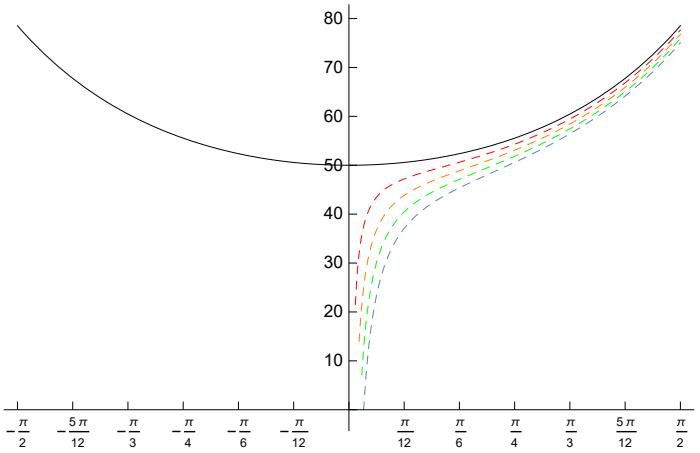

# Appendix 3

This appendix contains the Mathematica scripts used for the finite difference methods for a uniform strut, strut with a single hinge, multiple hinged struts.

In[ ]:=

# Finite Difference for Buckling Columns.

In[ ]:=

## Define the variables.

In[1]:=
```
e = 200 000; (*N/mm2 *)
```

In[2]:=
```
i = 33 500 000; (* units to be checked*)
```

In[3]:=
```
l = 4000.; (* length in m; define as a decimal to speed up calculation *)
```

In[4]:=
```
nn = 200;  (* number of segments *)
```

In[5]:=
```
lx = l / (nn - 1) (* length of segment *)
```

Out[5]= 20.1005

In[6]:=
```
theoreticalBuckling = (-1) π^2 e i / l^2 10^-3 // N
```

Out[6]= −4132.9

In[ ]:= Create the base matrix.

In[7]:=
```
lhs = DiagonalMatrix[ConstantArray[6, nn]] +
    DiagonalMatrix[ConstantArray[-4, nn - 1], 1] +
    DiagonalMatrix[ConstantArray[-4, nn - 1], -1] +
    DiagonalMatrix[ConstantArray[1, nn - 2], 2] +
    DiagonalMatrix[ConstantArray[1, nn - 2], -2];
```

In[8]:=
```
rhs = DiagonalMatrix[ConstantArray[-2, nn]] +
    DiagonalMatrix[ConstantArray[1, nn - 1], 1] +
    DiagonalMatrix[ConstantArray[1, nn - 1], -1] ;
```

In[ ]:= Now reduce the matrix for the boundaries known.

In[9]:=
```
mlhs = lhs[[ ;; -2, 2 ;;]];
```

In[10]:=
```
xredlhs = Drop[mlhs, 1, -1];
```

In[11]:=
```
mrhs = rhs[[ ;; -2, 2 ;;]];
```

In[12]:=
```
xredrhs = Drop[mrhs, 1, -1];
```

In[ ]:=

## Support definition.

In[ ]:= Simply supported at the ends needs a 5 inserting into the matrix, fixed ended needs a 7 inserting into the matrix

In[13]:=
```
supportend1 = 5;
```

In[14]:=
```
supportend2 = 5;
```

In[15]:=
```
xredlhs[[1, 1]] = supportend1;
```

In[16]:=
```
xredlhs[[nn - 2, nn - 2]] = supportend2;
```

In[ ]:=

# Define the loading matrix

Out[ ]= Define loading matrix the

In[17]:=
```
p = ConstantArray[0, nn - 2];
```

In[18]:=
```
p[[nn - 2]] = -1;
def = (e i) / (1000 * lx^2)
```

Out[19]= $1.65829 \times 10^{7}$

In[20]:=
```
tlhss = def xredlhs;
```

In[21]:=
```
{gvals, gvecs} = Eigensystem[{tlhss, xredrhs}];
```

In[22]:=
```
eigenbuckle = Max[gvals] // N
```

Out[22]= $-4132.81$

In[23]:=
```
error = 100 * (theoreticalBuckling - eigenbuckle) / theoreticalBuckling
```

Out[23]= 0.0020781

# Finite Difference with Central Hinge

In[ ]:=

## Define the variables.

In[ ]:=
```
e = 20 000 000 000;
 (*N/mm2 *)
```

In[ ]:=
```
numhinge = 1; (* Not really used at the minute,
but will be integrated for several hinges *)
```

In[ ]:=
```
segments = 17;
(* Number of nodes in order to place a
 hinge in the middle this must be an odd number *)
```

In[ ]:=
```
i = 33 500 000;
(* stiffness mm^4*)
```

In[ ]:=
```
l = 3000.;
(* length in mm; define as a decimal to speed up calculation,
otherwise symbolic engine grinds solution to a halt *)
```

Define the hinge stiffness:

In[ ]:=
```
moment = 50; (*Enter as kNm/rad *)
```

In[ ]:=
```
nn = numhinge * segments;
 (* number of nodes *)
```

In[ ]:=
```
lx = l / (nn - 1);
 (* length of segment *)
```

Taking E = (M R)/I determine R for the rotational springs, using an equivalent angle of a single radian to calculate.

Define the radius that should be used to determine the equivalent stiffness for the central hinged element. If the central element has a length of lx, then when 'flexed' to an angle of 1 radian the curved arc length also remains as lx.... the length of the arc of the circle is equal to Radius x Angle (radians) therefore the Radius = lx/1 or lx....

In[ ]:=
```
radius = lx;
```

In[ ]:=
```
ehinge = (moment * 1 000 000 * radius) / i
(* Need to determine the relationship between the stiffnesses *)
```

Out[ ]=
```
279.851
```

Create a scaling factor between the E values that can be applied to modify the hinges later on to mimic a rotational spring being inserted into the matrix.

In[ ]:=
```
eratio = e / ehinge
```

Out[ ]=
$$7.14667 \times 10^{7}$$

Develop a matrix for the youngs modulus to allow the introduction of a central hinge and develop the base matrix.

```
In[ ]:= lhs = DiagonalMatrix[ConstantArray[6, nn]] +
            DiagonalMatrix[ConstantArray[-4, nn - 1], 1] +
            DiagonalMatrix[ConstantArray[-4, nn - 1], -1] +
            DiagonalMatrix[ConstantArray[1, nn - 2], 2] +
            DiagonalMatrix[ConstantArray[1, nn - 2], -2];

In[ ]:= rhs = DiagonalMatrix[ConstantArray[-2, nn]] +
            DiagonalMatrix[ConstantArray[1, nn - 1], 1] +
            DiagonalMatrix[ConstantArray[1, nn - 1], -1] ;

In[ ]:= stiff = ConstantArray[e, nn - 2];
```

Now reduce the matrix for the boundaries known.

```
In[ ]:= mlhs = lhs[[ ;; -2, 2 ;;]];

In[ ]:= xredlhs = Drop[mlhs, 1, -1];

In[ ]:= mrhs = rhs[[ ;; -2, 2 ;;]];

In[ ]:= xredrhs = Drop[mrhs, 1, -1];
```

Simply supported at the ends needs a 5 inserting into the matrix, fixed ended needs a 7 inserting into the matrix

```
In[ ]:= supportend1 = 5;

In[ ]:= supportend2 = 5;

In[ ]:= xredlhs[[1, 1]] = supportend1;

In[ ]:= xredlhs[[nn - 2, nn - 2]] = supportend2;

In[ ]:=
```

# Define the loading matrix

```
In[ ]:= def = (stiff i) / (1000 * lx^2);

In[ ]:= (* Modify the hinge position by eratio *)

In[ ]:= def[[(Length[def] + 1) / (numhinge + 1)]] =
          def[[(Length[def] + 1) / (numhinge + 1)]] / eratio;

In[ ]:= tlhss = def xredlhs;
```

Extract the Eigensystem, save the EigenValues as gvals and the EigenVectors as gvecs

```
In[ ]:= {gvals, gvecs} = Eigensystem[{tlhss, xredrhs}];
```

Extract the largest value from the Eigen Values and display numerically, buckling load in kN.

## Output

```
In[ ]:= eigenbuckle = Max[gvals] // N
Out[ ]= -66.6657
```

Check for the percentage error.

```
In[ ]:= error = 100 * (2 * moment / (l / 2000)) / Abs[eigenbuckle] - 100
Out[ ]= 0.00151889
```

# Finite Difference with Multiple Hinges

In[ ]:=

## Define the variables.

In[ ]:=
```
e = 200 000;
 (*N/mm2 *)
```

In[ ]:=
```
numhinge = 3; (* Define the number of internal
 hinges on the strut*)
```

In[ ]:=
```
segments = 101;
(* Number of nodes per link,
subsequently multiplied by number of segments.*)
```

In[ ]:=
```
i = 33 500 000;
(* stiffness mm^4*)
```

In[ ]:=
```
l = 3000.;
(* length in mm;
define as a decimal to speed up calculation,
otherwise symbolic engine grinds solution to a
 halt *)
```

Define the hinge stiffness:

In[ ]:=
```
moment = 50; (*Enter as kNm/rad *)
```

In[ ]:=
```
nn = (numhinge + 1) * segments + 1
 (* number of nodes *)
```

Out[ ]= 405

In[ ]:=
```
lx = l / (nn - 1)
 (* length of segment *)
```

Out[ ]=
```
7.42574
```

Taking E = (M R)/I determine R for the rotational springs, using an equivalent angle of a single radian to calculate.

Define the radius that should be used to determine the equivalent stiffness for the central hinged element. If the central element has a length of lx, then when 'flexed' to an angle of 1 radian the curved arc length also remains as lx.... the length of the arc of the circle is equal to Radius x Angle (radians) therefore the Radius = lx/1 or lx....

In[ ]:=
```
radius = lx;
```

In[ ]:=
```
ehinge = (moment * 1 000 000 * radius) / i
(* Need to determine the relationship between
 the stiffnesses *)
```

Out[ ]=
```
11.0832
```

Create a scaling factor between the E values that can be applied to modify the hinges later on to mimic a rotational spring being inserted into the matrix.

In[ ]:=
```
eratio = e / ehinge
```

Out[ ]=
```
18 045.3
```

Develop a matrix for the youngs modulus to allow the introduction of a central hinge and develop  the base matrix.

```
lhs = DiagonalMatrix[ConstantArray[6, nn]] +
    DiagonalMatrix[ConstantArray[-4, nn - 1], 1] +
    DiagonalMatrix[ConstantArray[-4, nn - 1], -1] +
    DiagonalMatrix[ConstantArray[1, nn - 2], 2] +
    DiagonalMatrix[ConstantArray[1, nn - 2], -2];
```

```
rhs = DiagonalMatrix[ConstantArray[-2, nn]] +
    DiagonalMatrix[ConstantArray[1, nn - 1], 1] +
    DiagonalMatrix[ConstantArray[1, nn - 1], -1] ;
```

```
stiff = ConstantArray[e, nn - 2];
```

Now reduce the matrix for the boundaries known.

```
mlhs = lhs[[ ;; -2, 2 ;;]];
```

```
xredlhs = Drop[mlhs, 1, -1];
```

```
mrhs = rhs[[ ;; -2, 2 ;;]];
```

```
xredrhs = Drop[mrhs, 1, -1];
```

Simply supported at the ends needs a 5 inserting into the matrix, fixed ended needs a 7 inserting into the matrix

```
supportend1 = 5;
```

```
supportend2 = 5;
```

```
xredlhs[[1, 1]] = supportend1;
```

```
xredlhs[[nn - 2, nn - 2]] = supportend2;
```

# Define the loading matrix

```
maptable = Partition[Table[segments i, {i, numhinge}], 1]
```

```
{{101}, {202}, {303}}
```

```
def = (stiff i) / (1000 * lx^2);
```

```
In[•]:= realspring = def[[1]] / eratio
Out[•]= 6733.33

In[•]:= def = ReplacePart[def, maptable → realspring];

In[•]:= Length[def] / (numhinge + 1)
Out[•]= 403/4

In[•]:= (* Modify the hinge position by eratio *)

In[•]:= tlhss = def xredlhs;
```

Quickly check the matrices, to see that everything has been mapped across correctly.

```
In[•]:= (* def // MatrixForm
     tlhss // MatrixForm
   xredrhs // MatrixForm *)
```

Extract the Eigensystem, save the EigenValues as gvals and the EigenVectors as gvecs, inserting the N[blahblah, ##] Set the precision to ## digit precision.

```
In[•]:= NHoldAll[gvals];

In[•]:= {gvals, gvecs} = Eigensystem[N[{tlhss, xredrhs}, 100]];
```

Extract the largest value from the Eigen Values and display numerically, buckling load in kN.

## Output

```
In[•]:= eigenbuckle = Max[gvals] // N
Out[•]= -38.8598
```

```
In[•]:= NumberForm[eigenbuckle, 16]
```

```
Out[•]//NumberForm=
-38.85979101034772
```

Check for the ratio between the lowest and highest eigenvalues for a sense of the ill conditioning.

```
In[•]:= eigenratio = Min[gvals] / Max[gvals] // N
```

```
Out[•]= 1.2504 × 10^7
```

```
In[•]:= Precision[gvals]
```

```
Out[•]= MachinePrecision
```

Check for ill-conditioning effects creeping in, 3rd variable. (c and c2) are the conditioning numbers for the various square matrices. https://math.stackexchange.com/questions/675474/what-is-the-practical-impact-of-a-matrixs-condition-number

```
In[•]:= {lu, p, c} = LUDecomposition[xredrhs];
```

```
In[•]:= lu // MatrixForm;
```

```
In[•]:= c
```

```
Out[•]= 0
```

```
In[•]:= {lu2, p2, c2} = LUDecomposition[tlhss];
```

LUDecomposition: Result for LUDecomposition of badly conditioned matrix {≪1≫} may contain significant numerical errors.

In[•]:=
```
lu2 // MatrixForm
```

Out[•]//MatrixForm=

( ··· 1 ··· )

large output | show less | show more | show all | limit

In[•]:=
```
c2
```

Out[•]= $9.47508 \times 10^{11}$

In[•]:=
```
NumberForm[1.33366 × 10^8, 16]
```

Out[•]//NumberForm=

$1.333658186663053 \times 10^{8}$

In[•]:=
```
$MachinePrecision
```

Out[•]= 15.9546

In[•]:=
```
$MaxMachineNumber
```

Out[•]= $1.79769 \times 10^{308}$

In[•]:=
```
Precision[1.79769 × 10^308]
```

Out[•]= MachinePrecision

In[•]:=
```
Det[tlhss]
```

Out[•]= $3.431329859484362 \times 10^{3250}$

In[•]:=
```
{u, v, w} = SingularValueDecomposition[tlhss];
```

In[•]:=
```
Diagonal[v] // MatrixForm;
```

In[•]:=
```
{gvals, gvecs} =
  Eigensystem[N[{u.v.Transpose[w], xredrhs}, 100]];
```

In[•]:=
```
Max[gvals]
```

Out[•]=
```
-38.8575
```

In[•]:=
```
{lu2, p2, c2} = LUDecomposition[u.v.Transpose[w]];
```

LUDecomposition: Result for LUDecomposition of badly conditioned matrix {{6.07526 × 10^8, −4.86021 × 10^8, 1.21505 × 10^8, 2.18316 × 10^−7, 6.4917 × 10^−7, ≪42≫, −1.26401 × 10^−7, 1.11741 × 10^−7, −1.09099 × 10^−7, ≪353≫}, {≪1≫}, ≪47≫, {≪1≫}, ≪353≫} may contain significant numerical errors.

In[•]:=
```
c2
```

Out[•]=
```
9.47509 × 10^11
```